Iterative and Adaptive Processing for Multiuser Communication Systems

Lance Linton B.Eng., M.Eng.

College of Engineering and Science,
Victoria University

Submitted in fulfillment of the requirements of the degree of
Doctor of Philosophy

15th April 2016

Abstract

The huge demand of wireless communications has driven the requirement for highly-efficient multiple-access communications schemes that can accommodate multiple simultaneous users, yet provide performance similar to single-user systems. Recently, iterative multiuser detection schemes have shown to provide this high level of performance at a manageable level of complexity. This thesis is concerned with iterative detection of two non-orthogonal asynchronous access schemes: code-division multiple-access (CDMA); and interleave-division multiple-access (IDMA).

A multi-rate IDMA system is developed where different users transmit data at different rates. High-rate users support multiple sub-streams, each coded as an IDMA layer. The iterative receiver treats each IDMA layer as a virtual user. Variance transfer analysis is employed to analyse the receiver performance, which is then optimised by developing a power allocation strategy. Simulation results demonstrate that the performance of this proposed system is close to the theoretical limit in a Rayleigh flat-fading environment.

Next, receiver performance is optimised by forward error correction code allocation. For multiuser systems with dynamic loads, new users are allocated codes according to the existing system load in order to optimise receiver convergence. Small multiuser systems have performances that approach the theoretical single-user bound.

The Golden Code is a "perfect" space-time block-code for 2×2 multiple-antenna (MIMO) systems. It can simultaneously achieve both full-diversity and -rate. A MIMO-IDMA multiuser detector is developed to extend the golden code scheme to the multiuser case. Decoding is performed by an iterative receiver whose complexity is linear in the

number of users. In a Rayleigh flat-fading environment, simulation results show that the proposed scheme can outperform other common MIMO schemes and approaches within 0.25dB of the single-user bound.

The application of iterative multiuser detection to underwater acoustic communications is considered next. Designing reliable communication systems for the underwater acoustic channel has proven to be very challenging. A major channel impairment is the multipath interference caused by multiple reflections of the acoustic signal from the water surface and bottom. These reflections occur at small grazing angles and with small reflection losses, causing both long delay spread and large multipath amplitudes in the received signal.

The large delay-spread implies that single-carrier communication will be plagued by inter-symbol interference (ISI) that spans many symbols. As an alternative, multi-carrier modulation (MCM) has been proposed to increase the symbol interval and thereby decrease the ISI span. We combine Orthogonal Frequency-Division Multiplexing (OFDM), a low-complexity spectrally-efficient MCM technique, with an IDMA overlay to develop a multiple-access communications system that provides robust performance in the presence of large time-delay spread and the other impairments presented by the shallow water acoustic channel.

Finally, we consider multiuser communications in doubly-spread underwater acoustic channels, where the relative motion between the transmitter, receiver, and scattering objects imparts each path with a unique Doppler shift. In this case, the orthogonality of OFDM is lost, leading to subcarrier interference which greatly complicates optimal data detection. Therefore, single-carrier system is considered with a non-linear Kalman filter as equalizer. The doubly-selective channel is modelled using basis expansion models (BEMs), a low-rank channel model that exploits the inherent structure in the channel response. The use of basis functions can turn a time-varying system identification problem into a time-invariant one, thereby reducing the number of parameters to estimate. The receiver uses a semi-blind iterative channel estimation algorithm to estimate the channel parameters. Experimental results demonstrate robust performance in underwater channels with simultaneously large delay- and Doppler-spreads.

Declaration

I, Lance Linton, declare that this PhD thesis entitled "Iterative and Adaptive Processing for Multiuser Communication Systems" is no more than 100,000 words in length including quotes and exclusive of tables, figures, appendices, bibliography, references and footnotes. This thesis contains no material that has been submitted previously, in whole or in part, for the award of any other academic degree or diploma. Except where otherwise indicated, this thesis is my own work.

Lance Linton
15th April 2016

Acknowledgements

Of the many people who deserve thanks, some are particularly prominent, such as my supervisors, Prof. Michael Faulker, Assoc. Prof. Patrick Leung, and Dr. Phillip Conder. Their invaluable advice, guidance, and encouragement have made all of this possible.

Contents

Nomenclature

Notation

$\mathbb{R}, \mathbb{R}^n, \mathbb{R}^{n \times m}$	set of real numbers, vectors, and matrices
$\mathbb{C}, \mathbb{C}^n, \mathbb{C}^{n \times m}$	set of complex numbers, vectors, and matrices
$\mathbb{N}^*$	set of natural numbers $\{1, 2, 3 \ldots\}$
$\mathbb{Q}$	set of rational numbers
$\mathbb{Z}$	set of integers
$\star$	convolution
$\odot$	Hadamard product
$\otimes$	Kronecker product
$\mathbf{I}_n$	$n \times n$ identity matrix
$\mathbf{0}_{n \times m}$	$n \times m$ zero matrix
$\{\mathbf{A}\}_{i,j}$	i, j-th element of matrix $\mathbf{A}$
$\mathbf{A}^T$	transpose of matrix $\mathbf{A}$
$\mathbf{A}^H$	conjugate transpose of matrix $\mathbf{A}$
$\mathbf{A}^{-1}$	inverse of matrix $\mathbf{A}$
$\mathrm{diag}\{a_1, \ldots, a_n\}$	diagonal matrix with elements $a_1, \ldots, a_n$ on the main diagonal
$\mathrm{tr}(\mathbf{A})$	trace of matrix $\mathbf{A}$
$\arg\max_x f(x)$	denotes the value of x that maximises $f(x)$
$\arg\min_x f(x)$	denotes the value of x that minimises $f(x)$
$\mathrm{Cov}\{x, y\}$	covariance of x and y
$\delta(t)$	Dirac delta function
$\mathrm{E}\{x\}$	expected value of x
$\exp\{x\}$	exponential function, $\exp(x) = e^x$

$\mathrm{L}(x)$	log likelihood ratio of x
$\log(x)$	natural logarithm of x
$\mathcal{N}(\mu, \sigma^2)$	normal (Gaussian) distribution with mean μ and variance σ^2
$\mathcal{N}(\boldsymbol{\mu}, \mathbf{C})$	multivariate normal distribution with mean $\boldsymbol{\mu}$ and covariance $\mathbf{C}$
$p(x)$	probability density function of x
$p(x \mid y)$	conditional probability density function of x conditioned on y
$P(x)$	probability mass function of x
$P(x \mid y)$	conditional probability mass function of x conditioned on y
$\Re\{z\}, \Im\{z\}$	real and imaginary parts of z
$\mathrm{sgn}(x)$	signum function, $\mathrm{sgn}(x) = -1$ if $x < 0$; $\mathrm{sgn}(x) = 1$ if $x > 0$
$\mathrm{Var}\{x\}$	variance of x

Commonly used symbols

$\Lambda(x)$	*a posteriori* probability information in LLR form, $\Lambda(x) = L_{app}(x)$
$\Lambda_1(\,\cdot\,)$	*a posteriori* probability information (in LLR form) output from the soft equalizer or multiuser detector
$\Lambda_2(\,\cdot\,)$	*a posteriori* probability information (in LLR form) output from the soft FEC channel decoder(s)
$\lambda(x)$	extrinsic information in LLR form, $\lambda(x) = L_{ext}(x)$
$\lambda_1(\,\cdot\,)$	extrinsic information (in LLR form) output from the soft equalizer or soft multiuser detector, used as *a priori* information by the FEC channel decoder(s)
$\lambda_2(\,\cdot\,)$	extrinsic information (in LLR form) output from the soft FEC channel decoder(s), used as *a priori* information by the soft equalizer or soft multiuser detector
$b[i], b_k[i]$	i-th bit (single-user case), i-th bit for the k-th user (multiuser case), input to the symbol mapper or spreader (transmit side, coded or uncoded systems). $b[i], b_k[i]$ is coded and interleaved in coded systems
$\hat{b}[i], \hat{b}_k[i]$	estimate of $b[i]$, estimate of $b_k[i]$, output from the equalizer, detector, or multiuser detector (receive side, coded or uncoded systems)
$c[i], c_k[i]$	i-th coded bit (single-user case), i-th coded bit for the k-th user (multiuser case), output from the FEC encoder(s) (transmit side, coded systems)

$\hat{c}[i], \hat{c}_k[i]$	estimate of $c[i]$, estimate of $c_k[i]$, input to the FEC decoder(s) (receive side, coded systems)
$d[i], d_k[i]$	i-th input data bit (single-user case), i-th input data bit for the k-th user (multiuser case), input to the FEC encoder(s) (transmit side, coded systems)
$\hat{d}[i], \hat{d}_k[i]$	estimate of $d[i]$, estimate of $d_k[i]$, output from the FEC decoder(s) (receive side, coded systems)
K	number of users in the multiuser system
$n(t)$	continuous-time channel noise at time t
$x[i], x_k[i]$	i-th transmitted symbol (single-user case), i-th transmitted symbol or chip from user-k (multiuser case), discrete-time channel input
$x(t), x_k(t)$	transmitted signal at time t (single-user case), transmitted signal from user-k at time t (multiuser case), continuous-time channel input
$y[i]$	i-th received symbol, discrete-time channel output
$y(t)$	received signal at time t, continuous-time channel output

Abbreviations

APP	a posteriori probability
AR	autoregressive
AR(p)	autoregressive process of order p
AWGN	additive white Gaussian noise
BCJR	Bahl, Cocke, Jelenik and Raviv (algorithm)
BEM	basis expansion model
BER	bit error rate
BI-AWGN	binary-input additive white Gaussian noise
BPSK	binary phase shift keying
CDMA	code-division multiple-access
CE-BEM	complex exponential BEM (discrete Fourier BEM)
DFE	decision feedback equalizer
DFT	discrete Fourier transform
DPSS	discrete prolate spheroidal sequence (Slepian sequence)
EKF	extended Kalman filter

ESE	elementary signal estimator
EXIT	extrinsic information transfer
FEC	forward error correction
FFT	fast Fourier transform
FIR	finite impulse response
ICI	inter-carrier interference
i.i.d	independent and identically distributed
IDMA	interleave-division multiple-access
ISI	intersymbol interference
KF	Kalman filter
K-L	Karhunen-Loeve expansion
LD	linear dispersion
LDPC	low-density parity check
LLR	log-likelihood ratio
MAI	multiple-access interference
MAP	maximum a posteriori probability
MCM	multi-carrier modulation
MF	matched filter
MIMO	multiple-input multiple-output
ML	maximum likelihood
MMSE	minimum mean square error
MSE	mean square error
MUD	multiuser detection/detector
NKF	nonlinear Kalman filter
OFDM	orthogonal frequency division multiplexing
p.d.f	probability density function
QAM	quadrature amplitude modulation
QPSK	quadrature phase shift keying
SISO	soft-input soft-output
SNR	signal to noise ratio

ST	space-time
STBC	space-time block code/coding
UAC	underwater acoustic channel
US	uncorrelated scattering
V-BLAST	vertical Bell Labs layered space-time
VT	variance transfer
WSS	wide sense stationary
WSSUS	wide sense stationary uncorrelated scattering

Chapter 1

Introduction

The last two decades has witnessed a tremendous growth in wireless communications. Cellar mobile telephony and data services, and wireless networking were once rare but have become pervasive and an almost essential part of daily life. Future demand for these wireless devices and services show no sign of abating. In addition to the traditional network usage of wireless technology, the availability of low-cost wireless devices has enabled many new wireless applications over recent years. One notable application is distributed sensing, in which large numbers of inexpensive wireless nodes sense some ongoing process and wirelessly communicate with each other and wired access points. Environmental detection, surveillance, and health monitoring are just a few of the numerous potential uses of distributed sensor networks.

A defining feature of wireless communications is that all devices must share the electromagnetic spectrum in order to communicate with each other. Unlike in wired communications, where each communication channel could conceivably have a physical channel independent from all others, in wireless communication all channels come from a common medium. The scarcity of radio spectrum resource requires wireless communication systems to reuse the frequency bands In order to achieve reliable communications, some scheme must be developed for equitable sharing the usable frequencies. The issue of a large number of users sharing a single allocated spectrum in order to communicate is known as the *multiple-access* problem.

1.1 Multiple-Access Schemes

In a multiuser communication system, a large number of users share a common multiple-access channel to transmit information to a receiver. Multiple access systems generally require that when different transmitting sources are sending messages simultaneously through the same channel, the transmissions must be separated in some fashion so that they do not interfere with one another. This is usually accomplished by making the messages orthogonal to one another in the dimensions of frequency, time or code.

Frequency division multiple access (FDMA). In FDMA systems, the allocated frequency band is divided into non-overlapping sub-channels. Each transmitting source is assigned an individual sub-channel for data transmission, as shown in Figure 1.1a. A disadvantage of FDMA is that the frequency spectrum may not be used efficiently as no user can share the same frequency band at the same time and guard bands have to be maintained between adjacent signals spectra to minimise cross talk between sub-channels. FDMA also constrains the maximum bit rate per channel as increasing the bit rate requires the allocation of more frequency channels to a user.

Time division multiple access (TDMA). In TDMA systems, each user is allocated a unique cyclically repeating time slot within the channel. This allows a number of users to access and share a common channel without interfering with each other. Different users can transmit or receive messages, one after the next in the same bandwidth but in different time slots, as shown in Figure 1.1b. A disadvantages of TDMA is that it requires a significant amount of signal processing for synchronisation as the transmission of all users must be exactly synchronised. Additionally, TDMA needs guard times (the equivalent to guard bands in FDMA) between time intervals to reduce the effects of clock instabilities and transmission time delay.

Code-division multiple access (CDMA). CDMA is a spread-spectrum technique where the transmitted signal is spread over a wide frequency band, much wider that the minimum bandwidth required to transmit the information being sent.

The most common form of CDMA is direct sequence (DS) CDMA where all users share a common channel in time and frequency (Figure 1.1c). Each user modulates its data with a unique spreading sequence (pseudo-random modulation), which allows the users data to be distinguished at the receiver. In contrast to FDMA and TDMA, where the users communication channels are separated in frequency or time, in a DS-CDMA system the users data are distinguished by the separation (cross-correlation) between their spreading sequences.

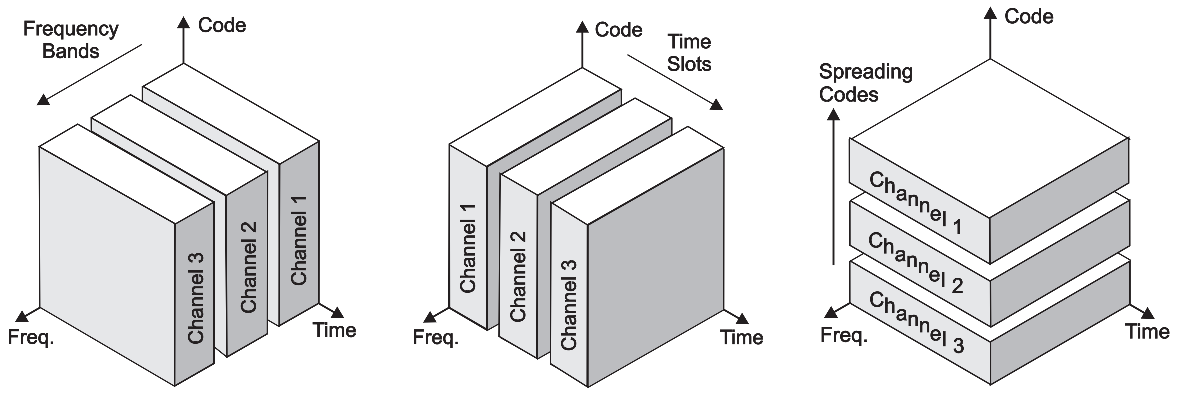

(a) FDMA **(b)** TDMA **(c)** CDMA

Figure 1.1: Multiple-access techniques: (a) Frequency-division multiple access (FDMA); (b) Time-division multiple access (TDMA); and (c) Code-division multiple access (CDMA).

CDMA schemes have become a very popular method for multiple-access communications, and multiuser detection algorithms for CDMA receivers will be the focus of this thesis. Since the users in a DS-CDMA system are distinguished by the separation (cross-correlation) between their spreading sequences, we can categorise DS-CDMA schemes according to the cross-correlation between users, i.e.,

- *orthogonal signalling* - where the cross-correlation between all users is zero; or
- *non-orthogonal signalling* - where the cross-correlation between users is non-zero.

Additionally, CDMA schemes can also be categorised according to the synchronism of the users' signals at the receiver, i.e.,

- *synchronous schemes* where the bit epochs of all the users are aligned at the receiver.
- *asynchronous schemes* where bit epochs of the users may be offset (not aligned) at the receiver.

Asynchronous schemes are also non-orthogonal because there are no known sets of spreading sequences that exhibit zero cross-correlation over a range of timing offsets.

In this thesis, we investigate asynchronous non-orthogonal CDMA schemes, and in particular, Interleave Division Multiple Access (IDMA) which is a multiple-access scheme where users are separated by unique interleaver sequences (instead of unique spreading sequences).

Iterative signal processing has proven to be an important technique in improving the performance of receivers in communications systems. Iterative techniques can be used to equalize inter-symbol interference channels (turbo equalization) and to resolve multiple-access interference (MAI) in multiuser receivers (turbo multiuser-detection, or turbo MUD). The origins of these techniques lie in error correction coding with the concepts of concatenated coding [29] and turbo codes. A brief review of error correction coding provides insight into the common building blocks of iterative processing.

1.2 Error Correction Coding

The approach to error correction coding taken by modern digital communication systems started in the late 1940's with the ground breaking work of Shannon [107], Hamming [38], and Golay [34]. In his paper, Shannon developed the theoretical basis for coding which has become known as *information theory*. By mathematically defining the entropy of an information source and the capacity of a communications channel, he showed that it was possible to achieve reliable communications over a noisy channel provided that the source's entropy is lower than the channel's capacity. Shannon did not explicitly state how channel capacity could be practically reached, only that it was attainable.

1.2.1 Block Codes

Hamming is generally credited with discovering the first error correcting code [68] when, in 1946, he developed an algorithm that enabled early computers to correct isolated errors detected in the input data. His method was to group the data into sets of four information bits and then calculate three check bits which are a linearly combination of the information bits, resulting in a seven bit code word. After reading in a code word, the Hamming's algorithm could detect errors and also determine the location of a single error. Hence, the Hamming code was able to correct a single error in a block of seven encoded bits.

While it was a major advancement, the Hamming code had a number of shortcomings. Firstly, it was inefficient, requiring three check bits for every four data bits, and secondly, it only had the ability to correct a single error within the block. These issues were addressed by Golay, who generalized Hamming's construction, and in the process, discovered two important codes: the binary Golay code; and ternary Golay code [137].

Reed-Muller (RM) codes [78] [99] were the next main class of linear block codes to be discovered, and were an important development because they allowed more flexibility in the size of the code word and the number of correctable errors per code word. They were followed by the discovery of *cyclic* codes, first discovered by Prange [90]. Cyclic codes are linear block codes that possess the additional property that any cyclic shift of a code word is also a code word. The cyclic property adds considerable structure to the code, which can be exploited by reduced complexity encoders and (more importantly) reduced complexity decoders. Important cyclic codes include the binary BCH codes [14] [43], and their non-binary extensions, the Reed and Solomon (RS) codes [100]. RS codes were a major advancement because their non-binary nature allows for protection against bursts of errors.

Although popular, block codes have two fundamental disadvantages: Firstly, their frame-oriented nature means that the entire code word must be received before decoding can be completed. This can introduce unacceptable latency into the system, particularly when block lengths are large. Secondly, most algebraic-based decoders for block codes work with hard-bit decisions, rather than with the unquantized, or "soft", outputs of the demodulator. With hard-decision decoding, the output of the channel is taken to be binary, while with soft-decision decoding the channel output is continuous-valued [125].

In order to achieve the Shannon performance bound, a continuous-valued channel output is required. Block codes can achieve good performance over relatively benign channels, but they are generally power inefficient and have poor performance when the signal-to-noise ratio (SNR) is low. This poor performance at low SNR is not a function of the code itself, but is actually a function of the sub-optimality of hard-decision decoding. It is possible to perform soft-decision decoding of block codes, although historically soft-decision decoding has generally been regarded as too complex [125].

1.2.2 Convolutional Codes

Convolutional codes, introduced by Elias [26], avoid both main disadvantages of block codes. Instead of segmenting data into distinct blocks, convolutional encoders add redundancy to a continuous stream of input data by using linear shift registers. Each set of n output bits is a linear combination of the current set of m input bits and the bits stored in the shift register. The total number of bits that each output depends on is called the *constraint length*, L. The *rate*, R_c, of the convolutional encoder is the number of data bits m taken in by the encoder in one coding interval, divided by the number of code bits n output during the same interval, i.e., $R_c = m/n$. Just as the data is continuously encoded, it can be continuously decoded with nominal latency. Additionally, the decoding algorithms can make full use of soft-decision information from the demodulator.

The first practical decoding algorithm for convolutional codes was the sequential decoder, introduced by Wozencraft and Reiffen [138]. However convolutional coding was not widely used until the introduction of the Viterbi algorithm (VA) [129], which was the first practical method for optimally (maximum likelihood) decoding convolutional codes.

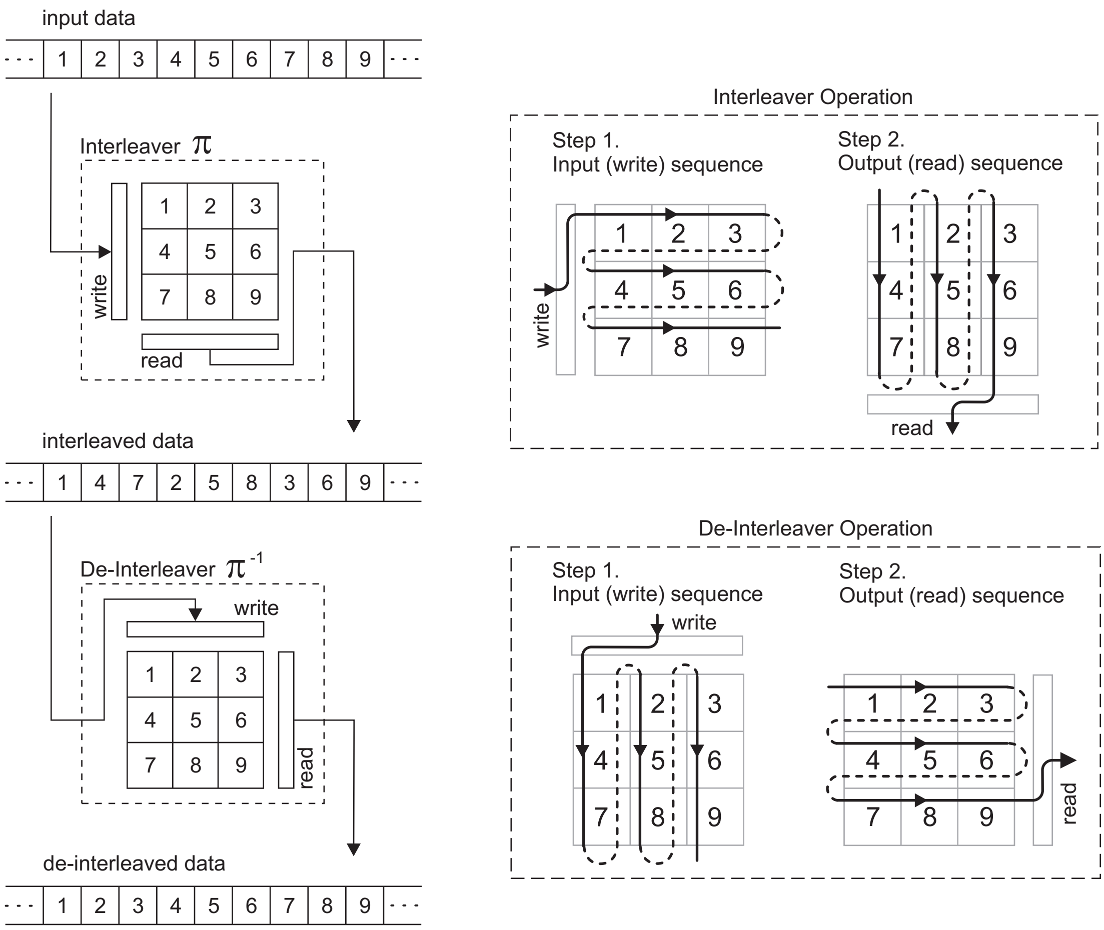

Figure 1.2: Block interleaver and de-interleaver operation

One of the main disadvantages of convolutional codes is their susceptibility to burst errors. This susceptibility can be mitigated by using an *interleaver*, which scrambles the order of the code bits prior to transmission. A *deinterleaver* at the receiver places the received code bits back in the proper order after demodulation and prior to decoding. By scrambling the order of the code bits at the transmitter, and then reversing the process at the receiver, burst errors can be spread out so that they appear independent to the decoder. The most common type of interleaver is the *block interleaver* (Figure 1.2), which is simply an $M_b \times N_b$ bit array. Data is placed into the array column-wise and then read out row-wise. A burst error of length up to N_b bits can be spread out by a block interleaver such that only one error occurs every M_b bits. There are also many other interleaver types [130].

1.2.3 Concatenated Codes

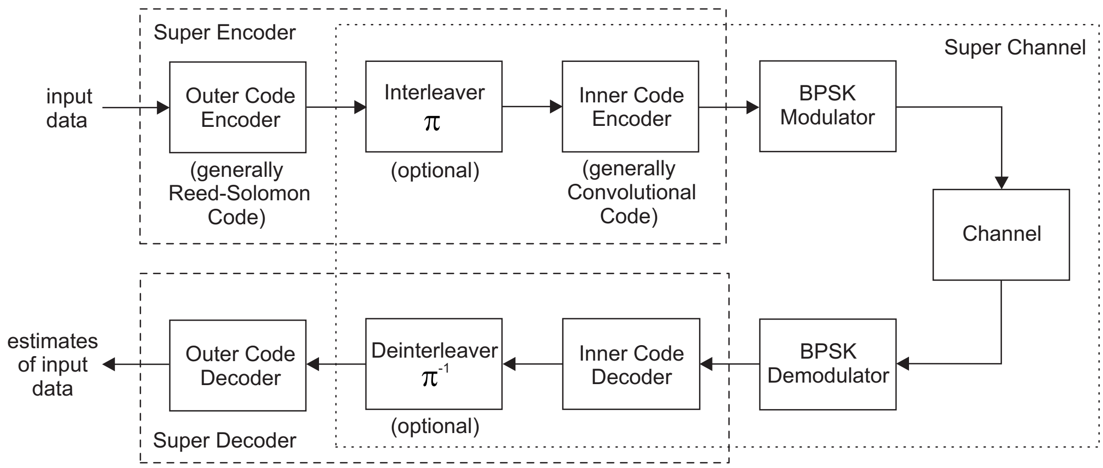

Figure 1.3: Serial concatenated coding system. Optional interleaver and deinterleaver are used for channels with very long error bursts.

Convolutional codes and Reed-Solomon (RS) codes have complimentary properties. Convolutional codes are susceptible to burst errors, while RS codes can cope with burst errors quite well [137]. By concatenating an RS code and a convolutional code in series, Forney was able to take advantage of these complimentary properties and create an efficient system design for power-limited channels [29].

Forney's concatenated coding scheme is shown in Figure 1.3. Data is first encoded by an RS *outer* encoder which then feeds an *inner* convolutional encoder. At the receiver, the *inner* convolutional decoder cleans up the data received over the noisy channel. The output of the convolutional decoder has a much improved SNR, but due to the nature of convolutional codes, errors are typically grouped into bursts. The *outer* RS decoder completes the decoding process by decoding data output from the convolutional decoder.

Hence, each decoder works with the appropriate type of data—the convolutional decoder works at low SNR with mostly independent errors, while the RS decoder works at high SNR with mostly burst errors. For cases with very long error bursts, a block interleaver can can be placed between the convolutional and RS encoders in order to spread long error bursts across several RS code words [137].

1.2.4 Turbo Codes

Although considerable progress had been made in coding theory, there was still a considerable gap between the performance of the best known codes and the theoretical limit predicted by Shannon. This changed when Berrou, Glavieux, and Thitimajshima [13] discovered *turbo codes*—a practical coding system that could approach Shannon's theoretical limit.

A turbo code is the parallel concatenation of two or more component codes. In its original form, the constituent codes were recursive systematic convolutional (RSC) codes [13], which are a subclass of convolutional codes. As shown in Figure 1.4a, two rate $R_c = 1/2$ RSC encoders work on the input data in parallel, with the input data interleaved before being fed into the lower encoder (Code 2 encoder). The encoders are *systematic* (one of the outputs is the input itself) and receive the same input (although in a different order), therefore, the systematic output of the Code 2 encoder is completely redundant and does not need to be transmitted. The overall code rate of the parallel concatenated code is $R_c = 1/3$, although higher code rates can be obtained by *puncturing* (i.e., selectively removing) the parity output with a multiplexer (MUX) circuit [48].

Due to the presence of the interleaver, optimal (maximal likelihood) decoding of turbo codes has prohibitive computational complexity. However, a suboptimal iterative decoding algorithm was presented in [13] which provides good performance at much lower complexity. The idea behind the decoding strategy is to break the overall decoding problem into two smaller problems (decoding each of the constituent codes) with locally optimal solutions and to share information in an iterative fashion. The decoder associated with each of the constituent codes is modified so that it produces soft-outputs in the form of *a posteriori probabilities* (APPs) of the data bits. The two decoders are cascaded as shown in Figure 1.4b so that the Code 2 decoder receives the soft-output of the Code 1 decoder. At the end of the first iteration, the soft-output of the Code 2 decoder is fed back to the upper decoder and used as *a priori* information during the next iteration. Decoding continues in an iterative fashion until the desired performance is attained.

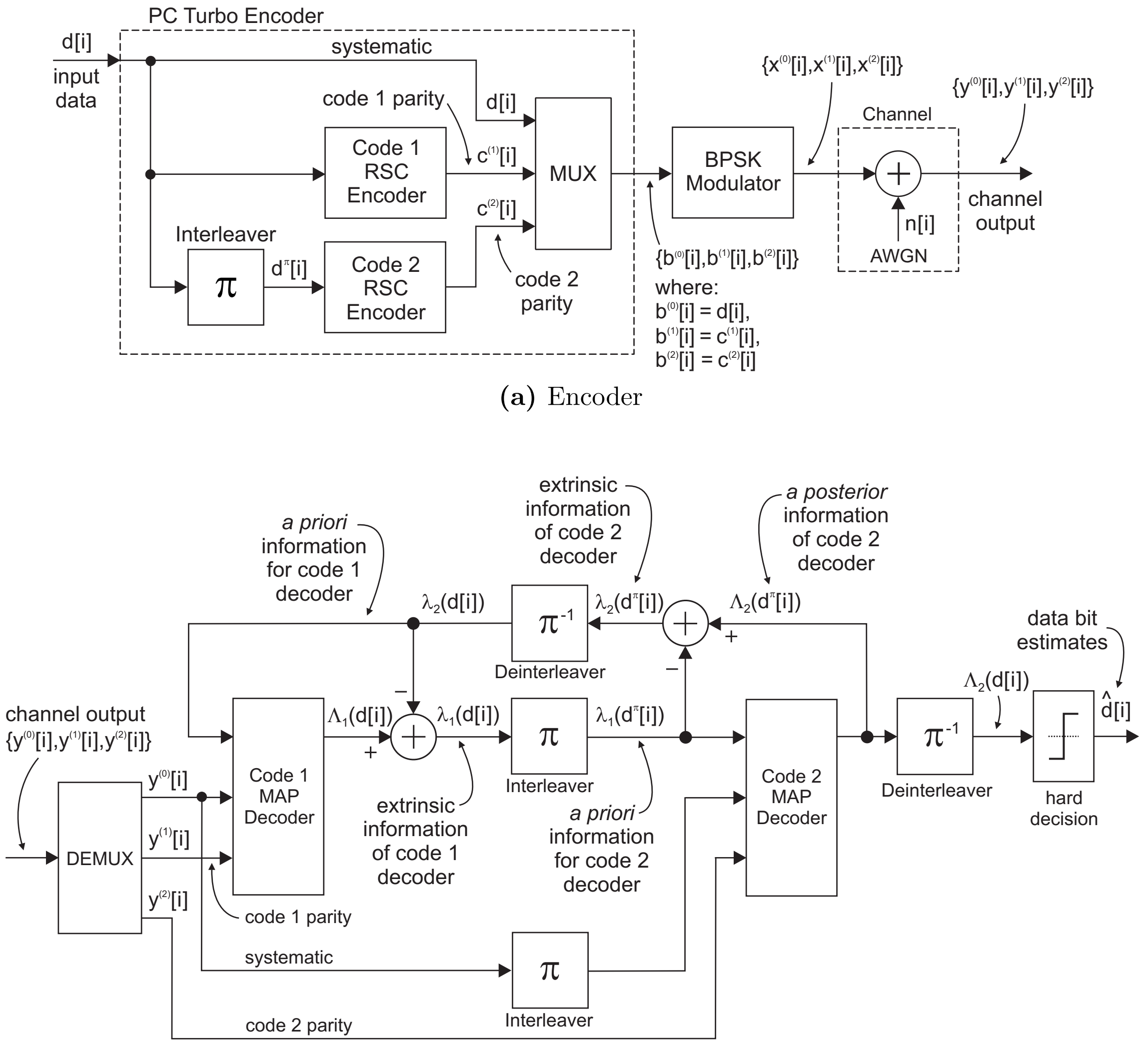

(a) Encoder

(b) Decoder

Figure 1.4: Parallel concatenated (PC) turbo encoder and decoder (systematic form).

However, iterative decoding obeys a law of diminishing returns and hence the incremental gain of each additional iteration is less than that of the previous iteration. It is the decoding method that gives turbo codes their name, since the feedback action of the decoder is similar to that of a turbo-charged engine [125].

Simulation results for the original turbo code of [13] showed that a bit error rate of 10^{-5} could be achieved at an E_b/N_0 ratio of just 0.7dB after 18 iterations of decoding, i.e., turbo codes could come within a 0.7dB of the Shannon limit. Other researchers began to look at using other concatenation configurations and other types of component codes. It was found that serial concatenated codes offer performance that is comparable to, or even exceeds, that of parallel concatenated codes [11]. Additionally, it was found that the performance with convolutional component codes could be matched or exceeded with block component codes [19] [94] [1]. As a result, it became clear that the real breakthrough from the introduction of turbo codes, was not the code construction, but the method of iterative decoding.

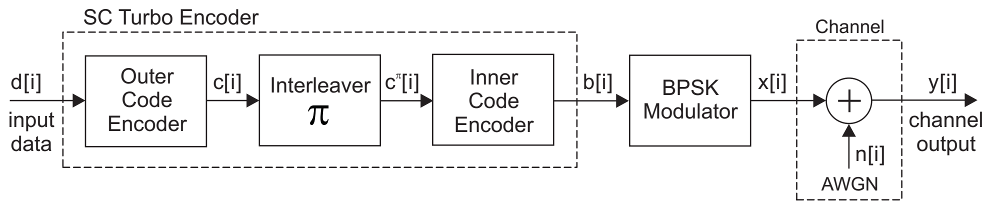

(a) Encoder

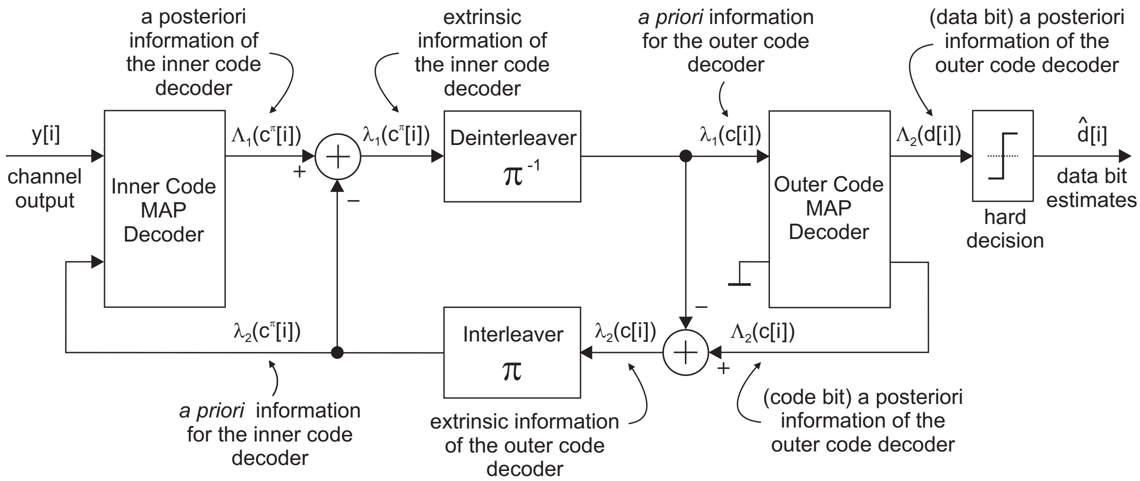

(b) Decoder

Figure 1.5: Serial concatenated (SC) turbo encoder and decoder (non-systematic form).

1.3 Applications of Iterative Decoding

After the introduction of turbo codes, it was quickly recognized that the iterative decoding method was suitable for many other applications, and could be used as a general methodology for receiver design. Communication receivers typically consist of a cascade of subsystems, each optimized to perform a single task. Examples of these subsystems include equalizers, multiuser detectors, channel decoders, and source decoders.

Traditionally, the interface between subsystems involves the passing of hard-decisions (e.g., bits) down the stages of the chain. Whenever hard-decisions are made, information is lost and becomes unavailable to subsequent stages. Additionally, stages at the beginning of the processing chain do not benefit from information derived by stages further down the chain. The interface between stages can be greatly improved by using the same strategy devised to decode turbo codes. This general strategy of iterative feedback decoding or detection is termed *turbo processing* [66].

Turbo processing frameworks are constructed using soft-input soft-output (SISO) subsystems. A SISO subsystem receives soft-decision values as input and produces soft-decision values as output. Soft-decision values are passed down the chain and refined by subsequent stages. The soft-output of the final stage is then fed back to the first stage and the next iteration of processing is initiated. Multiple iterations of turbo processing can be performed, although, as with turbo codes, the incremental improvement in performance diminishes with each additional iteration.

Turbo processing can be used to combine channel decoding with source decoding [36], and channel decoding with symbol detection [66]. Other examples include:

Turbo equalization. This is a method of combining equalization with channel decoding [23]. An equalizer is a subsystem that compensates for the intersymbol interference (ISI) present in frequency selective channels. A frequency selective channel can be described as a rate-one convolutional code defined over the field of real or complex numbers. The combination of a convolutional channel code and ISI channel can be viewed as a serial concatenation of two convolutional codes, which is a type of serially concatenated turbo code, and can therefore can be decoded using the turbo decoding algorithm.

Turbo multiuser detection. Here, the concept of turbo processing is applied to coded multiple-access channels [44]. In a multiple-access channel, several users transmit at the same time and frequency, producing multiple access interference (MAI), which can be described as a form of time varying ISI. Thus, the multiple access channel can be viewed as a rate-one convolutional code with time varying coefficients taken over the field of real numbers. The combination of convolutional channel code and MAI channel can also be viewed as a serial concatenation of two convolutional codes, and is therefore suitable for turbo decoding.

1.4 Summary of Thesis Work

This thesis is concerned with two main topics related to iterative multiuser receivers.

The first topic considers the optimisation of iteratively-decoded IDMA multiple-access communications systems. Using variance-transfer charts to analyse the performance of the iterative receiver, numerical methods are developed to maximise receiver performance by optimally allocating transmit power, and also dynamically allocating FEC codes for variable load systems. Optimal space-time coding (codes that provide both maximal spatial-multiplexing and diversity) are also investigated, and an efficient iterative multiuser receiver for the codes is developed.

The second topic considers the application of iteratively-decoded multiple-access communications in underwater acoustic network. We develop novel iterative receiver structures for underwater acoustic channels with delay-spread only, and with delay- and Doppler-spread (doubly-spread). Adaptive channel estimation for the doubly-spread channel is also developed.

1.4.1 Iterative Methods for Equalization and Multiuser Detection

An introduction and literature survey on applying the turbo principle to channel equalization and multiuser detection is presented.

Turbo Equalization. Equalization is the process of compensating for the effects of intersymbol interference (ISI) arising from the transmission of data over multipath delay-spread channels. We discuss the application of the turbo decoding algorithm to joint equalization and data detection.

Iterative Multiuser Detection. Multiuser detection (MUD) refers to the detection of data from multiple sources transmitting in a non-orthogonal multiple-access channel. For example, a CDMA system where users transmit using nonorthogonal spreading codes. We discuss the application of the turbo decoding algorithm to multiuser detection (MUD).

CDMA and IDMA. CDMA has become a widely used multiple-access technique. Recently, a new multiple-access scheme, interleave division multiple access (IDMA) has been proposed [85]. When used with low-complexity iterative receivers, IDMA has been shown to outperform coded CDMA. In contrast to CDMA, which separates users by specific spreading codes, IDMA separates users by unique interleaver sequences. We provide detailed system models for the iterative decoding of CDMA and IDMA systems.

1.4.2 IDMA Performance Optimisation using Variance Transfer Analysis

Variance Transfer (VT) charts [102] are used as a tool for analysing the iterative receiver performance. VT charts track the variance of the estimation error in the soft estimates that are exchanged between the multiuser detector (MUD) and the channel decoders, providing a graphical representation of the receiver's convergence process. Although similar in concept to Extrinsic Information Transfer (EXIT) charts [115], VT charts are better suited for analysing multiuser detectors. Using variance transfer analysis, numerical methods are devised to optimise the receiver performance. Two multiuser system scenarios are considered for optimisation:

Layered IDMA with Power Allocation. Firstly, the IDMA concept is extended to a multi-rate system where different users transmit data at different rates and the same low-complexity iterative receiver structure can still be used. High-rate users are supported by breaking up the input data stream into multiple sub-streams. An IDMA layer is created from each sub-stream, and the multiple layers are then combined and the composite layered signal is transmitted from a single antenna. The iterative receiver treats each IDMA layer as a virtual user.

Chayat et. al. [18] observed that the performance of an iterative receiver is improved if different users transmit at different powers. This allows the iterative decoder to operate in an "onion peeling" mode, where the higher-power layers converge first, decreasing their contribution to the residual noise, and then the lower-power layers converge. CDMA and IDMA systems utilising iterative receivers can exploit this power allocation strategy to gain an improvement in performance.

To improve the performance of our layered IDMA scheme, we develop a simple power allocation scheme, where the power levels for each IDMA layer are calculated using Variance Transfer (VT) analysis and linear programming techniques. In a Rayleigh flat-fading environment, simulation results demonstrate that the performance of this proposed system is close to the theoretical limit.

FEC Code Allocation for Dynamic Loads. Secondly, we propose an alternative optimisation approach for inducing "onion peeling" operation in the iterative receiver. Ten Brink [116] demonstrated that different FEC codes generate different variance transfer characteristics within an iterative receiver. Therefore, as an alternative to manipulating transmit power, the judicious selection of FEC codes can also be used to optimise receiver performance.

A simple FEC code allocation strategy for multiuser systems with dynamic loads is devised. New users are allocated FEC codes according to the existing system load, providing optimal system performance over a range of operating conditions. We derive a numerical method for optimising performance based on FEC code allocation, and present simulation results. For small multiuser systems, results demonstrate that the performance of the proposed system approaches the theoretical single user bound.

1.4.3 Optimal Space-Time Coding using the Golden Code

Multiple antenna systems (commonly referred MIMO systems) have proven to be an effective method for realising high-rate reliable wireless communications. Generally coding strategies for MIMO systems has focused on providing either higher-rate or increased diversity over traditional single antenna systems. Layered space-time (BLAST) coding schemes utilise spatial multiplexing to achieve high-throughput rates, but do not provide any diversity gain. Orthogonal space time block coding (STBC) schemes provide diversity gain, but generally have coding rates of 1/2 or less.

Linear dispersion (LD) codes are a generalised class of space-time codes that can theoretically provide both diversity gain and high-rate [39]. Cyclic division algebra techniques have provided the means for constructing LD codes that provide both full-diversity and full-rate [105]. Space-time codes that achieve both full-diversity and -rate are known as perfect codes. The *golden code* [7] is a perfect code for 2×2 multiple-antenna systems.

We extend the golden code (GC) system to the multiuser case, and develop a MIMO-IDMA multiuser detector to decode LD codes. The performance of this GC-IDMA scheme is compared against MIMO-IDMA schemes employing the Alamouti code and V-BLAST, and also against the single-user bound. In a Rayleigh flat-fading environment, simulation results show that GC-IDMA outperforms both Alamouti- and V-BLAST-IDMA at moderate and high signal to noise ratios. For an E_b/N_0 ratio of 8dB or greater, the GC-IDMA scheme employing 16 users approaches within 0.25dB of the single-user bound.

1.4.4 Multiuser Communications for Underwater Acoustic Channels

We consider the application of multiuser communications to underwater sensor networks. These networks enable a broad range of applications including environmental monitoring, undersea exploration, assisted navigation, and distributed surveillance [2]. Reliable high-performance sensor networks would need to be underpinned by a robust and efficient multiple-access underwater communications scheme.

Transmission of acoustic waves is considered the most practical means of underwater communications, as neither radio or optical systems have proved feasible. Radio systems are not feasible because only radio waves in the extra-low frequency range (< 300Hz) are capable of propagating any distance through conductive sea water. Optical systems are also not suitable because optic waves, while not suffering as significantly from attenuation, are severely affected by scattering and absorption [110]. However, designing reliable underwater acoustic communications (UAC) systems has proven to be very challenging, with the underwater acoustic channel being referred to as "quite possibly natures most unforgiving wireless medium" [16].

Delay-spread underwater acoustic channels

One of the main channel impairments is multipath interference caused by multiple reflections of the acoustic signal from the water surface and bottom. These reflections occur at small grazing angles and with small reflection losses, causing both large delay-spread and large multipath amplitudes to be present in the received signal [51].

Large delay-spread implies that single-carrier communication will be plagued by inter-symbol interference (ISI) that spans many symbols. As an alternative, multi-carrier modulation (MCM) has been proposed to increase the symbol interval and thereby decrease the ISI span. In multi-carrier modulation, the data stream is split into several substreams and transmitted, in parallel, on different subcarriers. This transforms the inter-symbol interference (ISI)-inducing channel into a set of independent parallel subchannels. The principle advantage of multi-carrier schemes, relative to single-carrier schemes, is that they facilitate simple equalization of delay-spread channels. The is significant as equalization of underwater acoustic channels is usually a complex task.

Orthogonal frequency division multiplexing (OFDM) [135], [20] is a practical MCM scheme that uses the computationally-efficient fast Fourier transform (FFT) to transmit data in parallel over a large number of orthogonal subcarriers. Typically, the number of subcarriers is chosen such that the symbol duration is large compared to the maximum delay of the channel, reducing the effects of ISI. However, to completely avoid the effects of ISI and thus, to maintain the orthogonality between the signals on the sub-carriers, a cyclic prefix (called a *guard interval*) is inserted between adjacent OFDM symbols. The guard time is chosen to be larger than the expected channel delay spread, such that multipath components from one symbol cannot interfere with the next symbol [28]. Maintaining subcarrier orthogonality eliminates intercarrier interference (ICI) and therefore allow simple (low-complexity) data detection.

We combine Orthogonal Frequency Division Multiplexing (OFDM) with an IDMA overlay to develop a multiple-access communications system that provides robust performance in the presence of large time-delay spread and the other impairments presented by the shallow water acoustic channel. The proposed OFDM-IDMA scheme utilises a low-complexity iterative decoding algorithm based on the turbo-decoding concept. The experimental results demonstrate that the OFDM-IDMA scheme provides robust performance in delay-spread underwater acoustic environments.

Doubly-spread underwater acoustic channels

We extend the underwater acoustic channel to the doubly-spread case. The relative motion between the transmitter, receiver, and scattering objects imparts each path with a unique Doppler shift, so that multipath propagation also induces a frequency-domain spreading effect on the information signal. Such channels are both delay- and Doppler-spread (or equivalently, frequency- and time-selective), and are referred to as "doubly-spread" or "doubly-selective".

OFDM schemes have been successfully used for time-invariant and slowly time-varying (TV) channels. But for doubly-spread (or rapidly TV) channels, using OFDM becomes problematic. For time-invariant channels, the data stream can be split up and transmitted in parallel on non-interfering subcarriers, with equalization being just a simple matter of adjusting the gain and phase on each received subcarrier. This approach can be easily extended to slowly TV channels, where a time-invariant channel is simulated by choosing an OFDM symbol duration that is shorter than the coherence time of the channel. However, this approach becomes impractical for rapidly TV channels. For time-invariant or slowly TV channels, the loss in spectral efficiency due to the inclusion of the guard intervals can be made small, since the channel delay spread (and hence the guard interval) is much smaller than the channel coherence time (and hence the OFDM symbol length). But for rapidly TV channels, the OFDM symbol length would need to be made extremely short, at which point the loss of spectral efficiency due to guard insertion would be severe [104].

Therefore, we consider single-carrier system with adaptive channel-estimation for the doubly-spread underwater channel. A single-carrier system with linear traversal equalizer would face complexity issues due to the large number of equalizer taps required to compensate for the long delay-spread. Instead, a Kalman filter (KF) is used as equalizer. KF-based equalizers have been shown to perform significantly better than linear traversal equalizers at a much lower complexity (fewer equalizer taps) [55], [101]. Moreover, the state-space formulation of the Kalman equalizer is well suited for iterative receivers and allows easy incorporation of soft (a-priori) information for channel-coded systems.

The doubly-selective channels are modeled using basis expansion models (BEMs). A basis expansion model is a parsimonious (economical while accurate) low-rank channel model that exploits the inherent structure in the channel response [32]. Modelling of linear systems by basis functions can turn a time-varying system identification problem into a time-invariant one, thereby reducing the number of channel parameters to estimate and simplifying the equalization task.

The receiver uses a semi-blind iterative channel estimation algorithm to initially estimate the channels using only the pilot sequences and then iteratively includes the decoded data into the channel estimates to improve the estimation accuracy. Experimental results show that the proposed system provides robust performance in doubly-spread underwater acoustic environments.

1.5 Original Contributions

The original contributions of this research include:

- Simulation results illustrating the performance of the Golden Code over the wireless channels with Doppler spread.
- A novel multiuser iterative receiver for linear dispersion codes developed specifically for decoding the Golden Code.

- A novel power allocation method for multirate IDMA systems, where the power allocation is calculated using variance-transfer charts and linear programming.
- A novel FEC code allocation method to optimise multiuser system performance over varying system loads.
- The novel application of OFDM-IDMA to underwater acoustic communications and simulation results of the system performance.
- A novel iterative receiver for underwater acoustic communications for doubly-spread underwater channels. The iterative receiver incorporates a non-linear Kalman filter to perform joint decoding and channel equalization. Superimposed training is used for channel estimation and the time-varying channels are modeled using low-rank basis expansion models (BEMs).

These works were new when they were published or completed.

1.6 Thesis Outline

In this thesis, our goals are twofold. Firstly, we consider methods to multiuesr iterative receiver performance using power allocation, FEC code allocation, and maximising MIMO diversity through the use of perfect space-time codes. Secondly, we consider the application of underwater acoustic communications and develop multiuser receiver structures for channels with severe delay-spread and also doubly-spread. Therefore we organise the rest of the thesis as follows

In Chapter 2, we provide an introduction and literature survey on turbo equalization and turbo multiuser detection techniques. Detailed system models of iterative receivers for CDMA and IDMA multiple-access systems are also presented.

In Chapter 3, we describe our method of selecting transmit power levels to optimise the system performance. Next, we describe our method of assigning different FEC codes to different users to optimise the multiuser receiver performance. Both methods use variance transfer charts and linear programming.

In Chapter 4, we discuss MIMO systems and perfect space-time codes – codes that maximise both diversity and coding-rate. We describe our new receiver structures for decoding multiple perfect space-time codes.

In Chapter 5, we describe propagation models and noise models to characterise the underwater acoustic channel. Next, we describe a multiple-access system that combines Orthogonal Frequency Division Multiplexing (OFDM) with an IDMA overlay to provide robust performance in the presence of large time-delay spread and the other impairments presented by the shallow water acoustic channel.

In Chapter 6, we extend our underwater channel model to include both delay- and doppler-spread, so-called doubly-spread channel. Next, we describe our multiuser receiver for doubly-spread channels. This is an iterative receiver that uses soft-input soft-output Kalman filter as an adaptive MIMO equalizer. The time-varying characteristics of the channel are modeled using low-rank basis expansion models.

In Chapter 7, we summarise the thesis work, state its major contributions, and finally suggest some possible future directions

1.7 Related Publications

Part of the thesis work have been published in major conferences or journals related to wireless communications or underwater acoustic oceanic communications. Below is an incomplete list:

Related Publications of Chapter 3 include:

- L. Linton, P. Conder, and M. Faulkner, "Multi-Rate Communications Using Layered Interleave-Division Multiple Access with Power Allocation," *2009 IEEE Wireless Communications and Networking Conference, WCNC 2009*, 5-8 April 2009, Budapest, Hungary
- L. Linton, P. Conder, and M. Faulkner, "Improved Interleave-Division Multiple Access (IDMA) Performance Using Dynamic FEC Code Allocation," *2010 IEEE Wireless Communications and Networking Conference, WCNC 2010*, 18-21 April 2010, Sydney, Australia

Related Publications of Chapter 4 include:

- L. Linton, P. Conder, and M. Faulkner, "On the Performance of Golden Codes in Rayleigh Fading Channels with Doppler Spread," *1st International Conference* *on Signal Processing and Communication Systems, ICSPCS-2007* 17-19 December 2007, Gold Coast, Australia

- L. Linton, P. Conder, and M. Faulkner, "Multiuser MIMO Communications using Interleave-Division Multiple-Access and Golden Codes," *2008 IEEE 67th Vehicular Technology Conference: VTC2008-Spring* 11-14 May 2008, Marina Bay, Singapore

Related Publications of Chapter 5 include:

- L. Linton, P. Conder, and M. Faulkner, "Multiuser Communications for Underwater Acoustic Networks using MIMO-OFDM-IDMA," *2nd International Conference on Signal Processing and Communication Systems, ICSPCS-2008*, 15-17 December 2008, Gold Coast, Australia

- L. Linton, P. Conder, and M. Faulkner, "Multiple-Access Communications for Underwater Acoustic Sensor Networks using OFDM-IDMA," *MTS/IEEE Oceans 2009 Conference*, 26-29 October 2009, Biloxi, Mississippi, USA

Related Publications of Chapter 6 include:

- L. Linton, P. Conder, and M. Faulkner, "Adaptive Multiuser Turbo Equalization for Doubly-Spread Underwater Acoustic Channels" *IEEE Journal of Oceanic Engineering (submitted)*

Chapter 2

Iterative Decoding for Equalization and Multiuser Detection

In this chapter, the turbo decoding principle is applied to the communications problems of channel equalization and multiuser detection. These fundamental techniques are the basis for the research described in the the subsequent chapters of this thesis.

First, convolutional coding over an AWGN channel is introduced. Convolutional codes are trellis-based (or state-machine based) codes that are commonly used for forward error correction (FEC) and are also a fundamental building block of iterative communication systems. An optimal decoding method for convolutional codes is the BCJR MAP algorithm which decodes the transmitted data by estimating the most probable state transitions of the encoder from the received (noisy) channel observations.

Next, the intersymbol interference (ISI) channel is presented. The traditional methods of data protection used in FEC do not work well when the channel over which the data is sent introduces additional distortions in the form of ISI. When the channel is bandlimited of for other reasons is time-dispersive in nature, then the receiver will generally need to compensate for the channel effects prior to employing a standard decoding algorithm for the FEC. Such methods for channel compensation are typically referred to as channel equalization .

One approach to the problem of coded transmission over an ISI channel is to consider the channel as a rate-1 convolutional code and consequently the time dispersion of the channel can be considered to be equivalent to the shift register elements of the convolutional encoder. The FEC encoder of the transmitter and the ISI channel can then be thought of as an example of Forney's serial concatenated coding scheme transmitting over a memoryless AWGN channel.

However, when the super-trellis of the combined states of the FEC encoder and ISI channel is constructed, it becomes apparent that the complexity of an optimal joint FEC and channel trellis decoder would be excessive for practical implementations. Therefore, suboptimal detection methods must be considered. For complexity reasons, the problems of FEC decoding and channel equalization have traditionally been considered separately, with limited interaction between the two blocks. As such, substantial performance degradation is typically induced through the separation of these inherently dependent tasks.

Recently, research in iterative methods for equalization, generally referred to as *turbo equalization*, has enabled feasible approaches to jointly solving the equalization and decoding tasks. As a result, the performance gap between optimal joint decoding and equalization and that achievable through systems with practical complexity has been narrowed in a manner similar to that of near Shannon-limit communications using turbo codes [12].

Finally, multiuser detection (MUD) is described. Communication channels that involve both forward error correction (FEC) coding and multiple-access signaling are of increasing interest in applications such as cellular telephony, wireless computer networks, and broadband local access. Optimal data detection and decoding in such channels generally requires a level of computational complexity that is prohibitive for these types of applications. Turbo multiuser detection (MUD) addresses this problem by applying the turbo principle of iteration among constituent decision algorithms, with intermediate exchanges of soft information (i.e., posterior probabilities) about tentative decisions. Here this principle is applied by considering MUD (which exploits the multiple-access signaling structure) and FEC decoding as the two constituent decision algorithms. The resulting iteration between soft MUD and soft channel decoding yields good results. The basic principles of MUD are presented and the basis for low-complexity turbo multiuser detectors that require minimal increased complexity over that of the standard channel decoder are also described. Turbo detection schemes for both CDMA (code-division multiple-access) and IDMA (interleave-division multiple-access) schemes are discussed.

2.1 Convolutional Coding for the Gaussian Channel

Convolutional codes are stream-oriented linear codes and are a building block of turbo code, turbo equalization, and turbo multiuser detection schemes. A convolutional encoder assigns code bits to an incoming information bit stream continuously, in a stream-oriented fashion. The convolutional code is named after its encoding method of using *modulo-2 convolutions* to generate the redundant bits.

2.1.1 Convolutional Encoding

The role of the encoder is to take the binary data sequence to be transmitted as input and produce an output that contains not only this data but also additional redundant information that can be used to protect the data from the possibility of errors that might occur in the data stream as a result of additive noise in the transmission or detection errors at the receiver.

A convolutional encoder can be represented by a finite-state machine, taking in a continuous stream of message bits and producing a continuous stream of output bits. The encoder has a memory of the past inputs, which is held in the encoder *state*. The output depends on the value of this state, as well as on the present message bits at the input, but is completely unaffected by any subsequent message bits.

The encoder memory is generally implemented using a linear finite-state shift register circuit where each shift register element represents a time delay of one unit. The bit at the output of the shift register element at time i is the bit that was present at the input of the element at time $i-1$. The set of all the shift registers elements together holds the encoder state. An encoder can have one or more shift registers, one or more inputs and one or more outputs.

Consider the convolutional encoder of Figure 2.1a. The serial-to-parallel converter splits the input message into vectors of m-bits length, i.e., $\mathbf{d}[i] = \left[\, d^{(1)}[i],\, \ldots,\, d^{(m)}[i] \,\right]^T$. At each state transition, i, the encoder receives a m-bit input vector and outputs a n-bit coded vector, $\mathbf{c}[i] = \left[\, c^{(1)}[i],\, \ldots,\, c^{(n)}[i] \,\right]^T$. The parallel-to-serial converter generates the output coded bit stream by concatenating the coded vectors $\mathbf{c}[i]$ from each state transition. The convolutional code is said to have rate $R_c = m/n$ if, at each time instant i, the convolutional encoder receives m input bits and produces n output bits.

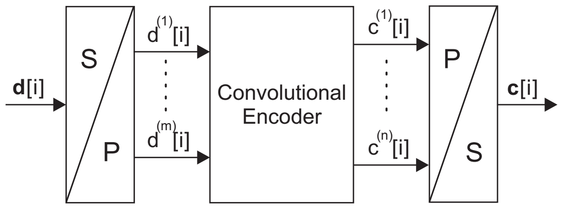

(a) Encoder schematic block

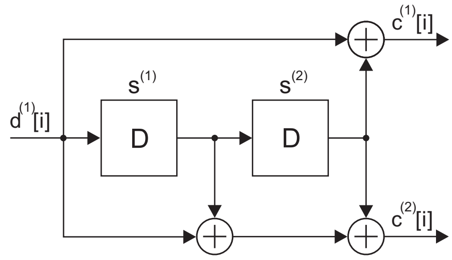

(b) Example rate-1/2 encoder circuit

Figure 2.1: Convolutional encoder schematic block code, and example rate-1/2 encoder for generator polynomial $(1 + D^2, 1 + D + D^2)$.

Without loss of generality, we consider the case where the input to the convolutional encoder is a single-bit vector, i.e., $m = 1$. For an input message of block length M, $\{d[i]\}_{i=0}^{M-1}$, the output coded message will have a block length of $N = nM$, i.e., $\{c[i]\}_{i=0}^{N-1}$.

Figure 2.1b shows an example binary convolutional encoder, where D represents the delay elements (shift register elements), and $\oplus$ represents modulo-2 addition. At time i the input to the encoder is one message bit $d^{(1)}[i]$ and the output is a two-bit vector, $\mathbf{c}[i] = [\, c^{(1)}[i],\, c^{(2)}[i]\,]^T$; thus the code rate is 1/2. The state of this encoder is given by $S = (s^{(1)}, s^{(2)})$, where $s^{(1)} \in \{1, 0\}$ and $s^{(2)} \in \{1, 0\}$ are the contents of the left-hand register element and the right-hand register element, respectively. Thus the encoder can be in one of four possible states, $S_0 = (0, 0)$, $S_1 = (0, 1)$, $S_2 = (1, 0)$, and $S_3 = (1, 1)$. As there is only one input, the message $\mathbf{d}$ is simply given by $[\, d^{(1)}[0],\, \ldots,\, d^{(1)}[M-1]\,]$, and therefore the superscript (1) can be dropped.

For the example encoder shown in Figure 2.1b, the output bits $c^{(1)}[i]$ and $c^{(2)}[i]$ (at time i) are computed as:

$$c^{(1)}[i] = d[i] \oplus s^{(2)}[i] \qquad \text{and} \qquad c^{(2)}[i] = d[i] \oplus s^{(1)}[i] \oplus s^{(2)}[i] \tag{2.1}$$

where $\oplus$ represents modulo-2 addition. The equations in (2.1) can be more concisely represented by the generator polynomial $(1 + D^2, 1 + D + D^2)$, where D is equivalent to the discrete-time delay operator z^{-1}.

Generally, convolutional coding schemes are designed so that the encoder starts from a known initial state, and ends at a known termination state. For the example encoder of Figure 2.1b, we assume that the two delay elements in the circuit are zero at the beginning of the encoding process (time $i = 0$) and at the end (time $i = M - 1$). To achieve the latter assumption, the last two input data bits, $d[M-2]$ and $d[M-1]$, must be zero, which implies a small rate loss. This loss can be controlled by using long sequences (i.e., large values of M), or can be avoided by using tail-biting encoding [136] [48].

Since a convolutional encoder can be thought of as a finite-state machine, the encoder behaviour can be described by a *state diagram* which portrays the temporal relationships between inputs, states and outputs. This representation is often helpful for both encoding and decoding purposes. For an encoder with L memory elements (i.e., L shift register elements), there are 2^L encoder states in the state diagram. The state diagram in Figure 2.2a provides a graphical representation of the state transitions of the encoder in Figure 2.1b. Each of the four states is represented by a node. The edges between nodes represent the possible state transitions. Each edge is labeled with the input bit that produced the transition and the output bits generated.

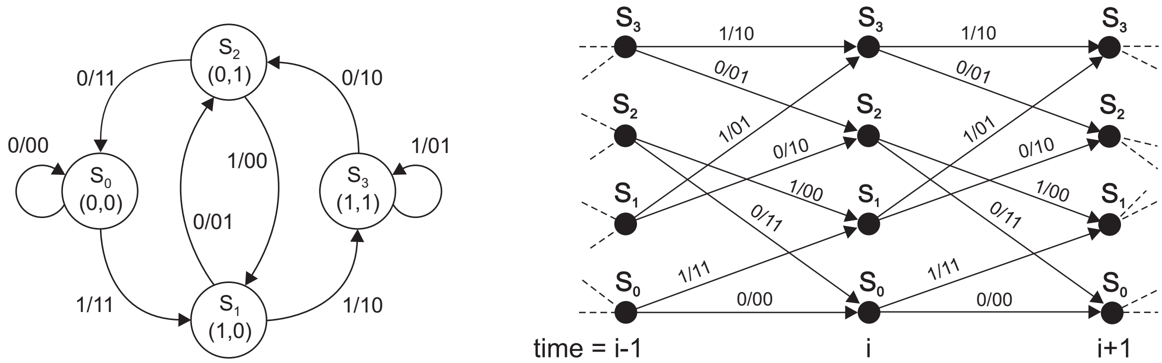

(a) State diagram **(b)** Trellis diagram

Figure 2.2: State diagram and trellis representations of the convolutional code of Figure 2.1b. The trellis states correspond to the content of the delay elements as $S_0 = (0, 0)$, $S_1 = (1, 0)$, $S_2 = (0, 1)$ and $S_3 = (1, 1)$.

Although the state diagram describes the convolutional encoder state and input-output relationship completely, it does not provide a record of how the state has evolved with time. For this we use a trellis diagram. Figure 2.2b shows the state diagram expanded in time to produce a trellis segment. On the left each state is represented for time i and on the right a copy of each state is represented for time $i + 1$. The state transition edges are joined from a state at time i to a state at time $i + 1$ to show the changes with time. Each path through the trellis is an evolution of the convolutional encoder for one of the 2^M possible input streams. Consequently the set of codewords for a convolutional code is the set of all possible paths through its trellis.

This trellis representation enables optimal decoding of convolutional codes with reasonable complexity. Each path in the trellis corresponds to a codeword, and so the maximum likelihood (ML) decoder (which finds the most likely codeword) searches for the most likely path in the trellis. Alternatively, each edge in the trellis can correspond to a particular input: the bit-wise maximum a posteriori (MAP) decoder, which searches for the maximum-probability input bit, calculates the probability of each trellis edge [48].

2.1.2 System Model

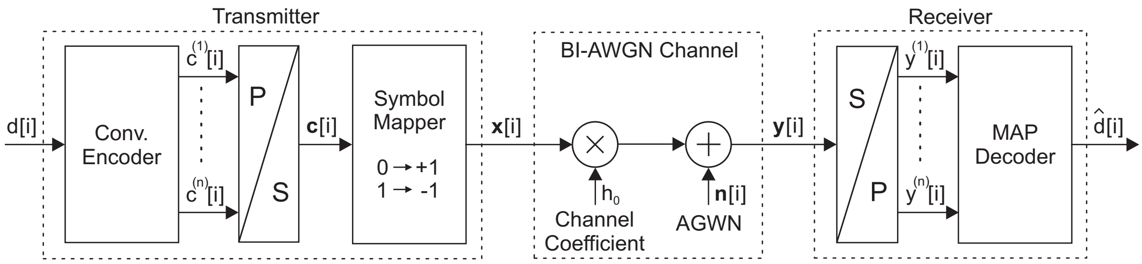

Figure 2.3: System model for a coded transmission over a memoryless AWGN channel

Figure 2.3 shows the system model for a convolutional-coded transmission scheme. The input data sequence $\mathbf{d} = [\, d[0],\, d[1],\, \ldots,\, d[M-1]\,]^T$ is encoded by the convolutional encoder (with rate R_c) generating a n-bit coded vector, $\mathbf{c}[i]$, for each data bit, $d[i]$, i.e.,

$$\mathbf{c} = \left[\, \mathbf{c}^T[0],\, \mathbf{c}^T[1],\, \ldots,\, \mathbf{c}^T[M-1] \,\right]^T \quad \text{where} \quad \mathbf{c}[i] = \left[\, c^{(1)}[i],\, \ldots,\, c^{(n)}[i] \,\right]^T \tag{2.2}$$

The parallel-to-serial converter (P/S) concatenates M of the $\mathbf{c}[i]$ vectors to form a N-bit frame. Hence, (2.2) can be restated as $\mathbf{c} = [\, c[0],\, c[1],\, \ldots,\, c[N-1]\,]^T$, where N is the frame length ($N = nM$), and the elements of $\mathbf{c}$ are referred to as coded bits. The coded bit sequence $\mathbf{c}$ is then BPSK modulated, producing the symbol sequence $\mathbf{x}$, which is defined as

$$\mathbf{x} = [\, x[0],\, x[1],\, \ldots,\, x[N-1]\,]^T \qquad (N \times 1 \text{ vector}) \tag{2.3}$$

where $x[i] \in \{+1, -1\}$. Finally, the sequence of BPSK symbols is transmitted over an AWGN channel. The decoder receives a noisy version of the transmitted symbol sequence from which to determine the message. The sequence of noise-corrupted symbols received from the channel are denoted by

$$\mathbf{y} = [\, y[0],\, y[1], \ldots, y[N-1]\,]^T. \qquad (N \times 1 \text{ vector}) \tag{2.4}$$

The serial-to-parallel converter (S/P) divides the received symbol sequence into M vectors of n-bits length, i.e.,

$$\mathbf{y} = \left[\, \mathbf{y}^T[0],\, \mathbf{y}^T[1],\, \ldots,\, \mathbf{y}^T[M-1] \,\right]^T \quad \text{where} \quad \mathbf{y}[i] = \left[\, y^{(1)}[i],\, \ldots,\, y^{(n)}[i] \,\right]^T \tag{2.5}$$

At each state transition, i, the MAP decoder receives a n-bit input vector $\mathbf{y}[i]$, and outputs the message bit estimate $\hat{d}[i]$. After M state transitions of the MAP decoder, the estimated message sequence can be formed as $\hat{\mathbf{d}} = [\, \hat{d}[0],\, \hat{d}[1],\, \ldots,\, \hat{d}[M-1]\,]$.

We consider the binary-input additive white Gaussian noise (BI-AWGN) channel, which is both symmetric and memoryless. A binary-input channel is *symmetric* if both input bits, $\{+1, -1\}$, are corrupted equally by the channel. A channel is considered *memoryless* if the channel output at any time instant depends only on the input at that time instant, and not on previously transmitted symbols. This property can be expressed in terms of channel transition probabilities as

$$p(\mathbf{y} \mid \mathbf{x}) = \prod_{i=0}^{N-1} p(y[i] \mid x[i]) \tag{2.6}$$

where $\mathbf{x}$ is the transmitted symbol sequence defined in (2.3), and $\mathbf{y}$ is the received symbol sequence defined in (2.4). A memoryless channel is therefore completely described by its input and output alphabets and the conditional probability distribution $p(y \mid x)$ for each input-output symbol pair.

The BI-AWGN channel of Figure 2.3 can be described by the equation

$$y[i] = h_0 x[i] + n[i] \tag{2.7}$$

where $x[i] \in \{-1, +1\}$ is the i-th transmitted symbol, $y[i]$ is the i-th received symbol and $n[i]$ is the additive noise sampled from a Gaussian random variable with zero mean and σ^2 variance, i.e., $n[i] \sim \mathcal{N}(0, \sigma^2)$. The probability density function for n is

$$p(n) = \frac{1}{\sqrt{2\pi\sigma^2}} \exp\left(-\frac{n^2}{2\sigma^2}\right), \tag{2.8}$$

where $\exp(\,\cdot\,)$ is the exponential function. If the source is equiprobable then $P(x[i] = -1) = P(x[i] = +1)$, then we have for the BI-AWGN channel:

$$p(y[i] \mid x[i] = \pm 1) = \frac{1}{\sqrt{2\pi\sigma^2}} \exp\left(-\frac{1}{2\sigma^2}\,(y[i] \mp h_0)^2\right) \tag{2.9}$$

2.1.3 Log Likelihood Ratios (LLRs)

When using probabilistic decoding methods (such as the BCJR algorithm) on binary codes, the probabilities input and output from the decoder are often expressed in log likelihood ratio (LLR) form.

For a binary variable x, the probabilities $P(x = 1)$ given $P(x = 0)$ are related since $P(x = 1) = 1 - P(x = 0)$. Therefore only a single value is needed in order to represent the set of probabilities for x. The log likelihood ratio (LLR) is used to represent the probability metrics for a binary variable by a single value, and is given by

$$L(x) = \log \frac{P(x = 0)}{P(x = 1)} \tag{2.10}$$

The sign of $L(x)$ provides a hard decision on x and the magnitude $|L(x)|$ gives the reliability of this decision. In iterative decoding, *a posteriori* probability (APP) LLRs are commonly denoted $\Lambda(\,\cdot\,)$, i.e., $\Lambda(x) = L_{app}(x)$. Similarly, extrinsic information LLRs are commonly denoted $\lambda(\,\cdot\,)$, i.e., $\lambda(x) = L_{ext}(x)$. LLRs can be translated back to probabilities as follows:

$$P(x = 1) = \frac{\exp\{-L(x)\}}{1 + \exp\{-L(x)\}} = \frac{1}{2}\left\{1 - \tanh\left(\frac{L(x)}{2}\right)\right\} \tag{2.11}$$

and

$$P(x = 0) = \frac{\exp\{L(x)\}}{1 + \exp\{L(x)\}} = \frac{1}{2}\left\{1 + \tanh\left(\frac{L(x)}{2}\right)\right\} \tag{2.12}$$

A benefit of the logarithmic representation of probabilities is that when probabilities need to be multiplied, log-likelihood ratios need only be added; which can reduce implementation complexity.

2.1.4 MAP Decoding using the BCJR Algorithm

The binary symbol MAP decoder will output the probability $p(d[i] \mid \mathbf{y})$ that the message bit $d[i]$ was 0 or 1 given all the information from the received vector $\mathbf{y}$ and the structure of the code. An efficient algorithm for performing MAP decoding using a trellis was first proposed Bahl et al. in [6] and is called the BCJR algorithm after its authors.

Since the convolutional encoder has memory, the codeword bit output at time i is influenced by the codeword bits sent before it and may itself influence the codeword bits sent after it. Thus all the bits in $\mathbf{y}$ may tell us something about the message bit at time i. To incorporate the information from both the bits transmitted before time i and the bits transmitted after time i, the BCJR decoding uses two passes through the trellis:

- a forward pass that provides the current message bit on the basis of only the codeword bits that were transmitted before it; and
- a backward pass that predicts the current message bit on the basis of only the codeword bits that were transmitted after it.

Since the message bits are the input to a binary convolutional encoder we can determine which message bit was sent by finding out which state transition occurred. We denote:

- $\mathcal{S}$ as the set of possible states,
- $\mathcal{T}^+$ as the set of state transitions (S_r, S_s) that correspond to a 1 input bit,
- $\mathcal{T}^-$ as the set of state transitions (S_r, S_s) that correspond to a 0 input bit, and
- $\mathcal{T}$ as the set of all valid state transitions (S_r, S_s), i.e., $\mathcal{T} = \mathcal{T}^+ \cup \mathcal{T}^-$.

For example, the convolutional encoder in Figure 2.1b has $\mathcal{S} = \{S_0, S_1, S_2, S_3\}$,

$$\mathcal{T}^+ = \{(S_0, S_1), (S_1, S_3), (S_2, S_1), (S_3, S_3)\}, \tag{2.13}$$

$$\mathcal{T}^- = \{(S_0, S_0), (S_1, S_2), (S_2, S_0), (S_3, S_2)\}, \quad \text{and} \tag{2.14}$$

$$\mathcal{T} = \{(S_0, S_0), (S_0, S_1), (S_1, S_2), (S_1, S_3), (S_2, S_0), (S_2, S_1), (S_3, S_3), (S_3, S_2)\}. \tag{2.15}$$

The probability that $d[i]$ was 1 is the probability that a state transition in the set $\mathcal{T}^+$ occurred at time i:

$$P(d[i] = 1 \mid \mathbf{y}) = \sum_{(S_r, S_s) \in \mathcal{T}^+} P(\psi_i = S_r, \psi_{i+1} = S_s \mid \mathbf{y}) \tag{2.16}$$

where ψ_i is the variable for the state at time i, and $\mathcal{S} = \{S_0, S_1, \ldots, S_{(2^L-1)}\}$ is the set of possible values that the state can take. We represent by S_r and S_s the values of the state at times $i-1$ and time i respectively. Similarly, the probability that $d[i]$ was 0 is the probability that a state transition in the set $\mathcal{T}^-$ occurred at time i:

$$P(d[i] = 0 \mid \mathbf{y}) = \sum_{(S_r,S_s)\in\mathcal{T}^-} P(\psi_i = S_r, \psi_{i+1} = S_s \mid \mathbf{y}) \tag{2.17}$$

For convenience, $P(\psi_i = S_r)$ will be denoted as $P(S_r)$, and $P(\psi_{i+1} = S_s)$ denoted as $P(S_s)$ when the context is clear.

Thus determining the message bit probabilities $P(d[i] \mid \mathbf{y})$ requires that we determine the probability of each state transition, $P(S_r, S_s \mid \mathbf{y})$, given that we have only the received vector $\mathbf{y}$. Using Bayes' rule we can rewrite $P(S_r, S_s \mid \mathbf{y})$ as

$$P(S_r, S_s \mid \mathbf{y}) = \frac{p(S_r, S_s, \mathbf{y})}{p(\mathbf{y})} \tag{2.18}$$

Substituting (2.18) into equations (2.16) and (2.17), the log-likelihood ratio (LLR) for bit $d[i]$ can be defined as

$$\Lambda(d[i] \mid \mathbf{y}) = \log \frac{\sum_{(S_r,S_s)\in\mathcal{T}^+} p(S_r, S_s, \mathbf{y})}{\sum_{(S_r,S_s)\in\mathcal{T}^-} p(S_r, S_s, \mathbf{y})} \tag{2.19}$$

Note that the term $p(\mathbf{y})$ in (2.18) cancels out when the ratio is taken, and therefore does not need to be explicitly calculated.

To enable the efficient calculation of $p(\psi_i, \psi_{i+1}, \mathbf{y})$, the received vector, $\mathbf{y}$, is split into three sets:

$$p(\psi_i, \psi_{i+1}, \mathbf{y}) = p(\psi_i, \psi_{i+1}, \mathbf{y}^-[i], \mathbf{y}[i], \mathbf{y}^+[i]) \tag{2.20}$$

where

- $\mathbf{y}^-[i]$ represents the values received for the set of bits sent before time i;
- $\mathbf{y}[i]$ represents the values received for the set of bits sent at time i; and
- $\mathbf{y}^+[i]$ represents the values received for the set of bits sent after time i.

The values received for the set of bits sent at time i, $\mathbf{y}[i]$, are written as a vector since the convolutional code may output more than one codeword bit at each time point (i.e., n may be greater than 1).

Applying Bayes' rule again,

$$\begin{aligned} p(\psi_i, \psi_{i+1}, \mathbf{y}) &= p(\psi_i, \psi_{i+1}, \mathbf{y}^-[i], \mathbf{y}[i], \mathbf{y}^+[i]) \\ &= p(\psi_i, \mathbf{y}^-[i])\, p(\psi_{i+1}, \mathbf{y}[i] \mid \psi_i, \mathbf{y}^-[i])\, p(\mathbf{y}^+[i] \mid \psi_i, \psi_{i+1}, \mathbf{y}^-[i], \mathbf{y}[i]) \end{aligned}$$

Since a convolutional encoder has been used to generate the codeword bits, we know that the codeword bits output at time i are completely determined by the state transition, ψ_i (at time i) to ψ_{i+1} (at time $i+1$). Also, since we are considering a memoryless channel, the channel output $\mathbf{y}[i]$ depends only on the transmitted codeword bit $\mathbf{c}[i]$ and the channel noise at time i, and is not affected by anything previously or subsequently transmitted through the channel. Putting these together, if we know the probability of the state transition ψ_i to ψ_{i+1} then the probability of $\mathbf{y}[i]$ is completely independent of $\mathbf{y}^+[i]$ and $\mathbf{y}^-[i]$, and so

$$p(\psi_{i+1}, \mathbf{y}[i] \mid \psi_i, \mathbf{y}^-[i]) = p(\psi_{i+1}, \mathbf{y}[i] \mid \psi_i).$$

Similarly, if we know the probability of the encoder state at time i then the probability of $\mathbf{y}^+[i]$ is independent of both the past states and past outputs and so

$$p(\mathbf{y}^+[i] \mid \psi_i, \psi_{i+1}, \mathbf{y}^-[i], \mathbf{y}[i]) = p(\mathbf{y}^+[i] \mid \psi_{i+1}).$$

Thus finally

$$p(\psi_i, \psi_{i+1}, \mathbf{y}) = p(\psi_i, \mathbf{y}^-[i])\, p(\psi_{i+1}, \mathbf{y}[i] \mid \psi_i)\, p(\mathbf{y}^+[i] \mid \psi_{i+1}). \tag{2.21}$$

The BCJR algorithm assigns a label to each term in (2.21), therefore (2.21) can be restated as [48]

$$m_i(\psi_i, \psi_{i+1}) = \alpha_i(\psi_i)\, \gamma_i(\psi_i, \psi_{i+1})\, \beta_{i+1}(\psi_{i+1}) \tag{2.22}$$

where

$$m_i(\psi_i, \psi_{i+1}) = p(\psi_i, \psi_{i+1}, \mathbf{y}), \tag{2.23}$$

$$\alpha_i(\psi_i) = p(\psi_i, \mathbf{y}^-[i]), \tag{2.24}$$

$$\beta_{i+1}(\psi_{i+1}) = p(\mathbf{y}^+[i] \mid \psi_{i+1}), \text{ and} \tag{2.25}$$

$$\gamma_i(\psi_i, \psi_{i+1}) = p(\psi_{i+1}, \mathbf{y}[i] \mid \psi_i). \tag{2.26}$$

Equation (2.22) shows that the probability of the state transition from state ψ_i at time i to state ψ_{i+1} at time $i+1$ is a function of three terms:

1. $\alpha_i(\psi_i)$, which is the probability that the encoder is in state ψ_i at time i based on what we know about $\mathbf{y}^-[i]$,

2. $\beta_{i+1}(\psi_{i+1})$, which is the probability that the encoder is in state ψ_{i+1} at time $i+1$ based on what we know about $\mathbf{y}^+[i]$, and

3. $\gamma_i(\psi_i, \psi_{i+1})$, which is the probability of a transition between the states ψ_i and ψ_{i+1} based on what we know about $\mathbf{y}[i]$

The calculation of the α values is called the forward recursion of the BCJR decoder, while the β values are calculated in the backward recursion.

Applying Bayes' rule to (2.26), $\gamma_i(S_r, S_s)$ can be written as follows:

$$\gamma_i(S_r, S_s) = p(S_s, \mathbf{y}[i] \mid S_r) = P(S_s \mid S_r)\, p(\mathbf{y}_i \mid S_r, S_s).$$

In this form it is easier to see that $p(S_s, \mathbf{y}[i] \mid S_r)$ has two parts.

- The first part, $P(S_r \mid S_s)$, is the probability that the state of the encoder moves to S_s at time $i+1$ if it started in state S_r at time i. Since the encoder will have moved from S_r to S_s for an input $d_{r,s}$, we know that $P(S_s \mid S_r) = P(d[i] = d_{r,s})$, which is given by the probability distribution of the message source.

- The second part, $p(\mathbf{y}[i] \mid S_r, S_s)$, is the probability that $\mathbf{y}[i]$ was received given the state transition S_r to S_s. Since this state transition produces the codeword bits $\mathbf{c}_{r,s}$, the probability that $\mathbf{y}[i]$ is received is equal to the probability that the channel turned $\mathbf{c}_{r,s}$ into $\mathbf{y}[i]$, i.e., $p(\mathbf{y}[i] \mid S_r, S_s) = p(\mathbf{y}[i] \mid \mathbf{c}[i] = \mathbf{c}_{r,s})$.

Thus $\gamma_i(S_r, S_s)$ is a function of the source probability $P(d[i] = d_{r,s})$ and the channel transition probability $p(\mathbf{y}[i] \mid \mathbf{c}_{r,s})$:

$$\gamma_i(S_r, S_s) = P(d[i] = d_{r,s})\, p(\mathbf{y}[i] \mid \mathbf{c}_{r,s}) \tag{2.27}$$

$$= P(d[i] = d_{r,s}) \prod_{q=1}^{n} p(y^{(q)}[i] \mid c_{r,s}^{(q)}) \tag{2.28}$$

Note that the transition probability $\gamma_i(S_r, S_s)$ is zero if the index pair is not in $\mathcal{T}$. The channel transition probability is a function of the modulation and channel model. For the system model shown in Figure 2.3, i.e., BI-AWGN channel with BPSK modulation,

$$p(y^{(q)}[i] \mid c_{r,s}^{(q)}) = \frac{1}{\sqrt{2\pi\sigma^2}} \exp\left\{-\frac{1}{2\sigma^2}\|y^{(q)}[i] - h_0(2c_{r,s}^{(q)} - 1)\|^2\right\} \tag{2.29}$$

The key to the BCJR decoder is that the values of α and β can be calculated recursively. Applying Bayes' rule to (2.24), the following recursive form of α can be obtained:

$$\alpha_i(\psi_i) = \sum_{\psi_{i-1}\in\mathcal{S}} \alpha_{i-1}(\psi_{i-1})\,\gamma_{i-1}(\psi_{i-1}, \psi_i) \tag{2.30}$$

Thus, for the forward recursion, the probability that the encoder is in state ψ_i at time i is the sum, over all of the states ψ_{i-1} at time $i-1$, of the probability that it is in state ψ_{i-1} times the probability of its moving from ψ_{i-1} to ψ_i. The encoder starts in the zero state and so at initialisation $\alpha_0(S_0) = 1$.

Similarly, by applying Bayes' rule to (2.25), the following recursive form of β can be obtained:

$$\beta_i(\psi_i) = \sum_{\psi_{i+1}\in\mathcal{S}} \beta_{i+1}(\psi_{i+1})\,\gamma_i(\psi_i, \psi_{i+1}) \tag{2.31}$$

For the backward recursion, the probability that the encoder is in state ψ_i at time i is the sum, over all the states ψ_{i+1} at time $i+1$, of the probability that it is in state ψ_{i+1} times the probability of its moving from ψ_i to ψ_{i+1} If the encoder is terminated then it finishes in the zero state and $\beta_M(S_0) = 1$. Alternatively, if the encoder has not been terminated, β is initialised in such a way that every state is equally likely, i.e., $\beta_M(\psi_M) = 1/2^L$ for all $\psi_M \in \mathcal{S}$.

The BCJR algorithm calculates the γ, α and β values and then puts them together to find the state transition probabilities using (2.22). Therefore, the log-likelihood ratio (LLR) for bit $d[i]$, (2.19), becomes [48]

$$\Lambda(d[i] \mid \mathbf{y}) = \log \frac{\sum_{(S_r,S_s)\in\mathcal{T}^+} \alpha_i(S_r)\gamma_i(S_r, S_s)\beta_{i+1}(S_s)}{\sum_{(S_r,S_s)\in\mathcal{T}^-} \alpha_i(S_r)\gamma_i(S_r, S_s)\beta_{i+1}(S_s)} \tag{2.32}$$

The calculation of α and β involves multiplying together small numbers, and numerical stability can become a problem. However, this can be avoided by normalizing α and β

at each step so that they sum to unity, i.e.,

$$\alpha'_i(S_r) = \frac{\alpha_i(S_r)}{\sum_{\psi_i \in \mathcal{S}} \alpha_i(\psi_i)} \quad \text{and} \quad \beta'_{i+1}(S_s) = \frac{\beta_{i+1}(S_s)}{\sum_{\psi_{i+1} \in \mathcal{S}} \beta_{i+1}(\psi_{i+1})}. \tag{2.33}$$

In summary, the BCJR algorithm consists of an initialization in (2.27), a forward pass to calculate α in (2.30), a backward pass to calculate β in (2.31), the calculation of each state probability using (2.22), and lastly, the calculation of message bit probabilities (in LLR form) using (2.32).

The source message bit probabilities $P(d[i])$ are called the *a priori probabilities* for $\mathbf{d}$ because they are known in advance before the BCJR decoder is run. The message bit probabilities $P(d[i] \,|\, \mathbf{y})$ output by the BCJR decoder are called the *a posteriori probabilities* for $\mathbf{d}$.

Matrix Formulation of the BCJR Algorithm

For notational purposes it is often convenient to express the BCJR algorithm in matrix form. Denote the vectors of the forward and backward probabilities as:

$$\boldsymbol{\alpha}_i = \left[\, \alpha_i(S_0),\, \alpha_i(S_1),\, \cdots, \alpha_i(S_{(2^L-1)}) \,\right]^T, \qquad (|\mathcal{S}| \times 1 \text{ vector}) \tag{2.34}$$

$$\boldsymbol{\beta}_i = \left[\, \beta_i(S_0),\, \beta_i(S_1),\, \cdots, \beta_i(S_{(2^L-1)}) \,\right]^T. \qquad (|\mathcal{S}| \times 1 \text{ vector}) \tag{2.35}$$

Let $\mathbf{P}_i$ be the probability matrix with dimensions $|\mathcal{S}| \times |\mathcal{S}|$ defined as

$$\{\mathbf{P}_i\}_{j,k} = \gamma_i(S_j, S_k) \tag{2.36}$$

where $\{\,\cdot\,\}_{j,k}$ denotes the entry of a matrix in the j-th row and k-th column. Then the forward recursion (2.30) can be expressed as

$$\boldsymbol{\alpha}_{i+1} = \mathbf{P}_i^T \boldsymbol{\alpha}_i, \qquad i = 1, 2, \ldots, N-1, \tag{2.37}$$

and the backward recursion (2.31) can be expressed as

$$\boldsymbol{\beta}_i = \mathbf{P}_i \boldsymbol{\beta}_{i+1}, \qquad i = N-1, N-2, \ldots, 1. \tag{2.38}$$

To compute (2.32), we need to define two matrices describing transitions in the trellis. Let matrices $\mathbf{T}(0)$ and $\mathbf{T}(1)$ be defined as

$$\{\mathbf{T}(0)\}_{j,k} = \begin{cases} 1, & \text{if } (S_j, S_k) \text{ is a state transition with } d_{j,k} = 0, \\ 0, & \text{otherwise} \end{cases}$$

$$\{\mathbf{T}(1)\}_{j,k} = \begin{cases} 1, & \text{if } (S_j, S_k) \text{ is a state transition with } d_{j,k} = 1, \\ 0, & \text{otherwise} \end{cases}$$

respectively. For example, for the trellis shown in Figure 2.2b,

$$\mathbf{T}(0) = \begin{bmatrix} 1 & 0 & 0 & 0 \\ 0 & 0 & 1 & 0 \\ 1 & 0 & 0 & 0 \\ 0 & 0 & 1 & 0 \end{bmatrix}, \quad \text{and} \quad \mathbf{T}(1) = \begin{bmatrix} 0 & 1 & 0 & 0 \\ 0 & 0 & 0 & 1 \\ 0 & 1 & 0 & 0 \\ 0 & 0 & 0 & 1 \end{bmatrix}. \tag{2.39}$$

Then the *a posteriori* probabilities for $d[i]$ in LLR form, (2.32), can be expressed as [77]:

$$\Lambda(d[i] \mid \mathbf{y}) = \log \left[\frac{\boldsymbol{\alpha}_i^T (\mathbf{T}(1) \odot \mathbf{P}_i) \boldsymbol{\beta}_{i+1}}{\boldsymbol{\alpha}_i^T (\mathbf{T}(0) \odot \mathbf{P}_i) \boldsymbol{\beta}_{i+1}} \right], \tag{2.40}$$

where $\odot$ denotes the element-by-element product of two matrices (Hadamard product).

2.2 Intersymbol Interference (ISI) Channels

Traditional forward error correction (FEC) methods do not work well when the data is transmitted over a channel that introduces additional distortions in the form of ISI. When the channel is bandlimited or for other reasons is time-dispersive in nature, then the receiver will generally need to compensate for the channel effects prior to employing a standard decoding algorithm for the FEC. Such methods for channel compensation are commonly referred to as channel equalization.

Given observations of the received data, the receiver must estimate the data that was transmitted, using knowledge of how the channel has corrupted the data together with the available redundancy that has been introduced to protect the data, in the form of the FEC. While the FEC alone would protect the data from additive noise, when the channel introduces intersymbol interfernce, adjacent channel symbols become smeared together, introducing additional dependencies among the transmitted channel symbols which degrades the decoder performance.

Three receiver structures for the reception of signals from an intersymbol interference channel are considered.

Optimal Receiver (Joint Equalization and Detection). To optimally estimate the data that was transmitted, in terms of minimizing the bit error rate (BER), the receiver must find the set of transmitted bits that are most probable, given knowledge of the complex statistical relationship between the observations and the transmitted bits. An optimal receiver takes into account the FEC, the interleaver, the symbol mapping, and knowledge of the channel. With so many factors involved, the resulting statistical relationship becomes difficult to manage efficiently. Therefore, in most practical applications, the optimal receiver is infeasible, as it essentially tries to fit all the possible sequences of transmitted bits to the received data, a task whose complexity grows exponentially in the length of the data transmitted.

Separate Equalization and Decoding. Traditionally, most practical receivers have been designed is to first process the received observations to account for the effects of the channel and then to make estimates of the transmitted channel symbols that best fit the observed data. Generally, the problem of mitigating the effects of an ISI channel on the transmitted data is called *equalization* or *detection*, while the subsequent problem of recovering the data bits from the equalized symbol stream, making use of the FEC, is called *decoding*.

In the traditional implementation of this separate equalization and decoding process, the equalizer makes hard decisions as to which sequence of channel symbols were transmitted and then maps these hard decisions into their constituent binary code bits. These code bits are then processed by the FEC decoder. However, the process of making hard decisions on the channel symbols destroys information relating to how likely each of the possible channel symbols might have been. This additional "soft" information can be converted into probabilities that each of the received code bits takes on the value of zero or one. This form of soft information can be readily exploited by a BER optimal decoding algorithm. Many practical systems use this type of soft-input FEC decoding by passing soft information between an equalizer and decoding algorithm.

Turbo Equalization. The remarkable performance of turbo codes demonstrated the benefits of passing soft information in both directions between constituent processing blocks. Once the FEC decoding algorithm processes the soft information it can, in turn, generate its own soft information indicating the relative likelihood of each of the transmitted bits. This soft information from the decoder could then be taken into account in the equalization process, creating a feedback loop between the equalizer and decoder, through which each of the constituent algorithms communicates its beliefs about the relative likelihood that each given bit takes on a particular value. This process is often termed "belief propagation" or "message passing". This feedback loop structure essentially describes the process of *turbo equalization*.

In this and the subsequent two sections, an overview of receivers for intersymbol interference channels, including turbo equalization are presented. The focus of this discussion will be the system model shown in Figure 2.4, which contains a system configuration for a digital transmitter as part of a communication link. These basic elements are contained in most practical communication systems and are essential components of a transmitter such that turbo equalization can be used in the receiver.

2.2.1 System Model

We consider the design of a communication system for ISI channels with the aim of transmitting M data bits, $\{d[i]\}_{i=0}^{M-1}$, over the channel in a manner that enables the receiver to correctly recover the original data stream with low probability of error.

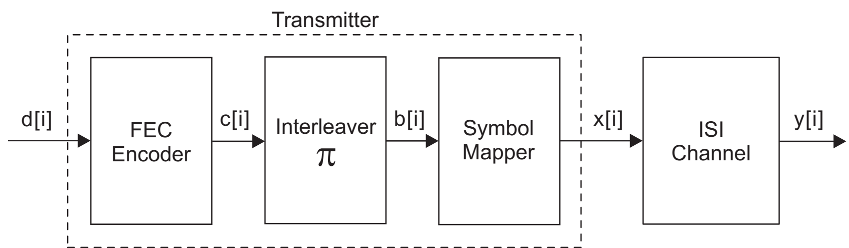

Figure 2.4: Coded transmitter structure and signal model for an ISI channel

The transmitter structure for this system is shown in Figure 2.4. The FEC encoder takes as in input the binary data sequence to be transmitted, $\{d[i]\}_{i=0}^{M-1}$, and produces a longer sequence of N coded bits, $\{c[i]\}_{i=0}^{N-1}$. The coded sequence contains addition redundant information that can be used to protect the data of interest in the event of transmission errors. The rate of the code, $R_c = M/N$, specifies the amount of added redundant information. In this section, we use the convolutional code given by the generator $(1 + D^2,\ 1 + D + D^2)$ [59] from Figure 2.1b. This code has rate-1/2, and therefore, M data bits $d[i]$ are encoded to $2M$ code bits $c[i]$.

During transmission, data errors may occur due to additive channel noise or receiver detection error. The ability of the FEC code to correct these errors can be improved by ensuring that the errors appear random and that long error bursts are are avoided. This is achieved by using an interleaver to randomize the order of the code bits prior to transmission. This process is completely reversible and is simply mirrored in the receiver.

The coded bit sequence $\{c[i]\}_{i=0}^{N-1}$ is permutated into $\{b[i]\}_{i=0}^{N-1}$ by the interleaver. Finally, the mapper converts the permuted code bits $b[i]$ into symbols or signal levels that can be modulated for transmission over a passband channel. Generally, this is is achieved by mapping a group of Q code bits onto a complex modulation waveform or channel symbol, $x[i]$. For example, Q bits would map onto a (2^Q)-QAM symbol. However in this chapter, binary phase shift keying (BPSK) modulation is used, where $Q = 1$ and the transmit pulse shape is modulated with either a $+1$ or -1, i.e., the bit $b[i] \in \{0, 1\}$ is mapped to a symbol $x[i]$ as $x[i] = (-1)^{b[i]}$. The series of transmit pulse shapes modulated with the symbols $\{x[i]\}_{i=0}^{N-1}$ is then transmitted over a linear time-invariant (LTI) channel with known channel impulse response (CIR).

The transmitted symbols, which are distorted by the dispersive nature of the channel and by additive white Gaussian noise (AWGN), are received by a coherent symbol-spaced receiver front-end that has precise knowledge of the signal phase and symbol timing. The received waveforms are passed through the receive filter, which is matched to the transmit pulse shape and the CIR. Sampling the receive filter output produces the sequence of samples $\{y[i]\}_{i=0}^{N-1}$ given by

$$y[i] = v[i] + n[i] \quad \text{where} \quad v[i] = \sum_{l=0}^{L} h_l\, x[i-l], \qquad i = 0, 1, \ldots, N-1 \tag{2.41}$$

where the real-valued coefficients h_l are the sampled values of the combined impulse response of the transmit filter, the channel, and the receive filter. The response is assumed to have a finite length of $L + 1$, and hence, $h_l = 0$ for $l > L$.

For BPSK modulation, the transmit symbols, $x[i]$, and the (noise-free) channel output, $v[i]$, are real-valued. Therefore, assuming that the receive filter satisfies the Nyquist criterion, the noise samples $n[i]$ are independent and identically distributed (i.i.d.) real-valued Gaussian noise samples, i.e., $n[i] \sim \mathcal{N}(0, \sigma^2)$, with p.d.f. described by (2.8).

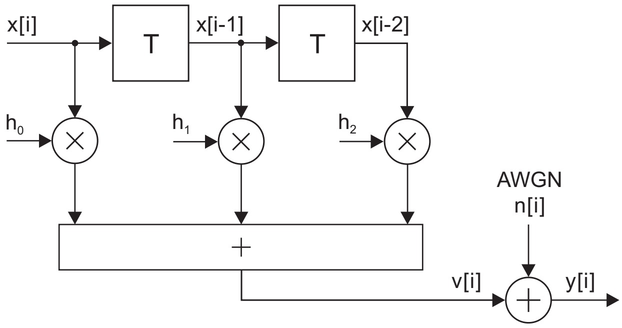

Figure 2.5: Tapped delay line model of an ISI channel with memory L = 2 (and coefficients $h_0 = 0.407$, $h_1 = 0.815$, and $h_2 = 0.407$)

The discrete-time model of data transmission in a bandlimited additive noise channel (2.41) can be represented by an equivalent tapped delay-line model. Figure 2.5 shows an example tapped delay-line model for a three-tap ISI channel ($L = 2$) with coefficients $h_0 = 0.407$, $h_1 = 0.815$, $h_2 = 0.407$. These coefficients are assumed to be time-invariant and known to the receiver. This example is from [92] and [53]. For channel shown in Figure 2.5, the system model of (2.41) can be expressed in matrix form as

$$\mathbf{y} = \mathbf{H}\mathbf{x} + \mathbf{n}, \tag{2.42}$$

where channel matrix $\mathbf{H}$ is given by

$$\mathbf{H} = \begin{bmatrix} h_0 & 0 & 0 & 0 & 0 & \cdots & 0 \\ h_1 & h_0 & 0 & 0 & 0 & \cdots & 0 \\ h_2 & h_1 & h_0 & 0 & 0 & \cdots & 0 \\ 0 & h_2 & h_1 & h_0 & 0 & \cdots & 0 \\ & & \ddots & \ddots & \ddots & & \\ 0 & 0 & \ldots & 0 & h_2 & h_1 & h_0 \end{bmatrix} \qquad (N \times N \text{ matrix})$$

and vectors $\mathbf{y}$, $\mathbf{x}$, and $\mathbf{n}$ are given by

$$\mathbf{y} = [\, y[0],\, y[1],\, \ldots,\, y[N-1]\,]^T \qquad (N \times 1 \text{ vector})$$
$$\mathbf{x} = [\, x[0],\, x[1],\, \ldots,\, x[N-1]\,]^T \qquad (N \times 1 \text{ vector})$$
$$\mathbf{n} = [\, n[0],\, n[1],\, \ldots,\, n[N-1]\,]^T \qquad (N \times 1 \text{ vector})$$

2.2.2 Optimal Detection

An optimal receiver seeks to minimize the bit error rate (BER) by finding the set of transmitted bits that are most probable, given knowledge of the complex statistical relationship between the observations and the transmitted bits. Such a receiver takes into account the FEC, the interleaver, the symbol mapping, and knowledge of the channel. In the general case, the decision rule minimizing the bit error probability is based on the maximization of the *a posteriori* probabilities (APP) of each data bit in the sequence, i.e.

$$\hat{d}[i] = \arg\max_{d \in \{0,1\}} P(d[i] = d \mid \mathbf{y}), \qquad i = 0, 1, \ldots, M-1 \tag{2.43}$$

where $d[i]$ is the data bit at time i, and $\mathbf{y}$ is the entire received symbol sequence [10]. Detection algorithms that implement the decision rule of (2.43) are commonly known as maximum *a posteriori* probability (MAP) algorithms. By applying Bayes' rule to (2.43), the data bit estimates can be calculated as follows

$$P(d[i] = d \mid \mathbf{y}) = \sum_{\mathbf{d}:d[i]=d} P(\mathbf{d} \mid \mathbf{y}) = \sum_{\mathbf{d}:d[i]=d} \frac{p(\mathbf{y} \mid \mathbf{d})P(\mathbf{d})}{p(\mathbf{y})}, \qquad d \in \{0,1\} \tag{2.44}$$

where $P(\mathbf{d})$ is the *a-priori* probability of the sequence $\mathbf{d}$, which can be used to include knowledge about the source producing the bits $d[i]$. The data bits, $d[i]$, are usually assumed to be independent, and hence

$$P(\mathbf{d}) = \prod_{i=0}^{M-1} P(d[i]). \tag{2.45}$$

It then follow that (2.44) can be restated as

$$P(d[i] = d \mid \mathbf{y}) = \sum_{\mathbf{d}:d[i]=d} \frac{p(\mathbf{y} \mid \mathbf{d})}{p(\mathbf{y})} \prod_{j=0}^{M-1} P(d[j]), \qquad d \in \{0,1\} \tag{2.46}$$

In log-likelihood ratio (LLR) form, (2.46) can be written as

$$\begin{aligned} \Lambda(d[i] \mid \mathbf{y}) &= \log \frac{\sum_{\mathbf{d}:d[i]=0} p(\mathbf{y} \mid \mathbf{d}) \prod_{j=0}^{M-1} P(d[j])}{\sum_{\mathbf{d}:d[i]=1} p(\mathbf{y} \mid \mathbf{d}) \prod_{j=0}^{M-1} P(d[j])} \\ &= \lambda(d[i] \mid \mathbf{y}) + \lambda(d[i]) \end{aligned} \tag{2.47}$$

where $\lambda(d[i] \mid \mathbf{y})$ is the extrinsic information about $d[i]$ contained in $\mathbf{y}$, defined as

$$\lambda(d[i] \mid \mathbf{y}) = \log \frac{\sum_{\mathbf{d}:d[i]=0} p(\mathbf{y} \mid \mathbf{d}) \prod_{j=1:j\neq i}^{M-1} P(d[j])}{\sum_{\mathbf{d}:d[i]=1} p(\mathbf{y} \mid \mathbf{d}) \prod_{j=1:j\neq i}^{M-1} P(d[j])}, \tag{2.48}$$

and $\lambda(d[i])$ is the *a priori* information about $d[i]$, defined as

$$\lambda(d[i]) = \log \frac{P(d[i]=0)}{P(d[i]=1)}. \tag{2.49}$$

Extrinsic information plays an important role in the iterative detection schemes described in later sections. Note that if the bits $d[i]$ are assumed to be uniformly distributed (i.e., they take on the values 0 or 1 equally likely), then the *a priori* information (in LLR form) is zero, i.e., $\lambda(d[i]) = 0$.

Using (2.47) to compute the *a posteriori* probabilities in LLR form, $\Lambda(d[i] \mid \mathbf{y})$, the MAP decision rule of (2.43) can be written in LLR form as

$$\hat{d}[i] = \begin{cases} 0, & \Lambda(d[i] \mid \mathbf{y}) \geq 0 \\ 1, & \Lambda(d[i] \mid \mathbf{y}) < 0 \end{cases} \qquad i = 0, 1, \ldots, M-1 \tag{2.50}$$

The main difficulty with optimal joint MAP detection is the computational complexity of computing $p(\mathbf{y} \mid \mathbf{d})$ in (2.44) and (2.47), which involves 2^M terms and becomes impractical for large block lengths M.

2.3 Separate Equalization and Decoding for ISI Channels

Optimal joint equalization and decoding using the MAP algorithm is rarely used in practice because of the computational complexity. The traditional approach to minimising receiver complexity is to split the detection task into a number of separate subtasks. First, the equalizer estimates the transmitted channel symbols. Then, the symbols are demapped into their associated code bits, deinterleaved, and finally, decoded using a BER optimal decoder for the FEC. This approach is shown in Figure 2.6.

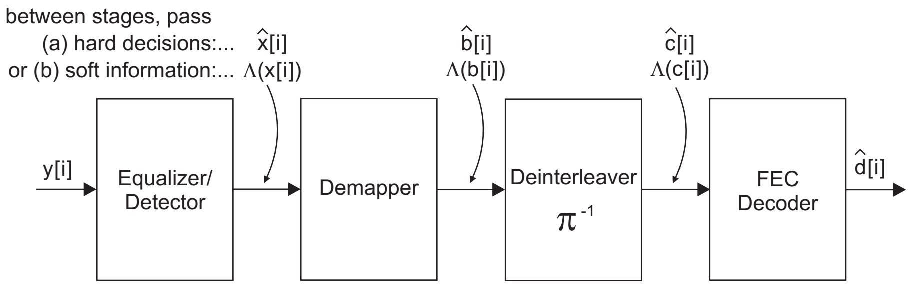

Figure 2.6: Receiver with separate equalization and decoding stages, using (a) hard decisions or (b) soft information between stages)

Traditionally, the equalizer generates hard decisions of the estimated symbols, i.e., $\hat{x}[i]$, which are then propagated through the demapper and deinterleaver, and presented as hard inputs, $\hat{c}[i]$, to the decoder. In this case, $\hat{x}[i]$, and $\hat{c}[i]$ are from the same alphabet as $x[i] \in \{-1, +1\}$ and $c[i] \in \{0, 1\}$, respectively. However, instead of providing hard decisions to the decoder, the equalizer can often provide the probabilities that $x[i]$ takes on a particular value from $\{-1, +1\}$. These probabilities convey more information to the decoder than hard decisions, and generally lead to better receiver performance. The principle of using probabilities (soft information) rather than hard decisions is generally referred to as *soft decoding*.

The most commonly used soft information about the transmitted symbols, $x[i]$, is the *a posteriori* probabilities (APPs) in LLR form, $\Lambda(x[i] \mid \mathbf{y})$. The concept of soft processing is illustrated in the receiver block diagram of Figure 2.6, by the flow of soft information, in LLR form $\Lambda(\,\cdot\,)$, between signal blocks.

While APP information is a "side product" of the MAP symbol detector, it can also be extracted from filter-based equalizers, but is generally more complicated [133], [121]. A common approach for filter-based equalizers is to assume that the estimation error, $\epsilon[i] = \hat{x}[i] - x[i]$, is Gaussian distributed with PDF $p(\epsilon[i])$. This approach can apply to other equalization algorithms producing estimates $\hat{x}[i]$ as well.

Various performance criteria have been used for equalizer design. Common techniques include: zero-forcing equalizers that attempt to simply invert the channel; linear and nonlinear equalizers based on minimizing a mean-squared error (MSE) metric; and symbol-error-rate (SER) optimal equalizers that maximize the likelihood of the observations given the channel and data model. In this chapter, two types of equalization algorithm are considered: trellis-based MAP symbol detection (Section 2.3.1); and equalization based on linear filtering (Section 2.3.2).

2.3.1 Trellis-Based MAP Symbol Detection

A MAP symbol detector computes symbol estimates, $\hat{x}[i]$, using a decision rule based on the maximization of the *a posteriori* probabilities (APP) of each individual symbol in the sequence, i.e., for BPSK transmission,

$$\hat{x}[i] = \underset{x \in \{+1,-1\}}{\arg\max}\, P(x[i] = x \mid \mathbf{y}), \qquad i = 0, 1, \ldots, N-1 \tag{2.51}$$

where $x[i]$ is the transmitted symbol at time i and $\mathbf{y}$ is the entire received sequence [10]. Note that the decision rule ignores the effect of the FEC code. MAP detection may appear intractably complex because of the large number of probabilities to be computed (c.f. (2.43)-(2.44)), however it can be performed efficiently using trellis-based methods.

Consider the tapped delay line model of the transmitter, channel, and receive filter shown in Figure 2.5. Given that the tapped delay line contains L delay elements and that the input symbols are BPSK modulated, $x[i] \in \{+1, -1\}$, the channel can be in one of 2^L states $S_l,\ l = 0, 1, \ldots, 2^L - 1$, corresponding to the 2^L different possible contents of the delay elements. The set of possible states is denoted $\mathcal{S} = \{S_0, S_1, \ldots, S_{(2^L-1)}\}$.

At each time instance $i = 0, 1, \ldots, N-1$ the state of the channel is a random variable $\psi_i \in \mathcal{S}$. If the channel is in state ψ_i at time i, then ψ_{i+1} (the state at time $i+1$) can only assume one of two values corresponding to a transmit symbol of $x[i] = +1$ or $x[i] = -1$ being input into the tapped delay line (channel model) at time i. This possible evolution of states can be described using a trellis diagram. Figure 2.7a and Figure 2.7b show the state and trellis diagrams, respectively, for the channel model of Figure 2.5. A branch of the trellis is a four-tuple $(S_r, S_s, x_{r,s}, v_{r,s})$ such that state $\psi_{i+1} = S_s$ at time $i+1$ can be reached from state $\psi_i = S_r$ at time i with input $x[i] = x_{r,s}$ and output $v[i] = v_{r,s}$, where $x_{r,s}$ and $v_{r,s}$ are uniquely identified by the index pair (S_r, S_s). The output symbol $v[i]$ at time i is the noise-free output of the channel model, (2.41), given by

$$v[i] = \sum_{l=0}^{L} h_l\, x[i-l].$$

The transitions from a state $\psi_i = S_r$ at time i to a state $\psi_{i+1} = S_s$ at time $i+1$ are labeled with the input/output pair $x_{r,s}/v_{r,s}$. The set of all index pairs (S_r, S_s) corresponding to valid trellis branches (i.e. valid state transitions) is denoted $\mathcal{T}$. The set $\mathcal{T}$ for the trellis in Figure 2.7b is

$$\mathcal{T} = \{ (S_0, S_0), (S_0, S_1), (S_1, S_2), (S_1, S_3), (S_2, S_0), (S_2, S_1), (S_3, S_3), (S_3, S_2) \}.$$

This trellis description can be used to efficiently compute the APPs, $P(x[i] \mid \mathbf{y})$.

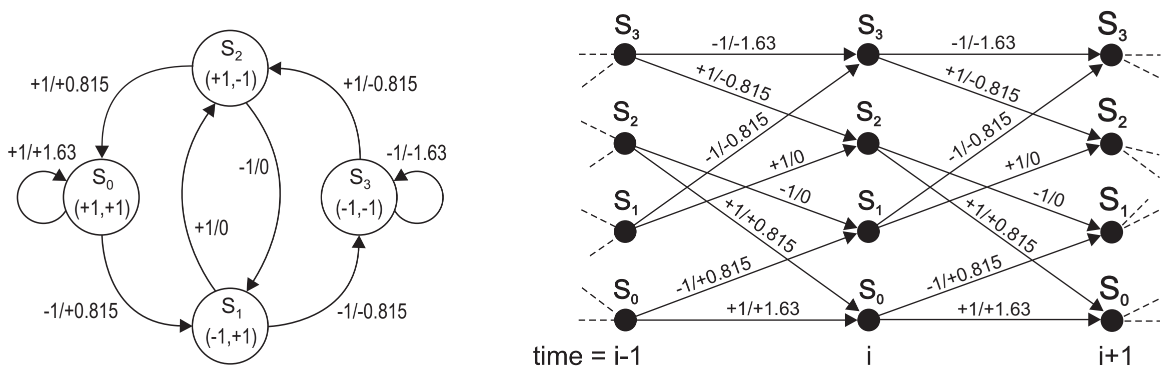

(a) State diagram **(b)** Trellis diagram

Figure 2.7: State diagram and trellis representations of the channel in Figure 2.5. The states $S_0 = (+1, +1)$, $S_1 = (-1, +1)$, $S_2 = (+1, -1)$, $S_3 = (-1, -1)$ are the possible contents of the channel model delay elements.

The approach of separating the equalization and decoding tasks assumes that the transmitted symbols, $x[i]$, are i.d.d. random variables, ie

$$P(\mathbf{x}) = \prod_{i=0}^{N-1} P(x[i]) \tag{2.52}$$

and $x[i]$ takes on values $+1$ and -1 equally for all i. With this assumption, the BCJR algorithm (of Section 2.1.4) can be adapted to efficiently compute $P(x[i] \mid \mathbf{y})$.

The probability that the transmitted sequence path in the trellis contained the branch $(S_r, S_s, x_{r,s}, v_{r,s})$ at time i, i.e., $P(\psi_i = S_r, \psi_{i+1} = S_s \mid \mathbf{y})$ can be computed by the BCJR algorithm [6], [97] based on the decomposition of the joint distribution $p(\psi_i, \psi_{i+1}, \mathbf{y})$ given by

$$p(\psi_i, \psi_{i+1}, \mathbf{y}) = P(\psi_i, \psi_{i+1} \mid \mathbf{y}) p(\mathbf{y}). \tag{2.53}$$

The received signal sequence $\mathbf{y}$ in $p(\psi_i, \psi_{i+1}, \mathbf{y})$ can be written as

$$p(\psi_i, \psi_{i+1}, \mathbf{y}) = p(\psi_i, \psi_{i+1}, (y[0], \ldots, y[i-1]), y[i], (y[i+1], \ldots, y[N-1])), \tag{2.54}$$

and applying the chain rule for joint probabilities, i.e., $P(a, b) = P(a)P(b|a)$, to (2.54) produces the decomposition:

$$p(\psi_i, \psi_{i+1}, \mathbf{y}) = \underbrace{p(\psi_i, y[0], \ldots, y[i-1])}_{\alpha_i(\psi_i)} \underbrace{p(\psi_{i+1}, y[i] \mid \psi_i)}_{\gamma_i(\psi_i, \psi_{i+1})} \underbrace{p(y[i+1], \ldots, y[N-1] \mid \psi_{i+1})}_{\beta_{i+1}(\psi_{i+1})}.$$

The term $\alpha_i(\psi)$ can be computed using the recursion of (2.30) with the initial value $\alpha_0(\psi) = P(\psi_0 = \psi)$, the distribution of the state at time $i = 0$. The term $\beta_i(\psi)$ can be computed using the recursion (2.30) with the initial value $\beta_N(\psi) = 1$ for all $\psi \in \mathcal{S}$. The term $\gamma_i(\psi_i, \psi_{i+1})$ can be decomposed into two parts:

$$\gamma_i(\psi_i, \psi_{i+1}) = P(\psi_{i+1} \mid \psi_i)p(y[i] \mid \psi_i, \psi_{i+1}), \tag{2.55}$$

where $P(\psi_{i+1} \mid \psi_i) = P(x[i] = x_{r,s})$, which is given by the probability of the message source; and $p(y[i] \mid \psi_i, \psi_{i+1}) = p(y[i] \mid v[i] = v_{r,s})$ is the channel transition probability, i.e., the probability that the channel turned $v_{r,s}$ into $y[i]$.

The transition probability $\gamma_i(S_r, S_s)$ is zero if the index pair (S_r, S_s) is not in $\mathcal{T}$. For pairs (S_r, S_s) from $\mathcal{T}$, $\gamma_i(S_r, S_s)$ is a function of the source probability and the channel transition probability, i.e.,

$$\gamma_i(S_r, S_s) = \begin{cases} P(x[i] = x_{r,s})p(y[i] \mid v[i] = v_{r,s}), & (S_r, S_s) \in \mathcal{T} \\ 0, & (S_r, S_s) \notin \mathcal{T} \end{cases} \tag{2.56}$$

The symbols are assumed to be i.d.d. and hence $P(x[i] = +1) = P(x[i]) = -1) = 1/2$. For the channel model of (2.41), i.e. $y[i] = v[i] + n[i]$, and the assumption that $n[i] \sim \mathcal{N}(0, \sigma^2)$, the channel transition probability is given by

$$p(y[i] \mid v[i]) = \frac{1}{\sqrt{2\pi\sigma^2}} \exp\left\{-\frac{1}{2\sigma^2}(y[i] - v[i])^2\right\}.$$

The BCJR algorithm calculates the $\alpha(\psi_i)$, $\gamma_i(\psi_i, \psi_{i+1})$, and $\beta_{i+1}(\psi_i)$ probabilities and puts them together to obtain the state transition probability $p(\psi_i, \psi_{i+1}, \mathbf{y})$. Therefore the conditional LLR $\Lambda(b[i] \mid \mathbf{y})$ of the code bit $b[i]$ can be written as

$$\Lambda(b[i] \mid \mathbf{y}) = \log \frac{\sum_{(S_r,S_s) \in \mathcal{T}: x_{r,s}=+1} \alpha_i(S_r)\gamma_i(S_r, S_s)\beta_{i+1}(S_s)}{\sum_{(S_r,S_s) \in \mathcal{T}: x_{r,s}=-1} \alpha_i(S_r)\gamma_i(S_r, S_s)\beta_{i+1}(S_s)} \tag{2.57}$$

Note that (2.57) includes the demapping operation $x[i] \rightarrow b[i]$, where

$$\Lambda(b[i] \mid \mathbf{y}) = \log \frac{P(b[i] = 0 \mid \mathbf{y})}{P(b[i] = 1 \mid \mathbf{y})} = \log \frac{P(x[i] = +1 \mid \mathbf{y})}{P(x[i] = -1 \mid \mathbf{y})}$$

Finally, the code bit estimates $\hat{b}[i]$ are computed from the sign of $\Lambda(b[i] \mid \mathbf{y})$ as in (2.50).

The BCJR algorithm for MAP equalization can be concisely described in terms of matrix operations. For a trellis with a set of states $\mathcal{S}$, denote the following vectors and matrices:

- $\boldsymbol{\alpha}_i$ as the set of $|\mathcal{S}| \times 1$ vectors of the forward probabilities ($\alpha_i(\psi)$ values), as defined in (2.34);
- $\boldsymbol{\beta}_i$ as the set of $|\mathcal{S}| \times 1$ vectors of backward probabilities ($\beta_i(\psi)$ values), as defined in (2.35);
- $\mathbf{P}_i$ as the set of $|\mathcal{S}| \times |\mathcal{S}|$ probability matrices as defined in (2.36); and
- $\mathbf{T}(x)$ for $x \in \{+1, -1\}$, as the two $|\mathcal{S}| \times |\mathcal{S}|$ trellis transition matrices, defined as

$$\{\mathbf{T}(x)\}_{j,k} = \begin{cases} 1, & (S_j, S_k) \text{ is a branch with } x_{j,k} = x, \\ 0, & \text{otherwise} \end{cases} \tag{2.58}$$

For the trellis in Figure 2.7, the matrices $\mathbf{T}(+1)$ and $\mathbf{T}(-1)$ are defined as

$$\mathbf{T}(+1) = \begin{bmatrix} 1 & 0 & 0 & 0 \\ 0 & 0 & 1 & 0 \\ 1 & 0 & 0 & 0 \\ 0 & 0 & 1 & 0 \end{bmatrix}, \quad \text{and} \quad \mathbf{T}(-1) = \begin{bmatrix} 0 & 1 & 0 & 0 \\ 0 & 0 & 0 & 1 \\ 0 & 1 & 0 & 0 \\ 0 & 0 & 0 & 1 \end{bmatrix}.$$

Then the BCJR algorithm for MAP equalization can be expressed as shown in Table 2.1. Note that the algorithm shown assumes that the channel is not in any predefined starting or ending state, but can be readily modified to include defined starting and ending states.

1. Initialization: calculate matrices $\mathbf{P}_i$ for $i = 0, 1, \ldots, N-1$, where

$$\{\mathbf{P}_i\}_{r,s} = \gamma_i(S_r, S_s) \quad \text{and}$$
$$\gamma_i(S_r, S_s) = \begin{cases} P(x[i] = x_{r,s})p(y[i] \mid v[i] = v_{r,s}), & (S_r, S_s) \in \mathcal{T} \\ 0, & (S_r, S_s) \notin \mathcal{T}. \end{cases}$$

2. Forward recursion: calculate vectors $\boldsymbol{\alpha}_i$ for $i = 0, 1, \ldots, N-1$, where

$$\boldsymbol{\alpha}_0 = [\,1,\ 1,\ \ldots,\ 1\,]^T \quad \text{and}$$
$$\boldsymbol{\alpha}_i = \mathbf{P}_{i-1}^T \boldsymbol{\alpha}_{i-1}, \quad i = 1, 2, \ldots, N-1.$$

3. Backward recursion: calculate vectors $\boldsymbol{\beta}_i$ for $i = N, N-1, \ldots, 0$, where

$$\boldsymbol{\beta}_N = [\,1,\ 1,\ \ldots,\ 1\,]^T \quad \text{and}$$
$$\boldsymbol{\beta}_i = \mathbf{P}_i \boldsymbol{\beta}_{i+1}, \quad i = N-1, N-2, \ldots, 1.$$

4. Output: calculate code bit APPs in LLR form, $\Lambda(b[i] \mid \mathbf{y})$, using

$$\Lambda(b[i] \mid \mathbf{y}) = \log \left[\frac{\boldsymbol{\alpha}_i^T (\mathbf{T}(+1) \odot \mathbf{P}_i) \boldsymbol{\beta}_{i+1}}{\boldsymbol{\alpha}_i^T (\mathbf{T}(-1) \odot \mathbf{P}_i) \boldsymbol{\beta}_{i+1}} \right], \quad i = 0, 1, \ldots, N-1.$$

Table 2.1: MAP equalization using the BCJR algorithm

In a practical implementation of the algorithm, a frequent re-normalization of the vectors is necessary to avoid numerical underflow. That is, after each step in the recursion to compute $\boldsymbol{\alpha}_i$ and $\boldsymbol{\beta}_i$, both vectors are normalized using (2.33).

2.3.2 Linear Equalization and Symbol Detection

The computational complexity of the trellis-based approaches is determined by the number of trellis states, equal to 2^{QL}, where Q is the number of bits mapped onto each symbol and L is the number of delay elements in the tapped delay line channel model (Figure 2.5). Therefore, the computational complexity of trellis-based equalization can become prohibitive for large signal constellations or long channel-delay spreads.

In contrast to trellis-based equalization, linear-filter-based approaches perform only simple operations on the received symbols, which are applied sequentially to a subset of the observed symbols. Consider the transmitted symbols in the interval $\{x[i-\delta], \ldots, x[i], \ldots, x[i+\delta]\}$, where, for example, $\delta = 6$. This subset of transmitted symbols, denoted $\mathbf{x}_i$ is given by

$$\mathbf{x}_i = [\, x[i-6],\, x[i-5],\, \ldots,\, x[i],\, \ldots,\, x[i+6]\,]^T \qquad ((\Delta + L) \times 1 \text{ vector})$$

where $\Delta + L = 2\delta + 1$, and L is the number of delay elements in the channel model. For the 3-tap ISI channel model of Figure 2.5, $L = 2$ and hence $\Delta = 11$. The signal model can be expressed as

$$\mathbf{y}_i = \tilde{\mathbf{H}}\mathbf{x}_i + \mathbf{n}_i \tag{2.59}$$

where channel matrix $\tilde{\mathbf{H}}$ is given by

$$\tilde{\mathbf{H}} = \begin{bmatrix} h_2 & h_1 & h_0 & 0 & 0 & \cdots & 0 \\ 0 & h_2 & h_1 & h_0 & 0 & \cdots & 0 \\ \vdots & & \ddots & \ddots & \ddots & & \vdots \\ 0 & \cdots & 0 & h_2 & h_1 & h_0 & 0 \\ 0 & \cdots & 0 & 0 & h_2 & h_1 & h_0 \end{bmatrix} \qquad (\Delta \times (\Delta + L) \text{ matrix})$$

and received symbol vector, $\mathbf{y}_i$, and channel noise vector, $\mathbf{n}_i$, are given by

$$\mathbf{y}_i = [\, y[i-4],\, y[i-3],\, \ldots,\, y[i],\, \ldots,\, y[i+6]\,]^T, \qquad (\Delta \times 1 \text{ vector})$$
$$\mathbf{n}_i = [\, n[i-4],\, n[i-3],\, \ldots,\, n[i],\, \ldots,\, n[i+6]\,]^T, \qquad (\Delta \times 1 \text{ vector})$$

respectively. Define vector $\mathbf{w}_i$ as:

$$\mathbf{w}_i = [\, w_\delta,\, w_{\delta-1},\, \ldots,\, w_0,\, \ldots,\, w_{-\delta+L}\,]^T, \qquad (\Delta \times 1 \text{ vector})$$

then the linear processing of $\mathbf{y}_i$ to compute $\hat{x}[i]$ can be expressed with the linear (affine) function

$$\hat{x}[i] = \mathbf{w}_i^T \mathbf{y}_i + a_i, \tag{2.60}$$

where vector $\mathbf{w}_i \in \mathbb{R}^{\Delta}$ and scalar $a_i \in \mathbb{R}$ are the parameters subject to optimization. The general form on the linear equalizer is shown in Figure 2.8.

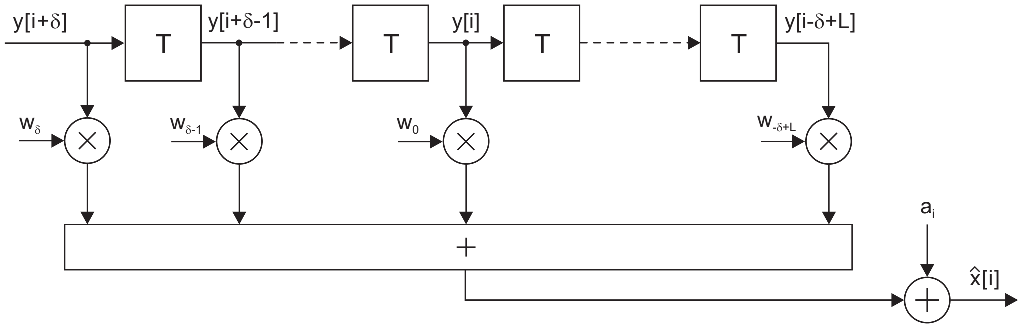

Figure 2.8: Linear-filter-based equalizer

The zero-forcing (ZF) equalizer optimizes $\mathbf{w}_i$ so that $\hat{x}[i]$ is recovered perfectly from $\mathbf{y}_i$ in the absence of noise. However, with noise present, an estimate $\hat{x}[i] = x[i] + \mathbf{w}_i^T \mathbf{n}_i$ is obtained and the equalizer can suffer from severe "noise enhancement" if $\tilde{\mathbf{H}}$ is ill conditioned [92]. This effect can be avoided using linear minimum mean square error (MMSE) estimation [87].

A linear MMSE estimator computes $\hat{x}[i]$ such that the mean squared error (MSE) $\mathrm{E}\{|\, x[i] - \hat{x}[i]\,|^2\}$ is minimized, i.e., $\mathbf{w}_i$ is computed such that

$$\mathbf{w}_i = \arg\min_{\mathbf{w} \in \mathbb{R}^{\Delta}} \mathrm{E}\{|\, x[i] - \mathbf{w}^T \mathbf{y}_i\,|^2\} \tag{2.61}$$

where $\mathrm{E}\{\,\cdot\,\}$ denotes expectation. This is achieved by the affine model

$$\hat{x}[i] = \mathbf{w}_i^T (\mathbf{y}_i - \mathrm{E}\{\mathbf{y}_i\}) + \mathrm{E}\{x[i]\}, \tag{2.62}$$

where

$$\mathbf{w}_i = \mathrm{Cov}\{\mathbf{y}_i, \mathbf{y}_i\}^{-1} \mathrm{Cov}\{\mathbf{y}_i, x[i]\}. \tag{2.63}$$

Note that (2.62) is not purely linear because of the bias terms $\mathrm{E}\{x[i]\}$ and $\mathrm{E}\{\mathbf{y}_i\}$. From (2.59), the following statistics can be defined:

$$\mathrm{Cov}\{\mathbf{y}_i, \mathbf{y}_i\} = \sigma^2 \mathbf{I}_{\Delta} + \tilde{\mathbf{H}}\,\mathrm{Cov}\{\mathbf{x}_i, \mathbf{x}_i\} \tilde{\mathbf{H}}^T, \tag{2.64}$$

$$\mathrm{Cov}\{\mathbf{y}_i, x[i]\} = \tilde{\mathbf{H}}\,\mathrm{Cov}\{\mathbf{x_i}, x[i]\}, \tag{2.65}$$

$$E\{\mathbf{y}_i\} = \tilde{\mathbf{H}}\,\mathrm{E}\{\mathbf{x}_i\}, \tag{2.66}$$

where $\mathbf{I}_\Delta$ is the $\Delta \times \Delta$ identity matrix. Furthermore, assuming symbols $x[i]$ are independent, then

$$\mathrm{Cov}\{x[i], x[j]\} = 0 \quad \text{for} \quad i \neq j \tag{2.67}$$

and hence, covariance matrix $\mathrm{Cov}\{\mathbf{x}_i, \mathbf{x}_i\}$ is diagonal. Additionally,

$$\mathrm{Cov}\{\mathbf{x}_i, x[i]\} = \mathbf{e}\,\mathrm{Cov}\{x[i], x[i]\} = \mathbf{e}\,\mathrm{Var}\{x[i]\} \tag{2.68}$$

where

$$\mathbf{e} = [\,\mathbf{0}_{1\times\delta},\ 1,\ \mathbf{0}_{1\times\delta}\,]^T \qquad\qquad ((\Delta + L) \times 1 \text{ vector})$$

Note that the element set to one in vector $\mathbf{e}$ corresponds to the $x[i]$ element in vector $\mathbf{x}_i$. Using these definitions, the MMSE linear equalizer of (2.62)-(2.63) can be restated as [53]

$$\hat{x}[i] = \mathbf{w}_i^T(\mathbf{y}_i - \tilde{\mathbf{H}}\,\mathrm{E}\{\mathbf{x}_i\}) + \mathrm{E}\{x[i]\}, \tag{2.69}$$

where

$$\mathbf{w}_i = \left(\sigma^2\mathbf{I}_\Delta + \tilde{\mathbf{H}}\,\mathrm{Cov}\{\mathbf{x}_i, \mathbf{x}_i\}\tilde{\mathbf{H}}^T\right)^{-1}\tilde{\mathbf{H}}\mathbf{e}\,\mathrm{Var}\{x[i]\}, \tag{2.70}$$

and the remaining statistics, $\mathrm{E}\{x[i]\}$ and $\mathrm{Cov}\{x[i], x[i]\}$, are obtained from the symbol *a priori* probabilities, $P(x[i])$, using

$$\mathrm{E}\{x[i]\} = \sum_{x\in\{+1,-1\}} x\,P(x[i] = x), \quad \text{and} \tag{2.71}$$

$$\mathrm{Var}\{x[i]\} = \sum_{x\in\{+1,-1\}} |x - \mathrm{E}(x[i])|^2\,P(x[i] = x). \tag{2.72}$$

In turbo equalization configurations (described in later sections), the *a priori* probabilities, $P(x[i])$, would be provided by the soft FEC decoder.

When *a priori* information is not available (for example, in non-iterative configurations), then symbols $x[i]$ are assumed to be i.d.d. and it follows that

$$\mathrm{E}\{x[i]\} = 0, \qquad \mathrm{Var}\{x[i]\} = 1, \quad \text{and} \quad \mathrm{Cov}\{\mathbf{x}_i, \mathbf{x}_i\} = \mathbf{I}_{(\Delta+L)}. \tag{2.73}$$

Substituting (2.73) into (2.69) and (2.69), the MMSE linear equalizer (for the case where there is no *a priori* information about the symbols available) is given by [112] [92]

$$\hat{x}[i] = \mathbf{w}_i^T \mathbf{y}_i, \quad \text{where} \quad \mathbf{w}_i = \left(\sigma^2 \mathbf{I}_\Delta + \tilde{\mathbf{H}}\tilde{\mathbf{H}}^T\right)^{-1} \tilde{\mathbf{H}}\mathbf{e}. \tag{2.74}$$

The estimates $\hat{x}[i]$ are usually not in the symbol alphabet $\{+1, 1\}$ and the decision whether $\hat{x}[i] = +1$ or $\hat{x}[i] = -1$ is usually based on the estimation error $\epsilon[i] = x[i] - \hat{x}[i]$. Given the estimator (2.62)-(2.63), the p.d.f. of the estimation error, $p(\epsilon[i])$, can be assumed to be Gaussian and is given by [41]

$$p(\epsilon[i]) = \frac{1}{\sqrt{2\pi \mathrm{Var}\{\epsilon[i]\}}} \exp\left\{\frac{\epsilon^2[i]}{2\mathrm{Var}\{\epsilon[i]\}}\right\},$$

where the mean and variance are given by

$$\mathrm{E}\{\epsilon[i]\} = 0, \quad \text{and} \quad \mathrm{Var}\{\epsilon[i]\} = \mathrm{Var}\{x[i]\} - \mathbf{w}_i^T \tilde{\mathbf{H}}\mathbf{e},$$

respectively. The hard decision of $\hat{x}[i]$ is the symbol $x \in \{+1, -1\}$ that maximizes $p(\epsilon[i])$, which is the symbol x of closest distance to $\hat{x}[i]$, i.e.,

$$\hat{x}[i] = \arg\min_{x \in \{+1,-1\}} |\, x - \hat{x}[i]\,|.$$

2.3.3 Trellis-Based MAP FEC Decoding

The symbol *a posteriori* probabilities in LLR form, $\Lambda(x[i] \mid \mathbf{y})$), output from the equalizer/detector are demapped and deinterleaved to form the code bit probabilities, $\Lambda(c[i] \mid \mathbf{y})$, input to the FEC decoder. In LLR form, the code bit probabilities $\Lambda(c[i] \mid \mathbf{y})$ can be converted back to probability form using

$$P(c[i] = 1 \mid \mathbf{y}) = \frac{1}{2}\left\{1 - \tanh\left(\frac{\Lambda(c[i] \mid \mathbf{y})}{2}\right)\right\} \tag{2.75}$$

and

$$P(c[i] = 0 \mid \mathbf{y}) = \frac{1}{2}\left\{1 + \tanh\left(\frac{\Lambda(c[i] \mid \mathbf{y})}{2}\right)\right\}. \tag{2.76}$$

The set of probabilities input to the FEC decoder is denoted $\mathbf{p}$, where

$$\mathbf{p} = [\, P(c[0] \mid \mathbf{y}),\, P(c[1] \mid \mathbf{y}),\, \ldots,\, P(c[N-2] \mid \mathbf{y}),\, P(c[N-1] \mid \mathbf{y})\,]^T \tag{2.77}$$

Using these input probabilities, the decoder is tasked with decoding the FEC code, which in this case, is a binary convolutional code. The BCJR algorithm operating on a trellis description for the code can used here as an efficient MAP decoder for computing estimates of the transmitted data bits, $\hat{d}[i]$. In Section 2.1.4, the BCJR algorithm was used as a MAP decoder for convolutional codes, but for case where channel observations are used as input. In this section, the BCJR algorithm is modified for the case where code bit probabilities are used as input.

Consider the convolutional encoder of Figure 2.1b and the corresponding trellis description of Figure 2.2b. The trellis branches are denoted by the tuple $(S_r,\, S_s,\, d_{r,s},\, c_{r,s}^{(1)},\, c_{r,s}^{(2)})$, where $d_{r,s}$ is the input bit $d[i]$ and $(c_{r,s}^{(1)},\, c_{r,s}^{(2)})$ are the two output bits $(c^{(1)}[i],\, c^{(2)}[i])$ belonging to the state transition $(\psi_i = S_r,\, \psi_{i+1} = S_s)$. The set $\mathcal{T}$ of valid transitions is listed in (2.15).

The MAP decoder processes the N-bit block of coded bit probabilities in M state transitions. Therefore, for notational convenience, the set of coded bit probabilities in (2.77) can be restated as

$$\mathbf{p} = \left[\, P(c^{(1)}[0] \mid \mathbf{y}),\, P(c^{(2)}[0] \mid \mathbf{y}),\, \ldots,\, P(c^{(1)}[M-1] \mid \mathbf{y}),\, P(c^{(2)}[M-1] \mid \mathbf{y})\,\right]^T \tag{2.78}$$

where there are two coded bits per state transition since the FEC encoder uses a rate-1/2 code, i.e., $N = 2M$ for $R_c = 1/2$. The change in notation from (2.77) to (2.78) represents the serial-to-parallel conversion process at the input of the MAP decoder (as shown, for example, in Figure 2.3).

To apply the BCJR MAP algorithm from Section 2.1.4, the computation of the transition probabilities, $\gamma_i(\psi_i, \psi_{i+1})$, must be modified to use code bit probabilities as input (instead of channel observations). For probabilistic input, $\gamma_i(\psi_i, \psi_{i+1})$ is computed as

$$\gamma_i(S_r, S_s) = \begin{cases} P(d[i] = d_{r,s}) P(c^{(1)}[i] = c_{r,s}^{(1)} \mid \mathbf{y}) P(c^{(2)}[i] = c_{r,s}^{(2)} \mid \mathbf{y}), & (S_r, S_s) \in \mathcal{T} \\ 0, & (S_r, S_s) \notin \mathcal{T} \end{cases} \tag{2.79}$$

where $P(d[i]=0) = P(d[i]=1) = 1/2$ from the assumption that the data bits, $d[i]$, are i.i.d. The code bit probabilities are computed from (2.75) and (2.76).

The matrices $\mathbf{T}(x)$ for $x \in \{0, 1\}$ are defined as

$$\{\mathbf{T}(x)\}_{j,k} = \begin{cases} 1, & (S_j,\, S_k) \text{ is a branch with } d_{j,k} = x, \\ 0, & \text{otherwise.} \end{cases} \tag{2.80}$$

and the BCJR algorithm for MAP FEC decoding (with probabilistic input) can be expressed as shown in Table 2.2. Note that the initialization of the $\boldsymbol{\alpha}_i$ and $\boldsymbol{\beta}_i$ vectors assumes that the encoder starts from state S_0 at time $i = 0$ and terminates at state S_0 at time $i = M - 1$.

When the soft FEC decoder is used in turbo equalization or turbo multiuser-detection configurations (described in later sections), the decoder is required to compute the code bit APPs, $\Lambda(c[i] \mid \mathbf{p})$, in addition to the data bit APPs, $\Lambda(d^[i] \mid \mathbf{p})$. In turbo configurations, the code bit APPs, $\Lambda(c[i] \mid \mathbf{p})$, serve as *a priori* information for the equalizer or multiuser detector algorithm. Code bit APPs can be computed using the BCJR algorithm in Table 2.2 by changing the definitions of the $\mathbf{T}(x)$ matrices. For APPs $\Lambda(c^{(1)}[i] \mid \mathbf{p})$, $i = 0, 1, \ldots, M-1$ (in LLR from), matrices $\mathbf{T}(x)$ for $x \in \{0, 1\}$ are defined as

$$\{\mathbf{T}(x)\}_{j,k} = \begin{cases} 1, & (S_j,\, S_k) \text{ is a branch with } c^{(1)}_{j,k} = x, \\ 0, & \text{otherwise.} \end{cases} \tag{2.81}$$

Similarly, for APPs $\Lambda(c^{(2)}[i] \mid \mathbf{p})$, $i = 0, 1, \ldots, M-1$ (in LLR form), matrices $\mathbf{T}(x)$ for $x \in \{0, 1\}$ are defined as

$$\{\mathbf{T}(x)\}_{j,k} = \begin{cases} 1, & (S_j,\, S_k) \text{ is a branch with } c^{(2)}_{j,k} = x, \\ 0, & \text{otherwise.} \end{cases} \tag{2.82}$$

1. Initialization: calculate matrices $\mathbf{P}_i$ for $i = 0, 1, \ldots, M-1$, where

$$\{\mathbf{P}_i\}_{r,s} = \gamma_i(S_r, S_s) \quad \text{and}$$
$$\gamma_i(S_r, S_s) = \begin{cases} P(d[i] = d_{r,s})P(c^{(1)}[i] = c^{(1)}_{r,s} \mid \mathbf{y})P(c^{(2)}[i] = c^{(2)}_{r,s} \mid \mathbf{y}), & (S_r, S_s) \in \mathcal{T} \\ 0, & (S_r, S_s) \notin \mathcal{T} \end{cases}$$

2. Forward recursion: calculate vectors $\boldsymbol{\alpha}_i$ for $i = 0, 1, \ldots, M-1$, where

$$\boldsymbol{\alpha}_0 = [\,1,\ 0,\ \ldots,\ 0\,]^T \quad \text{and}$$
$$\boldsymbol{\alpha}_i = \mathbf{P}_{i-1}^T \boldsymbol{\alpha}_{i-1}, \quad i = 1, 2, \ldots, M-1.$$

3. Backward recursion: calculate vectors $\boldsymbol{\beta}_i$ for $i = M, M-1, \ldots, 1$, where

$$\boldsymbol{\beta}_M = [\,1,\ 0,\ \ldots,\ 0\,]^T \quad \text{and}$$
$$\boldsymbol{\beta}_i = \mathbf{P}_i \boldsymbol{\beta}_{i+1}, \quad i = M-1, M-2, \ldots, 1.$$

4. Output: calculate data bit APPs in LLR form, $\Lambda(d[i] \mid \mathbf{p})$, using

$$\Lambda(d[i] \mid \mathbf{p}) = \log \left[\frac{\boldsymbol{\alpha}_i^T (\mathbf{T}(0) \odot \mathbf{P}_i) \boldsymbol{\beta}_{i+1}}{\boldsymbol{\alpha}_i^T (\mathbf{T}(1) \odot \mathbf{P}_i) \boldsymbol{\beta}_{i+1}} \right], \quad i = 0, 1, \ldots, M-1.$$

   where $\mathbf{T}(x)$ is defined in (2.80). $\Lambda(c^{(1)}[i] \mid \mathbf{p})$ and $\Lambda(c^{(2)}[i] \mid \mathbf{p})$ are computed similarly, using $\mathbf{T}(x)$ defined in (2.81) and (2.82), respectively.

Table 2.2: MAP FEC decoding using the BCJR algorithm

2.3.4 System Performance

The performance of the separate equalization and decoding schemes is evaluated for the ISI channel model of Figure 2.5. The schemes use an input data block length (M) of 512 bits with forward error correction performed by the rate-1/2 convolutional encoder of Figure 2.1b, resulting in a coded block length (N) of 1024 bits. The coded bits are scrambled using a random interleaver and mapped onto BPSK symbols. Figure 2.9 compares the receiver performance using the MAP symbol detector ('MAP/APP Det.') of Section 2.3.1 and the MMSE linear equalizer ('LMMSE Eq.') of Section 2.3.2. In both cases, FEC decoding is performed using the BCJR algorithm of Section 2.3.3. The effect of passing hard bit estimates and soft information from the equalizer to the decoder is also compared.

It can be seen that MAP symbol detection (using the BCJR algorithm) provides superior performance compared to the MMSE linear equalizer, but at the cost of additional computational complexity. Note also that passing soft information between the equalizer and decoder provides a 2dB gain in SNR compared to passing hard bit decisions.

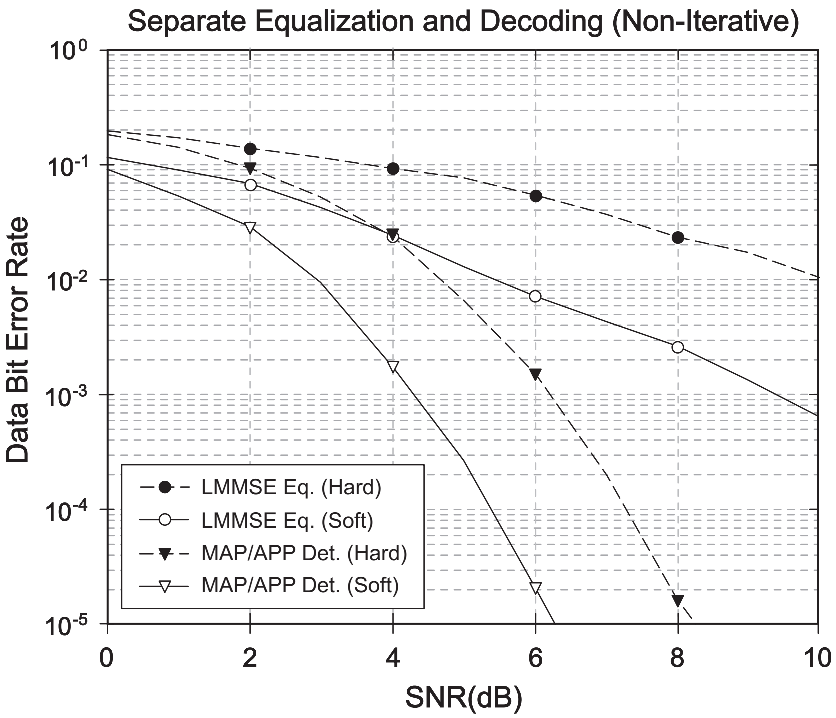

Figure 2.9: System performance of separate equalization and decoding schemes. Performance of equalizer types (MAP symbol detection, and linear MMSE equalization) is compared. System performance when passing hard estimates, and soft information, from the equalizer to the decoder is also compared.

The performance of these separate equalization and decoding schemes is suboptimal because of assumptions of independence in the derivation of the soft information exchanged. In particular, the computation of the APPs $P(x[i] \mid \mathbf{y})$ assumes that all 2^N possible sequences $\{x[i]\}_{i=0}^{N-1}$ are equally likely, i.e., $P(\mathbf{x}) = 1/2^N$ (from the assumption that symbols, $x[i]$, are i.d.d). However, there are only 2^M valid sequences of $\{x[i]\}_{i=0}^{N-1}$, each belonging to a particular input data sequence $\{d[i]\}_{i=0}^{M-1}$. Therefore, the equalizer performance would be significantly improved if the APPs were computed as

$$P(x[i] = x \mid \mathbf{y}) \quad = \sum_{\substack{\text{all } 2^M \text{ valid } \mathbf{x}: \\ x[i]=x}} \frac{p(\mathbf{y} \mid \mathbf{x})P(\mathbf{x})}{p(\mathbf{y})}, \tag{2.83}$$

where $P(\mathbf{x}) = 1/2^M$ for valid $\mathbf{x}$. However, this approach would require exhaustive search methods, since trellis-based methods (such as the BCJR algorithm) could no longer be used, and the resulting computational complexity would be prohibitive.

2.4 Turbo Equalization for ISI Channels

The MAP symbol detector computes symbol estimates using the MAP rule

$$\hat{x}[i] = \underset{x \in \{+1,-1\}}{\arg\max}\, P(x[i] = x \mid \mathbf{y}), \qquad i = 0, 1, \ldots, N-1, \tag{2.84}$$

where, using Bayes' rule, the *a posteriori* probabilities can be computed from

$$P(x[i] = x \mid \mathbf{y}) = \sum_{\mathbf{x}:x[i]=x} p(\mathbf{y} \mid \mathbf{x})P(\mathbf{x}), \qquad x \in \{+1, -1\}. \tag{2.85}$$

Here $p(\mathbf{y} \mid \mathbf{x})$ is the likelihood function and $P(\mathbf{x})$ is the *a priori* probability. Note that the marginal probability, $p(\mathbf{y})$, does not have to be included in this form of the equation. Hence, MAP detection can be thought of as a process that takes a series of observations, $\mathbf{y}$, and bit-wise *a priori* probabilities, $\{P(x[i])\}_i$, and computes bit-wise *a posteriori* probabilities, $\{P(x[i] \mid \mathbf{y})\}_i$, as shown in the block diagram model in Figure 2.10.

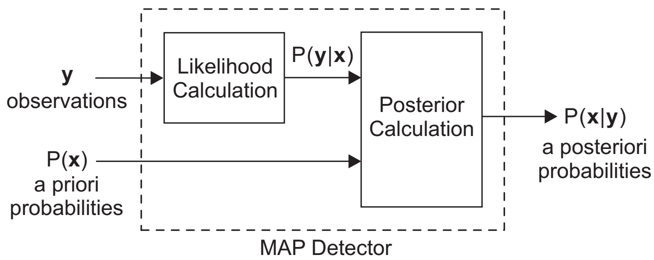

Figure 2.10: The MAP detection process in block diagram form, which takes *a priori* probabilities and observations as input and produces *a posteriori* probabilities as output

In the BCJR equalization algorithm of Section 2.3.1, the *a posteriori* probabilities are formed from the transition probabilities, $\gamma_i(S_r, S_s)$, computed from (2.56), i.e.,

$$\gamma_i(S_r, S_s) = P(x[i] = x_{r,s})p(y[i] \mid v[i] = v_{r,s}) \tag{2.86}$$

where:

- $p(y[i] \mid v[i] = v_{r,s})$ is the likelihood function, and can be interpreted as "local" evidence about which branch in the trellis was traversed; and
- $P(x[i] = x_{r,s})$ is the *a priori* information, which accounts for any prior knowledge about the probability of trellis branch being traversed.

In the separate equalization and decoding strategy of Section 2.3, the equalizer does not have any *a priori* information available, the symbols are assumed to be i.d.d ($P(x[i] = +1) = P(x[i]) = -1) = 1/2$), and the transition probabilities, $\gamma_i(S_r, S_s)$, are computed solely from the observed data $y[i]$. However, the performance of the BCJR algorithm can be greatly improved if good *a priori* information is available. In turbo equalization, the *a posteriori* probabilities from the MAP FEC decoder are fed back and used as *a priori* information by the MAP equalizer. This is performed in an iterative process where the symbol and data bit estimates become more accurate as the quality of the *a priori* information improves over a number of iterations.

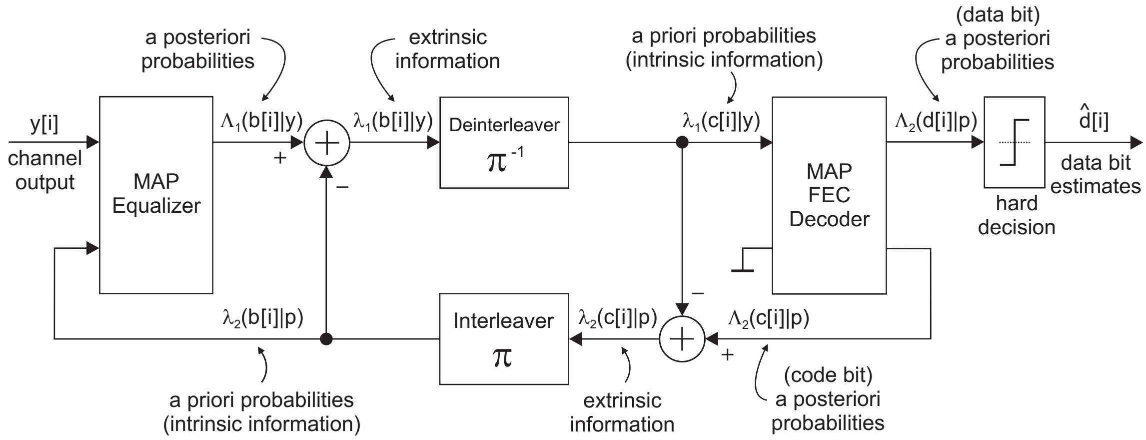

Figure 2.11: Block diagram of a turbo equalization receiver.

When designing the feedback loop structure, it is important to consider the effect that soft information generated from one bit in one of the constituent algorithms (equalizer or decoder) will have on the other bits in the other constituent algorithm.

When processing soft information input to the equalizer or the decoder, it is assumed that the soft information about each bit (or channel symbol) is independent. This assumption reduces the complexity of the equalizer and decoder algorithms. However, if the decoder formulates its soft information about a given bit, based on soft information provided to it from the equalizer about exactly the same bit, then the equalizer cannot consider this information to be independent of its channel observations. In effect, this would create a feedback loop in the overall process of length two: the equalizer informs the decoder about a given bit; and then the decoder simply reiterates to the equalizer what it already knows.

To avoid short cycles in the feedback, local minima, and limit cycle behavior in the iterative process, when soft information is passed between constituent algorithms, such information is never formed based on the information passed into the algorithm concerning the same bit. Essentially, this amounts to the equalizer only telling the decoder new information about a given bit based on information it gathered from distant parts of the received signal. Similarly, the decoder only tells the equalizer information it gathered from distant parts of the encoded bit stream. This consideration leads to the concept of extrinsic and intrinsic information [53].

For the optimal receiver in Section 2.2.2, it was shown (from (2.47)-(2.49)) that the *a posteriori* LLR, $\Lambda(d[i] \mid \mathbf{y})$, can be separated into extrinsic LLR, $\lambda(d[i] \mid \mathbf{y})$, and the intrinsic (*a priori*) LLR, $\lambda(d[i])$. Also, that $\lambda(d[i] \mid \mathbf{y})$ does not depend on $\lambda(d[i])$. In the case of the (BCJR) MAP equalization algorithm, the same functional relation can be applied to the output *a posteriori* LLRs in order to separate the two contributions. That is, the *a posteriori* LLRs, $\Lambda(b[i] \mid \mathbf{y})$, can be split into:

- extrinsic information, $\lambda(b[i] \mid \mathbf{y}) = \Lambda(b[i] \mid \mathbf{y}) - \lambda(b[i])$; and
- intrinsic information, $\lambda(b[i])$.

It is essential to the performance of turbo decoding algorithms that only *extrinsic information* is passed between the constituent decoders.

The block diagram of a turbo equalization receiver is shown in Figure 2.11. The two MAP algorithms form the core of the turbo equalizer. The MAP equalizer operates on channel observations and *a priori* information about individual bits, while the MAP FEC decoder operates on *a priori* information only. (In Figure 2.11, the observation input of the MAP decoder is grounded to indicate that it is not used). Only the extrinsic information is fed back in the iterative loop.

1. Turbo equalizer inputs:
   a) observation sequence, $\mathbf{y} = [\, y[0],\, y[1], \ldots,\, y[N-1]\,]^T$
   b) channel coefficients, $h_0, h_1, \ldots, h_L$
2. Initialization: initialize the MAP equalizer *a priori* information to all zeros, i.e., $\lambda_2(\mathbf{b} \mid \mathbf{p}) = [\,\mathbf{0}_{N\times 1}\,]$
3. Recursively compute (for a predetermined number of iterations):

$$
\begin{aligned}
\Lambda_1(\mathbf{b} \mid \mathbf{y}) &= \text{MAP Equalizer}(\ \lambda_2(\mathbf{b} \mid \mathbf{p})\ ) \\
\lambda_1(\mathbf{b} \mid \mathbf{y}) &= \Lambda_1(\mathbf{b} \mid \mathbf{y}) - \lambda_2(\mathbf{b} \mid \mathbf{p}) \\
\lambda_1(\mathbf{c} \mid \mathbf{y}) &= \text{Deinterleaver}(\ \lambda_1(\mathbf{b} \mid \mathbf{y})) \\
\Lambda_2(\mathbf{c} \mid \mathbf{p}) &= \text{MAP FEC Decoder}(\ \lambda_1(\mathbf{c} \mid \mathbf{y})\ ) \\
\lambda_2(\mathbf{c} \mid \mathbf{p}) &= \Lambda_2(\mathbf{c} \mid \mathbf{p}) - \lambda_1(\mathbf{c} \mid \mathbf{y}) \\
\lambda_2(\mathbf{b} \mid \mathbf{p}) &= \text{Interleaver}(\ \lambda_2(\mathbf{c} \mid \mathbf{p})\ )
\end{aligned}
$$

4. Turbo equalizer output: compute the data bit estimates, $\hat{d}[i]$, from the probabilities, $\Lambda_2(d[i] \mid \mathbf{y})$, using:

$$
\hat{d}[i] = \operatorname{sgn}\left(\Lambda_2(d[i] \mid \mathbf{y})\right), \quad i = 0, 1, \ldots, M-1
$$

Table 2.3: Turbo equalization algorithm

The interleaver and deinterleaver are incorporated into the iterative loop to further disperse the direct feedback effect. In particular, the BCJR algorithm creates output that is locally highly-correlated, but the use of an interleaver can largely suppress the correlations between neighboring symbols.

The operation of the turbo equalization receiver is shown in Table 2.3. The notation:

$$
\Lambda_1(\mathbf{b} \mid \mathbf{y}) = \text{MAP Equalizer}(\lambda_2(\mathbf{b} \mid \mathbf{p}))
$$

represents the generation of APP LLRs, $\Lambda_1(\mathbf{b} \mid \mathbf{y})$, by the MAP Equalizer from observations, $\mathbf{y}$, and *a priori* LLRs, $\lambda_2(\mathbf{b} \mid \mathbf{p})$, using the BCJR algorithm described in Table 2.1.

Similarly, the notation:

$$\Lambda_2(\mathbf{c} \mid \mathbf{p}) = \text{MAP FEC Decoder}(\lambda_1(\mathbf{c} \mid \mathbf{y}))$$

represents the generation of APP LLRs, $\Lambda_1(\mathbf{b} \mid \mathbf{y})$, by the MAP FEC Decoder from the *a priori* LLRs, $\lambda_2(\mathbf{c} \mid \mathbf{y})$, using the BCJR algorithm described in Table 2.2.

While the turbo equalization algorithm presented is based on two MAP algorithms, any pair of equalization and FEC decoding algorithms that make use of soft information can be used as constituent algorithms in the turbo equalizer.

For example, the linear MMSE equalizer in Section 2.3.2 can use *a priori* information about the transmitted symbol $x[i]$ to compute symbol statistics $\mathrm{E}\{x[i]\}$ and $\mathrm{Var}\{x[i]\}$ (using (2.71)-(2.72)) which are then incorporated into the MMSE filter, (2.69)-(2.70), to compute symbol estimate, $\hat{x}[i]$, and APP LLR, $\Lambda_1(x[i] \mid \mathbf{y})$. As with the MAP equalization algorithm, the APP LLR is computed the constraint that $\Lambda_1(x[i] \mid \mathbf{y})$ is not a function of the *a priori* LLR, $\lambda_2(b[i] \mid \mathbf{p})$, at the same index i. This helps to avoid short feedback cycles, and is equivalent to extracting only the extrinsic part of the information in the iterative scheme [53]. Note also that there are several low-complexity alternatives for re-estimating $\hat{x}[i]$, e.g. [53], [121], [122], [33], [120], [98], [139].

Figure 2.12 shows the performance of the turbo equalization scheme (of Figure 2.11 and Table 2.3) for the ISI channel model of Figure 2.5. The scheme is evaluated for an input data block length (M) of 512 bits with forward error correction performed by the rate-1/2 convolutional encoder of Figure 2.1b, resulting in a coded block length (N) of 1024 bits. The coded bits are scrambled using a random interleaver and mapped onto BPSK symbols.

Figure 2.12a shows the effect of receiver iterations for a turbo equalizer using the MAP symbol detector of Section 2.3.1, while Figure 2.12b shows the effect of receiver iterations for a turbo equalizer using the MMSE linear equalizer of Section 2.3.2. In both cases, FEC decoding is performed using the BCJR algorithm of Section 2.3.3. Note that zero-iterations represents the first pass when there is no *a-priori* information available for APP equalizer–this is equivalent to the separate equalization and decoding scheme (with soft information) evaluated in Section 2.3.4. The ISI-free bound represents the lower BER performance bound of the underlying rate-1/2 code used over an ISI-free channel, i.e., the performance bound for the evaluated system.

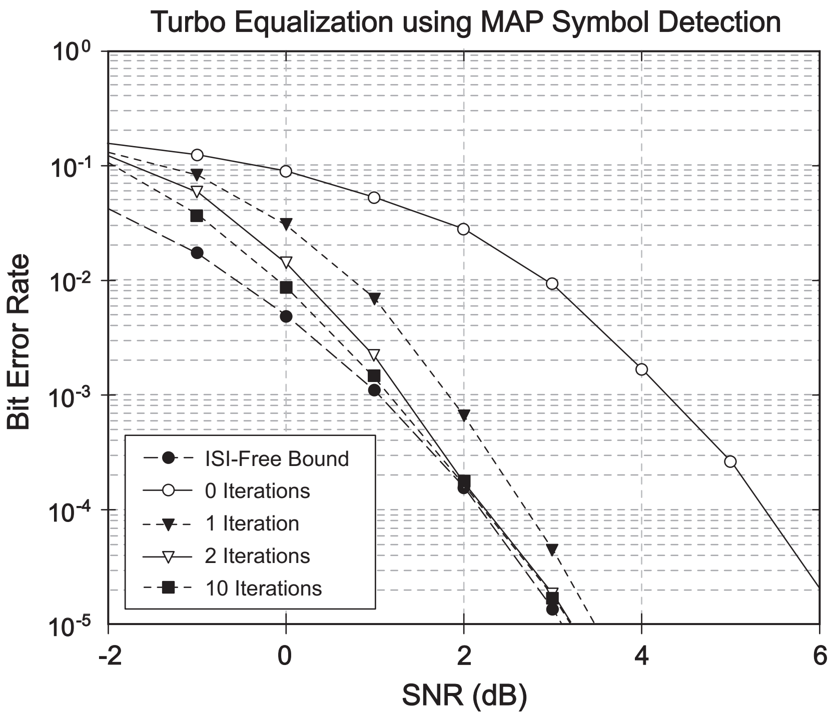

(a) Performance of turbo equalization using MAP symbol detection

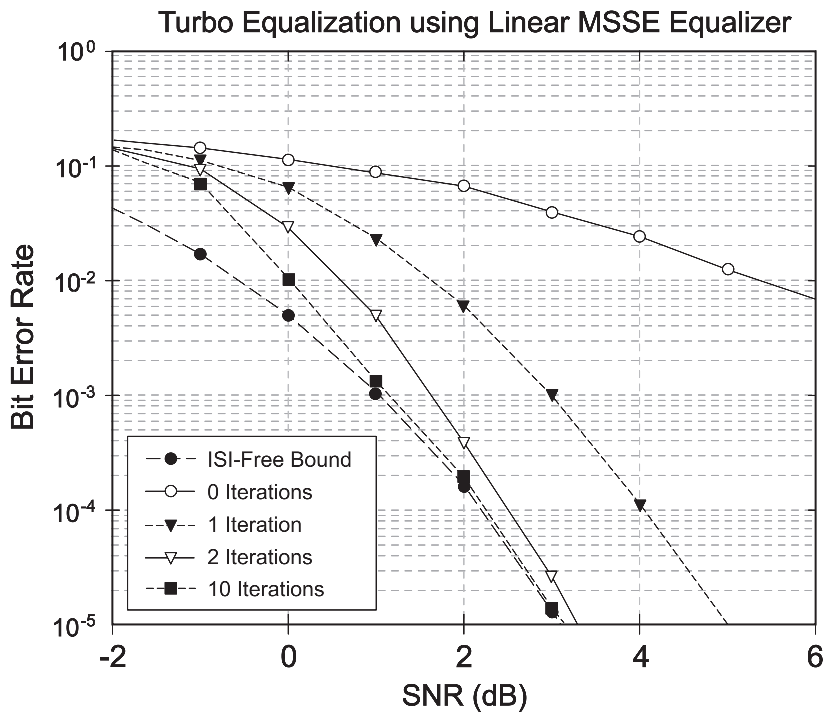

(b) Performance of turbo equalization using linear MMSE equalization

Figure 2.12: Performance of turbo equalization after 0, 1, 2, and 10 iterations using: (a) MAP symbol detection; and (b) linear MMSE equalization.

Both schemes show significant BER performance gain over the iterations, with performance approaching the ISI-free bound after 10 iterations. It is observed that turbo equalization using MAP symbol detection provides superior performance compared to the MMSE linear equalizer based scheme, but at the cost of additional computational complexity. However, it is noted that for larger block lengths, M, the performance of linear MMSE equalizer approaches that of the MAP detector [53], [121].

2.5 Code Division Multiple Access (CDMA) and Multiuser Detection

For multiuser communications, CDMA is an attractive multiple-access technique that has become widely used. Using the direct sequence spread-spectrum technique, each user spreads its signal over the entire bandwith, such that when demodulating any particular user's data, the other users' signals appear as pseudo white noise. A CDMA systems are interference limited, meaning that multiple-access interference and intersymbol interference (ISI) limit the system performance [127].

Multiuser detection (MUD) is the detection of data from multiple terminals in a communication network when observed in a nonorthogonal multiplex, that is, when derived from a nonorthogonal multiple-access channel. This situation may be the result of system design, for example, in code-division multiple-access (CDMA) systems using nonorthogonal spreading codes. It may also be the result of channel impairments in orthogonally multiplexed systems, for example, in time-division multiple-access (TDMA) wireless systems transmitting over multipath-fading delay-spread channels. Another example is digital subscriber line (DSL) systems that are impaired by crosstalk and other types of interference.

The fundamental concept of MUD is to make use of the known structure of all the users' transmitted signals, and the cross-correlations among these signals, in order to improve the data detection process. Research has shown that the use of MUD can provide significant performance advantages in interference-limited channels, and many advances have been made in recent years [127], [134], [88], [102].

Optimal MUD techniques, based on maximum-likelihood (ML) or maximum a posteriori probability (MAP) criteria, often achieve performance close to that of an interference-free system. hat is free of interference. However, these methods have high computational complexity, particularly when compared with the processing resources available in most communications receivers. As a result, considerably effort has been made to develop sub-optimal low-complexity techniques that can achieve good performance. Linear multiuser detection is a popular low-complexity technique that uses linear processing to suppress interference, followed by simple quantization to perform data detection.

The computational complexity of optimal MUD techniques is further increased when forward error correction (FEC) is considered in addition to nonorthogonal signaling. In particular, the complexity of joint MUD and FEC decoding (based on ML or MAP criteria) is prohibitively high. However, this combination can be considered as a serially concatenated coding system, where the FEC code and multiple-access channel take the roles of outer code and inner code, respectively [102]. This interpretation, provides the basis for iterative MUD techniques to be developed using the turbo decoding concept [12]. In these techniques, which are commonly known as turbo MUD [134], [88], the MUD is used to provide tentative channel-symbol decisions to the FEC channel decoders, and similarly, tentative channel-symbol decisions are produced by the channel decoders which are fed back to the MUD. Several iterations between these two constituent processes are made, with intermediate exchanges of soft channel symbol information. These turbo MUD techniques have modest computational complexity, yet have been shown to provide near-optimal performance.

2.5.1 Synchronous CDMA Signal Model

In CDMA systems, multiple users can share a common frequency band at the same time by using different signature waveforms. Consider a CDMA channel that is shared by by K simultaneous users. For simplicity, it is assumed that binary antipodal (BPSK) signals are used to transmit the information from each user. The received signal, $y(t)$, will consist of the sum of antipodally modulated synchronous signature waveforms embedded in additive white Gaussian noise:

$$y(t) = \sum_{k=1}^{K} A_k b_k s_k(t) + n(t), \qquad t \in [\,0, T\,] \tag{2.87}$$

where

- T is the symbol interval
- $s_k(t)$ is the deterministic signature waveform assigned to the k-th user.

- A_k is the received amplitude of the k-th user's signal. A_k^2 is referred to as the energy of the k-th user.
- b_k is the bit transmitted by the k-th user, $b_k \in \{-1, +1\}$
- $n(t)$ is a zero-mean white Gaussian noise (AWGN) process with power spectral density σ^2. This models noise sources that are unrelated to the transmitted signal, including thermal noise.

Each user is assigned a signature waveform $s_k(t)$ of duration T. A signature waveform may be expressed as

$$s_k(t) = \sum_{n=0}^{L-1} a_k(n) p_c(t - nT_c), \qquad t \in [\,0, T\,] \tag{2.88}$$

where $\{a_k(n), 0 \leq n \leq L-1\}$ is a pseudo-noise (PN) code sequence consisting of L chips that take values $\{\pm 1\}$, $p_c(t)$ is a pulse of duration T_c, and T_c is the chip interval. Thus, there are L chips per symbol and $T = LT_c$. The signature waveforms are assumed to be zero outside the interval $[0, T]$, and therefore, there is no intersymbol interference. Additionally, it is also assumed that all K signature waveforms have unit energy, i.e.,

$$\|s_k\|^2 = \int_0^T s_k^2(t)\,\mathrm{d}t = 1 \tag{2.89}$$

The performance of various demodulation strategies depends on the signal-to-noise ratios, A_k/σ, and on the similarity between the signature waveforms, quantified by their cross-correlations, which for the synchronous case is defined as

$$\rho_{ij} \;=\; \rho_{ij}(0) \;=\; \int_0^T s_i(t) s_j(t)\,\mathrm{d}t. \tag{2.90}$$

for the synchronous case.

2.5.2 Asynchronous CDMA Signal Model

In the synchronous model, bit epochs are aligned at the receiver. However, symbol-synchronism is not necessary for CDMA to operate, and it is possible to let the users transmit completely asynchronously. The asynchronous CDMA model is shown in Figure 2.13 where time offsets are introduced to model the lack of alignment of the bit epochs at the receiver: $\tau_k \in [0, T),\ k = 1, \ldots, K$. The symbol epochs are defined with

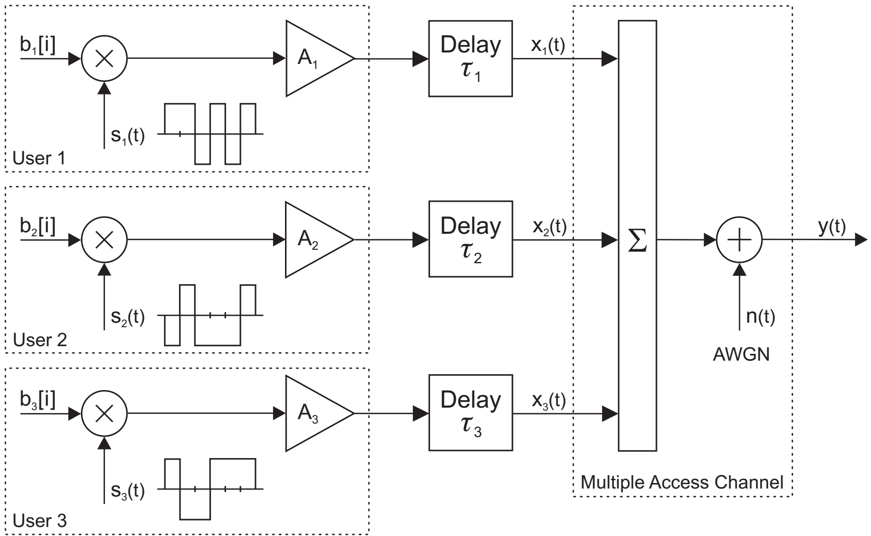

(a) Asynchronous CDMA channel model for 3 users ($K = 3$)

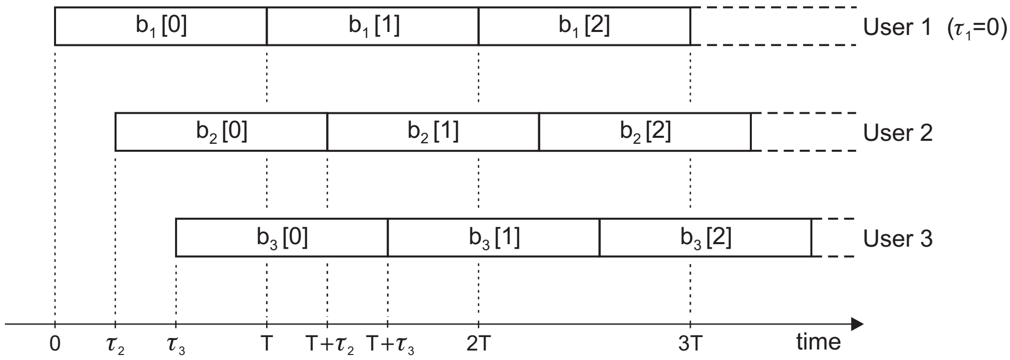

(b) Asynchronism modelling using time offsets. Bit epochs for 3 users ($K = 3$)

Figure 2.13: Asynchronous CDMA channel model and asynchronism modelling using time offsets for 3 users ($K = 3$)

respect to an arbitrary origin (it is often advantageous to take $\tau_1 = 0$). Without loss of generality, we assume that $0 \leq \tau_1 \leq \tau_2 \leq \cdots \leq \tau_K < T$. Note that we still require the symbol interval be identical for all users.

For the synchronous model it is sufficient to restrict attention to the received waveform in an interval of length T, the bit duration. In the asynchronous case we must take into account the fact that the users send a stream of bits. Without loss of generality, we assume that all users transmit packets or frames of length N. Therefore the data block for the k-th user is $\{b_k[i]\}_{i=0}^{N-1}$ Generalising (2.87) to the asynchronous case, the CDMA channel model now becomes

$$y(t) = \sum_{k=1}^{K} A_k \sum_{i=0}^{N-1} b_k[i] s_k(t - iT - \tau_k) + \sigma n(t), \qquad t \in [\,0, NT\,],\ \tau_k \in [\,0, T\,) \tag{2.91}$$

The synchronous channel corresponds to the special case of (2.91) where all the offsets are identical, $\tau_k = 0$ for $1 \leq k \leq K$.

As with the synchronous channel, asynchronous channel performance depends on the cross-correlation between the user signature waveforms. However for asynchronous CDMA, the synchronous cross-correlation definition of (2.90) is not sufficient to determine the performance, and two cross-correlations between every pair of signature waveforms must be defined, as shown in Figure 2.14. Note that $\tau = |\tau_k - \tau_j|$.

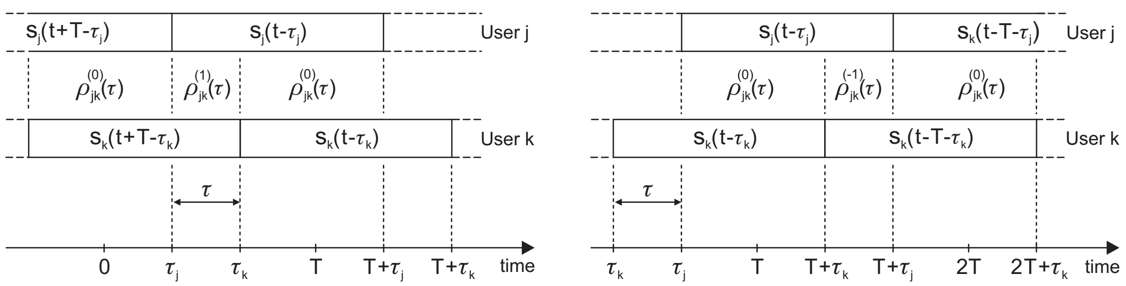

(a) $\tau_j < \tau_k$ case **(b)** $\tau_j > \tau_k$ case

Figure 2.14: Definition of asynchronous cross correlations ($0 \leq \tau_j, \tau_k < T$)

For the case where $\tau_j < \tau_k$, the cross-correlations are defined as:

$$\rho_{jk}^{(0)}(\tau) = \int_{\tau_k}^{T+\tau_j} s_j(t - \tau_j) s_k(t - \tau_k)\, \mathrm{d}t \tag{2.92}$$

$$\rho_{jk}^{(+1)}(\tau) = \int_{\tau_j}^{\tau_k} s_j(t - \tau_j) s_k(t + T - \tau_k)\, \mathrm{d}t \tag{2.93}$$

and $\rho_{jk}^{(-1)}(\tau) = 0$. For the case where $\tau_j > \tau_k$, the cross-correlations are defined as:

$$\rho_{kj}^{(-1)}(\tau) = \int_{T+\tau_k}^{T+\tau_j} s_j(t - \tau_j) s_k(t - T - \tau_k)\, \mathrm{d}t \tag{2.94}$$

$$\rho_{jk}^{(0)}(\tau) = \int_{\tau_j}^{T+\tau_k} s_j(t - \tau_j) s_k(t - \tau_k)\, \mathrm{d}t \tag{2.95}$$

and $\rho_{jk}^{(+1)}(\tau) = 0$. Note that the length of the integration interval is τ for $\rho_{jk}^{(+1)}(\tau)$ or $\rho_{kj}^{(-1)}(\tau)$ and $T - \tau$ for $\rho_{jk}^{(0)}(\tau)$.

2.5.3 Single-User Matched Filter Detector

The simplest approach to demodulate CDMA signals is the single-user matched filter (MF). This is the demodulator that was first adopted in CDMA receivers, and is often called the *conventional detector*. The matched filter is the optimal receiver for both the single-user CDMA channel and the multiuser orthogonal CDMA channel. However for the multiuser non-orthogonal CDMA channel, the performance of the matched filter is degraded by multiple-access interference (interference from other users) and is sub-optimal.

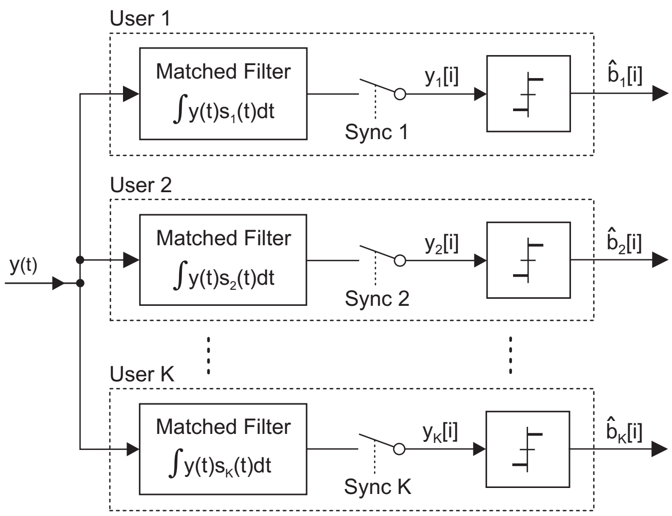

Figure 2.15: Bank of single-user matched filters

In the conventional single-user detection, the receiver for each user consist of a demodulator that correlates (or match filters) the received signal with the signature sequence of the user and passes the correlator output to the detector, which makes a decision based on the single correlator output. Thus, the conventional detector neglects the presence of the other users of the channel or, equivalently, assumes that the aggregate noise plus interference is white and Gaussian.

For the case of synchronous transmission, the output of the correlator for the k-th user for the signal in i-th code bit interval, i.e., $iT \leq t \leq (i+1)T$ is

$$y_k \triangleq \int_{iT}^{(i+1)T} y(t) s_k(t - iT)\, \mathrm{d}t \tag{2.96}$$

$$= A_k b_k[i] + \sum_{\substack{j=1 \\ j \neq k}}^{K} A_j \rho_{jk}(0) b_j[i] + n_k[i] \tag{2.97}$$

where the noise component $n_k[i]$ is given as

$$n_k[i] \triangleq \int_{iT}^{(i+1)T} n(t) s_k(t) \, \mathrm{d}t \tag{2.98}$$

If the signature sequences are orthogonal, the interference from the other users given by the middle term in (2.97) vanishes and the conventional single-user detector is optimum. On the other hand, if one or more of the other signature sequences are not orthogonal to the k-th user signature sequence, the interference from the other users can become excessive if the power levels of one or more of the other users is sufficiently larger that the power level of the k-th user. This situation is generally called the *near-far problem* in multiuser communications, and necessitates some form of power control for conventional detection.

For synchronous transmission, (2.97) can also be expressed in discrete-time matrix form:

$$\mathbf{y}[i] = \mathbf{RAb}[i] + \mathbf{n}[i] \tag{2.99}$$

where

$$\mathbf{y}[i] = [\, y_1[i],\, y_2[i],\, \ldots,\, y_K[i]\,]^T \qquad (K \times 1 \text{ vector}) \tag{2.100}$$

$$\mathbf{A} = \mathrm{diag}\{\, A_1,\, A_2,\, \ldots,\, A_K\,\} \qquad (K \times K \text{ matrix}) \tag{2.101}$$

$$\mathbf{b}[i] = [\, b_1[i],\, b_2[i],\, \ldots,\, b_K[i]\,]^T \qquad (K \times 1 \text{ vector}) \tag{2.102}$$

$$\mathbf{n}[i] = [\, n_1[i],\, n_2[i],\, \ldots,\, n_K[i]\,]^T \qquad (K \times 1 \text{ vector}) \tag{2.103}$$

and $\mathbf{R}$ is the $K \times K$ cross-correlation matrix, defined as

$$\{\mathbf{R}\}_{j,k} \;=\; \rho_{jk} \;\triangleq\; \int_0^T s_j(t) s_k(t) \, \mathrm{d}t \tag{2.104}$$

The diagonal elements of $\mathbf{R}$ are the autocorrelation factors, ρ_{jj}, and are equal to 1. For the synchronous case, $\mathbf{R}$ is symmetric and the cross-correlation factors have the feature: $\rho_{jk} = \rho_{kj}$.

In asynchronous transmission, the conventional detector is more vulnerable to interference from other users. This is because it is not possible to design signature sequences for any pair of users that are orthogonal for all time offsets. Consequently, interference from other users is unavoidable in asynchronous transmission with the conventional single-user detection. In such a case, the near-far problem resulting from unequal power in the signals transmitted by the various users is particularly serious. The practical solution generally requires a power adjustment method that is controlled by the receiver via a separate communications channel that all users are continuously monitoring. Another option is to employ one of the multiuser detectors described in the following sections.

2.6 The Optimum Multiuser Receiver

The optimum receiver is defined as the receiver that selects the most probable sequence of bits $\{b_k[i], 0 \leq i \leq N-1,\ 1 \leq k \leq K\}$ given the received signal $y(t)$ observed over the time interval $0 \leq t \leq NT$ for synchronous transmission, or $0 \leq t \leq NT + 2T$ for asynchronous transmission.

2.6.1 Synchronous Transmission

In synchronous transmission, each (user) interferer produces exactly one symbol which interferes with the desired symbol. In additive white Gaussian noise, it is sufficient to consider the signal received in one signal interval, $iT \leq t \leq (i+1)T$, and determine the optimum receiver. Hence $y(t)$ may be expressed as

$$y(t) = \sum_{k=1}^{K} A_k b_k[i] s_k(t) + n(t), \qquad t \in [\, iT,\, (i+1)T\,]. \tag{2.105}$$

The optimum maximum-likelihood receiver computes the likelihood function, $L(\mathbf{b}[i])$, for all 2^K possible combinations of information sequence $\mathbf{b}[i] = [b_1[i], b_2[i], \ldots, b_K[i]]^T$, and then selects the sequence of $\mathbf{b}[i]$ that maximises $L(\mathbf{b}[i])$. For synchronous CDMA, $L(\mathbf{b}[i]) = f(y(t) \mid \mathbf{b}[i])$, and [127]

$$f(y(t) \mid \mathbf{b}[i]) = \exp\left\{ -\frac{1}{2\sigma^2} \int_{iT}^{(i+1)T} [\, y(t) - x(t; \mathbf{b}[i])\,]^2 \,\mathrm{d}t \right\},\ t \in [\, iT,\, (i+1)T\,] \tag{2.106}$$

where

$$x(t;\mathbf{b}[i]) = \sum_{k=1}^{K} b_k[i] A_k s_k(t), \quad t \in [\, iT,\, (i+1)T\,] \tag{2.107}$$

Equivalently, the most likely $\mathbf{b}[i]$ also maximises [127]

$$\begin{aligned}\Omega(\mathbf{b}[i]) &= 2\int_{iT}^{(i+1)T} \left[\sum_{k=1}^{K} A_k b_k[i] s_k(t)\right] y(t)\,\mathrm{d}t - \int_{iT}^{(i+1)T} \left[\sum_{k=1}^{K} A_k b_k[i] s_k(t)\right]^2 \mathrm{d}t \\ &= 2\mathbf{b}^T[i]\mathbf{A}\mathbf{y}[i] - \mathbf{b}^T[i]\mathbf{A}\mathbf{R}\mathbf{A}\mathbf{b}[i] \end{aligned} \tag{2.108}$$

The expression (2.108) shows that the dependence of the likelihood function of the received signals is through the vector of matched filter outputs $\mathbf{y}[i]$, which is therefore a sufficient statistic for demodulating the transmitted data.

There are 2^K possible choices of the bits in the information sequences of the K users. The optimum detector computes the correlation metrics for each sequence and selects the sequence that yields the largest correlation metric. Therefore the optimum detector has a complexity that grows exponentially with the number of users K.

2.6.2 Asynchronous Transmission

In this case, there are exactly two consecutive symbols from each interferer that overlap a desired symbol. We assume that the receiver knows the received signal energies $\{A_k^2\}$ for the K users and the transmission delays $\{\tau_k\}$. We view the K-user N-frame asynchronous channel as a $(K \times N)$-user asynchronous channel. Let us define $\mathbf{b}_n$, a KN-vector, with components

$$\mathbf{b}_n = \left[\, \mathbf{b}^T[0],\, \mathbf{b}^T[1],\, \ldots,\, \mathbf{b}^T[N-1]\,\right]^T \qquad (KN \times 1 \text{ vector}) \tag{2.109}$$

and the KN-vector of matched-filter outputs $\mathbf{y}_n$,

$$\mathbf{y}_n = \left[\, \mathbf{y}^T[0],\, \mathbf{y}^T[1],\, \ldots,\, \mathbf{y}^T[N-1]\,\right]^T \qquad (KN \times 1 \text{ vector}) \tag{2.110}$$

where $\mathbf{y}[i] = [\ y_1[i],\ y_2[i],\ \ldots,\ y_K[i]\ ]^T$ with components

$$y_k[i] \triangleq \int_{iT+\tau_k}^{(i+1)T+\tau_k} y(t) s_k(t - iT - \tau_k)\, \mathrm{d}t \qquad 0 \leq i \leq N-1 \tag{2.111}$$

The integral (2.111) represents the outputs of the correlator or matched filter for the k-th user in each of the signal intervals. This means that the $y_k[i]$ is the output of the k-th matched filter applied to the signal in the interval $[\tau_k + iT, \tau_k + (i+1)T]$, that is, the interval corresponding to $b_k[i]$.

Using vector notation, the $K \times N$ correlator or matched filter outputs $\{y_k[i]\}$ can be expressed in the form

$$\mathbf{y}_n = \mathbf{R}_n \mathbf{A}_n \mathbf{b}_n + \mathbf{n}_n \tag{2.112}$$

with the following vector and matrix definitions: $\mathbf{R}_n$ is the asynchronous cross-correlation matrix,

$$\mathbf{R}_n = \begin{bmatrix} \mathbf{R}^{(0)} & \mathbf{R}^{(-1)} & \mathbf{0} & \mathbf{0} & \cdots & \mathbf{0} \\ \mathbf{R}^{(1)} & \mathbf{R}^{(0)} & \mathbf{R}^{(-1)} & \mathbf{0} & \cdots & \mathbf{0} \\ \mathbf{0} & \ddots & \ddots & & & \vdots \\ \vdots & & & \ddots & \ddots & \mathbf{0} \\ \mathbf{0} & \cdots & \mathbf{0} & \mathbf{R}^{(1)} & \mathbf{R}^{(0)} & \mathbf{R}^{(-1)} \\ \mathbf{0} & \cdots & \mathbf{0} & \mathbf{0} & \mathbf{R}^{(1)} & \mathbf{R}^{(0)} \end{bmatrix} \qquad (KN \times KN \text{ matrix}) \tag{2.113}$$

where $\mathbf{R}^{(-1)}$, $\mathbf{R}^{(0)}$, and $\mathbf{R}^{(1)}$ are $K \times K$ matrices with elements

$$\{\mathbf{R}^{(-1)}\}_{j,k} = \rho_{jk}^{(-1)}(\tau), \quad \{\mathbf{R}^{(0)}\}_{j,k} = \rho_{jk}^{(0)}(\tau), \quad \text{and} \quad \{\mathbf{R}^{(1)}\}_{j,k} = \rho_{jk}^{(1)}(\tau).$$

Note that the asynchronous cross-correlations, $\rho_{jk}^{(-1)}(\tau)$, $\rho_{jk}^{(0)}(\tau)$, and $\rho_{jk}^{(1)}(\tau)$, are defined in (2.92)-(2.95). $\mathbf{A}_n$ is the diagonal matrix,

$$\mathbf{A}_n = \begin{bmatrix} \mathbf{A} & \mathbf{0} & \cdots & \mathbf{0} \\ \mathbf{0} & \mathbf{A} & & \mathbf{0} \\ \vdots & \vdots & \ddots & \vdots \\ \mathbf{0} & \mathbf{0} & \cdots & \mathbf{A} \end{bmatrix} \qquad (KN \times KN \text{ matrix}) \tag{2.114}$$

where $\mathbf{A}$ is the $K \times K$ diagonal matrix defined in (2.101), and $\mathbf{n}_N$ is the vector,

$$\mathbf{n}_n = \left[\, \mathbf{n}^T[0],\ \mathbf{n}^T[1],\ \cdots,\ \mathbf{n}^T[N-1] \,\right]^T \qquad (KN \times 1 \text{ vector}) \tag{2.115}$$

For the asynchronous case, the maximum-likelihood receiver computes the likelihood function $L(\mathbf{b_n})$ for all 2^{KN} possible combinations of $\mathbf{b}_n$, and then selects the sequence $\mathbf{b}_n$ that maximises $L(\mathbf{b_n})$. For this case, $L(\mathbf{b_n}) = f(y(t) \mid \mathbf{b}_n)$, and [127]

$$f(y(t) \mid \mathbf{b}_n) = \exp\left\{ -\frac{1}{2\sigma^2} \int_0^{NT+2T} \left[\, y(t) - x(t; \mathbf{b}_n) \,\right]^2 \,\mathrm{d}t \right\},\ t \in [0, NT+2T] \tag{2.116}$$

where

$$x(t; \mathbf{b}_n) = \sum_{k=1}^{K} \sum_{i=0}^{N-1} b_k[i] A_k s_k(t - iT - \tau_k), \quad t \in [0, NT+2T]. \tag{2.117}$$

Equivalently, the most likely $\mathbf{b}_n$ also maximises [127]

$$\begin{aligned} \Omega(\mathbf{b}_n) &= 2\int_0^{NT+2T} x(t; \mathbf{b}_n) y(t) \,\mathrm{d}t - \int_0^{NT+2T} \left(\, x(t; \mathbf{b}_n) \,\right)^2 \,\mathrm{d}t \\ &= 2\mathbf{b}_n^T \mathbf{A}_n \mathbf{y}_n - \mathbf{b}_n^T \mathbf{A}_n \mathbf{R}_n \mathbf{A}_n \mathbf{b}_n. \end{aligned} \tag{2.118}$$

Once more, the observations enter in the function to be maximised by jointly optimum decisions on through the matched filter outputs. Therefore, $\mathbf{y}_n$ is a sufficient statistic for $\mathbf{b}_n$. The vector $\mathbf{y}_n$ given by (2.112) constitutes a set of sufficient statistics for estimating the transmitted bits $b_k[i]$.

If we adopt a block processing approach, the optimum ML detector must compute 2^{KN} likelihood functions and select the K sequences of length N that corresponds to the greatest likelihood value. Clearly such an approach is much too complex computationally to be implemented in practice, especially when K and N are large. An alterative approach is ML sequence estimation employing the Viterbi algorithm. In order to construct a sequential-type detector, we make use of the fact that each transmitted symbol overlaps at most with $2K-2$ symbols. Thus, a significant reduction in computational complexity is obtained with respect to the block-size parameter N, but the exponential dependence on K cannot be reduced. It is apparent that the optimum ML receiver employing the Viterbi algorithm also involves such a high computational complexity that its practical use is limited. In the following sections, a number of suboptimum detectors whose complexity grows linearly with K are considered.

2.7 Linear Multiuser Detectors

The matched filter (conventional detector) has a complexity that grows linearly with the number of users, K. But susceptibility to MAI from non-orthogonal users means that the matched filter may make errors even in the absence of noise. In contrast, the optimum receiver demodulates the data error-free in the absence of noise, but has a computational complexity that grows exponentially with the number of users, K. In this section, we consider linear multiuser detectors with computational complexities that grow linearly with K, but do not exhibit vulnerability to interference from other users.

2.7.1 Decorrelating Detector

Firstly, the case of symbol-synchronous transmission is considered. In this case, the output of the K matched filters in the i-th code bit interval is represented by the received signal vector, $\mathbf{y}[i]$, given by

$$\mathbf{y}[i] = \mathbf{RAb}[i] + \mathbf{n}[i] \tag{2.119}$$

where $\mathbf{R}$, $\mathbf{A}$, $\mathbf{b}[i]$, and $\mathbf{n}[i]$ are defined in (2.104), (2.101), (2.102), and (2.103), respectively. Noise vector $n[i]$ has a covariance

$$E\{\mathbf{n}[i]\mathbf{n}^T[i]\} = \sigma^2\mathbf{R}. \tag{2.120}$$

Since the noise is Gaussian, $\mathbf{y}[i]$ is described by a K-dimensional Gaussian PDF with mean $\mathbf{RAb}[i]$ and covariance $\mathbf{R}$. That is [93],

$$p(\mathbf{y}[i] \mid \mathbf{b}[i]) = \frac{1}{\sqrt{(2\pi\sigma^2)^K \det \mathbf{R}}} \exp\left\{-\frac{1}{2\sigma^2}(\mathbf{y}[i] - \mathbf{RAb}[i])^T\mathbf{R}^{-1}(\mathbf{y}[i] - \mathbf{RAb}[i])\right\} \tag{2.121}$$

The best linear estimate of $\mathbf{b}[i]$, denoted by $\mathbf{b}^0[i]$, is defined as the value of $\mathbf{b}[i]$ that minimises the likelihood function

$$L(\mathbf{b}[i]) = (\mathbf{y}[i] - \mathbf{RAb}[i])^T \mathbf{R}^{-1} (\mathbf{y}[i] - \mathbf{RAb}[i]), \tag{2.122}$$

and hence [69],

$$\mathbf{b}^0[i] = \arg\min_{\mathbf{b}[i]} (\mathbf{y}[i] - \mathbf{RAb}[i])^T \mathbf{R}^{-1} (\mathbf{y}[i] - \mathbf{RAb}[i]). \tag{2.123}$$

The result of this minimisation yields

$$\mathbf{b}^0[i] = \mathbf{A}^{-1}\mathbf{R}^{-1}\mathbf{y}[i], \tag{2.124}$$

and the ML estimates of the detected symbols, $\hat{b}_k[i]$, is given by

$$\begin{aligned}\hat{b}_k[i] &= \operatorname{sgn}\left(\frac{1}{A_k}\left\{\mathbf{R}^{-1}\mathbf{y}[i]\right\}_k\right) \\ &= \operatorname{sgn}\left(\left\{\mathbf{R}^{-1}\mathbf{y}[i]\right\}_k\right) \quad \text{for } k = 1, \ldots, K.\end{aligned} \tag{2.125}$$

Note that the estimate $\mathbf{b}^0[i]$ is also the best linear estimate that maximises the likelihood function given by (2.108). Since $\mathbf{y}[i] = \mathbf{RAb}[i] + \mathbf{n}[i]$, it follows from (2.124) that [69]

$$\mathbf{b}^0[i] = \mathbf{b}[i] + \mathbf{A}^{-1}\mathbf{R}^{-1}\mathbf{n}[i] \tag{2.126}$$

Therefore, $\mathbf{b}^0[i]$ is an unbiased estimate of $\mathbf{b}$. The transformation $\mathbf{R}^{-1}$ has eliminated the interference components between the users, and as a consequence, the near-far problem is also eliminated. The decorrelating detector is so-called because the linear transformation $\mathbf{R}^{-1}$ is used to tune out or *decorrelate* the multiuser interference. Figure 2.16 illustrates the receiver structure. The symbol estimates $\hat{b}_k[i]$ are obtained by performing the linear transformation $\mathbf{R}^{-1}$ on the vector of matched filter outputs $\mathbf{y}[i]$, and therefore, the computational complexity is linear in K.

In asynchronous transmission, the received signal at the output of the matched filters is given by (2.112). The best linear estimate of $\mathbf{b}_n$, denoted by $\mathbf{b}_n^0$, is the value of $\mathbf{b}_n$ that minimises the likelihood function [93]

$$L(\mathbf{b}_n) = (\mathbf{y}_n - \mathbf{R}_n\mathbf{A}_n\mathbf{b}_n)^T \mathbf{R}_n^{-1} (\mathbf{y}_n - \mathbf{R}_n\mathbf{A}_n\mathbf{b}_n) \tag{2.127}$$

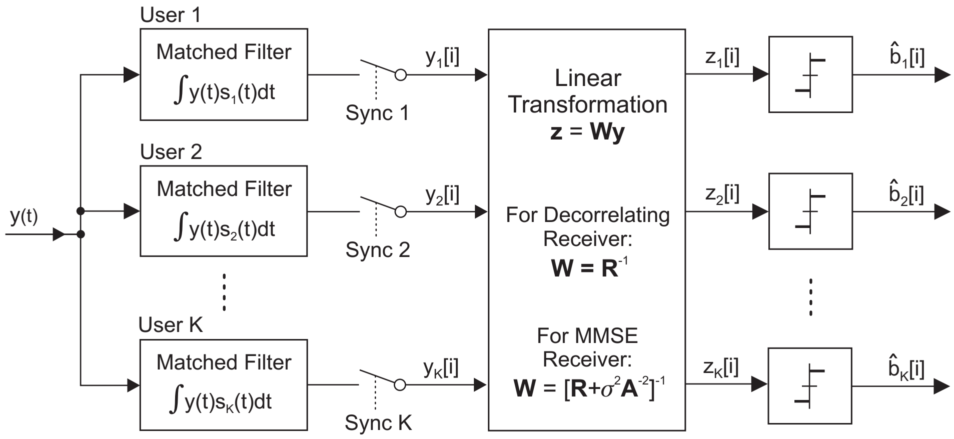

Figure 2.16: Linear multiuser detector for synchronous CDMA systems

and hence,

$$\mathbf{b}_n^0 = \arg\min_{\mathbf{b}[i]} (\mathbf{y}_n - \mathbf{R}_n\mathbf{A}_n\mathbf{b}_n)^T\mathbf{R}_n^{-1}(\mathbf{y}_n - \mathbf{R}_n\mathbf{A}_n\mathbf{b}_n). \tag{2.128}$$

The result of this minimisation yields [70]

$$\mathbf{b}_n^0 = \mathbf{A}_n^{-1}\mathbf{R}_n^{-1}\mathbf{y}_n \tag{2.129}$$

This is the ML estimate of $\mathbf{b}_n$ and it is again obtained by performing a linear transformation of the outputs from the bank of correlators or matched filters. The estimate $\mathbf{b}_n^0$ is unbiased, and therefore the multiuser interference has been completely eliminated. Therefore the linear decorrelating detector is effective in eliminating multiuser interference for both synchronous and asynchronous transmissions.

2.7.2 Minimum Mean-Square-Error Detector

In the previous section, the decorrelating detector obtains the linear ML estimate of $\mathbf{b}[i]$ by minimising the quadratic likelihood function of (2.122) for synchronous CDMA, or (2.127) for asynchronous CDMA. This is achieved by applying the linear transformation $\mathbf{b}^0[i] = \mathbf{R}^{-1}\mathbf{y}[i]$ to the outputs of the bank of correlators or matched filters, $\mathbf{y}[i]$.

Another approach is to seek the linear transformation $\mathbf{b}^0[i] = \mathbf{W}\mathbf{y}[i]$, where the matrix $\mathbf{W}$ is to be determined so as to minimise the mean square error (MSE) [93]:

$$\begin{aligned}\mathrm{MSE}(\mathbf{b}[i]) &= \mathrm{E}\left\{\mathbf{A}(\mathbf{b}[i]-\mathbf{b}^0[i])^T\mathbf{A}(\mathbf{b}[i]-\mathbf{b}^0[i])\right\}\\ &= \mathrm{E}\left\{(\mathbf{A}\mathbf{b}[i]-\mathbf{W}\mathbf{y}[i])^T(\mathbf{A}\mathbf{b}[i]-\mathbf{W}\mathbf{y}[i])\right\}\end{aligned} \tag{2.130}$$

where the expectation is with respect to the data vector $\mathbf{b}[i]$ and the additive noise $\mathbf{n}[i]$. The optimum matrix $\mathbf{W}$ may be found by forcing the error $(\mathbf{b}[i]-\mathbf{W}\mathbf{y}[i])$ to be orthogonal to the data vector $\mathbf{y}[i]$. Thus

$$\begin{aligned}\mathrm{E}\left\{(\mathbf{A}\mathbf{b}[i]-\mathbf{W}\mathbf{y}[i])\mathbf{y}^T[i]\right\} &= 0\\ \mathrm{E}\left\{\mathbf{A}\mathbf{b}[i]\mathbf{y}^T[i]\right\}-\mathbf{W}\mathrm{E}\left\{\mathbf{y}[i]\mathbf{y}^T[i]\right\} &= 0\end{aligned} \tag{2.131}$$

Consider the case of synchronous transmission. We have

$$\mathrm{E}\{\mathbf{A}\mathbf{b}[i]\mathbf{y}^T[i]\} = \mathrm{E}\{\mathbf{A}\mathbf{b}[i]\mathbf{A}\mathbf{b}^T[i]\}\mathbf{R}^T = \mathbf{A}^2\mathbf{R}^T \tag{2.132}$$

and

$$\begin{aligned}\mathrm{E}\{\mathbf{y}[i]\mathbf{y}^T[i]\} &= \mathrm{E}\left\{(\mathbf{R}\mathbf{A}\mathbf{b}[i]+\mathbf{n}[i])(\mathbf{R}\mathbf{A}\mathbf{b}[i]+\mathbf{n}[i])^T\right\}\\ &= \mathbf{R}\mathbf{A}^2\mathbf{R}^T+\sigma^2\mathbf{R}^T\end{aligned} \tag{2.133}$$

By substituting (2.132) and (2.133) into (2.131) and solving for $\mathbf{W}$. We obtain

$$\mathbf{W} = \left(\mathbf{R}+\sigma^2\mathbf{A}^{-2}\right)^{-1} \tag{2.134}$$

Therefore, the minimum mean square error (MMSE) estimate of $\mathbf{b}[i]$ is [140] [73]

$$\mathbf{b}^0[i] = \mathbf{A}^{-1}\left(\mathbf{R}+\sigma^2\mathbf{A}^{-2}\right)^{-1}\mathbf{y}[i] \tag{2.135}$$

and the estimated symbols are obtained by

$$\begin{aligned}\hat{b}_k[i] &= \mathrm{sgn}\left(\frac{1}{A_k}\left\{\left(\mathbf{R}+\sigma^2\mathbf{A}^{-2}\right)^{-1}\right\}_k\right)\\ &= \mathrm{sgn}\left(\left\{\left(\mathbf{R}+\sigma^2\mathbf{A}^{-2}\right)^{-1}\right\}_k\right) \quad \text{for } k=1,\ldots,K\end{aligned} \tag{2.136}$$

The MMSE criterion produces a biased estimate of $\mathbf{b}$, hence there is some residual multiuser interference. Note that in the high-SNR case when $\sigma^2 \to 0$, then

$$\left(\mathbf{R} + \sigma^2 \mathbf{A}^{-2}\right)^{-1} \to \mathbf{R}^{-1} \tag{2.137}$$

and the MMSE solution approaches the ML solution in (2.129). In this case, the MMSE detector becomes equivalent to the decorrelator detector. On the other hand, in the low-SNR case when $\sigma^2 \mathbf{A}^{-2} \gg \mathbf{R}$, then

$$\left(\mathbf{R} + \sigma^2 \mathbf{A}^{-2}\right)^{-1} \to \sigma^{-2} \mathbf{A}^2 \tag{2.138}$$

and the detector essentially ignores the interference from other users because the additive noise is the dominant term . In this case the MMSE detector becomes equivalent to the matched filter detector with amplitude scaling to compensate for the received power levels. Figure 2.16 illustrates the receiver structure for linear MMSE detector.

Similarly, for asynchronous transmission, the matrix $\mathbf{W}$ is chosen so as to minimise the mean square error (MSE):

$$\mathrm{MSE}(\mathbf{b}_n) = \mathrm{E}\left\{(\mathbf{A}_n \mathbf{b}_n - \mathbf{W}\mathbf{y}_n)^T (\mathbf{A}_n \mathbf{b}_n - \mathbf{W}\mathbf{y}_n)\right\} \tag{2.139}$$

In this case, the optimum choice of $\mathbf{W}$ is

$$\mathbf{W} = \left(\mathbf{R}_n + \sigma^2 \mathbf{A}_n^{-2}\right)^{-1} \tag{2.140}$$

and, hence the MMSE estimate of $\mathbf{b}_n$ is [140] [73]

$$\mathbf{b}_n^0 = \mathbf{A}_n^{-1} \left(\mathbf{R}_n + \sigma^2 \mathbf{A}_n^{-2}\right)^{-1} \mathbf{y}_n \tag{2.141}$$

The output of the MMSE detector is then $\hat{\mathbf{b}}_n = \mathrm{sgn}(\mathbf{b}_n^0)$.

2.8 Turbo Multiuser Detection for Synchronous CDMA

We consider a convolutionally coded synchronous real-valued CDMA system with K users, employing normalised signature waveforms $s_1, s_2, \ldots, s_K$, and tranmitting through an additive white Gaussian noise channel. The block diagram of the transmitter structure for this system is shown in Figure 2.17. The binary data sequence $\{d_k[i]\}_{i=0}^{M-1}$ for user

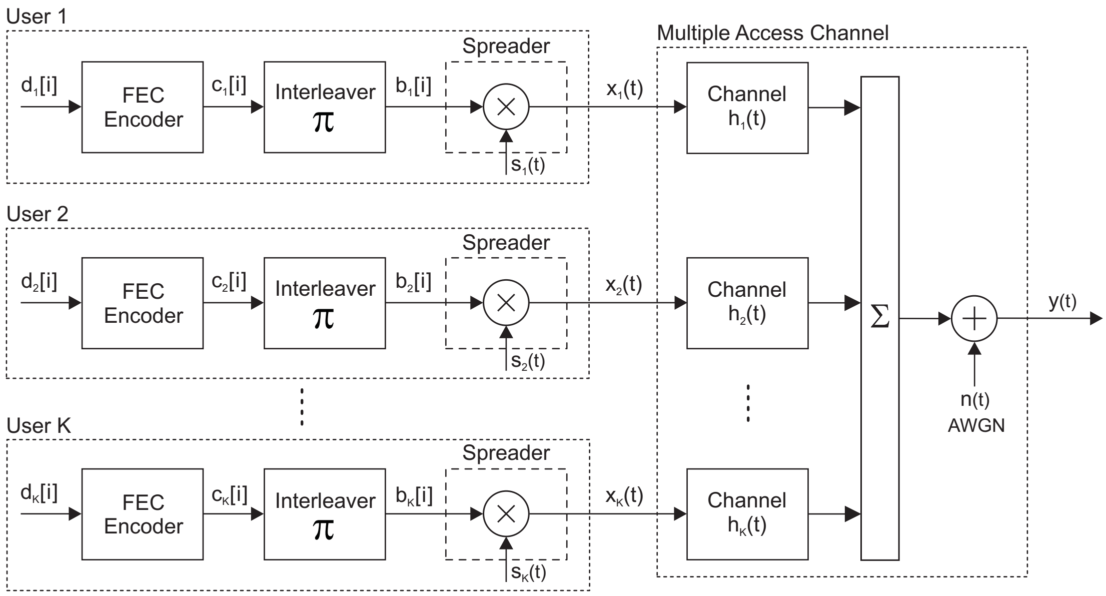

Figure 2.17: Coded CDMA Transmitter Structure

k, $k = 1, \ldots, K$, is convolutionally encoded with code rate R_c, by the FEC encoder, producing the code-bit sequence $\{c_k[i]\}_{i=0}^{N-1}$ for user k. A code-bit interleaver is used to reduce the influence of the error bursts at the input of each channel decoder. The interleaved code bits of the k-th user are BPSK modulated, yielding data symbols of duration T. Each data symbol $b_k[i]$ is then spread by a signature waveform $s_k[t]$ and transmitted through the channel.

The received continuous-time signal, $y(t)$, can be written as

$$y(t) = \sum_{k=1}^{K} A_k \sum_{i=0}^{N-1} b_k[i] s_k(t - iT) + n(t), \tag{2.142}$$

where $n(t)$ is a zero-mean white Gaussian noise process with power spectral density σ^2, and A_k is the amplitude of the k-th user.

The turbo receiver structure is shown in Figure 2.18. It consists of two stages: a soft-input soft-output (SISO) multiuser detector, followed by K parallel single-user MAP channel decoders. The two stages are separated by deinterleavers and interleavers. The SISO multiuser detector computes the *a posteriori* log-likelihood ratio (LLR) of a transmitted "+1" and a transmitted "-1" for every code bit of each user, i.e.,

$$\Lambda_1(b_k[i]) \triangleq \log \frac{P(b_k[i] = +1 \mid y(t))}{P(b_k[i] = -1 \mid y(t))}, \qquad k = 1, \ldots, K, \quad i = 0, \ldots, N-1. \tag{2.143}$$

Using Bayes' rule, (2.143) can be rewritten as

$$\Lambda_1(b_k[i]) \triangleq \underbrace{\log \frac{p(y(t) \mid b_k[i] = +1)}{p(y(t) \mid b_k[i] = -1)}}_{\lambda_1(b_k[i])} + \underbrace{\log \frac{P(b_k[i] = +1)}{P(b_k[i] = -1)}}_{\lambda_2(b_k[i])}, \tag{2.144}$$

where the second term in (2.144), denoted by $\lambda_2(b_k[i])$, represents the *a priori* LLR of the code bit $b_k[i]$, which is computed by the MAP channel decoder of the k-th user in the previous iteration, interleaved and then fed back to the SISO multiuser detector. For the first iteration, assuming equally likely code bits (i.e., no prior information available), we then have $\lambda_2(b_k[i]) = 0$ for $1 \leq k \leq K$ and $0 \leq i < N$. The first term in (2.144), denoted by $\lambda_1(b_k[i])$, represents the *extrinsic* information delivered by the SISO multiuser detector based on the received signal $y(t)$, the structure of the multiuser signal given by (2.142), the prior information about the code bits of all the other users, $\{\lambda_2(b_l[i])\}_{i;\, l\neq k}$, and the prior information about the code bits of the k-th user other than the i-th bit, $\{\lambda_2(b_k[j])\}_{j\neq i}$. The extrinsic information $\{\lambda_1(b_k[i])\}_i$, of the k-th user, which is not influenced by the *a priori* information $\{\lambda_2(b_k[i])\}_i$ provided by the MAP channel decoder, is then reverse interleaved and fed into the k-th user's channel decoder as the *a priori* information in the next iteration.

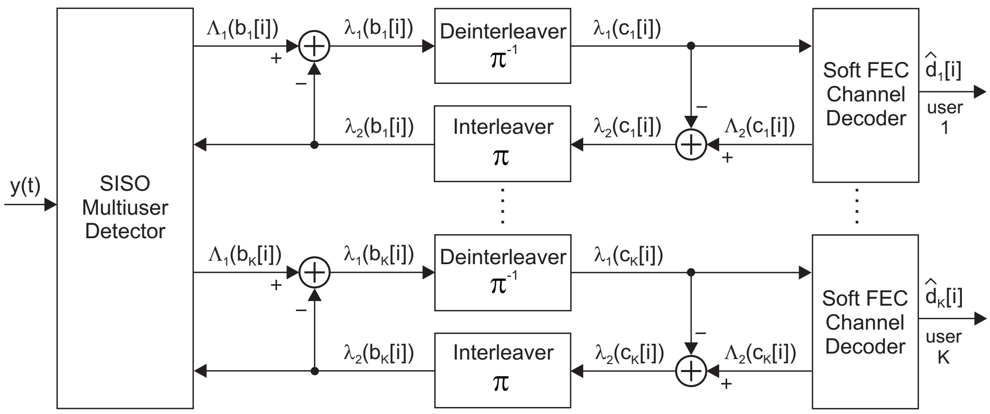

Figure 2.18: Coded CDMA Turbo Multiuser Receiver Structure

Denote the code-bit sequence of the k-th user after deinterleaving as $\{c_k[i]\}_i$. Based on the prior information $\{\lambda_1(c_k[i])\}_i$ and the trellis structure of the channel code (i.e., the constraints imposed by the code), the k-th user's MAP channel decoder computes the *a posteriori* LLR of each code bit,

$$\Lambda_2(c_k[i]) \triangleq \log \frac{P(c_k[i] = +1 \mid \{\lambda_1(c_k[i])\}_i \,;\, \text{code structure})}{P(c_k[i] = -1 \mid \{\lambda_1(c_k[i])\}_i \,;\, \text{code structure})}$$
$$= \lambda_2(c_k[i]) + \lambda_1(c_k[i]), \tag{2.145}$$

for $k = 1, \ldots, K$, and $i = 0, \ldots, N-1$. From (2.145), it can be seen that the output of the MAP channel decoder is the sum of the prior information $\lambda_1(c_k[i])$ and the extrinsic information $\lambda_2(c_k[i])$ delivered by the MAP channel decoder. This extrinsic information is the information about the code bit $c_k[i]$ gathered from prior information about the other code bits, $\{\lambda_1(c_k[j])\}_{j \neq i}$, based on the trellis constraint of the code. The MAP channel decoder also computes the *a posteriori* LLR of every information bit, which is used to make a decision on the decoded bit at the last iteration. After interleaving, the extrinsic information delivered by the K MAP channel decoders $\{\lambda_2(b_k[i])\}_{i;k}$ is then fed back to the SISO multiuser detector, as the prior information about the code bits of all users, in the next iteration. Note that at the first iteration, the extrinsic information quantities $\{\lambda_1(b_k[i])\}_{i;k}$ and $\{\lambda_2(b_k[i])\}_{i;k}$ are statistically independent. But subsequently, since they use the same information indirectly, they will become more and more correlated, which will result in diminishing improvement through iteration.

2.8.1 Optimal SISO Multiuser Detector

For the synchronous CDMA system, a sufficient statistic for demodulating the i-th code bits of the K users is given by the K-vector $\mathbf{y}[i] = [\, y_1[i], \, \ldots, \, y_K[i] \,]^T$, whose k-th component is the output of a filter matched to $s_k(\,\cdot\,)$ in the i-th code bit interval, i.e., (2.96). From Section 2.5.3, the sufficient statistic vector $\mathbf{y}[i]$ can be written as (2.99)

$$\mathbf{y}[i] = \mathbf{R}\mathbf{A}\mathbf{b}[i] + \mathbf{n}[i], \tag{2.146}$$

In what follows, the symbol index i is dropped whenever possible to simplify the notation. Denote

$$\mathcal{B}_k^+ \triangleq \{(b_1, \ldots, b_{k-1}, +1, b_{k+1}, \ldots, b_K) \;:\; b_j \in \{+1, -1\}\}\,,$$
$$\mathcal{B}_k^- \triangleq \{(b_1, \ldots, b_{k-1}, -1, b_{k+1}, \ldots, b_K) \;:\; b_j \in \{+1, -1\}\}\,,$$

From (2.146), the extrinsic information $\lambda_1(b_k)$ delivered by the SISO multiuser detector is then given by [134]

$$\begin{aligned}\lambda_1(b_k) &\triangleq \log \frac{p(\mathbf{y} \mid b_k = +1)}{p(\mathbf{y} \mid b_k = -1)} \\ &= \log \frac{\sum_{\mathbf{b} \in \mathcal{B}_k^+} \left\{ \exp\left\{ -\frac{1}{2\sigma^2} (\mathbf{y} - \mathbf{RAb})^T \mathbf{R}^{-1} (\mathbf{y} - \mathbf{RAb}) \right\} \prod_{j \neq k} P(b_j) \right\}}{\sum_{\mathbf{b} \in \mathcal{B}_k^-} \left\{ \exp\left\{ -\frac{1}{2\sigma^2} (\mathbf{y} - \mathbf{RAb})^T \mathbf{R}^{-1} (\mathbf{y} - \mathbf{RAb}) \right\} \prod_{j \neq k} P(b_j) \right\}} \end{aligned} \tag{2.147}$$

where $P(b_j) \triangleq P(b_j[i] = b_j)$ for $b_j \in \{+1, -1\}$. In (2.147), the summation in the numerator is over all the 2^{K-1} possible vectors $\mathbf{b}$ in $\mathcal{B}_k^+$. Similarly, the summation in the denominator is over all the 2^{K-1} possible vectors $\mathbf{b}$ in $\mathcal{B}_k^-$.

In (2.147), the *a priori* probabilities of the code bits, $P(b_j)$, can be expressed in terms of their LLRs $\lambda_2(b_j[i])$, as follows.

$$\begin{aligned} P(b_j) &\triangleq P(b_j[i] = b_j) \text{ for } b_j \in \{+1, -1\} \\ &= \frac{1}{2}\left[1 + b_j \tanh\left(\frac{\lambda_2(b_j[i])}{2}\right)\right] \end{aligned} \tag{2.148}$$

Substituting (2.148) into (2.147) and simplifying, we obtain [134]

$$\begin{aligned}\lambda_1(b_k[i]) &= \frac{2A_k y_k[i]}{\sigma^2} \\ &+ \log \frac{\sum_{\mathbf{b} \in \mathcal{B}_k^+} \left\{ \exp\left\{ \frac{-1}{2\sigma^2} \mathbf{b}^T \mathbf{ARAb} \right\} \prod_{j \neq k} \left[1 + b_j \tanh\left(\frac{A_j y_j[i]}{\sigma^2}\right)\right] \left[1 + b_j \tanh\left(\frac{\lambda_2(b_j[i])}{2}\right)\right] \right\}}{\sum_{\mathbf{b} \in \mathcal{B}_k^-} \left\{ \exp\left\{ \frac{-1}{2\sigma^2} \mathbf{b}^T \mathbf{ARAb} \right\} \prod_{j \neq k} \left[1 + b_j \tanh\left(\frac{A_j y_j[i]}{\sigma^2}\right)\right] \left[1 + b_j \tanh\left(\frac{\lambda_2(b_j[i])}{2}\right)\right] \right\}} \end{aligned} \tag{2.149}$$

It can be seen from (2.149) that the extrinsic information $\lambda_1(b_k[i])$ at the output of the SISO multiuser detector consists of two parts; the first term contains the channel value of the desired user $y_k[i]$ and the second term is the information extracted from the other users' channel values $\{y_j[i]\}_{j \neq k}$ as well as their prior information $\{\lambda_2(b_j[i])\}_{j \neq k}$.

2.8.2 Low-Complexity SISO Multiuser Detector

From (2.149), it is clear that the computational complexity of the optimal SISO multiuser detector is exponential in terms of the number of users K, which is prohibitive for channels with moderate to large numbers of users. In this section, a low-complexity SISO multiuser detector based on a novel technique of combined soft interference cancelation and linear MMSE filtering proposed by Wang and Poor [133] is presented. The structure of this low-complexity multiuser detector is shown in Figure 2.19.

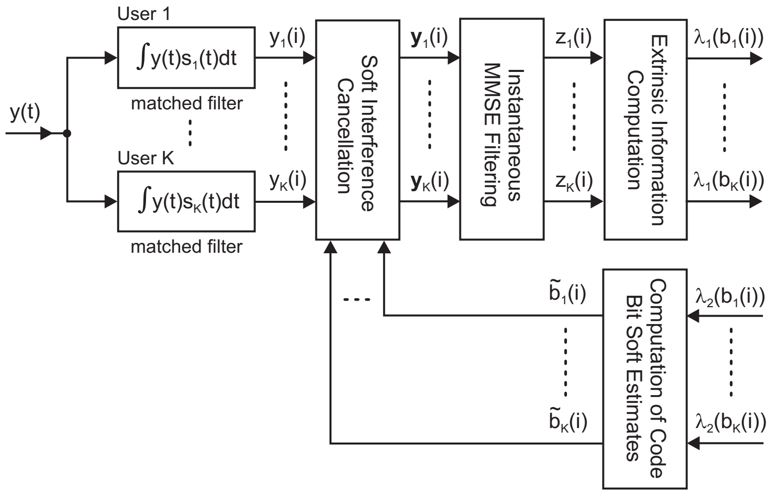

Figure 2.19: Low-complexity soft multiuser detector for synchronous CDMA

Soft Interference Cancellation and Instantaneous Linear MMSE Filtering

Based in the *a priori* LLR of the code bits of all users, $\{\lambda_2(b_k[i])\}_{k=1}^{K}$, provided by the MAP channel decoder from the previous iteration, we first form soft estimates of the code bits of all the users (i.e., for $k = 1, \ldots, K$) as

$$\begin{aligned}\tilde{b}_k[i] &\triangleq \mathrm{E}\{b_k[i]\} = \sum_{b\in\{+1,-1\}} b\, P(b_k[i] = b) \\ &= \sum_{b\in\{+1,-1\}} \frac{b}{2}\left[1 + b\tanh\left(\frac{\lambda_2(b_k[i])}{2}\right)\right] \qquad (2.150)\\ &= \tanh\left(\frac{\lambda_2(b_k[i])}{2}\right) \qquad (2.151)\end{aligned}$$

where (2.150) follows from (2.148). Define

$$\tilde{\mathbf{b}}[i] \triangleq \left[\tilde{b}_1[i],\, \tilde{b}_2[i],\, \ldots,\, \tilde{b}_K[i]\right]^T \qquad (2.152)$$

$$\begin{aligned}\tilde{\mathbf{b}}_k[i] &\triangleq \tilde{\mathbf{b}}[i] - \tilde{b}_k[i]\mathbf{e}_k \\ &= \left[\tilde{b}_1[i],\, \ldots,\, \tilde{b}_{k-1}[i],\, 0,\, \tilde{b}_{k+1}[i],\, \ldots,\, \tilde{b}_K[i]\right]^T \qquad (2.153)\end{aligned}$$

where $\mathbf{e}_k$ denotes a K-vector of all zeros, except for the k-th element, which is 1. Therefore, $\tilde{\mathbf{b}}_k[i]$ is obtained from $\tilde{\mathbf{b}}[i]$ by setting the the k-th element to zero. For each user, a soft interference cancellation is performed on the matched filter output $\mathbf{y}[i]$ in (2.146), to obtain

$$\begin{aligned}\mathbf{y}_k[i] &\triangleq \mathbf{y}[i] - \mathbf{R}\mathbf{A}\tilde{\mathbf{b}}_k[i] \\ &= \mathbf{R}\mathbf{A}\left(\mathbf{b}[i] - \tilde{\mathbf{b}}_k[i]\right) + \mathbf{n}[i], \qquad k = 1, \ldots, K\end{aligned} \tag{2.154}$$

Such a soft inference cancellation scheme was first proposed by Hagenauer [37]. Next, in order to further suppress the residual interference in $\mathbf{y}_k[i]$, an instantaneous linear minimum mean-square error (MMSE) filter $\mathbf{w}_k[i]$ is applied to $\mathbf{y}_k[i]$ to obtain

$$z_k[i] = \mathbf{w}_k^T[i]\mathbf{y}_k[i] \tag{2.155}$$

where the filter $\mathbf{w}_k[i] \in \mathbb{R}^K$ is chosen to minimise the mean-square error between the code bit and the filter output $z_k[i]$:

$$\begin{aligned}\mathbf{w}_k[i] &= \arg\min_{\mathbf{w}\in\mathbb{R}^K} \mathrm{E}\left\{\left(b_k[i] - \mathbf{w}^T\mathbf{y}_k[i]\right)^2\right\} \\ &= \arg\min_{\mathbf{w}\in\mathbb{R}^K} \mathbf{w}^T\mathrm{E}\left\{\mathbf{y}_k[i]\mathbf{y}_k^T[i]\right\}\mathbf{w} - 2\mathbf{w}^T\mathrm{E}\left\{b_k[i]\mathbf{y}_k[i]\right\}\end{aligned} \tag{2.156}$$

where using (2.154), we have

$$\mathrm{E}\{\mathbf{y}_k[i]\mathbf{y}_k^T[i]\} = \mathbf{R}\mathbf{A}\,\mathrm{Cov}\left\{\mathbf{b}[i] - \tilde{\mathbf{b}}_k[i]\right\}\mathbf{A}\mathbf{R} + \sigma^2\mathbf{R} \tag{2.157}$$

and

$$\begin{aligned}\mathrm{E}\{b_k[i]\mathbf{y}_k[i]\} &= \mathbf{R}\mathbf{A}\,\mathrm{E}\left\{b_k[i]\left(\mathbf{b}[i] - \tilde{\mathbf{b}}_k[i]\right)\right\} \\ &= \mathbf{R}\mathbf{A}\mathbf{e}_k\end{aligned} \tag{2.158}$$

Substituting (2.157) and (2.158) into (2.156), we have

$$\begin{aligned}\mathbf{w}_k[i] &= \left(\mathbf{R}\mathbf{V}_k[i]\mathbf{R} + \sigma^2\mathbf{R}\right)^{-1}\mathbf{R}\mathbf{A}\mathbf{e}_k \\ &= A_k\mathbf{R}^{-1}\left(\mathbf{V}_k[i] + \sigma^2\mathbf{R}^{-1}\right)^{-1}\mathbf{e}_k\end{aligned} \tag{2.159}$$

where $\mathbf{V}_k[i]$ is defined as

$$\begin{aligned}\mathbf{V}_k[i] &\triangleq \mathbf{A}\mathrm{Cov}\left\{\mathbf{b}[i]-\tilde{\mathbf{b}}_k[i]\right\}\mathbf{A}\\ &= \sum_{\substack{j=1\\ j\neq k}}^{K} A_j^2\left(1-\tilde{b}_j^2[i]\right)\mathbf{e}_j\mathbf{e}_j^T + A_k^2\mathbf{e}_k\mathbf{e}_k^T. \end{aligned} \tag{2.160}$$

Substituting (2.154) and (2.159) into (2.155), we obtain [133]

$$z_k[i] = A_k\mathbf{e}_k^T\left(\mathbf{V}_k[i]+\sigma^2\mathbf{R}^{-1}\right)^{-1}\left(\mathbf{R}^{-1}\mathbf{y}[i]-\mathbf{A}\tilde{\mathbf{b}}_k[i]\right). \tag{2.161}$$

Note that the term $\mathbf{R}^{-1}\mathbf{y}[i]$ in (2.161) is the output of a linear decorrelating multiuser detector (Section 2.7.1).

Gaussian Approximation of Linear MMSE Filter Output

The distribution of the residual interference plus noise at the output of a linear MMSE multiuser detector is well approximated by a Gaussian distribution [89]. Therefore, the output $z_k[i]$ of the instantaneous linear MMSE filter in (2.155) can be modelled as the output of an equivalent additive white Gaussian noise channel having $b_k[i]$ as its input symbol. This equivalent channel model can be represented as

$$z_k[i] = \mu_k[i]b_k[i] + \eta_k[i], \tag{2.162}$$

where $\mu_k[i]$ is the equivalent amplitude of the k-th user's signal at the output and $\eta_k[i] \sim \mathcal{N}(0, \nu_k^2[i])$ is a Gaussian noise sample. Using (2.154) and (2.155), the parameters $\mu_k[i]$ and $\nu_k^2[i]$ can be computed as follows,

$$\begin{aligned}\mu_k[i] &\triangleq \mathrm{E}\{z_k[i]b_k[i]\}\\ &= A_k\mathbf{e}_k^T\left(\mathbf{V}_k[i]+\sigma^2\mathbf{R}^{-1}\right)^{-1}\mathrm{E}\left\{b_k[i]\mathbf{A}\left(\mathbf{b}[i]-\tilde{\mathbf{b}}_k[i]\right)+b_k[i]\mathbf{n}[i]\right\}\\ &= A_k^2\left[\left(\mathbf{V}_k[i]+\sigma^2\mathbf{R}^{-1}\right)^{-1}\right]_{k,k} \end{aligned} \tag{2.163}$$

and

$$\begin{aligned}\nu_k^2[i] &\triangleq \mathrm{Var}\{z_k[i]\} = E\{z_k^2[i]\} - \mu_k^2[i] \\ &= \mathbf{w}_k^T[i]\mathrm{E}\{\mathbf{y}_k[i]\mathbf{y}_k^T[i]\}\mathbf{w}_k[i] - \mu_k^2[i] \\ &= \mu_k[i] - \mu_k^2[i] \end{aligned} \tag{2.164}$$

where the expectation is taken with respect to the code bits of interfering users $\{b_j[i]\}_{j\neq k}$ and the channel noise vector $\mathbf{n}[i]$. Using (2.154) and (2.154), the extrinsic information delivered by the instantaneous linear MMSE filter is then [133]

$$\begin{aligned}\lambda_1(b_k[i]) &\triangleq \log \frac{p(z_k[i] \,|\, b_k[i] = +1)}{p(z_k[i] \,|\, b_k[i] = -1)} \\ &= -\frac{(z_k[i] - \mu_k[i])^2}{2\nu_k^2[i]} + \frac{(z_k[i] + \mu_k[i])^2}{2\nu_k^2[i]} \\ &= \frac{2z_k[i]}{1 - \mu_k[i]} \end{aligned} \tag{2.165}$$

Recursive Procedure for Computing Soft Output

In order to form the extrinsic LLR $\lambda_1(b_k[i])$ at the instantaneous linear MMSE filter, $z_k[i]$ and $\mu_k[i]$ must be computed first (2.165). From (2.161) and (2.163) the computation of $z_k[i]$ and $\mu_k[i]$ involves inverting a $K \times K$ matrix:

$$\mathbf{\Phi}_k[i] \triangleq \left(\mathbf{V}_k[i] + \sigma^2\mathbf{R}^{-1}\right)^{-1}. \tag{2.166}$$

This matrix inversion, $\mathbf{\Phi}_k[i]$, can computed efficiently using the following recursive procedure. Define $\mathbf{\Psi}^{(0)} \triangleq (1/\sigma^2)\mathbf{R}$, and

$$\mathbf{\Psi}^{(k)} \triangleq \left(\sigma^2\mathbf{R}^{-1} + \sum_{j=1}^{k} A_j^2\left(1 - \tilde{b}_j^2[i]\right)\mathbf{e}_j\mathbf{e}_j^T\right)^{-1}, \quad k = 1, \ldots, K. \tag{2.167}$$

Using the matrix inversion lemma, $\mathbf{\Psi}^{(k)}$ can be computed recursively as

$$\mathbf{\Psi}^{(k)} = \mathbf{\Psi}^{(k-1)} - \left(\frac{1}{A_k^{-2}\left(1 - \tilde{b}_k^2[i]\right)^{-1}\{\mathbf{\Psi}^{(k-1)}\}_{k,k}}\right)\left(\mathbf{\Psi}^{(k-1)}\mathbf{e}_k\right)\left(\mathbf{\Psi}^{(k-1)}\mathbf{e}_k\right)^T,$$

$$k = 1, \ldots, K. \tag{2.168}$$

Denote $\boldsymbol{\Psi} \triangleq \boldsymbol{\Psi}^{(K)}$. Using the definition of $\mathbf{V}_k[i]$ given by (2.160), we can then compute $\boldsymbol{\Phi}_k[i]$ from $\boldsymbol{\Psi}$ as follows [133]:

$$\begin{aligned}\boldsymbol{\Phi}_k[i] &= \left(\boldsymbol{\Psi}^{-1} + A_k^2 \tilde{b}_k^2[i]\mathbf{e}_k\mathbf{e}_k^T\right)^{-1} \\ &= \boldsymbol{\Psi} - \left(\frac{1}{\left(A_k\tilde{b}_k[i]\right)^{-2}\{\boldsymbol{\Psi}\}_{k,k}}\right)(\boldsymbol{\Psi}\mathbf{e}_k)(\boldsymbol{\Psi}\mathbf{e}_k)^T, \quad k = 1, \ldots, K. \qquad (2.169)\end{aligned}$$

Finally, the low-complexity SISO multiuser detection algorithm for synchronous CDMA systems is summarised in Table 2.4.

1. Given the extrinsic information (in LLR form), $\{\lambda_2(b_k[i])\}_k$, from the FEC decoders, calculate the soft bit estimates (for $k = 1, \ldots, K$) using:

$$\begin{aligned}\tilde{b}_k[i] &= \tanh\left(\frac{1}{2}\lambda_2(b_k[i])\right), \\ \tilde{\mathbf{b}}[i] &= \left[\tilde{b}_1[i], \;\cdots,\; \tilde{b}_K[i]\right]^T \\ \tilde{\mathbf{b}}_k[i] &= \tilde{\mathbf{b}}[i] - \tilde{b}_k[i]\mathbf{e_k}\end{aligned}$$

2. Using the recursive procedure of (2.167), (2.168), and (2.169), calculate the matrix inversion:

$$\boldsymbol{\Phi}^{(k)} = (\mathbf{V}_k[i] + \sigma^2\mathbf{R}^{-1})^{-1}, \quad \text{for } k = 1, \ldots, K,$$

3. Perform soft interference cancellation and linear MMSE filtering (for $k = 1, \ldots, K$) using:

$$z_k[i] = A_k\mathbf{e}_k^T\boldsymbol{\Phi}_k[i]\left(\mathbf{R}^{-1}\mathbf{y}[i] - \mathbf{A}\tilde{\mathbf{b}}_k[i]\right)$$

4. Calculate the extrinsic information $\{\lambda_1(b_k[i])\}_k$, for $k = 1, \ldots, K$, using:

$$\lambda_1(b_k[i]) = \frac{2z_k[i]}{1 - \mu_k[i]} \quad \text{where} \quad \mu_k[i] = A_k^2\{\boldsymbol{\Phi}_k[i]\}_{k,k}$$

Table 2.4: Algorithm: Low-Complexity Soft MUD for Synchronous CDMA

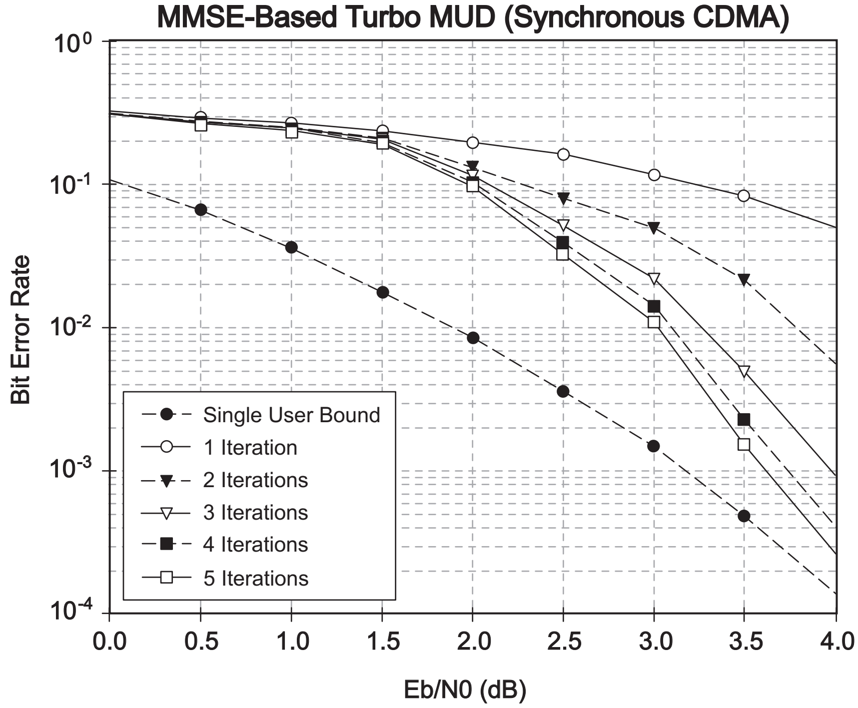

Figure 2.20: Performance of MMSE-based low-complexity turbo MUD: four users ($K = 4$), equal power, equal cross-correlations ($\rho = 0.7$); each user employs a rate-1/2 constraint-length-5 convolutional code and length-128 interleaver.

Typical performance results show that near-interference-free performance can be readily achieved when there is sufficient signal-to-noise ratio (SNR) for the initial SISO MUD to gain useful information about the channel symbols. Figure 2.20 shows an example of such a result in which there are $K = 4$ users with equal power and equal cross-correlations of $\rho = 0.7$. Each user employs a rate-1/2, constraint-length-5 convolutional code with a length-128 interleaver. Note that near-single-user performance is achieved after only five iterations with very moderate SNR.

2.9 Turbo Multiuser Detection for CDMA with Multipath Fading

In this section, the low complexity SISO multiuser detector for synchronous CDMA systems (presented in Section 2.8.2) is extended to incorporate asynchronous CDMA systems with multipath fading channels. This low-complexity SISO multiuser detector for asynchronous CDMA systems, which is also based on combined soft interference cancelation and linear MMSE filtering, was proposed by Li, Wang, and Georghiades [57].

2.9.1 Signal Model and Sufficient Statistics

We consider a K-user asynchronous CDMA system transmitting over multipath fading channels. The transmitted signal due to the k-th user is given by

$$x_k(t) = A_k \sum_{i=0}^{N-1} b_k[i] s_k(t - iT) \tag{2.170}$$

where N is the number of data symbols per user per frame; T is the symbol interval; A_k is the amplitude of the k-th user; $b_k[i]$ is i-th transmitted bit of the k-th user; and $\{s_k(t);\ 0 \leq t \leq T\}$ is the normalised signature waveform of the k-th user. It is assumed that $s_k(t)$ is supported only on the interval $[0, T]$ and has unit energy.

The k-th user's signal $x_k(t)$ propagates through a multipath channel with impulse response

$$h_k(t) = \sum_{l=1}^{L} g'_{k,l}(t) \delta(t - \tau_{k,l}) \tag{2.171}$$

where L is the number of paths in the k-th user's channel, and where $g'_{k,l}(t)$ and $\tau_{k,l}$ are the complex fading process and the delay of the l-th path of the k-th user's signal, respectively. It is assumed that the fading processes are known to the receiver and do not vary during one coded symbol interval, but may vary from symbol to symbol, i.e.,

$$g'_{k,l}(t) = g'_{k,l}(iT) \triangleq g_{k,l}[i] \quad \text{for} \quad iT \leq t < (i+1)T$$

The received signal, $y(t)$, is the superposition of the K users' signals plus the additive white Gaussian noise, given by

$$\begin{aligned} y(t) &= \sum_{k=1}^{K} x_k(t) \star h_k(t) + n(t) &\quad (2.172)\\ &= \sum_{k=1}^{K} A_k \sum_{i=0}^{N-1} b_k[i] \sum_{l=1}^{L} g_{k,l}[i] s_k(t - iT - \tau_{k,l}) + n(t) &\quad (2.173) \end{aligned}$$

where $n(t)$ is a zero-mean complex AWGN process with power spectral density σ^2.

From (2.102) and (2.109), denote

$$\mathbf{b}[i] \triangleq [\,b_1[i],\, b_2[i],\, \ldots,\, b_K[i]\,]^T \quad \text{and} \quad \mathbf{b}_n \triangleq \left[\,\mathbf{b}^T[0],\, \mathbf{b}^T[1], \ldots,\, \mathbf{b}^T[N-1]\,\right]^T.$$

Using the Cameron-Martin formula [87], the likelihood function of the received waveform $y(t)$ in (2.173) conditioned on all the transmitted symbols $\mathbf{b}_n$ of all users can be written as

$$L(y(t) \mid \mathbf{b}_n) = C \exp\left\{\frac{\Omega(\mathbf{b}_n)}{\sigma^2}\right\}, \qquad -\infty < t < \infty \tag{2.174}$$

where C is some positive scalar constant, and

$$\Omega(\mathbf{b}_n) \triangleq 2\Re\left\{\int_{-\infty}^{\infty} S(t;\mathbf{b}_n)^* y(t)\, dt\right\} - \int_{-\infty}^{\infty} |S(t;\mathbf{b}_n)|^2\, \mathrm{d}t \tag{2.175}$$

and

$$S(t;\mathbf{b}_n) \triangleq \sum_{k=1}^{K} A_k \sum_{i=0}^{N-1} b_k[i] \sum_{l=1}^{L} g_{k,l}[i] s_k(t - iT - \tau_{k,l}) \tag{2.176}$$

The first integral in (2.175) can be expressed as [57]

$$\int_{-\infty}^{\infty} S(t;\mathbf{b}_n)^* y(t)\, dt \triangleq \sum_{k=1}^{K} A_k \sum_{i=0}^{N-1} b_k[i] \overbrace{\sum_{l=1}^{L} g_{k,l}^*[i] \underbrace{\int_{-\infty}^{\infty} y(t) s_k(t - iT - \tau_{k,l})\, \mathrm{d}t}_{y_{k,l}[i]}}^{y_k[i]} \tag{2.177}$$

Since the second integral in (2.175) does not depend on the received signal $y(t)$, from (2.177) it can be seen that the sufficient statistic for detecting the multiuser symbols $\mathbf{b}_n$ is $\{y_k[i]\}_{k=1;i=0}^{K;\ N-1}$ and that this sufficient statistic is obtained by passing the received signal $y(t)$ through a bank of K maximal-ratio multipath combiners, i.e., a Rake receiver [91] (as shown in Figure 2.21).

Next, the expression for this sufficient statistic is restated in terms of the multiuser channel parameters and transmitted symbols, which is fundamental to the development of the SISO multiuser detector.

We assume that the multipath spread of any user's channel is within one symbol interval, that is, $\tau_{k,l} \in [0, T)$ for $k = 1, \ldots, K$ and $l = 1, \ldots, L$. Define the following

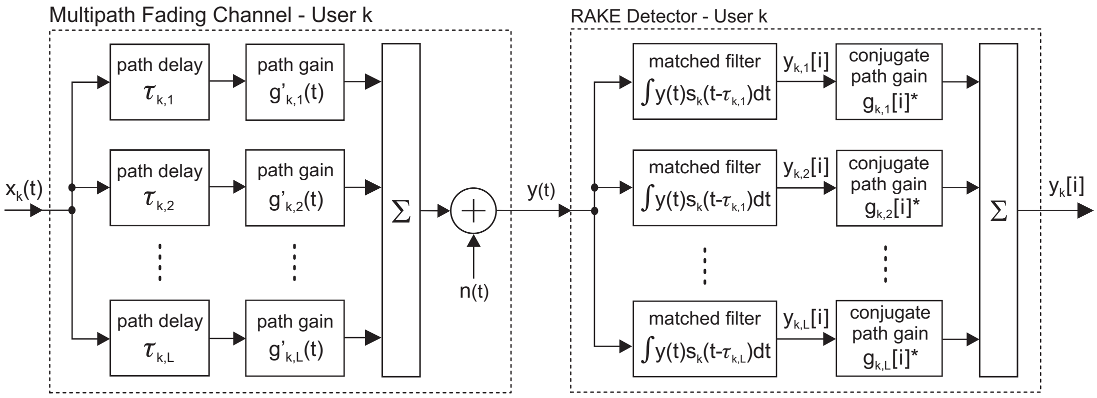

Figure 2.21: CDMA Rake receiver for multipath fading channels

correlation of the delayed signalling waveforms:

$$\rho^{(j)}_{(k,l)(k',l')} \triangleq \int_{-\infty}^{\infty} s_k(t-\tau_{k,l})s_{k'}(t+jT-\tau_{k',l'})\,\mathrm{d}t,$$
$$j \in \mathcal{J}, \quad 1 \le k,k' \le K, \quad 1 \le l,l' \le L \tag{2.178}$$

where $\mathcal{J} \triangleq \{-1,0,+1\}$. Since $\tau_{k,l} \le T$ and $s_{i,k}(t)$ is nonzero only $t \in [0,T]$, it then follows that $\rho^{(j)}_{(k,l)(k',l')} = 0$ for $j \notin \{-1,0,+1\}$. Now substituting (2.173) into (2.177), we have

$$\begin{aligned} y_{k,l}[i] &= \sum_{i'=0}^{N-1}\sum_{k'=1}^{K} A_{k'}b_{k'}[i']\sum_{l'=1}^{L} g_{k',l'}[i']\int_{-\infty}^{\infty} s_{k'}(t-i'T-\tau_{k',l'})s_k(t-iT-\tau_{k,l})\,\mathrm{d}t + u_{k,l}[i] \\ &= \sum_{j\in\mathcal{J}}\sum_{k'=1}^{K} A_{k'}b_{k'}[i+j]\sum_{l'=1}^{L} g_{k',l'}[i]\rho^{(-j)}_{(k,l)(k',l')} + u_{k,l}[i] \end{aligned} \tag{2.179}$$

where $\{u_{k,l}[i]\}$ are zero-mean complex Gaussian random sequences, defined as

$$u_{k,l}[i] = \int_{-\infty}^{\infty} n(t)s_k(t-iT-\tau_{k,l})\,\mathrm{d}t \tag{2.180}$$

with covariance

$$\begin{aligned} \mathrm{Cov}\{u_{k,l}[i], u_{k',l'}[i']\} &= \mathrm{E}\left\{u_{k,l}[i]u^*_{k',l'}[i']\right\} \\ &= \int_{-\infty}^{\infty} s_k(t-iT-\tau_{k,l})s_{k'}(t'-i'T-\tau_{k',l'})\,\mathrm{d}t \\ &= \rho^{(i-i')}_{(k,l)(k',l')} \end{aligned} \tag{2.181}$$

Define the following quantities:

$$\mathbf{R}^{(j)}_{(k,k')} \triangleq \begin{bmatrix} \rho^{(j)}_{(k,1)(k',1)} & \rho^{(j)}_{(k,1)(k',2)} & \cdots & \rho^{(j)}_{(k,1)(k',L)} \\ \rho^{(j)}_{(k,2)(k',1)} & \rho^{(j)}_{(k,2)(k',2)} & \cdots & \rho^{(j)}_{(k,1)(k',L)} \\ \vdots & \vdots & & \vdots \\ \rho^{(j)}_{(k,L)(k',1)} & \rho^{(j)}_{(k,L)(k',2)} & \cdots & \rho^{(j)}_{(k,L)(k',L)} \end{bmatrix} \qquad (L \times L - \text{matrix})$$

$$\mathbf{R}^{(j)} \triangleq \begin{bmatrix} \mathbf{R}^{(j)}_{(1,1)} & \mathbf{R}^{(j)}_{(1,2)} & \cdots & \mathbf{R}^{(j)}_{(1,K)} \\ \mathbf{R}^{(j)}_{(2,1)} & \mathbf{R}^{(j)}_{(2,2)} & \cdots & \mathbf{R}^{(j)}_{(2,K)} \\ \vdots & \vdots & & \vdots \\ \mathbf{R}^{(j)}_{(K,1)} & \mathbf{R}^{(j)}_{(K,2)} & \cdots & \mathbf{R}^{(j)}_{(K,K)} \end{bmatrix} \qquad (KL \times KL - \text{matrix})$$

$$\begin{aligned} \mathbf{\Upsilon}[i] &\triangleq [\, y_{1,1}[i], \ldots, y_{1,L}[i], \ldots, y_{K,1}[i], \ldots, y_{K,L}[i]\,]^T && (KL \times 1 - \text{vector}) \\ \mathbf{u}[i] &\triangleq [\, u_{1,1}[i], \ldots, u_{1,L}[i], \ldots, u_{K,1}[i], \ldots, u_{K,L}[i]\,]^T && (KL \times 1 - \text{vector}) \\ \mathbf{g}_k[i] &\triangleq [\, g_{k,1}[i], g_{k,2}[i], \ldots, g_{k,L}[i]\,]^T && (L \times 1 - \text{vector}) \\ \mathbf{G}[i] &\triangleq \text{diag}\{\, \mathbf{g}_1[i], \mathbf{g}_2[i], \ldots, \mathbf{g}_K[i]\,\} && (KL \times K - \text{matrix}) \\ \mathbf{A} &\triangleq \text{diag}\,\{\, A_1, A_2, \ldots, A_K \,\} && (K \times K - \text{matrix}) \\ \mathbf{y}[i] &\triangleq [\, y_1[i], y_2[i], \ldots, y_K[i]\,]^T && (K \times 1 - \text{vector}) \end{aligned}$$

The sufficient statistic of (2.179) can be rewritten in vector form as follows:

$$\mathbf{\Upsilon}[i] = \sum_{j \in \mathcal{J}} \mathbf{R}^{(-j)} \mathbf{G}[i] \mathbf{A}\, \mathbf{b}[i+j] + \mathbf{u}[i]. \tag{2.182}$$

From (2.180), the complex Gaussian vector sequence $\{\mathbf{u}[i]\}$ has the covariance matrix of

$$\begin{aligned} \text{Cov}\{\mathbf{u}[i], \mathbf{u}[i+j]\} &= \text{E}\{\mathbf{u}[i]\mathbf{u}^H[i+j]\} \\ &= \sigma^2 \mathbf{R}^{(-j)}. \end{aligned} \tag{2.183}$$

Substituting (2.182) into (2.177), the expression for the sufficient statistic $\mathbf{y}[i]$ is given by

$$\mathbf{y}[i] = \mathbf{G}^H[i] \mathbf{\Upsilon}[i] = \sum_{j \in \mathcal{J}} \mathbf{H}^{(-j)}[i] \mathbf{A}\, \mathbf{b}[i+j] + \mathbf{v}[i] \tag{2.184}$$

where $\mathbf{H}^{(-j)}[i]$ is defined as

$$\mathbf{H}^{(-j)}[i] = \mathbf{G}^H[i]\mathbf{R}^{(-j)}\mathbf{G}[i], \tag{2.185}$$

and $\mathbf{v}[i]$ is a sequence of zero-mean complex Gaussian vectors, defined as

$$\mathbf{v}[i] = \mathbf{G}^H[i]\mathbf{u}[i] \tag{2.186}$$

and has the covariance matrix of

$$\begin{aligned}\mathrm{Cov}\{\mathbf{v}[i], \mathbf{v}[i+j]\} &= \mathrm{E}\{\mathbf{v}[i]\mathbf{v}^H[i+j]\} \\ &= \sigma^2\mathbf{G}^H[i]\mathbf{R}^{(-j)}\mathbf{G}[i] \triangleq \sigma^2\mathbf{H}^{(-j)}[i].\end{aligned} \tag{2.187}$$

Note that $\rho^{(j)}_{(k,l)(k',l')} = \rho^{(-j)}_{(k',l')(k,l)}$ by definition of (2.178). It then follows that $\mathbf{R}^{(-j)} = (\mathbf{R}^{(j)})^T$, and therefore, $\mathbf{H}^{(-j)}[i] = (\mathbf{H}^{(j)}[i])^H$.

2.9.2 SISO Multiuser Detector in Multipath Fading Channels

The structure of the soft multiuser detector for multipath fading channels is shown in Figure 2.22. First, the received signal $y(t)$ is passed through a bank of K maximum-ratio multipath combiners (i.e. Rake receivers) to obtain the sufficient statistic. Then, soft interference cancellation is applied to the outputs of the combiners, followed by linear MMSE filtering. Finally, the extrinsic information is computed from the MMSE filter outputs.

Define the following quantities:

$$\begin{aligned}\mathbf{H}[i] &\triangleq \left[\,\mathbf{H}^{(1)}[i],\ \mathbf{H}^{(0)}[i],\ \mathbf{H}^{(-1)}[i]\,\right] && (K \times 3K - \text{matrix}) \\ \mathbf{A_a} &\triangleq \mathrm{diag}\,\{\,\mathbf{A},\ \mathbf{A},\ \mathbf{A}\,\} && (3K \times 3K - \text{matrix}) \\ \mathbf{b_a}[i] &\triangleq \left[\,\mathbf{b}^T[i-1],\ \mathbf{b}^T[i],\ \mathbf{b}^T[i+1]\,\right]^T && (3K \times 1 - \text{vector})\end{aligned}$$

We can then write (2.184) in matrix form as

$$\mathbf{y}[i] = \mathbf{H}[i]\mathbf{A_a}\mathbf{b_a}[i] + \mathbf{v}[i] \tag{2.188}$$

where by (2.187), $\mathbf{v}[i] \sim \mathcal{N}_c(\mathbf{0}, \sigma^2\mathbf{H}^{(0)}[i])$.

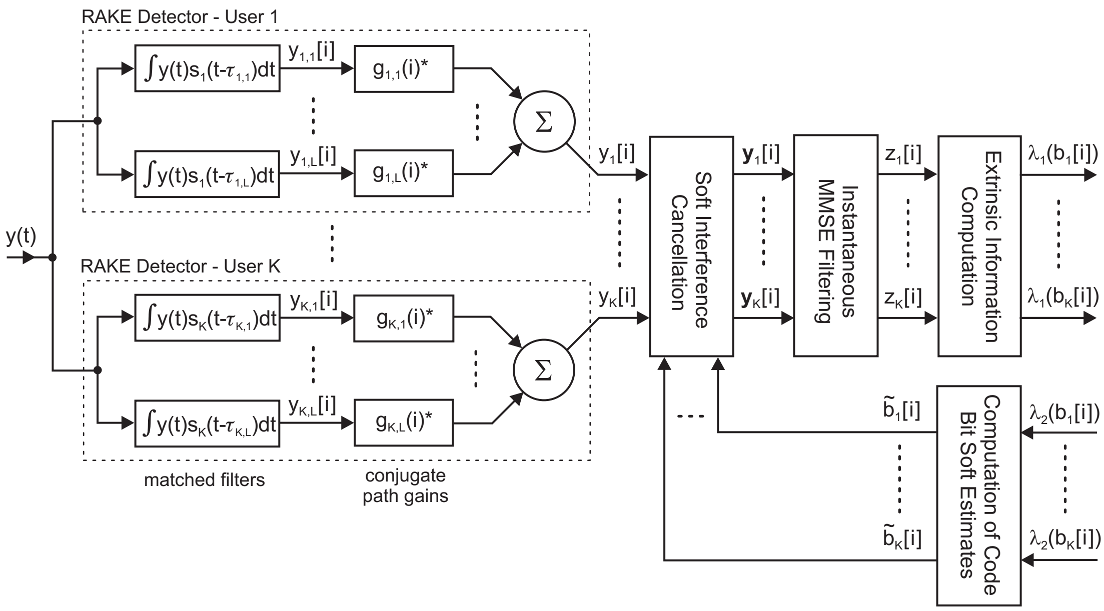

Figure 2.22: Low-complexity soft multiuser detector for asynchronous CDMA systems with multipath fading channels

Based on the *a priori* LLR of the code bits of all users, $\{\lambda_2(b_k[i]\}_{i;k}$ provided by the MAP channel decoder, we first form soft estimates of the user code bits:

$$\tilde{b}_k[i] \triangleq \tanh\left(\frac{1}{2}\lambda_2(b_k[i])\right), \quad i = 0, \ldots, N-1; \quad k = 1, \ldots, K. \tag{2.189}$$

Denote

$$\tilde{\mathbf{b}}[i] \triangleq \left[\tilde{b}_1[i],\, \tilde{b}_2[i],\, \ldots,\, \tilde{b}_K[i]\right]^T \qquad (K \times 1 - \text{vector}) \tag{2.190}$$

$$\tilde{\mathbf{b}}_{\mathbf{a}}[i] = \left[\tilde{\mathbf{b}}^T[i-1],\ \tilde{\mathbf{b}}^T[i],\ \tilde{\mathbf{b}}^T[i+1]\right]^T \qquad (3K \times 1 - \text{vector}) \tag{2.191}$$

$$\tilde{\mathbf{b}}_k[i] \triangleq \tilde{\mathbf{b}}_{\mathbf{a}}[i] - \tilde{b}_k[i]\mathbf{e}_k \qquad (3K \times 1 - \text{vector}) \tag{2.192}$$

where $\mathbf{e}_k$ denotes a $3K$-vector of all zeroes, except for the $(K+k)$-th element, which is 1.

At the symbol time i, for each user, a soft interference cancellation is performed on the received discrete-time signal $\mathbf{y}[i]$ in (2.188), to obtain

$$\mathbf{y}_k[i] \triangleq \mathbf{y}[i] - \mathbf{H}[i]\mathbf{A}_{\mathbf{a}}\tilde{\mathbf{b}}_k[i] \tag{2.193}$$

$$= \mathbf{H}[i]\mathbf{A}_{\mathbf{a}}\left(\mathbf{b}_{\mathbf{a}}[i] - \tilde{\mathbf{b}}_k[i]\right) + \mathbf{v}[i], \quad k = 1, \ldots, K \tag{2.194}$$

An instantaneous linear MMSE filter is then applied to $\mathbf{y}_k[i]$, to obtain

$$z_k[i] = \mathbf{w}_k^H[i]\mathbf{y}_k[i] \tag{2.195}$$

where the filter $\mathbf{w}_k[i] \in \mathbb{C}^K$ is chosen to minimize the mean-square error between the code bit $b_k[i]$ and the filter output $z_k[i]$;

$$\begin{aligned}\mathbf{w}_k[i] &= \arg\min_{\mathbf{w}\in\mathbb{C}^K} \mathrm{E}\left\{\left|b_k[i] - \mathbf{w}^H\mathbf{y}_k[i]\right|^2\right\}\\ &= \arg\min_{\mathbf{w}\in\mathbb{C}^K} \mathbf{w}^H \mathrm{E}\left\{\mathbf{y}_k[i]\mathbf{y}_k^H[i]\right\}\mathbf{w} - 2\Re\left[\mathbf{w}^H \mathrm{E}\left\{b_k[i]\mathbf{y}_k[i]\right\}\right]\end{aligned} \tag{2.196}$$

where

$$\mathrm{E}\left\{\mathbf{y}_k[i]\mathbf{y}_k^H[i]\right\} = \mathbf{H}[i]\mathbf{A_a}\boldsymbol{\Delta}_k[i]\mathbf{A_a}\mathbf{H}^H[i] + \sigma^2\mathbf{H}^{(0)}[i], \qquad \text{and} \tag{2.197}$$

$$\mathrm{E}\left\{b_k[i]\mathbf{y}_k[i]\right\} = \mathbf{H}[i]\mathbf{A_a}\mathbf{e}_k = A_k\mathbf{H}[i]\mathbf{e}_k \tag{2.198}$$

with

$$\boldsymbol{\Delta}_k[i] \triangleq \mathrm{Cov}\left\{\mathbf{b}_r[i] - \tilde{\mathbf{b}}_k[i]\right\} = \mathrm{diag}\left\{\,\mathbf{D}[i-1],\, \mathbf{D}_k[i],\, \mathbf{D}[i+1]\,\right\}$$

and

$$\begin{aligned}\mathbf{D}_k[i] &\triangleq \mathrm{diag}\left\{1-\tilde{b}_1^2[i], \ldots, 1-\tilde{b}_{k-1}^2[i],\, 1,\, 1-\tilde{b}_{k+1}^2[i], \ldots, 1-\tilde{b}_K^2[i]\right\}\\ \mathbf{D}[i+j] &\triangleq \mathrm{diag}\left\{1-\tilde{b}_1^2[i+j],\, 1-\tilde{b}_2^2[i+j],\, \ldots, 1-\tilde{b}_K^2[i+j]\right\},\end{aligned}$$

for $j = -1, +1$. The solution to (2.196) is given by [57]

$$\mathbf{w}_k[i] = A_k\left(\mathbf{H}[i]\mathbf{A_a}\boldsymbol{\Delta}_k[i]\mathbf{A_a}\mathbf{H}^H[i] + \sigma^2\mathbf{H}^{[0]}[i]\right)^{-1}\mathbf{H}[i]\mathbf{e}_k \tag{2.199}$$

As before, in order to form the LLR of the code bit $b_k[i]$, we approximate the instantaneous linear MMSE filter output $z_k[i]$ in (2.195) as being Gaussian, i.e., $z_k[i] \sim \mathcal{N}_c(\mu_k[i]b_k[i], \nu_k^2[i])$. Conditioned on the code bit $b_k[i]$, the mean and variance of $z_k[i]$ are given, respectively by

$$\begin{aligned}\mu_k[i] &\triangleq E\left\{z_k[i]b_k[i]\right\}\\ &= \mathbf{e}_k^H\mathbf{H}^H[i]\left(\mathbf{H}[i]\boldsymbol{\Delta}_k[i]\mathbf{H}^H[i] + \sigma^2\mathbf{H}^{(0)}[i]\right)^{-1}\mathbf{H}[i]\mathbf{e}_k\end{aligned} \tag{2.200}$$

and

$$\begin{aligned}\nu_k[i] &\triangleq \mathrm{Var}\left\{z_k[i]\right\} = E\left\{|z_k[i]|^2\right\} - \mu_k^2[i] \\ &= \mathbf{w}_k^H \mathrm{E}\left\{\mathbf{y}_k[i]\mathbf{y}_k^H[i]\right\}\mathbf{w}_k - \mu_k^2[i] \\ &= \mu_k[i] - \mu_k^2[i] \end{aligned} \tag{2.201}$$

Therefore, the extrinsic information $\lambda_1(b_k[i])$ delivered by the instantaneous linear MMSE filter is given by [57]

$$\begin{aligned}\lambda_1[b_k(i)] &= -\frac{|z_k[i]-\mu_k[i]|^2}{\nu_k^2[i]} + \frac{|z_k[i]+\mu_k[i]|^2}{\nu_k^2[i]} \\ &= \frac{4\Re\{z_k[i]\}}{1-\mu_k[i]}\end{aligned} \tag{2.202}$$

Recursive Algorithm for Computing Soft Output

The extrinsic information can be computed efficiently by employing reduced-complexity recursive techniques for performing matrix inversions. The $K \times K$ matrix inversion,

$$\mathbf{\Psi}_k[i] \triangleq \left(\mathbf{H}[i]\mathbf{\Delta}_k[i]\mathbf{H}^H[i] + \sigma^2\mathbf{H}^{(0)}[i]\right)^{-1}, \tag{2.203}$$

can be computed efficiently using the following procedure. Note that $\mathbf{\Delta}_k[i]$ can be written as

$$\mathbf{\Delta}_k[i] = \mathbf{\Delta}[i] + \tilde{b}_k^2[i]\mathbf{e}_k\mathbf{e}_k^T \tag{2.204}$$

where

$$\mathbf{\Delta}[i] = \mathrm{diag}\left\{\, \mathbf{D}[i-1],\, \mathbf{D}[i],\, \mathbf{D}[i+1]\,\right\} \tag{2.205}$$

and

$$\mathbf{D}[i+j] \triangleq \mathrm{diag}\left\{1-\tilde{b}_1^2[i+j],\, 1-\tilde{b}_2^2[i+j],\, \ldots, 1-\tilde{b}_K^2[i+j]\right\},$$

for $j = -1, 0, +1$. Substituting (2.204) into (2.203), we have

$$\mathbf{\Psi}_k[i] = \left(\mathbf{H}[i]\mathbf{\Delta}[i]\mathbf{H}^H[i] + \sigma^2\mathbf{H}^{(0)}[i] + \tilde{b}_k^2[i]\{\mathbf{H}[i]\}_{(:,K+k)}\{\mathbf{H}^H[i]\}_{(:,K+k)}\right)^{-1} \tag{2.206}$$

where $\{\mathbf{H}[i]\}_{(:,K+k)}$ denotes the $(K+k)$-th column of $\mathbf{H}[i]$. Define

$$\mathbf{\Psi}[i] \triangleq \left(\mathbf{H}[i]\mathbf{\Delta}[i]\mathbf{H}^H[i] + \sigma^2\mathbf{H}^{(0)}[i]\right)^{-1} \tag{2.207}$$

1. Given the extrinsic information (in LLR form), $\{\lambda_2(b_k[i])\}_{i,k}$, from the FEC decoders, calculate the soft bit estimates (for $i = 0, \ldots, N-1$ and $k = 1, \ldots, K$) using:

$$\begin{aligned} \tilde{b}_k[i] &= \tanh\left(\frac{1}{2}\lambda_2(b_k[i])\right) \\ \tilde{\mathbf{b}}[i] &= \left[\tilde{b}_1[i],\ \tilde{b}_2[i],\ \ldots,\ \tilde{b}_K[i]\right]^T \\ \tilde{\mathbf{b}}_{\mathbf{a}}[i] &= \left[\tilde{\mathbf{b}}^T[i-1],\ \tilde{\mathbf{b}}^T[i],\ \tilde{\mathbf{b}}^T[i+1]\right]^T, \\ \tilde{\mathbf{b}}_k[i] &= \tilde{\mathbf{b}}_{\mathbf{a}}[i] - \tilde{b}_k[i]\mathbf{e}_k \end{aligned}$$

2. Using the recursive procedure of (2.207) and (2.208), calculate the matrix inversions:

$$\begin{aligned} \mathbf{\Psi}_k[i] &\triangleq \left(\mathbf{H}[i]\mathbf{\Delta}_k[i]\mathbf{H}^H[i] + \sigma^2\mathbf{H}^{(0)}[i]\right)^{-1}, \\ \mathbf{\Phi}_k[i] &\triangleq \left(\mathbf{H}[i]\mathbf{A}_{\mathbf{a}}\mathbf{\Delta}_k[i]\mathbf{A}_{\mathbf{a}}\mathbf{H}^H[i] + \sigma^2\mathbf{H}^{(0)}[i]\right)^{-1} \end{aligned}$$

3. Perform soft interference cancellation and linear MMSE filtering (for $i = 0, \ldots, N-1$ and $k = 1, \ldots, K$) using:

$$\begin{aligned} \mathbf{y}_k[i] &= \mathbf{y}[i] - \mathbf{H}[i]\mathbf{A}_{\mathbf{a}}\tilde{\mathbf{b}}_k[i] \\ z_k[i] &= \mathbf{w}_k^H[i]\mathbf{y}_k[i] \quad \text{where} \quad \mathbf{w}_k[i] = A_k\mathbf{\Phi}_k[i]\mathbf{H}[i]\mathbf{e}_k \end{aligned}$$

4. Calculate the extrinsic information $\{\lambda_1(b_k[i])\}_{i,k}$, for $i = 0, \ldots, N-1$ and $k = 1, \ldots, K$, using:

$$\lambda_1(b_k[i]) = \frac{4\Re\{z_k[i]\}}{1 - \mu_k[i]} \quad \text{where} \quad \mu_k[i] = \mathbf{e}_k^H\mathbf{H}^H[i]\mathbf{\Psi}_k[i]\mathbf{H}[i]\mathbf{e}_k$$

Table 2.5: Algorithm: Low-Complexity Soft MUD for Multipath Fading Channels

Then by the matrix inversion lemma, (2.206) can be written as [57]

$$\mathbf{\Psi}_k[i] = \mathbf{\Psi}[i] - \left(\frac{1}{\tilde{b}_k^{-2}[i] + \{\mathbf{H}^H[i]\}_{(:,K+k)} \mathbf{\Psi}[i] \{\mathbf{H}[i]\}_{(:,K+k)}} \right) \cdot \left(\mathbf{\Psi}[i]\{\mathbf{H}[i]\}_{(:,K+k)}\right) \left(\mathbf{\Psi}[i]\{\mathbf{H}[i]\}_{(:,K+k)}\right)^H, \quad k = 1, \ldots, K \quad (2.208)$$

Equations (2.207) and (2.208) form the recursive procedure for computing $\Psi_k[i]$ in (2.203). Similarly, the recursive procedure can be easily adapted to compute the $K \times K$ matrix inversion $\mathbf{\Phi}_k[i]$ where

$$\mathbf{\Phi}_k[i] \triangleq \left(\mathbf{H}[i]\mathbf{A_a}\mathbf{\Delta}_k[i]\mathbf{A_a}\mathbf{H}^H[i] + \sigma^2\mathbf{H}^{(0)}[i]\right)^{-1}. \quad (2.209)$$

Finally, the SISO multiuser detection algorithm for asynchronous CDMA systems with multipath fading channels is summarised in Table 2.5.

2.10 Interleave-Division Multiple Access (IDMA)

Recently, a new multiple access system, interleave division multiple access (IDMA) has been proposed by Ping, Liu, Wu, and Leung [86], [85]. IDMA when used with low-complexity iterative receivers has been shown to outperform coded CDMA. In contrast to CDMA, which separates users by specific spreading codes, IDMA separates users by unique interleaver sequences. IDMA can be regarded as a special case of chip interleaved CDMA, and therefore inherits many advantages of CDMA including diversity against fading, and mitigation of the worst-case other-cell user interference problem [74].

2.10.1 Transmitter Structure

Figure 2.23 shows the transmitter structure of the multiuser IDMA scheme with K simultaneous users [85]. The input data sequence $\{d_k[i]\}_{i=0}^{M-1}$ of user-k is encoded by the FEC encoder (with rate R_k) generating a coded sequence $\{c_k[i]\}_{i=0}^{N-1}$, where N is the frame length. The elements $c_k[i]$ are referred to as coded bits. Then $\{c_k[i]\}_{i=0}^{N-1}$ is permutated by the user-specific interleaver π_k, producing $\{b_k[i]\}_{i=0}^{N-1}$. Finally, the interleaved coded bit sequence is BPSK modulated, producing $\{x_k[i]\}_{i=0}^{N-1}$. The elements $x_k[i]$ are referred to as chips in accordance with CDMA convention.

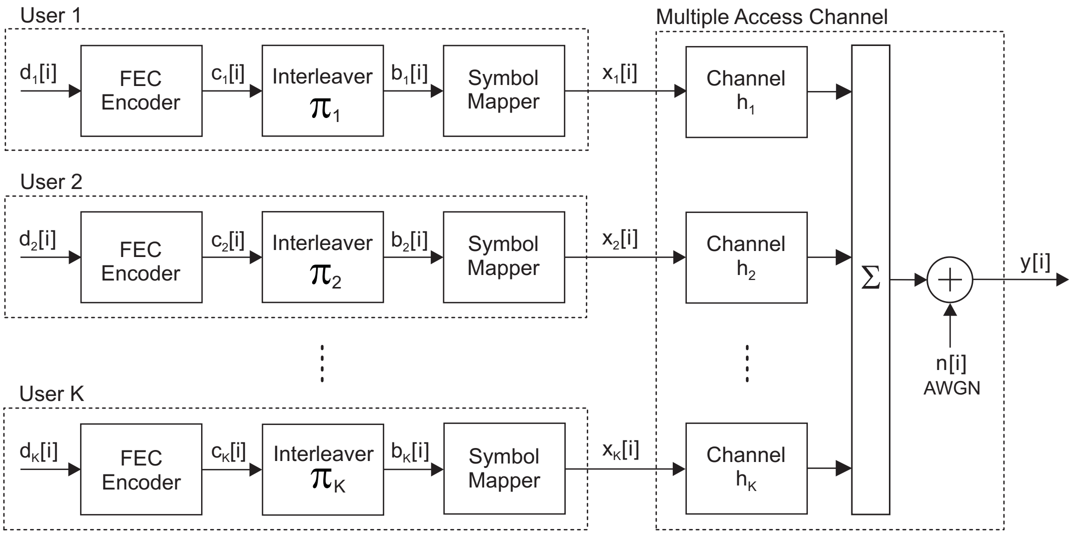

Figure 2.23: IDMA Transmitter Structure and Signal Model

The interleaver sequence π_k must be different for each user since IDMA system users are distinguished soley by their interleaver sequence. The interleavers are assumed to be generated randomly and independently. These interleavers disperse the coded sequences so that the adjacent chips are approximately uncorrelated.

2.10.2 Iterative Receiver and Signal Model

We consider the case of a Rayleigh flat-fading channel. Each received sample can be expressed as

$$y[i] = \sum_{k=1}^{K} h_k x_k[i] + n[i] \tag{2.210}$$

where $x_k[i]$ is the i-th chip transmitted by user k, h_k is the channel coefficient for user k, and $n[i]$ is additive noise sampled from a Gaussian random variable, i.e., $n[i] \sim \mathcal{N}(0, \sigma^2)$.

The joint multiple-access system with FEC coding in Figure 2.23 can be considered as a serially concatenated coding system, in which the FEC code and the multiple-access channel take the roles of the outer code and the inner code, respectively [102]. Using this interpretation, an iterative receiver algorithm based on the turbo decoding concept [12] can be developed. The receiver structure for the multiuser IDMA system is shown in Figure 2.24. It consists of a soft-output elementary signal estimator (ESE) and K

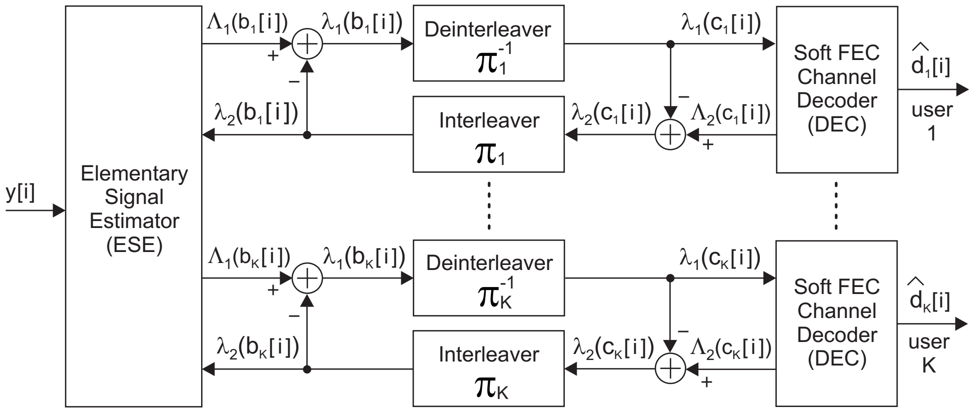

Figure 2.24: IDMA Multiuser Receiver Structure

single-user *a posteriori* probability FEC decoders (DECs). The two stages are separated by interleavers and deinterleavers.

Using the received signal $y[i]$, and the interleaved extrinsic log likelihood ratios (LLRs) of the code bits of the K-users (from the K single-user DECs) as inputs, the soft-output ESE calculates the *a posteriori* LLRs of the code bits of all K-users. These *a posteriori* LLRs are then deinterleaved and fed to the DECs.

Using the deinterleaved extrinsic LLRs of the code bits from the soft-output ESE as input, the DEC of the k-user calculates the *a posteriori* LLRs of the code bits, as well as the LLRs of the information bits. These *a posteriori* LLRs are then interleaved and fed back to the ESE.

This iterative decoding process is sub-optimal as the multiple access and FEC coding constraints are considered separately, however this approach has greatly reduced complexity compared to optimal detection approaches. Next, the receiver components are described.

Elementary Signal Estimator (ESE)

The ESE is developed from [85]. At a given iteration, the ESE estimates the *a posteriori* probabilities (in LLR form) of the code bits $b_k[i]$, which are denoted by $\Lambda_1(b_k[i])$,

$$\Lambda_1(b_k[i]) \triangleq \log \frac{P(b_k[i] = 1 \mid \mathbf{y})}{P(b_k[i] = 0 \mid \mathbf{y})}, \qquad i = 0, \ldots, N-1, \quad k = 1, \ldots, K \tag{2.211}$$

Where $\mathbf{y}$ denotes the received signal vector, given by $\mathbf{y} = [\,y[0], \ldots, y[N-1]\,]^T$. Using Bayes' rule, (2.211) can be rewritten as

$$\Lambda_1(b_k[i]) = \underbrace{\log \frac{P(\mathbf{y} \mid b_k[i]=1)}{P(\mathbf{y} \mid b_k[i]=0)}}_{\lambda_1(b_k[i])} + \underbrace{\log \frac{P(b_k[i]=1)}{P(b_k[i]=0)}}_{\lambda_2(b_k[i])}. \tag{2.212}$$

The first term in (2.212), denoted by $\lambda_1(b_k[i])$, is the extrinsic information calculated by the ESE. The second term, denoted by $\lambda_2(b_k[i])$, is the *a priori* probability (in LLR form) of $b_k[i]$. An estimate of the *a priori* probability is calculated by the DEC of the k-th user at the previous iteration. At the first iteration, no prior information about the code bits is available, therefore all bit values are assumed equiprobable and the *a priori* LLR values are set to zero. Finally, the sequence of extrinsic information, $\{\lambda_1(b_k[i])\}_i$, is deinterleaved by the deinterleaver of the k-th user (producing $\{\lambda_1(c_k[i])\}_i$) and fed into the corresponding DEC as *a priori* information for the next iteration.

The computation of the extrinsic information for each user is now described in detail. For a particular user, k, we can rewrite (2.210) as

$$y[i] = h_k x_k[i] + \zeta_k[i] \tag{2.213}$$

where $\zeta_k[i]$ is the distortion (comprising of AWGN channel noise and interference from other users) contained in sample $y[i]$ with respect to $x_k[i]$, and is given by

$$\zeta_k[i] \triangleq y[i] - h_k x_k[i] = \sum_{\substack{j=1 \\ (j \neq k)}}^{K} h_j x_j[i] + n[i] \tag{2.214}$$

From the central limit theorem, $\zeta_k[i]$ can be approximated as a Gaussian variable, and $y[i]$ can be characterised by a conditional Gaussian probability density function

$$P(y[i] \mid b_k[i] = \pm 1) = \frac{1}{\sqrt{2\pi \mathrm{Var}\{\zeta_k(i)\}}} \exp\left(-\frac{\left(y[i] - (\pm h_k + \mathrm{E}\{\zeta_k[i]\})\right)^2}{2\mathrm{Var}\{\zeta_k[i]\}} \right) \tag{2.215}$$

where $\mathrm{E}\{\,\cdot\,\}$ and $\mathrm{Var}\{\,\cdot\,\}$ denote expectation and variance, respectively. Using (2.213)-(2.215), the chip-by-chip ESE detection algorithm for IDMA systems can be developed as shown in Table 2.6.

1. Given the extrinsic information (in LLR form), $\{\lambda_2(b_k[j])\}_k$, from the FEC decoders, calculate the soft bit statistics for each user ($k = 1, \ldots, K$):

$$\mathrm{E}\{x_k[i]\} = \tanh\left(\frac{1}{2}\lambda_2(b_k[i])\right),$$
$$\mathrm{Var}\{x_k[i]\} = 1 - \left(\mathrm{E}\{x_k[i]\}\right)^2,$$

2. Calculate the received signal statistics:

$$\mathrm{E}\{y[i]\} = \sum_{k=1}^{K} h_k \mathrm{E}\{x_k[i]\},$$
$$\mathrm{Var}\{y[i]\} = \sum_{k=1}^{K} |h_k|^2 \mathrm{Var}\{x_k[i]\} + \sigma^2.$$

3. Calculate the estimated interference mean and variance for each user ($k = 1, \ldots, K$):

$$\mathrm{E}\{\zeta_k[i]\} = \mathrm{E}\{y[i]\} - h_k \mathrm{E}\{x_k[i]\},$$
$$\mathrm{Var}\{\zeta_k[i]\} = \mathrm{Var}\{y[i]\} - |h_k|^2 \mathrm{Var}\{x_k[i]\}$$

4. Perform soft interference cancellation for each user:

$$y_k[i] = y[i] - \mathrm{E}\{\zeta_k[i])\}, \quad k = 1, \ldots, K$$

5. Calculate the extrinsic information, $\{\lambda_1(b_k[i])\}_k$, using:

$$\lambda_1(b_k[i]) = 2h_k \cdot \left(\frac{y_k[i]}{\mathrm{Var}\{\zeta_k[i]\}}\right), \quad k = 1, \ldots, K$$

Table 2.6: Algorithm: Soft Elementary Signal Estimator (ESE) MUD for IDMA

Soft Channel Decoders (DEC)

The channel decoder for the k-th user estimates the *a posteriori* probabilities (APP) in LLR form of the code bits, $\Lambda_2(c_k[i])$, which are given by

$$\begin{aligned}\Lambda_2(c_k[i]) &\triangleq \log \frac{P(c_k[i]=1 \mid \{\lambda_1(c_k[i])\}_i\,;\,\text{code structure})}{P(c_k[i]=0 \mid \{\lambda_1(c_k[i])\}_i\,;\,\text{code structure})}, \\ &= \lambda_2(c_k[i]) + \lambda_1(c_k[i]),\end{aligned} \tag{2.216}$$

for $i = 0, \ldots, N-1$. These *a posteriori* probabilities are computed using the BCJR algorithm [6] (from Section 2.3.3) based on the *a priori* information from the ESE, $\{\lambda_1(c_k[i])\}_i$, and knowledge of the code structure.

As in (2.212), $\Lambda_2(c_k[i])$ can be expressed as the sum of extrinsic information $\lambda_2(c_k[i])$ and *a priori* information $\lambda_1(c_k[i])$. The sequence of extrinsic information, $\{\lambda_2(c_k[i])\}_i$, is interleaved (producing $\{\lambda_2(b_k[i])\}_i$) and fed back to the ESE as *a priori* information for the next iteration.

Additionally, the DEC estimates the *a posteriori* LLRs of the information bits, $\{\Lambda_2(d_k[i])\}_i$, and at the final iteration, performs a hard decision on the information bits, producing $\{\hat{d}_k[i]\}_i$.

2.11 Conclusion

In this chapter, the iterative decoding principles from turbo coding were applied to channel equalization and multiuser detection. The techniques presented will be the basis for the work described in the following chapters. First, the BCJR MAP algorithm was introduced for decoding convolutional codes over an AWGN channel. The BCJR algorithm is a fundamental building block of turbo decoding schemes.

Next, the inter-symbol interference (ISI) channel was presented. For coded data transmissions, the FEC encoder of the transmitter and the ISI channel can be modelled as a serial concatenated coding scheme transmitting over a memoryless channel. This model is similar to a standard serial encoder for turbo coding, and therefore, iterative decoding techniques can be used at the receiver. Iterative decoding for ISI channels is known as turbo equalization. Turbo equalization receiver structures were discussed and performance results presented.

Finally, the multiple-access channel and multiuser detection using iterative decoding was presented. For coded data transmissions, the FEC encoder of the transmitter and the MAI (multiple-access interference) channel can also be modelled as a serial concatenated coding scheme, and therefore, iterative decoding techniques can be utilised. Iterative decoding of multiple-access channels is commonly known as turbo MUD. Low-complexity multiuser detectors for use in turbo MUD receivers were presented for synchronous CDMA, asynchronous CDMA, and asynchronous IDMA systems.

Chapter 3

IDMA Performance Optimisation using Variance Transfer Analysis

In this chapter, Variance Transfer (VT) charts are used to analyse and optimise iterative receiver performance of a multiuser IDMA system. Introduced by Schlegel and Grant [102], VT charts are similar in concept to Extrinsic Information Transfer (EXIT) charts [115], but are better suited for analysing multiuser iterative receivers. VT Charts provide a graphical interpretation of the reliability of information passed between the constituent components of an iterative receiver. Once the VT characteristic curves have been determined, receiver performance can be optimised by attempting to closely match the VT characteristics of the multiuser detector (MUD) and the forward error correction (FEC) channel decoders. The MUD VT characteristic can be manipulated by the selection of multiuser detection algorithm and the number of simultaneous users (system load). The FEC channel decoder VT characteristic can be manipulated by the selection of error correction code.

Two multiuser system scenarios are considered for optimisation:

Layered IDMA with Power Allocation. Firstly, We extend the IDMA concept to a multi-rate system where different users transmit data at different rates and the same low-complexity iterative receiver structure can still be used. High-rate users are supported by breaking up the input data stream into multiple sub-streams. An IDMA layer is created from each sub-stream, and the multiple IDMA layers are then combined and the composite layered signal is transmitted from a single antenna. The iterative receiver treats each IDMA layer as a virtual user.

Chayat et. al. [18] observed that the performance of an iterative receiver is improved if different users transmit at different powers. This allows the iterative decoder to operate in an "onion peeling" mode, where the higher-power layers converge first, decreasing their contribution to the residual noise, and then the lower-power layers converge. CDMA and IDMA systems utilising iterative receivers can exploit this power allocation strategy to gain an improvement in performance. Caire et. al. [17] have shown that this power optimisation problem can be solved by optimising the partial loads, and developed simple optimisation methods based on linear programming techniques. In [103], Schlegel et al. applied the work of [18] and [17] to develop allocation schemes for iterative CDMA receivers that are based on combined soft interference cancellation and MMSE filtering (i.e., CDMA multiuser detector schemes of the type described in Section 2.8.2).

To improve the performance of our layered IDMA scheme, we develop a simple power allocation scheme, where the power levels for each IDMA layer are calculated using Variance Transfer (VT) analysis and linear programming techniques. In a Rayleigh flat-fading environment, simulation results demonstrate that the performance of this proposed system is close to the theoretical limit. This original contribution was published in [63].

FEC Code Allocation for Dynamic Loads. Secondly, we propose an alternative optimisation approach for inducing "onion peeling" operation in the iterative receiver. Ten Brink [116] demonstrated that different FEC codes generate different FEC channel decoder VT characteristics. As an alternative to transmit power allocation, the judicious selection of FEC codes can also be used to match the receiver VT characteristics for optimal performance.

A simple FEC code allocation strategy for multiuser systems with dynamic loads is devised. New users are allocated FEC codes according to the existing system load, which allows the FEC decoder VT curve to dynamically match the MUD VT curve as it changes with system load, providing optimal system performance over a range of operating conditions. We derive a numerical method for optimising performance based on FEC code allocation, and present simulation results. For small multiuser systems, results demonstrate that the performance of the proposed system approaches the theoretical single user bound. This original contribution was published in [65].

3.1 Variance Transfer Charts and Analysis

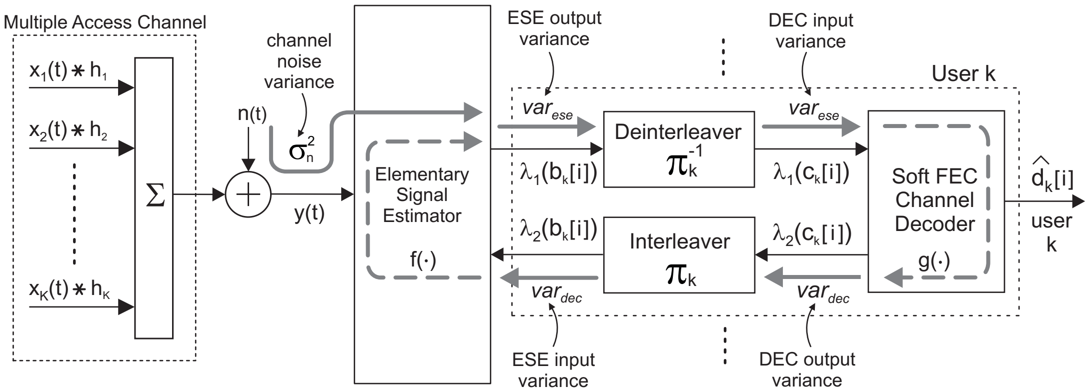

Figure 3.1: Variance transfer between constituent iterative receiver components

The Variance Transfer (VT) chart method [102] analyses the transfer functions of the multiuser detector and the channel decoders in order to predict the behaviour of the iterative receiver. Figure 3.1 shows the variance transfer paths for the IDMA iterative receiver from Section 2.10.2. There are two VT functions:

- The ESE VT function is defined as the variance in the ESE output, var_{ese}, as a function of the error variance in the soft-bit estimates from the FEC decoders, $var_{dec,k}$, and the channel noise variance, σ_n^2, i.e., $var_{ese} = f(var_{dec,k}\ ,\ \sigma_n^2)$
- The FEC channel decoder (DEC) VT function is defined as the variance in the k-th user DEC output, $var_{dec,k}$, as a function of the estimation error variance from the ESE, var_{ese}, i.e., $var_{dec,k} = g(var_{ese})$

3.1.1 ESE Variance Transfer Function

For our IDMA system, the multiuser interference is proportional to the system load, β, and the variance of the estimation error, $var_{dec,k}$. The system load is defined as the ratio of users, K, to bandwidth expansion, R, (i.e. $\beta = K/R$), and the estimation error variance is defined as

$$\mathrm{var}_{dec,k} = \mathrm{E}\left\{(c_k[i] - \hat{c}_k[i])^2\right\} \tag{3.1}$$

We first consider the case of equal power for all users, $P_k = P$. For this case, the estimation error for all users will be equal, $var_{dec,k} = var_{dec}$. For the ESE, the expression for the residual multiple access interference plus channel noise at the input to the FEC decoder is given by

$$\begin{aligned}\mathrm{var}_{ese}(\,\mathrm{var}_{dec}\,) &= \left(\frac{K-1}{R}\right) P\,\mathrm{var}_{dec} + \sigma_n^2 \\ &= \lim_{K\to\infty} \beta P\,\mathrm{var}_{dec} + \sigma_n^2 \qquad (3.2)\end{aligned}$$

where σ_n^2 is the channel noise, and the soft FEC decoder estimation error variance, var_{dec}, is the average power of the residual symbol interference. Therefore, given var_{dec}, equation (3.2) describes the noise variance in the input signal to the FEC decoder for the next iteration. Figure 3.2a shows the ESE VT function (3.2) for a typical IDMA system.

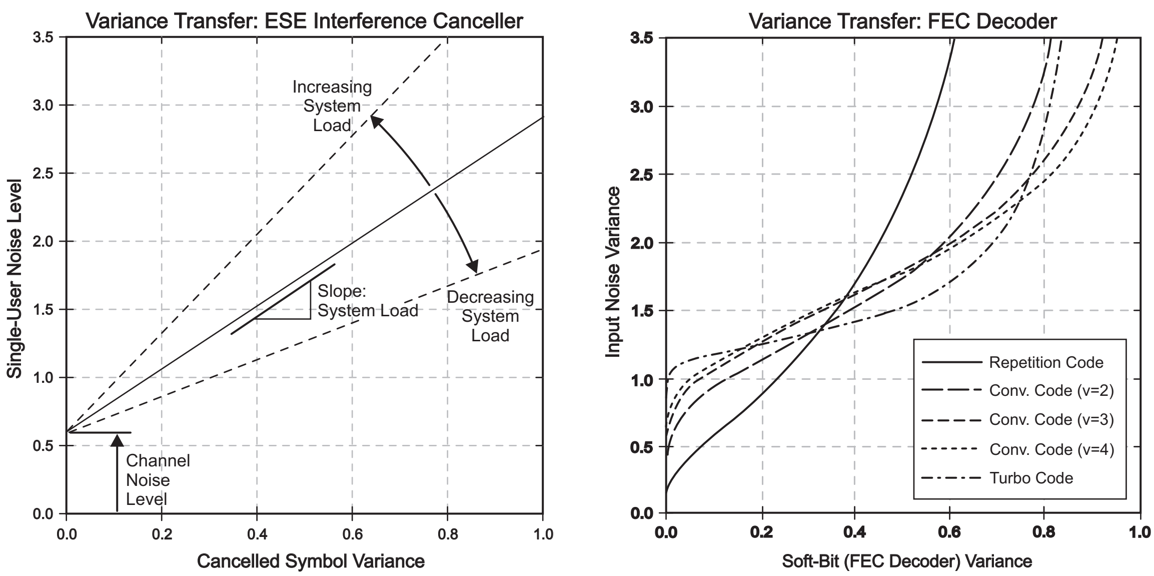

(a) ESE interference canceller **(b)** FEC decoder

Figure 3.2: Variance transfer functions for (a) ESE interference canceller, and (b) FEC decoder (for various 1/3-rate codes)

The more accurate the symbol estimates of the other interfering users, the smaller the residual noise that the error control decoder has to overcome. But even if the interfering symbols are known exactly, the FEC decoder still has to overcome the AWGN channel noise.

3.1.2 FEC Decoder Variance Transfer Function

At the input of the k-th soft FEC decoder, the input sequence has an additive Gaussian noise distortion with associated variance var_{ese} per symbol. Therefore the decoder can be analysed in the same manner as an AWGN channel. The output of the decoder are the soft bit estimates, and the primary measure of their reliability is the variance var_{dec}. Unfortunately, no closed form expression exists for var_{dec} as a function of var_{ese} other than for very simple codes. The VT functions $var_{dec} = g(var_{ese})$ are found using numerical methods by simulating the input-output behaviour of the FEC code. Figure 3.2b shows the VT functions for a repetition code, best known convolutional codes (with constraint lengths, v, of 2, 3, and 4) [54], and a turbo code [12]. All the codes shown have a rate of 1/3.

3.1.3 Example Variance Transfer Chart

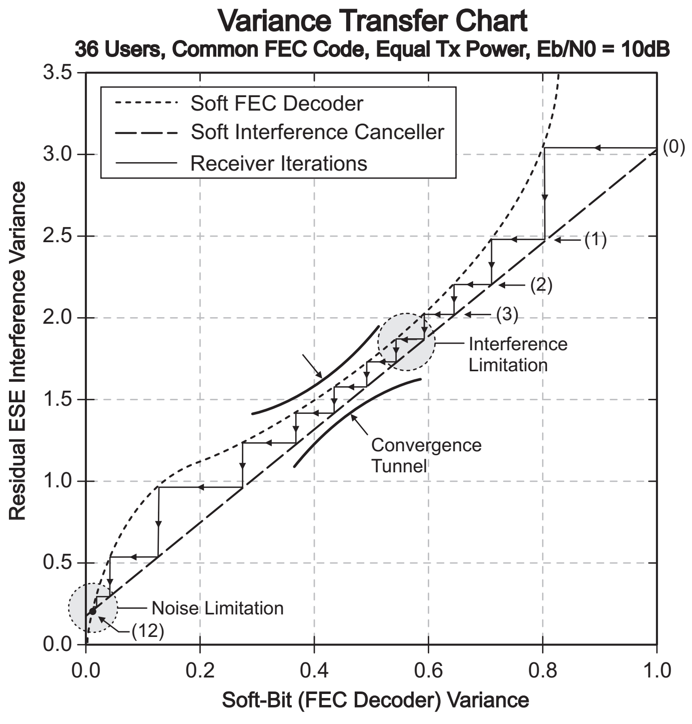

Figure 3.3: Variance transfer chart for an IDMA system with 36 users using equal transmit power and a common FEC code (Eb/N0 = 10dB)

Figure 3.3 shows a VT chart for our IDMA system with all users transmitting at equal power, and a receiver $Eb/N0$ value of 10dB. Decoding starts at point (0) where the FEC decoders have to work with full interference and noise. After the first iteration, the receiver reduces the interference by subtracting estimates of the interfering signals, this leads to point (1). The vertical distance between point (0) and point (1) is the resultant reduction in noise variance at the input of the soft-output FEC decoder. In the next iteration, the noise variance can be further reduced to point (2), and so on, until the iterations reach the intersection point between the two curves, point (12). At this point virtually all the interference has been canceled, and only channel noise is left. The performance of the individual decoders at this point is essentially that of the decoders in Gaussian noise, and is known as the *noise limitation* fix point of the iterative decoder.

In Figure 3.3, note that along the iterative trajectory there is a section which forms a narrow channel through which the trajectory progresses in small steps. This area is the *interference limitation*. An increase in the system load, or reduction in $Eb/N0$ ratio will create another intersection point between the two VT curves (within this interference limitation region), and the variance will stop improving at this *interference limitation* fix point, rather than at the *noise limitation* fix point. Under these conditions, the decoder does not function due to an excessive system load. As the load decreases, or the $Eb/N0$ ratio increases, the channel opens up and convergence to the noise limitation fix point is suddenly enabled. This effect happens at a sharp $Eb/N0$ threshold, and gives rise to the abrupt, cliff-like behaviour of the error rate performance in iterative receivers. This bound on the VT curve allows us to derive the optimal parameters for our IDMA system in order to optimise system performance.

Figure 3.4 demonstrates the iterative receiver operating modes and the effect of $Eb/N0$ on performance. Figure 3.4a shows the VT for an $Eb/N0$ of 1.5dB, the receiver is interference limited and the BER performance is poor regardless of the number of iterations. Figure 3.4b shows the VT for a slightly higher $Eb/N0$ of 3.0dB, here the receiver is no longer interference limited, but “bottlenecked”. Convergence is slow and a large number of iterations are required to achieve good BER performance. Figure 3.4c shows that at the higher $Eb/N0$ of 4.5dB, the bottleneck region has been opened up and convergence is achieved quickly with only a small number of iterations required to achieve good BER performance. These operating regions are also reflected in the BER graph in Figure 3.4d.

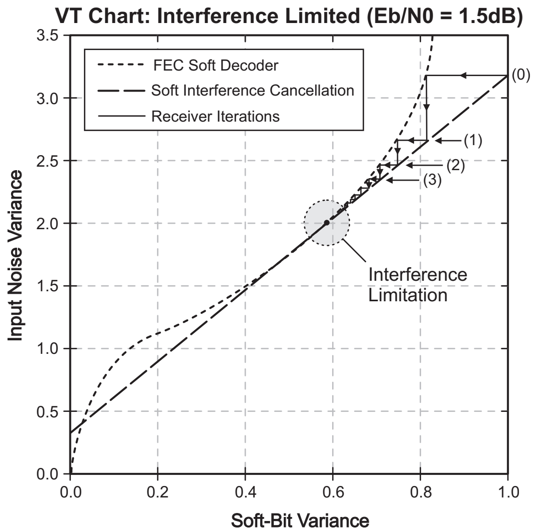

(a) VT at Eb/N0 = 1.5dB

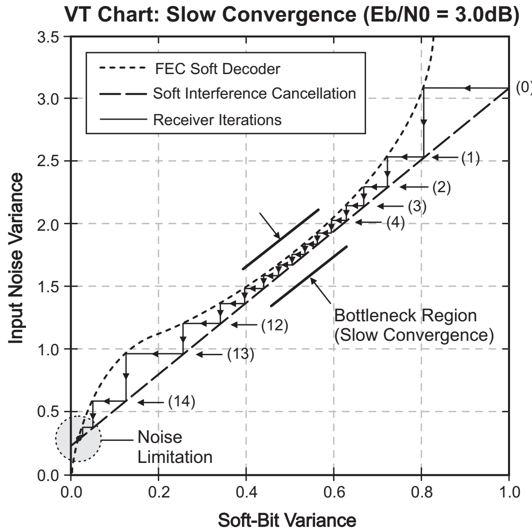

(b) VT at Eb/N0 = 3.0dB

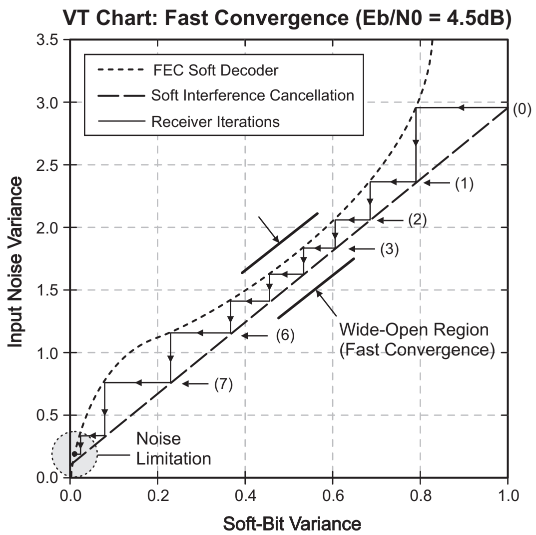

(c) VT at Eb/N0 = 4.5dB

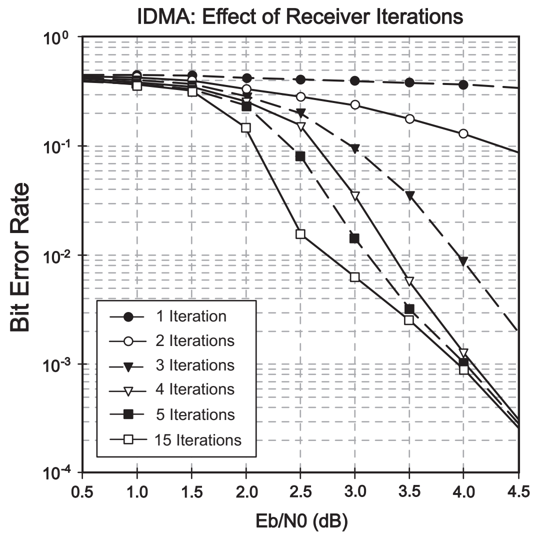

(d) BER Performance

Figure 3.4: Variance transfer charts demonstrating iterative receiver operating modes: (a) interference limited; (b) slow convergence; and (c) fast convergence.

3.2 Multi-Rate IDMA with Power Allocation

We extend the IDMA multiple-access system (from Section 2.10) to a multi-rate system where different users transmit data at different rates and the same low-complexity iterative receiver structure can still be used. High-rate users are supported by breaking up the input data stream into multiple sub-streams. An IDMA layer is created from each sub-stream, and the multiple IDMA layers are then combined and the composite layered signal is transmitted from a single antenna.

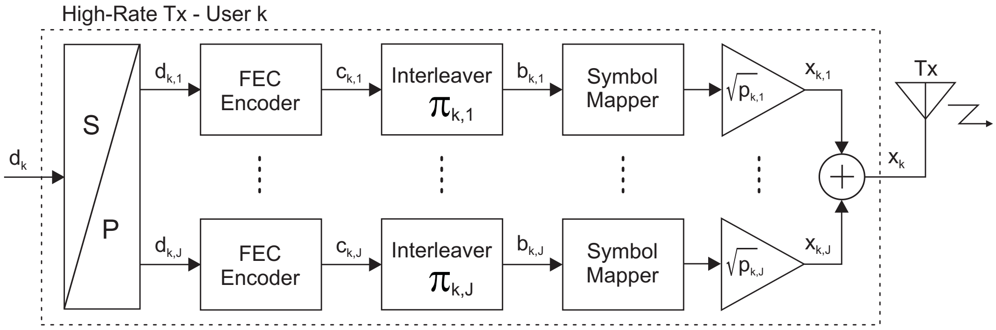

Figure 3.5: Transmitter Structure for the Multi-Rate IDMA System

Figure 3.5 shows the transmitter structure for multi-rate users of the multiple-access scheme. For the high-rate user, a serial-to-parallel converter breaks up the input data stream is into J sub-streams. An IDMA layer is created from each sub-stream, and the multiple layers are then combined and transmitted from a single antenna. Each layer is of equal rate, but unequal power. In order to achieve optimal receiver performance, transmit power is allocated to the various IDMA layers in accordance to the strategy developed in Section 3.2.1.

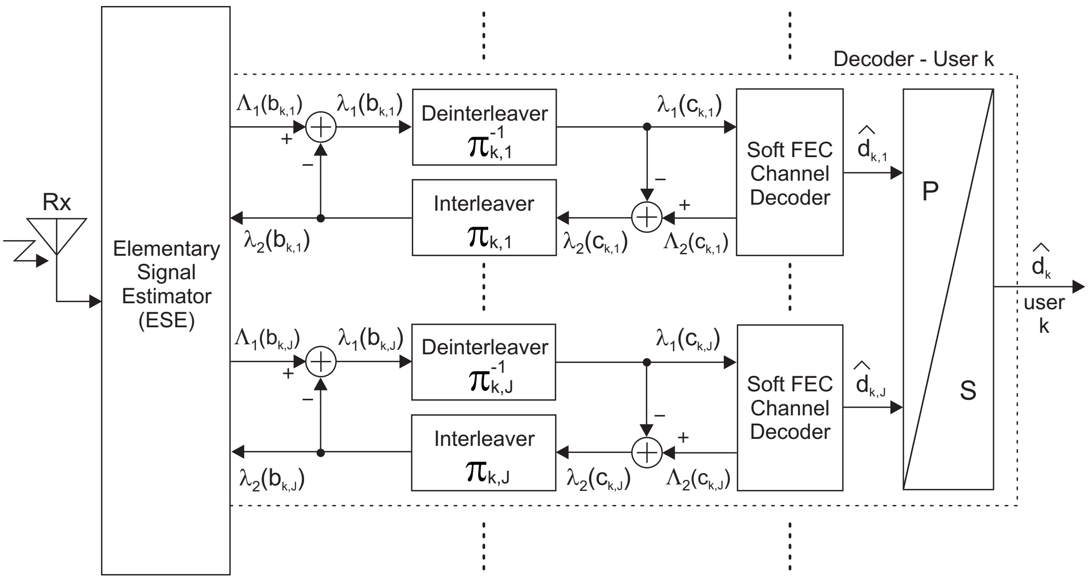

Figure 3.6: Receiver Structure for the Multi-Rate IDMA System

Figure 3.6 shows the receiver structure for the multi-rate IDMA system. The iterative receiver operates as described in Section 2.10.2 and each IDMA layer is treated as a virtual user. After the receiver has decoded the data for each virtual user, a parallel-to-serial converter recombines the IDMA layers into the appropriate high-rate streams for each multi-rate user.

3.2.1 Transmit Power Allocation

Chayat et. al. [18], observed that differences in received power levels are beneficial to the operation of the joint iterative decoder, and that in practice, only a few different power levels are needed to achieve good performance.

We develop a power allocation scheme to improve the performance of our layered IDMA system based on the methods from [102]. First, we extend the VT chart method to the case of unequal received power levels. Denote σ_ι^2 as the error variance in the ESE output, var_{ese}, at iteration ι. The residual interference and noise variance of an arbitrary user, at iteration ι, is given by

$$\sigma_\iota^2 = \frac{1}{R} \sum_{k=1}^{K} P_k \, g\left(\frac{\sigma_{\iota-1}^2}{P_k}\right) + \sigma_n^2 \tag{3.3}$$

where $g(\,\cdot\,)$ is VT function of the FEC decoder (Section 3.1.2). In the case where the users are grouped into J power groups, we find

$$\sigma_\iota^2 = \sum_{j=1}^{J} \frac{K_j P_j}{R} \, g\left(\frac{\sigma_{\iota-1}^2}{P_k}\right) + \sigma_n^2 \tag{3.4}$$

where K_j, is the number of users in group j. Since different users now contribute with different received power levels, we need to consider the *average* system load. The average system load is defined as $\beta_{av} = \sum_{j=1}^{J} \beta_j P_j$. We now obtain

$$\begin{aligned} \sigma_\iota^2 &= \beta_{av} \sum \frac{\beta_j P_j}{\beta_{av}} \, g\left(\frac{\sigma_{\iota-1}^2}{K_j}\right) + \sigma_n^2 \\ &= \beta_{av} \, g_{av}(\sigma_{\iota-1}^2) + \sigma_n^2 \end{aligned} \tag{3.5}$$

where $g_{av}(\sigma_{\iota-1}^2)$ is an *average* variance transfer function. It is obtained by weighing the individual code VT functions by the weight factor $\beta P_j/\beta_{av}$ (composed of their loads and powers). Equation (3.5) can be visualised and charted in a similar manner as the equal power case, where the FEC VT function of the code in the equal power case corresponds to the composite FEC VT function $g_{av}(\,\cdot\,)$ in the unequal power levels case.

If we assume that there are J different power levels, each with a partial load β_j, then the power levels can be optimised using numerical techniques. The number of levels J is arbitrary and determines the complexity of the numerical method. Caire et. al. [17] observed that the power optimisation problem can be solved by optimizing the partial loads. This turns the optimisation into a well-known linear programming problem.

Using the residual recursive interference equation (3.4),

$$\sigma_\iota^2 = \sum_{j=1}^{J} \frac{K_j P_j}{R}\, g\left(\frac{\sigma_{\iota-1}^2}{P_j}\right) + \sigma_n^2 = f(\mathbf{P},\, \boldsymbol{\beta},\, z = \sigma_{\iota-1}^2) \tag{3.6}$$

where $\mathbf{P} = (P_1, \ldots, P_J)$, and $\boldsymbol{\beta} = (\beta_1, \ldots, \beta_J)$. The condition that the VT curves of the FEC decoders and the ESE do not intersect can be reformulated as

$$f(\mathbf{P},\, \boldsymbol{\beta},\, z) < z; \qquad z \in [\sigma_{min}^2, \infty] \tag{3.7}$$

where the lower limit σ_{min}^2 is an arbitrary limit dictated by some minimal performance criterion. In this case we use the error probability of the lowest power level group as the performance criterion. Given the power P_j and the error control codes used, we can calculate the maximum tolerable error variance σ_{min}^2 and (3.7) ensures that no intersection point exist for larger residual interference variances, therefore enforcing this minimal performance criterion. This results in the following optimization problem:

$$\text{minimise} \quad \sum_{j=1}^{J} \beta_j P_j \quad \text{subject to:} \begin{cases} f(\mathbf{P}, \boldsymbol{\beta}, z) \leq z - \varepsilon \\ \sum_{j-1}^{J} \beta_j = \beta \\ \beta_j \geq 0 \end{cases} \tag{3.8}$$

where $z \in [\sigma_{min}^2, \infty]$. The optimisation criterion in (3.8) minimises the average E_b/N_0, which is equivalent to optimising the system load of a given average E_b/N_0. The parameter ε controls the width of the *convergence tunnel* and ensures that there is a sufficient opening for the iterations to proceed through. A wider convergence tunnel allows for faster convergence, but at the cost of a decreased system load. Equation (3.8) becomes a linear optimisation problem which can be solved by numerical techniques.

We consider the optimisation problem for a high-rate transmitter with 3 IDMA layers. Figures 3.7a & 3.7b both show the VT charts for 3 equal-sized power groups. Figure 3.7a uses a FEC code consisting of a 1/3-rate convolutional code serially concatenated with

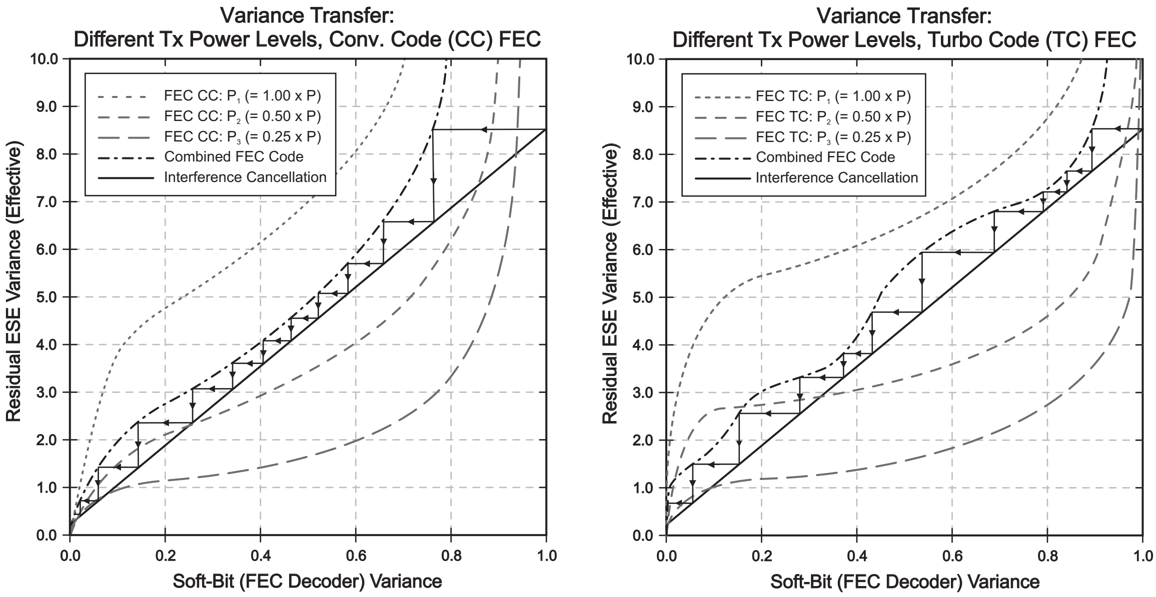

(a) Convolutional code **(b)** Turbo code

Figure 3.7: VT charts for layered-IDMA with power allocation using (a) convolutional code FEC, and (b) turbo code FEC

a 1/6-rate repetition code. Figure 3.7b uses 1/3-rate turbo code concatenated with a 1/6-rate repetition code. In both cases, the optimal power levels are found to be $P_1 = 0.25 \times P, P_2 = 0.50 \times P$, and $P_3 = 1.00 \times P$.

Note that the optimisation strategy does not take into account the physical constraints of the transmitter power amplifier (e.g., power budget and dynamic range). However, the optimisation results are pleasing in that the optimal power levels do not make any untoward demands on the underlying physical hardware and the scheme could be readily implemented using standard transmitter components.

3.2.2 Simulation Results

The simulations assume the receiver has perfect channel knowledge. The system is evaluated for fast time-varying Rayleigh flat-fading channels where the individual user channels are independent and uncorrelated.

Figure 3.8a compares the average bit error rate (BER) for 3 high-rate users after 12 receiver iterations versus the signal to noise ratio (SNR) $Eb/N0$ for layered-IDMA with and without power allocation, and with 2 types of FEC code (convolutional code, and turbo code). For $Eb/N0$ values of 4 dB and greater we observe a performance improvement of 0.5dB to 1.0dB for layered IDMA with power allocation when compared to the equal power case. We also observe a modest improvement (of 0.25dB to 0.5dB) when comparing IDMA with Turbo code FEC against IDMA with convolutional code FEC.

Figure 3.8b compares the average bit error rate (BER) for 9 high-rate users after 12 receiver iterations versus the signal to noise ratio (SNR) $Eb/N0$ for layered-IDMA with and without power allocation, and with 2 types of FEC code (convolutional code, and turbo code). For $Eb/N0$ values of 4 dB and greater we observe a performance improvement of 0.5dB to 1.0dB for layered IDMA with power allocation when compared to the equal power case. We also observe minimal difference between IDMA with Turbo code FEC against IDMA with convolutional code FEC.

3.3 FEC Allocation for Dynamic System Loads

From Figure 3.3 we observe that for good system performance, we need to *match* the FEC decoder VT curve to ESE VT curve, such that the FEC decoder VT curve is always above the ESE VT curve (maintaining an acceptable convergence tunnel width), and only crossing the ESE VT curve at the *noise limitation* fix point. From Figure 3.2b we observe that strong FEC codes are a good match for light system loads, and that weaker FEC codes are a better match for heavier system loads.

We consider a system consisting of a number of persistent users (primary users) and a number of intermittent users (secondary and tertiary users, where the tertiary users are more sporadic that the secondary users). From our observations, we hypothesise that the optimal FEC code allocation strategy is for assign strong FEC codes to primary users, and increasingly weaker FEC codes to the secondary and tertiary users. The composite FEC decoder VT function would be dominated by the strong codes at light loads, and dominated by the weaker codes at heavy loads. We now develop optimisation techniques to test our hypothesis

Caire et. al. [17] observed that the power optimisation problem can be solved by optimising the partial loads, and developed simple optimisation methods based on well-known linear programming techniques. This optimisation method splits the system load into a number of sub-groups (or partial loads), where each sub-groups represents

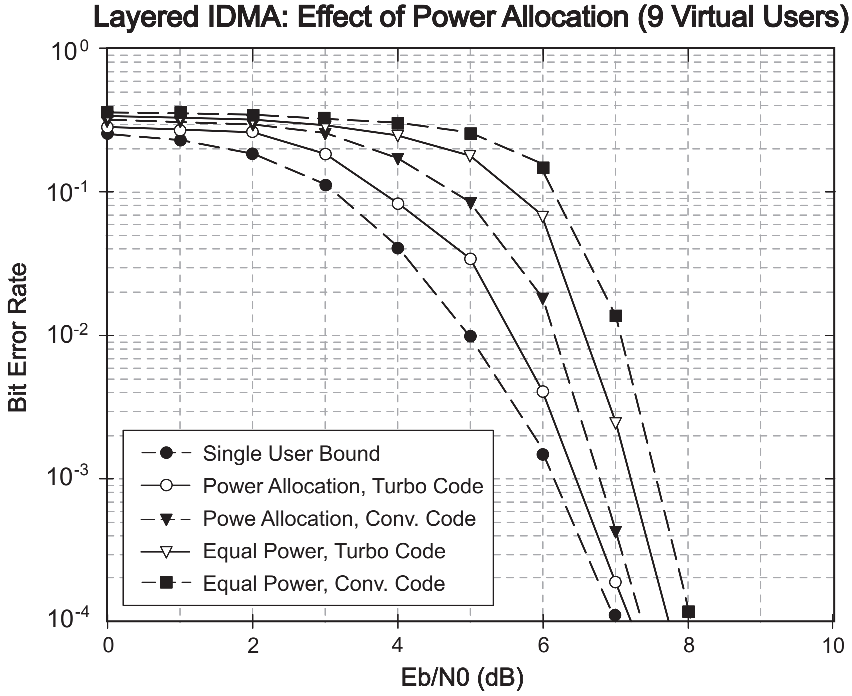

(a) 3 Users with 3-Layers/User

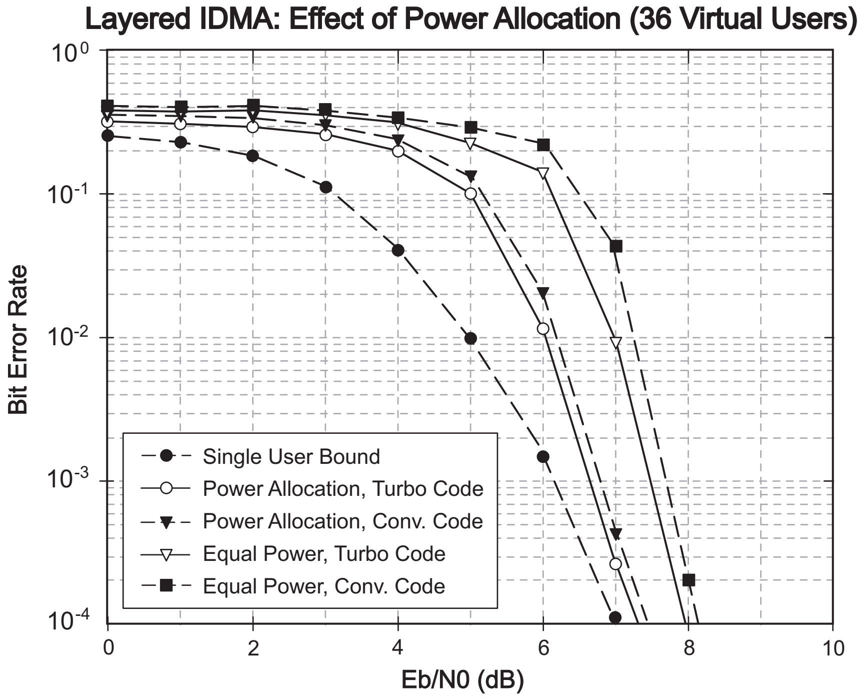

(b) 12 Users with 3-Layers/User

Figure 3.8: Effect of power allocation on layered IDMA Performance for (a) 3 Users with 3-Layers/User; and (b) 12 Users with 3-Layers/User.

a different power level. These sub-groups can be optimised using numerical techniques. The number of sub-groups (power levels) is arbitrary and determines the complexity of the numerical method.

Adapting the optimisation techniques from [17], we develop a simple method for FEC code allocation that optimises the overall system performance.

Denote σ_ι^2 as the error variance in the ESE output, var_{ese}, at iteration ι. The residual interference and noise variance of an arbitrary user, at iteration ι, is given by

$$\sigma_\iota^2 = \frac{1}{R}\sum_{k=1}^{K} P\, g_k\left(\frac{\sigma_{\iota-1}^2}{P_k}\right) + \sigma_n^2 \tag{3.9}$$

where $g_k(\,\cdot\,)$ is the VT function of the FEC decoder for user k (Section 3.1.2). In the case where the users are grouped into J FEC code groups (each group uses a different FEC code), we find

$$\sigma_\iota^2 = \sum_{j=1}^{J} \frac{K_j P}{R}\, g_j\left(\frac{\sigma_{\iota-1}^2}{P}\right) + \sigma_n^2 \tag{3.10}$$

where K_j, is the number of users in group j. Since different users now contribute with different FEC code VT functions, we consider the *average* system load. The average system load is defined as $\beta_{av} = \sum_{j=1}^{J}\beta_j g_j(\,\cdot\,)$. We now obtain

$$\begin{aligned}\sigma_\iota^2 &= \beta_{av}\sum \frac{\beta_j P}{\beta_{av}}\, g_j\left(\frac{\sigma_{\iota-1}^2}{K_j}\right) + \sigma_n^2 \\ &= \beta_{av}\, g_{av}(\sigma_{\iota-1}^2) + \sigma_n^2 \end{aligned} \tag{3.11}$$

where $g_{av}(\sigma_{\iota-1}^2)$ is the *average* VT function, which is obtained by weighing the individual code VT functions by the weight factor β_j/β_{av} (composed of their loads). Equation (3.11) can be graphed in a similar manner as the common FEC code case, where the FEC VT function of the code in the common code case corresponds to the composite FEC VT function $g_{av}(\,\cdot\,)$ in the multiple code groups case.

The residual recursive interference equation, (3.10), can be restated as

$$\sigma_\iota^2 = f\left(\mathbf{g}(\frac{\sigma_{\iota-1}^2}{P}),\, \boldsymbol{\beta},\, z = \sigma_{\iota-1}^2\right) \tag{3.12}$$

where $\mathbf{g}(\,\cdot\,) = (g_1(\,\cdot\,), \ldots, g_J(\,\cdot\,))$, and $\boldsymbol{\beta} = (\beta_1, \ldots, \beta_J)$. By choosing the maximum error probability as the minimum performance criterion, the condition that the VT curves of the FEC decoders and the ESE do not intersect can be reformulated as the following linear optimisation problem:

$$\text{minimise} \quad \sum_{j=1}^{J} \beta_j P g_j(\,\cdot\,) \quad \text{subject to:} \begin{cases} f(\mathbf{g}(\frac{\sigma^2_{\iota-1}}{P}),\, \boldsymbol{\beta},\, z) \leq z - \varepsilon \\ \sum_{j=1}^{J} \beta_j = \beta \\ \beta_j \geq 0 \end{cases} \tag{3.13}$$

where $z \in [\sigma^2_{min}, \infty]$, and σ^2_{min} is the arbitrary lower limit dictated by the minimal performance criterion. The optimisation criterion in (3.13) minimises the average E_b/N_0, which is equivalent to optimising the system load of a given average E_b/N_0. The parameter ε controls the width of the *convergence tunnel* and ensures that there is a sufficient opening for the iterations to proceed through. A wider convergence tunnel allows for faster convergence, but at the cost of a decreased system load. Equation (3.13) can be solved by numerical techniques.

We consider the optimisation problem for an IDMA system with 8 primary users (always present), 8 secondary users and 16 tertiary users (where the secondary and tertiary users are intermittent users, the tertiary users are more sporadic than the secondary users). To minimise the complexity of the optimisation problem, we consider an allocation of 3 FEC codes (one code for each user group). Each of the following candidate codes are considered for optimisation: convolutional codes with constraint lengths,v, of $2, 3, 4, 5,$ and 6; and turbo codes with RSC encoders of constraint lengths 2 and 3. All candidate codes are rate 1/3.

The optimal FEC code allocation for the three user groups are found to be turbo code (with RSC encoders of constraint length 2) for the primary user group; convolutional code with constraint length of 3 for the secondary user group; and convolutional code code with constraint length of 2 for the tertiary user group.

We also consider the optimisation problem for an IDMA system where FEC code allocation is not used, and all 32 users (8 primary, 8 secondary, and 16 tertiary) employ the same FEC code. Using the same candidate group of codes, the optimal FEC code is found to be the convolutional code with constraint length of 3.

3.3.1 Simulation Results

The simulations assume the receiver has perfect channel knowledge. The system is evaluated for fast time-varying Rayleigh flat-fading channels where the individual user channels are independent and uncorrelated.

We consider the scenario of an IDMA system with up to 32 simultaneous users (consisting of 8 primary users, which are always present; 8 secondary users; and 16 tertiary users, where the secondary and tertiary users are intermittent users, and the tertiary users are more sporadic than the secondary users). We compare the performance of a system employing FEC code allocation against a system using a common FEC code for all users (in this latter case, the FEC code is a convolutional code with constraint length of 3, which was found to be the optimal code for a 32-user system without code allocation).

Figure 3.9a compares the average bit error rate (BER) for 9 users after 12 receiver iterations versus the signal to noise ratio (SNR) $Eb/N0$ for an IDMA system with and without FEC code allocation. For $Eb/N0$ values of 4 dB and greater we observe a performance improvement of up 0.5dB to 0.8dB for IDMA with FEC code allocation when compared to the standard FEC code case. We also observe that performance of the IDMA system with FEC code allocation is generally within 0.5dB of the single user bound.

Figure 3.9b compares the average BER for 16 and 32 users after 12 receiver iterations versus the SNR $Eb/N0$ for an IDMA system with and without FEC code allocation. For $Eb/N0$ values of 4 dB and greater, with 16 users, we observe a performance improvement of approximately 0.5dB to 1.0dB for IDMA with FEC code allocation when compared to the standard FEC code case. For 32 users, we observe a modest performance improvement of approximately 0.3dB when comparing FEC code allocation against standard FEC code case.

3.4 Conclusion

The analysis of iterative multiuser receiver performance using Variance Transfer (VT) analysis has been presented. It was shown that receiver performance is optimal when the VT characteristics of the constituent components are "matched". Using linear programming techniques, allocation schemes for transmitter power and FEC codes were

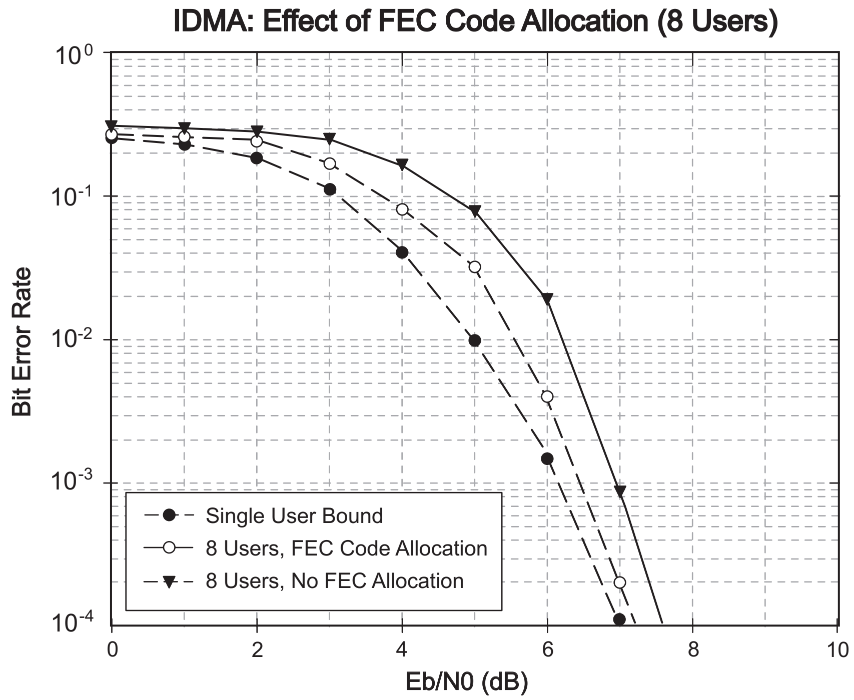

(a) 8 simultaneous users

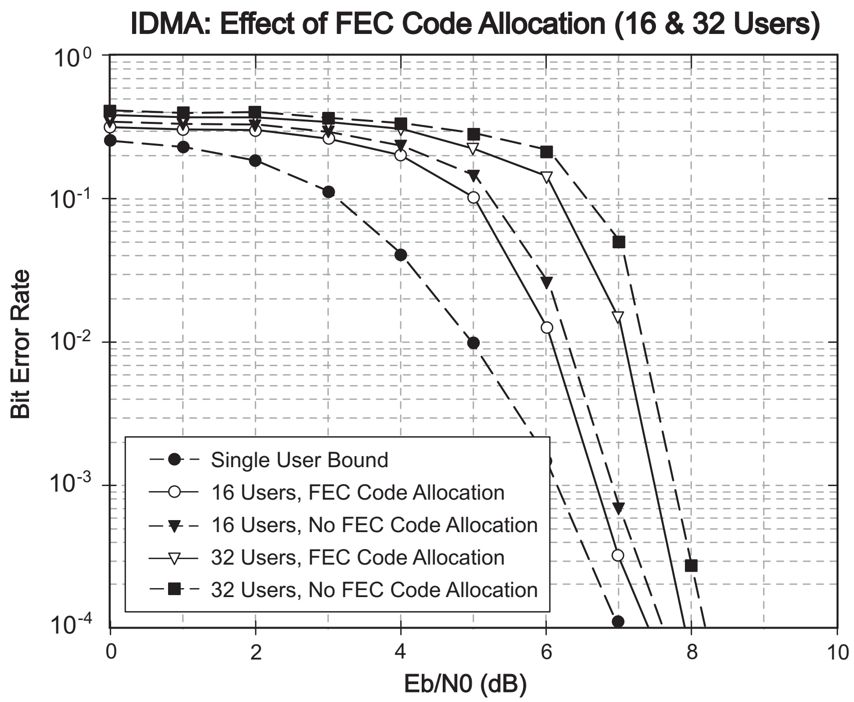

(b) 16 and 32 simultaneous users

Figure 3.9: Effect of FEC allocation on IDMA performance for (a) 8 simultaneous users; and (b) 16 and 32 simultaneous users

developed to achieve optimal system performance. Two multiuser system scenarios were considered for optimisation.

First, a multi-rate multiuser scheme using the layered-IDMA with power allocation was presented and compared with a layered scheme without power allocation (equal power). The layered IDMA scheme with power allocation was shown to provide superior performance at moderate and high SNR levels while using the same low-complexity iterative decoding receiver structure as the other IDMA schemes. In a Rayleigh flat-fading environment, simulation results show that for $Eb/N0$ values of 6dB and greater, the performance of layered IDMA system with power allocation is within 0.5dB of the single user bound.

Second, an IDMA multiuser scheme employing FEC code allocation for dynamic loads was presented and compared with a IDMA scheme without FEC code allocation (all users employ the same FEC code). The IDMA scheme with FEC code allocation was shown to provide superior performance at moderate and high SNR levels while using the same low complexity iterative decoding receiver structure as the other IDMA schemes. In a Rayleigh flat-fading environment, simulation results show that for $Eb/N0$ values of 6.5dB and greater, the performance of the IDMA system with FEC code allocation and 32 simultaneous users is within 0.7dB of the single user bound.

Chapter 4

Optimal Space-Time Coding using the Golden Code

In recent years, multiple antenna systems (commonly referred to as multi-input multi-output or MIMO systems) have proven to be an effective method for realising high-rate reliable wireless communications. Research in MIMO systems has generally focused on providing either higher-rate or increased diversity over traditional single antenna (SISO) systems.

Foschini [30] introduced the layered space-time (BLAST) architecture where a high throughput rate is achieved by using multiple transmit antennas to transmit multiple independent data sub-streams in parallel. Multiple receive antennas and multi-user detection algorithms are used at the receiver end to separate and decode the individual sub-streams. Although providing high-rate, BLAST has the shortcoming that it does not provide diversity gain as each data symbol is only transmitted once from one antenna.

Alamouti [3] introduced a simple orthogonal space time block code (STBC) that provided diversity gain for 2×1 and 2×2 multi-antenna systems. This scheme was generalised and extended by Tarokh et. al. [113] to include higher-dimension MIMO systems, using real and complex orthogonal STBCs. Although providing diversity gain, orthogonal STBCs have the shortcoming that (with the exception of a few sporadic codes) the coding rate does not exceed 1/2.

A generalised class of space-time codes that encompassed both orthogonal STBCs and BLAST architectures was proposed by Hassibi and Hochwald [39]. This generalised class of codes, which are known as linear dispersion (LD) codes, are defined as codes that break up the input data stream into sub-streams that are dispersed in linear combinations over space and time. Theoretically, LD codes can provide both diversity gain and high-rate. In general, LD codes can outperform their orthogonal STBC and BLAST sub-classes.

Sethuraman et. al. [105] proposed a methodology for designing full-diversity high-rate LD codes using cyclic division algebras. A division algebra is used to provide a structured set of invertible matrices to construct LD space-time codes. Using this technique, Belfiore et. al. [7] developed the *Golden Code*, a 2×2 LD code that provides both diversity gain and full-rate.

In the first part of this chapter, we investigate the effect of Doppler spread on the performance of the 2×2 Golden Code single-user system. Doppler spread is a measure of spectral broadening caused by the relative motion between the transmitter and receiver antennas or by the movement of reflecting objects in the channel. Doppler spread is an important consideration in the design of mobile communication systems.

The decoding methodology for the Golden code is presented, followed by performance comparisons with the Alamouti code and V-BLAST in Rayleigh fading environments with Doppler spread. Simulation results show that the Golden Code outperforms both the Alamouti code and V-BLAST at high SNR levels. For a symbol error rate of 10^{-4} the Eb/N0 requirement for the Golden code is 5dB less than the Alamouti code and V-BLAST. This original contribution was published in [60].

The second part of this chapter considers the multiuser case, and we develop a MIMO framework for IDMA that can provide both diversity gain and high-rate.

Recently multiuser MIMO-IDMA has been proposed [81], where IDMA has been generalised to multiple antenna systems where users employ V-BLAST (vertical-encoded layered space time) spatial multiplexing to achieve higher data rates. Decoding is still performed by an iterative receiver whose complexity is linear in the number of users. We further extend the MIMO-IDMA concept from IDMA with V-BLAST spatial multiplexing to IDMA with linear dispersion (LD) codes.

In particular, we investigate the performance of the MIMO-IDMA using the Golden Code. The Golden Code (GC), is 2×2 LD code derived from cyclic division algebra that provides both diversity gain and full-rate [7]. We compare the performance of this GC-IDMA scheme against MIMO-IDMA schemes employing the Alamouti code and V-BLAST, and also against the single-user bound. In a Rayleigh flat-fading environment, simulation results show that GC-IDMA outperforms both Alamouti- and V-BLAST-IDMA at moderate and high SNR levels. For signal to noise ratios of 8dB and greater, the GC-IDMA scheme employing 16 users approaches within 0.25dB of the single-user bound. This original contribution was published in [62].

4.1 Single-User MIMO System Model

The system model for a multiple-antenna communications system with N transmit and M receive antennas is shown in Figure 4.1.

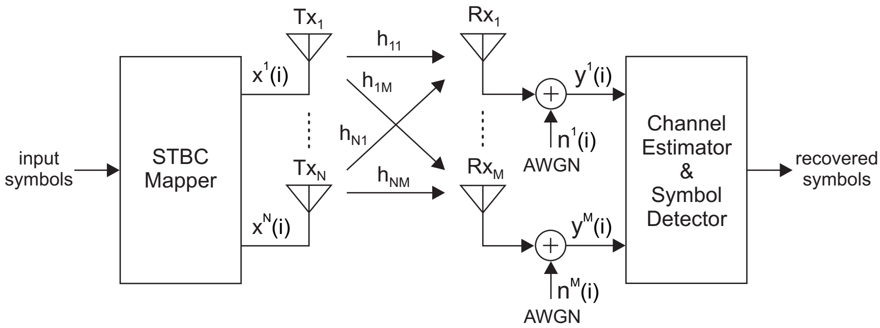

Figure 4.1: MIMO communications system model

If we assume a narrow-band flat-fading wireless channel which is constant for at least P channel uses, then the transmitted and received signals are related by

$$\mathbf{y}(i) = \sqrt{\frac{\rho}{N}}\mathbf{H}\mathbf{x}(i) + \mathbf{n}(i) \qquad i = 1, 2, \ldots, P \tag{4.1}$$

where i is an individual channel use, and we define

$$\mathbf{y}(i) = \begin{bmatrix} y^1(i) \\ y^2(i) \\ \vdots \\ y^M(i) \end{bmatrix}, \quad \mathbf{x}(i) = \begin{bmatrix} x^1(i) \\ x^2(i) \\ \vdots \\ x^N(i) \end{bmatrix}, \quad \mathbf{n}(i) = \begin{bmatrix} n^1(i) \\ n^2(i) \\ \vdots \\ n^M(i) \end{bmatrix} \tag{4.2}$$

where $\mathbf{y}(i)$ is the M-dimensional vector of complex received signals during channel use i, $\mathbf{x}(i)$ is the N-dimensional vector of complex transmitted signals, $\mathbf{H}$ is the $M \times N$ channel matrix, and $\mathbf{n}(i)$ is the M-dimensional vector of additive complex-Gaussian noise (assumed to be zero-mean and unit-variance).

If we assume that $\mathbf{H}$, $\mathbf{x}(\tau)$ and $\mathbf{n}(\tau)$ are random and independent quantities, the signal power normalisation $\sqrt{\rho/N}$ ensures that ρ is the signal-to-noise ratio (SNR) at each receive antenna, independently of N. It is assumed that the channel matrix is known by the receiver.

We define the matrices $\mathbf{Y}$, $\mathbf{X}$, and $\mathbf{V}$ as:

$$\mathbf{Y} = \begin{bmatrix} \mathbf{y}^T(1) \\ \mathbf{y}^T(2) \\ \vdots \\ \mathbf{y}^T(P) \end{bmatrix}, \quad \mathbf{X} = \begin{bmatrix} \mathbf{x}^T(1) \\ \mathbf{x}^T(2) \\ \vdots \\ \mathbf{x}^T(P) \end{bmatrix}, \quad \mathbf{V} = \begin{bmatrix} \mathbf{n}^T(1) \\ \mathbf{n}^T(2) \\ \vdots \\ \mathbf{n}^T(P) \end{bmatrix}$$

where the superscript T denotes transpose. Equation (4.1) is usually more convenient in its transposed form, i.e.,

$$\mathbf{Y} = \sqrt{\frac{\rho}{N}}\mathbf{X}\mathbf{H} + \mathbf{V} \tag{4.3}$$

where the transpose notation is omitted from $\mathbf{H}$, and the channel matrix is simply redefined to have dimension $N \times M$. $\mathbf{Y}$ is the $P \times M$ received signal matrix, $\mathbf{X}$ is the $P \times N$ transmitted signal matrix, and $\mathbf{n}$ is the $P \times M$ additive noise matrix. In matrices $\mathbf{Y}$, $\mathbf{X}$, and $\mathbf{V}$, time runs vertically and space runs horizontally.

4.2 Space-Time Coding and Linear Dispersion Codes

A space-time block code (STBC) is defined by a $(P \times N)$ code matrix $\mathbf{X}$, where N denotes the number of transmit antennas or the *spatial* transmitter diversity order, and P denotes the number of channel usages for transmitting a STBC codeword or the *temporal* transmitter diversity order [113].

The STBC encoder takes as input a code vector, $\mathbf{x}$, and transmits each row of symbols as specified in $\mathbf{X}$ at P consecutive channel usages. At each channel usage, the symbols contained in the N-dimensional row vector of $\mathbf{X}$ are transmitted through N transmitter antennas simultaneously.

As an example, consider the 2×2 Alamouti STBC (ie., $P = 2, N = 2$). The Alamouti STBC matrix $\mathbf{X}$ is defined by

$$\mathbf{X} = \begin{bmatrix} x(1) & x(2) \\ -x^*(2) & x^*(1) \end{bmatrix} \tag{4.4}$$

where $(\cdot)^*$ denotes the complex conjugate operation. The input to this STBC is the code vector $\mathbf{x} = [\,x(1),\, x(2)\,]^T$. During the first channel use, the two symbols of the top row of $\mathbf{X}$, $[\,x(1),\, x(2)\,]$, are transmitted simultaneously from the two transmit antennas; and during the second channel use, the symbols in the second row of $\mathbf{X}$, $[\,-x^*(2),\, x^*(1)\,]$, are transmitted.

A Linear Dispersion (LD) code is a general class of space time block code (STBC) that breaks up the input data stream into sub-streams that are dispersed in linear combinations over space and time. Specifically, a linear dispersion code is defined as:

$$\mathbf{X} = \sum_{q=1}^{Q} (x_q \mathbf{C}^q + x_q^* \mathbf{D}^q) \tag{4.5}$$

where the data sequence is broken up into Q sub-streams, $x_1, \ldots, x_Q$ are complex symbols from an arbitrary constellation (typically r-PSK or r-QAM), and $\mathbf{C}^q$ and $\mathbf{D}^q$ are fixed $P \times N$ complex matrices. The code is completely determined by the set of dispersion matrices $\{\mathbf{C}^q,\, \mathbf{D}^q\}$.

It is generally more convenient to decompose the complex scalar x_q into its real and imaginary components

$$x_q = \alpha_q + j\beta_q, \qquad q = 1, \ldots, Q \tag{4.6}$$

The LD code can then be redefined in terms of real and imaginary components as follows:

$$\mathbf{X} = \sum_{q=1}^{Q} (\alpha_q \mathbf{A}^q + j\beta_q \mathbf{B}^q) \tag{4.7}$$

where $\mathbf{A}^q = \mathbf{C}^q + \mathbf{D}^q$ and $\mathbf{B}^q = \mathbf{C}^q - \mathbf{D}^q$. The dispersion matrices $\{\mathbf{A}^q,\, \mathbf{B}^q\}$ also completely specify the code. LD codes include many commonly used ST codes including the Alamouti Scheme and V-BLAST (Vertical-encoding spatial multiplexing).

4.3 Decoding of Linear Dispersion Codes

This LD decoding method for the single-user case was developed from the framework proposed by Hassibi and Hochwald [39]. An important property of LD codes (4.7) is their linearity in the variables α_q, β_q, leading to efficient decoding schemes. To see this, we substitute the LD code equation (4.7) into the received signal equation (4.3) which forms the following block equation:

$$\mathbf{Y} = \sqrt{\frac{\rho}{N}}\mathbf{XH} + \mathbf{V} = \sqrt{\frac{\rho}{N}}\sum_{q=1}^{Q}(\alpha_q \mathbf{A}^q + j\beta_q \mathbf{B}^q)\mathbf{H} + \mathbf{V} \tag{4.8}$$

The matrices in (4.8) can be decomposed into their real and imaginary components to obtain:

$$\mathbf{Y}_R = \sqrt{\frac{\rho}{N}}\sum_{q=1}^{Q}\left[(\mathbf{A}_R^q\mathbf{H}_R - \mathbf{A}_I^q\mathbf{H}_I)\alpha_q + (-\mathbf{B}_I^q\mathbf{H}_R - \mathbf{B}_R^q\mathbf{H}_I)\beta_q\right] + \mathbf{V}_R$$
$$\mathbf{Y}_I = \sqrt{\frac{\rho}{N}}\sum_{q=1}^{Q}\left[(\mathbf{A}_I^q\mathbf{H}_R - \mathbf{A}_R^q\mathbf{H}_I)\alpha_q + (\mathbf{B}_R^q\mathbf{H}_R - \mathbf{B}_I^q\mathbf{H}_I)\beta_q\right] + \mathbf{V}_I$$

where

$$\begin{array}{llll} \mathbf{Y}_R = \Re\{\mathbf{Y}\}, & \mathbf{H}_R = \Re\{\mathbf{H}\}, & \mathbf{V}_R = \Re\{\mathbf{V}\}, & \text{and} \\ \mathbf{Y}_I = \Im\{\mathbf{Y}\}, & \mathbf{H}_I = \Im\{\mathbf{H}\}, & \mathbf{V}_I = \Im\{\mathbf{V}\}. & \end{array}$$

Where $\Re\{z\}$ and $\Im\{z\}$ denote the real and imaginary parts respectively of the complex value z.

We denote the columns of $\mathbf{Y}_R$, $\mathbf{Y}_I$, $\mathbf{H}_R$, $\mathbf{H}_I$, $\mathbf{V}_R$ and $\mathbf{V}_I$ by $\mathbf{y}_R^m$, $\mathbf{y}_I^m$, $\mathbf{h}_R^m$, $\mathbf{h}_I^m$, $\mathbf{n}_R^m$ and $\mathbf{n}_I^m$ respectively, and define:

$$\mathcal{A}^q = \begin{bmatrix} \mathbf{A}_R^q & -\mathbf{A}_I^q \\ \mathbf{A}_I^q & \mathbf{A}_R^q \end{bmatrix}, \quad \mathcal{B}^q = \begin{bmatrix} -\mathbf{B}_I^q & -\mathbf{B}_R^q \\ \mathbf{B}_R^q & -\mathbf{B}_I^q \end{bmatrix}, \quad \underline{\mathbf{h}}^m = \begin{bmatrix} \mathbf{h}_R^m \\ \mathbf{h}_I^m \end{bmatrix} \tag{4.9}$$

where $m = 1, \ldots, M$. The equations in $\mathbf{Y}_R$ and $\mathbf{Y}_I$ can be assembled to form the single real system of equations

$$\begin{bmatrix} \mathbf{y}_R^1 \\ \mathbf{y}_I^1 \\ \vdots \\ \mathbf{y}_R^M \\ \mathbf{y}_I^M \end{bmatrix} = \sqrt{\frac{\rho}{N}}\mathcal{H} \begin{bmatrix} \alpha_1 \\ \beta_1 \\ \vdots \\ \alpha_Q \\ \beta_Q \end{bmatrix} + \begin{bmatrix} \mathbf{n}_R^1 \\ \mathbf{n}_I^1 \\ \vdots \\ \mathbf{n}_R^M \\ \mathbf{n}_I^M \end{bmatrix} \tag{4.10}$$

where the equivalent $2MP \times 2Q$ real channel matrix is given by:

$$\mathcal{H} = \begin{bmatrix} \mathcal{A}^1\underline{\mathbf{h}}^1 & \mathcal{B}^1\underline{\mathbf{h}}^1 & \ldots & \mathcal{A}^Q\underline{\mathbf{h}}^1 & \mathcal{B}^Q\underline{\mathbf{h}}^1 \\ \vdots & \vdots & \vdots & \vdots & \vdots \\ \mathcal{A}^1\underline{\mathbf{h}}^M & \mathcal{B}^1\underline{\mathbf{h}}^M & \ldots & \mathcal{A}^Q\underline{\mathbf{h}}^M & \mathcal{B}^Q\underline{\mathbf{h}}^M \end{bmatrix} \tag{4.11}$$

We now have a linear relation between the input vector $\mathbf{x}$ and the output vector $\mathbf{y}$:

$$\mathbf{y} = \sqrt{\frac{\rho}{N}}\mathcal{H}\mathbf{x} + \mathbf{n} \tag{4.12}$$

where the equivalent channel $\mathcal{H}$ is known to the receiver because the original channel $\mathbf{H}$, and the dispersion matrices are all known to the receiver. The receiver uses (4.11) to find the equivalent channel. The system of equations between the transmitter and receiver is not under-determined as long as $Q \leq MP$.

Any decoding scheme that can solve a well-conditioned system of linear equation can be used for decoding of LD codes. Suitable decoding techniques include successive nulling and canceling (as used for V-BLAST), and sphere decoding.

4.4 The Golden Code

Sethuraman et. al. [105] proposed a methodology for designing full-diversity high-rate LD codes using cyclic division algebras. A division algebra is used to provide a structured set of invertible matrices to construct LD space-time codes. In general, LD codes derived from cyclic division algebra have been found to provide better performance than LD

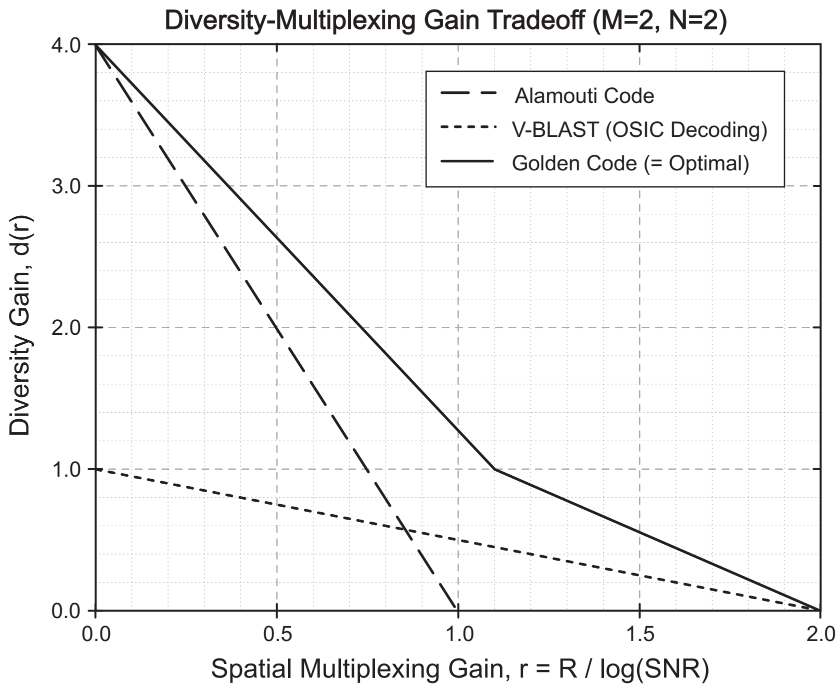

Figure 4.2: Diversity-Multiplexing Gain Tradeoff (M=2, N=2) [142] [83]

codes derived using the original information theoretic approach proposed by Hassibi and Hochwald [39].

The Golden Code is a full-rate 2×2 LD code and is defined as subset of the cyclic division algebra $(\mathbb{Q}(i, \sqrt{5}), i)$ with centre $\mathbb{Q}(i)$ [7]. The 2×2 Golden Code has the structure:

$$\mathbf{X} = \frac{1}{\sqrt{5}} \begin{bmatrix} \alpha\{x(1) + x(2)\theta\} & \alpha\{x(3) + x(4)\theta\} \\ j\bar{\alpha}\{x(3) + x(4)\bar{\theta}\} & \bar{\alpha}\{x(1) + x(2)\bar{\theta}\} \end{bmatrix} \tag{4.13}$$

where

$$\theta = \frac{1 + \sqrt{5}}{2}, \qquad \bar{\theta} = \frac{1 - \sqrt{5}}{2} = (1 - \theta), \qquad \alpha = j(1 - \theta), \qquad \bar{\alpha} = 1 + j(1 - \bar{\theta})$$

and $j = \sqrt{-1}$. In [114], Tarokh et. al. defined the rank criterion and determinant criterion for designing ST codes. Oggier et. al. [82] extended this design criteria to include: (a) full rate; (b) full diversity; (c) non-vanishing determinant for increasing spectral efficiency; (d) good shaping of the constellation; and (e) uniform average transmitted energy per antenna. ST Codes that meet all of these criteria are termed *perfect* space-time block codes. The Golden Code has been found to be the best *perfect* code for MIMO systems with 2 transmit and 2 or more receive antennas.

Elia et. al. [25] have shown that the Golden code achieves the optimal diversity-multiplexing tradeoff for a 2×2 MIMO system. Zheng and Tse [142] developed a simple characterisation of the optimal tradeoff between diversity and degrees of freedom (multiplexing gain), and then used it to evaluate the performance of existing multiple antenna schemes. The concept is that for a given MIMO channel, both diversity and multiplexing gain can be simultaneously obtained, but there is a fundamental tradeoff between how much of each type of gain any coding scheme achieve. For example, for a particular coding scheme, increased spatial multiplexing gain comes at the cost of reduced diversity gain. Figure 4.2 uses Zheng's and Tse's method to compare the Alamouti STBC, V-BLAST and the Golden Code STBC.

From Figure 4.2 we see that neither the Alamouti STBC nor V-BLAST are optimal. The Alamouti STBC does not provide full spatial-multiplexing gain, while V-BLAST does not provide full diversity gain. The Golden Code however provides both the full spatial-muliplexing gain and the full diversity gain available for a 2×2 system.

4.5 Single-User System Performance

The simulations assume the receiver has perfect channel knowledge. The individual channels in the channel matrix are uncorrelated, and the system does not use error correction coding. The constellations of each of the coding schemes has been chosen to ensure a common spectral efficiency of 8-bits per channel use. The V-BLAST and Golden code simulations both use 16-QAM constellations, while the Alamouti code simulations use 256-QAM (the higher-order constellation is required to compensate for the absence of spatial multiplexing gain).

In Figure 4.3 we compare the performance of the Golden Code STBC against the Alamouti code and V-BLAST in a Rayleigh flat-fading environment. The figure shows the superior performance of the Golden code, particularly at higher SNR values. For a symbol error rate of 10^{-4} the Eb/N0 requirement for the Golden code is 5dB less than the Alamouti code and V-BLAST.

Figure 4.4a compares the performance of the Golden code over a range of Doppler frequencies that would be typical in mobile communications scenarios. We observe

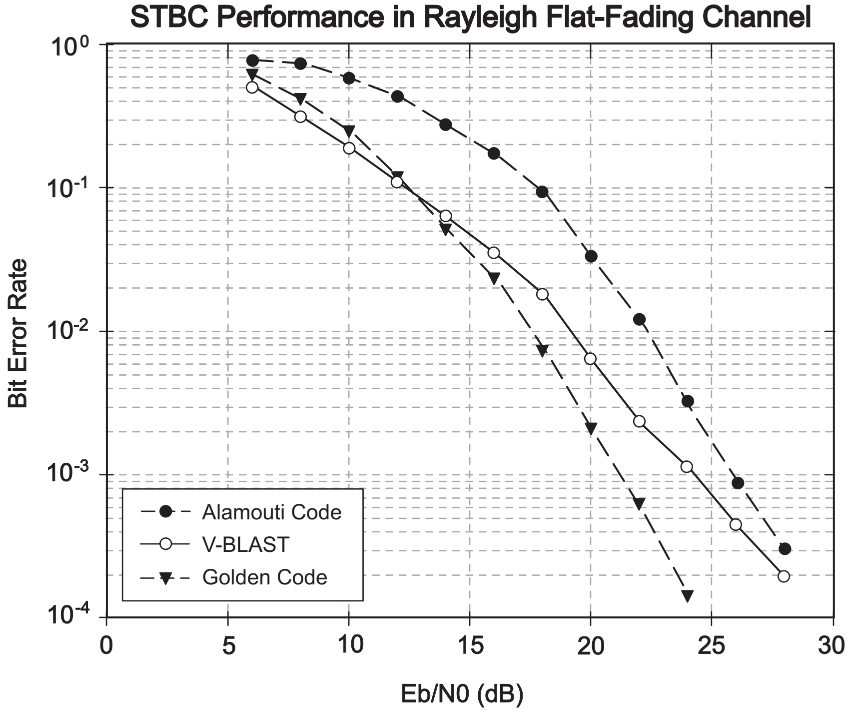

Figure 4.3: Alamouti, V-BLAST and Golden Code Performance (M=2, N=2)

a performance degradation of approximately 2dB for every 5Hz increase in Doppler frequency.

Figure 4.4b compares the Golden code performance against the Alamouti code at selected Doppler frequencies. The performance degradation of approximately 2dB for every 5Hz increase in Doppler frequency previously observed with the Golden code is also observe with the Alamouti code. The 5dB performance advantage at high SNR levels of the Golden code compared to the Alamouti code is maintained over the range of Doppler frequencies investigated.

4.6 Multiuser MIMO System Model

4.6.1 Multiuser Transmitter Structure

Figure 4.5 shows the transmitter structure of the multiple-access IDMA scheme with K simultaneous users. The input data sequence $\{d_k[i]\}_i$ of user-k is encoded by the FEC encoder generating a coded sequence $\{c_k[i]\}_{i=0}^{J-1}$, where J is the frame length. Then $\{c_k[i]\}_{i=0}^{J-1}$ is permutated by the interleaver π_k, producing $\{b_k[i]\}_{i=0}^{J-1}$. IDMA users are

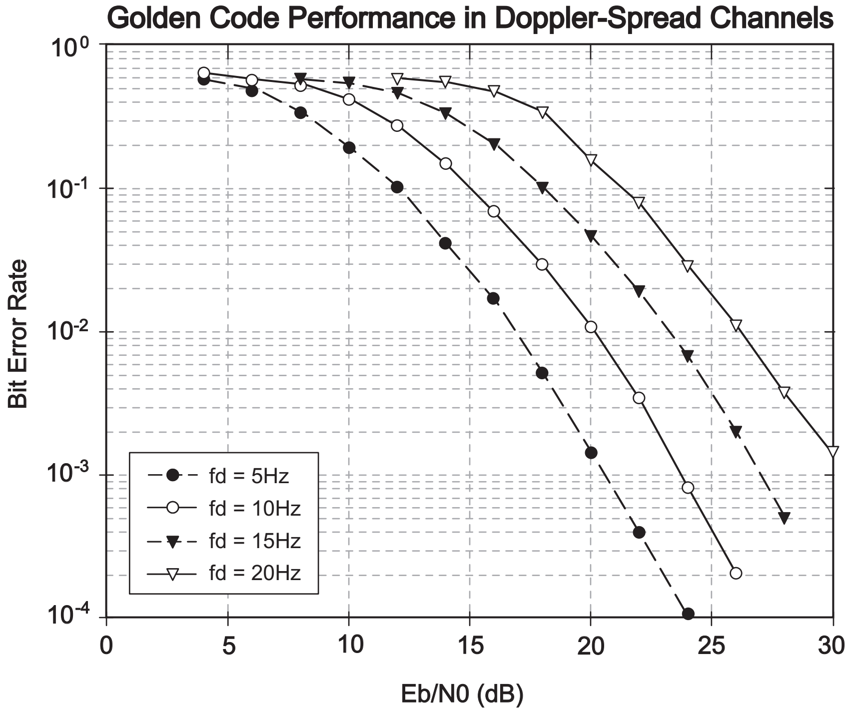

(a) Golden Code Performance at Various Doppler Frequencies

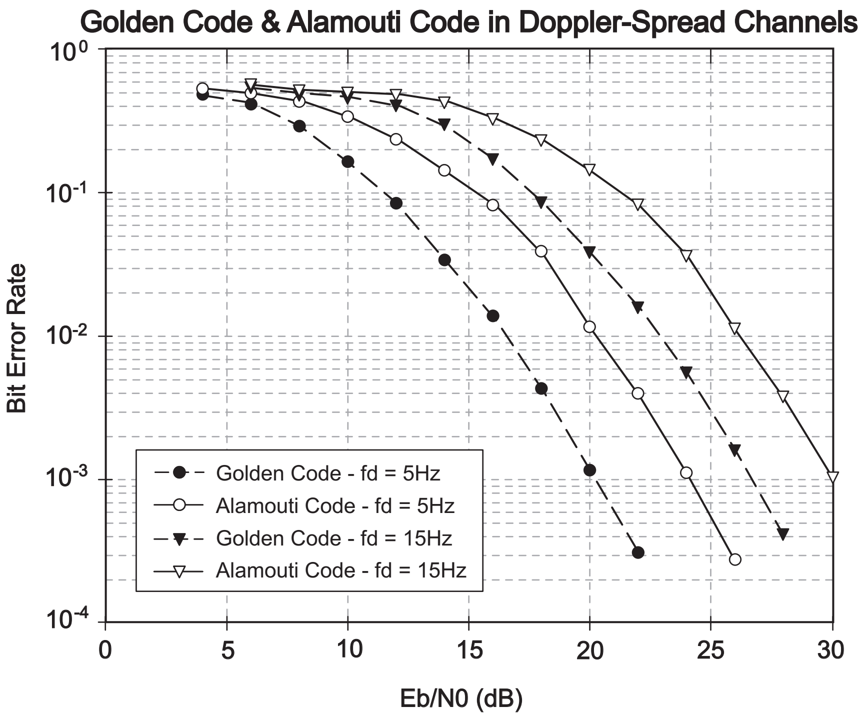

(b) Golden Code and Alamouti Code Performance Comparison

Figure 4.4: Golden Code Performance in Doppler-Spread Channels

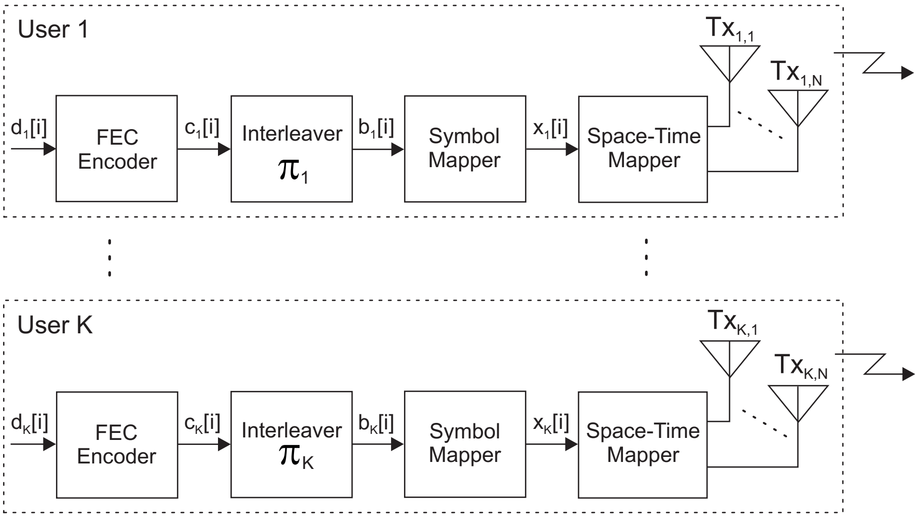

Figure 4.5: Transmitter structure for the multiuser MIMO-IDMA system

distinguished solely by their interleaver sequence, and therefore the interleaver π_k must be different for each user. Finally, the interleaved chip sequence, $\{b_k[i]\}_{i=0}^{J-1}$, is QPSK-modulated producing $\{x_k[i]\}_i$ which is then space-time mapped as specified by the code matrix, $\mathbf{X}$. Three different STBC matrices are used in our simulations: the Alamouti code (4.4), the Golden code (4.13), and V-BLAST. The STBC matrix for 2-transmit antenna V-BLAST is $\mathbf{X} = [\, x(1),\ x(2)\,]^T$.

4.6.2 Multiuser MIMO Signal Model

We develop the signal model for the MIMO-IDMA system by way of example. We assume a flat-fading channel between each transmit and receive antenna pair. We also assume that the fading remains constant over an entire signal frame, but may vary from one frame to another.

Consider a single user ($K = 1$) STBC system with two transmit antennas ($N = 2$), and M receiver antennas, employing the Alamouti code matrix, $\mathbf{X}$, from (4.4), the received signal at the m-th receiver antenna for this single user can be written as

$$\begin{bmatrix} y^m(1) \\ y^m(2) \end{bmatrix} = \begin{bmatrix} x(1) & x(2) \\ -x^*(2) & x^*(1) \end{bmatrix} \begin{bmatrix} h_{m,1} \\ h_{m,2} \end{bmatrix} + \begin{bmatrix} n^m(1) \\ n^m(2) \end{bmatrix} \tag{4.14}$$

where $y^m(p)$ is the received signal vector from channel usage p, $h_{m,n}$ is the complex fading gain from the n-th transmitter antenna to the m-th receiver antenna, $n^m(p)$ is the additive Gaussian noise samples from channel usage p, and $m = 1, 2, \ldots, M$.

Combining the channel matrix with the STBC code matrix $\mathbf{X}$, (and conjugating $y^m[2]$ to simplify notation), (4.14) can be written in the following alternative form

$$\mathbf{y^m} = \mathbf{H_1^m x_1} + \mathbf{n^m} \tag{4.15}$$

where $m = 1, 2, \ldots, M$ and we define

$$\mathbf{y^m} = \begin{bmatrix} y^m(1) \\ y^m(2)^* \end{bmatrix}, \ \mathbf{H_1^m} = \begin{bmatrix} h_{m,1} & h_{m,2} \\ h_{m,2} & h_{m,1} \end{bmatrix}, \ \mathbf{x_1} = \begin{bmatrix} x(1) \\ x(2) \end{bmatrix}, \text{ and } \mathbf{n^m} = \begin{bmatrix} n^m(1) \\ n^m(2)^* \end{bmatrix}$$

We see that $\mathbf{H_1^m}$ combines information of the channel response related to the m-th receiver antenna and the code constraint of the STBC, $\mathbf{X}$.

By stacking the $\mathbf{y^m}$ vectors from (4.15) for all M receiver antennas, the following signal model is obtained

$$\mathbf{y} = \begin{bmatrix} \mathbf{y^1} \\ \mathbf{y^2} \\ \vdots \\ \mathbf{y^M} \end{bmatrix} = \begin{bmatrix} \mathbf{H_1^1} \\ \mathbf{H_1^2} \\ \vdots \\ \mathbf{H_1^M} \end{bmatrix} \begin{bmatrix} x(1) \\ x(2) \end{bmatrix} + \begin{bmatrix} \mathbf{n^1} \\ \mathbf{n^2} \\ \vdots \\ \mathbf{n^M} \end{bmatrix} \tag{4.16}$$

We now consider the multiuser case of a STBC system with K users, each employing N transmitter antennas. At the receiver, M receiver antennas are employed. In this case, the received signal can be written as

$$\begin{bmatrix} \mathbf{y^1} \\ \mathbf{y^2} \\ \vdots \\ \mathbf{y^M} \end{bmatrix} = \begin{bmatrix} \mathbf{H_1}, & \mathbf{H_2}, & \ldots, & \mathbf{H_K} \end{bmatrix} \begin{bmatrix} \mathbf{x^1} \\ \mathbf{x^2} \\ \vdots \\ \mathbf{x^K} \end{bmatrix} + \begin{bmatrix} \mathbf{n^1} \\ \mathbf{n^2} \\ \vdots \\ \mathbf{n^M} \end{bmatrix} \tag{4.17}$$

where $\mathbf{y^m} \triangleq [\,y_m(1),\, y_m(2),\, \ldots, y_m(P)\,]^T,\ m = 1, 2, \ldots, M$, and contains the received signal vectors from channel usages 1 to P, at the m-th antenna; $\mathbf{H_k},\ k = 1, 2, \ldots, K$ is the channel response matrix for the kth user; $\mathbf{x^k} \triangleq [\, x_k(1),\, x_k(2),\, \ldots, x_k(N)\,]^T$ is the code vector for the k-th user; and $\mathbf{n^m} \triangleq [\, n^m(1),\, n^m(2),\, \ldots, n^m(P)\,]^T$ contains the additive Gaussian noise samples from channel usages 1 to P at the m-th receiver antenna.

In addition to the Alamouti code, we use this same methodology to develop signal models for the Golden code and V-BLAST. For the Golden code case, signal vectors are separated into their real and imaginary components. This method was first developed in [79] and [67].

4.6.3 Multiuser Iterative Receiver Structure

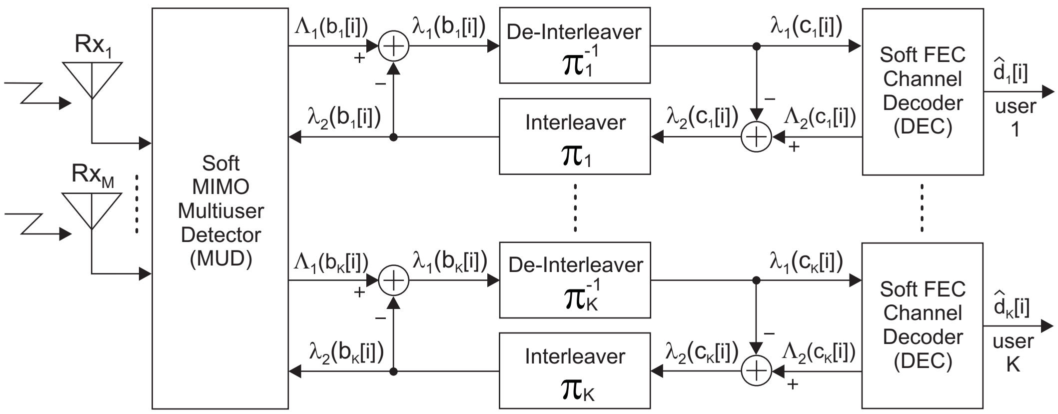

Figure 4.6: Receiver structure for the multiuser MIMO-IDMA system

The iterative receiver structure for the MIMO IDMA system is shown in Figure 4.6. It consists of a soft-output multiuser detector (MUD) and K single users *a posteriori* probability decoders (DECs). The two stages are separated by interleavers and deinterleavers. The soft-output MUD takes as input the received signals from the M receiver antennas and the interleaved extrinsic log likelihood ratios (LLRs) of the code bits of all users (which are fed back by the K single-user DECs), and computes as the output the a posteriori LLRs of the code bits of all users. The DEC of kth users takes as input the deinterleaved extrinsic LLRs of the code bits from the soft-output MUD and computes as output the *a posteriori* LLRs of the code bits, as well as the LLRs of the information bits.

At a given iteration, the MUD estimates the *a posteriori* LLRs of the code bits, i.e.,

$$\Lambda_1(b_k[i]) \triangleq \log \frac{P(b_k[i] = 1 \mid \mathbf{y})}{P(b_k[i] = 0 \mid \mathbf{y})}, \quad i = 0, \ldots, J-1, \quad k = 1, \ldots, K \tag{4.18}$$

where $\mathbf{y}$ denotes the received vectors from all M antennas. With Bayes' rule, (4.18) can be rewritten as

$$\Lambda_1(b_k[i]) = \underbrace{\log \frac{P(\mathbf{y} \mid b_k[i]=1)}{P(\mathbf{y} \mid b_k[i]=0)}}_{\lambda_1(b_k[i])} + \underbrace{\log \frac{P(b_k[i]=1)}{P(b_k[i]=0)}}_{\lambda_2(b_k[i])} \tag{4.19}$$

The first term in (4.19), denoted by $\lambda_1(b_k[i])$, is the extrinsic information calculated by the MUD. The second term, denoted by $\lambda_2(b_k[i])$, is the *a priori* information (in LLR form) of $b_k(i)$. An estimate of the *a priori* LLR is calculated by the DEC of the k-th user at the previous iteration. At the first iteration, no prior information about the code bits is available, therefore all bit values are assumed equiprobable and the *a priori* LLR values are set to zero. Finally, the sequence of extrinsic information, $\{\lambda_1(b_k(i))\}_i$, is deinterleaved by the deinterleaver of the k-th user (producing $\{\lambda_1(c_k(i))\}_i$) and fed into the corresponding DEC as *a priori* information for the next iteration.

The channel decoder for the k-th user estimates the *a posteriori* probabilities (in LLR form) of the code bits, i.e.,

$$\begin{aligned}\Lambda_2(c_k[i]) &\triangleq \log \frac{P(c_k[i]=1 \mid \{\lambda_1(c_k[i])\}_i\,;\text{ code structure})}{P(c_k[i]=0 \mid \{\lambda_1(c_k[i])\}_i\,;\text{ code structure})}, \\ &= \lambda_2(c_k[i]) + \lambda_1(c_k[i]).\end{aligned} \tag{4.20}$$

These *a posteriori* probabilities are computed using the BCJR algorithm [6] based on the *a priori* information from the MUD, $\{\lambda_1(c_k[i])\}$, and knowledge of the code structure. Additionally, the DEC estimates the *a posteriori* LLRs of the information bits, $\{\Lambda_2(d_k[i])\}$, and at the final iteration, performs a hard decision on the information bits, producing $\{\hat{d}_k[i])\}$.

4.7 Soft Multiuser Detector (MUD)

The MUD operation is now described in more detail. The MUD is developed largely from the concepts described in [67].

First, the soft estimate $\tilde{x}_k(i)$ of the k-th users i-th code symbol $x_k(i)$ is calculated by

$$\tilde{x}_k(i) \triangleq E\{x_k(i)\} = \sum_{x\in\mathcal{X}} xP(x_k(i)=x) \tag{4.21}$$

where $\mathcal{X}$ is the set of possible code symbols. At first iteration, all code symbols are assumed to be equiprobable. In subsequent iterations, the probability $P(x_k(i) = x)$ is computed from the extrinsic information provided by the DEC.

For our multi-user system, where each user employs multiple transmit antennas, we use the concept of treating each transmit antenna as a virtual user. Therefore, for a system with K-users, where each user employs N transmit antennas, there are (NK) virtual users in the system. We define an (NK)-dimensional soft code vector

$$\begin{aligned}\tilde{\mathbf{x}} &\triangleq [\,\tilde{\mathbf{x}}_1^T,\, \tilde{\mathbf{x}}_2^T,\, \ldots,\, \tilde{\mathbf{x}}_K^T\,]^T \\ &= [\,\tilde{x}_1(1),\, \ldots,\, \tilde{x}_1(N),\, \tilde{x}_2(1),\, \ldots,\, \tilde{x}_2(N),\, \ldots,\, \tilde{x}_K(1),\, \ldots,\, \tilde{x}_K(n)\,]^T \end{aligned} \tag{4.22}$$

where every element in $\tilde{\mathbf{x}}$ as a virtual user. We use the notation $_k(i)$ to index a virtual user, and define

$$\tilde{\mathbf{x}}_k(i) \triangleq \tilde{\mathbf{x}} - \tilde{x}_k(i)\mathbf{e}_k(i) \tag{4.23}$$

where $\mathbf{e}_k(i)$ is an (NK)-vector of all zeros, except for the “1” value in the vector element corresponding to the $_k(i)$-th virtual user. That is, $\mathbf{x}_k(i)$ is obtained from $\mathbf{x}$ by setting the $_k(i)-$th element to zero.

Subtracting the soft estimate of the interfering signals of the other virtual users from the received signal $\mathbf{y}$, we get

$$\mathbf{y}_k(i) \triangleq \mathbf{y} - \mathbf{H}\tilde{\mathbf{x}}_k(i) = \mathbf{H}[\mathbf{x} - \tilde{\mathbf{x}}_k(i)] + \mathbf{n} \tag{4.24}$$

In order to further suppress the residual interference in $\mathbf{y}_k(i)$, we apply an instantaneous linear minimum mean square error (MMSE) filter to $\mathbf{y}_k(i)$. The linear MMSE weight vector $\mathbf{w}_k(i)$ is chosen to minimise the mean square error between the transmitted symbol $x_k(i)$ and the filter output $\hat{x}_k(i) \triangleq \mathbf{w}_k^H(i)\mathbf{x}_k(i)$, (where $(\,\cdot\,)^H$ denotes the Hermitian transpose operation), hence

$$\begin{aligned}\mathbf{w}_k(i) &= \arg\min_{\mathbf{w}\in\mathbb{C}^{MP}} \mathrm{E}\left\{\|x_k(i) - \mathbf{w}^H\mathbf{y}_k(i)\|^2\right\} \\ &= \mathrm{E}\left\{\mathbf{y}_k(i)\mathbf{y}_k^H(i)\right\}^{-1}\mathrm{E}\left\{x_k^*(i)\mathbf{y}_k(i)\right\}\end{aligned} \tag{4.25}$$

Using (4.24) and assuming that the symbol $x_k(i)$ is of unit energy, ie., $\|x_k(i)\|^2 = 1$ and $E\{\mathbf{n}\mathbf{n}^H\} = \sigma^2\mathbf{I}$, where $\mathbf{I}$ is the identity matrix, we have

$$\mathrm{E}\{x_k^*(i)\mathbf{y}_k(i)\} = \mathbf{H}\mathrm{E}\left\{x_k^*(i)[\mathbf{x} - \tilde{\mathbf{x}}_k(i)]\right\} = \mathbf{H}\mathbf{e}_k(i) \tag{4.26}$$

$$\mathrm{E}\{\mathbf{y}_k(i)\mathbf{y}_k^H(i)\} = \mathbf{H}\mathbf{V}_k(i)\mathbf{H}^H + \sigma^2\mathbf{I} \tag{4.27}$$

with

$$\begin{aligned} \mathbf{V}_k(i) &\triangleq \mathrm{Cov}\{\mathbf{x} - \tilde{\mathbf{x}}_k(j)\} \\ &= \mathrm{diag}\{\, 1 - \|\tilde{x}_1(1)\|^2, \, \ldots, \, 1 - \|\tilde{x}_1(N)\|^2, \ldots, \\ &\qquad 1 - \|\tilde{x}_k(i-1)\|^2, \, 1, \, 1 - \|\tilde{x}_k(i+1)\|^2, \\ &\qquad \ldots, \, 1 - \|\tilde{x}_K(1)\|^2, \, \ldots, \, 1 - \|\tilde{x}_K(N)\|^2 \,\} \end{aligned} \tag{4.28}$$

Using equations (4.25) to (4.28), the instantaneous MMSE estimate for $x_k(i)$ is given by

$$\begin{aligned} x_k(i) &\triangleq \mathbf{w}_k^H(i)\mathbf{y}_k(i) \\ &= \mathbf{e}_k^T(i)\mathbf{H}^H \left[\mathbf{H}\mathbf{V}_k(i)\mathbf{H}^H + \sigma^2\mathbf{I}\right]^{-1} \mathbf{y}_k(i) \end{aligned} \tag{4.29}$$

The instantaneous MMSE filter can be modeled by an equivalent additive white Gaussian noise channel (with $\mu_k(i)$ mean and $v_k^2(i)$ variance) having $x_k(i)$ as its input symbol. The output of this filter can then be written as

$$\hat{x}_k(i) = \mu_k(i)x_k(i) + \eta_k(i) \tag{4.30}$$

with

$$\begin{aligned} \mu_k(i) &\triangleq \mathrm{E}\{\hat{x}_k(i)x_k^*(i)\} \\ &= \left\{\mathbf{H}^H \left[\mathbf{H}\mathbf{V}_k(i)\mathbf{H}^H + \sigma^2\mathbf{I}\right]^{-1} \mathbf{H}\right\}_{k,k} \end{aligned} \tag{4.31}$$

and

$$v_k^2(i) \triangleq \mathrm{Var}\{x_k(i)\} = \mu_k(j)x_k(i) - \mu_k^2(i) \tag{4.32}$$

where $\{\,\cdot\,\}_{j,k}$ denotes the matrix element at the j-th row and k-th column. Equations (4.30) to (4.32) give the probability distribution of the code symbol $\hat{x}_k(i)$, which is used to calculate the *a posteriori* probability of the code bits.

4.8 Multiuser System Performance

The simulations assume the receiver has perfect channel knowledge. The system is evaluated for fast time-varying Rayleigh flat-fading channels where the individual channels in the channel matrix are independent and uncorrelated. The transmitter FEC is a 1/2-rate convolutional code serially concatenated with a 1/16-rate repetition code (producing an overall code rate of $R = 1/32$). The transmitter generates QPSK symbols (before space-time mapping)

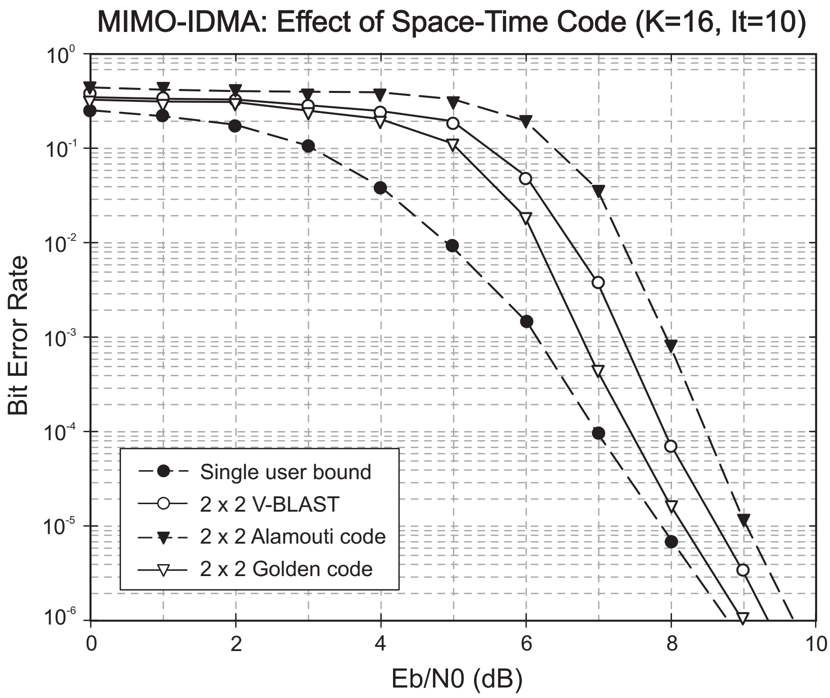

Figure 4.7: Alamouti-, V-BLAST- and GC-IDMA Performance

Figure 4.7 compares the bit error rate (BER) averaged over all (16) users after 10 receiver iterations versus the signal to noise ratio (SNR) $Eb/N0$ for IDMA with three space-time coding schemes (the Golden code, the Alamouti code, and V-BLAST). For BER of 10^{-5} or less, the $Eb/N0$ requirement for the Golden code is 1.5dB less than the Alamouti code and 1dB less that V-BLAST.

Figure 4.8a compares the effect of the number of receiver iterations on BER for a Golden code IDMA system with 16 simultaneous users. We observe receiver convergence after 7 iterations for $Eb/N0$ values of 7dB or less, and convergence after 5 iterations for $Eb/N0$ values greater than 7dB.

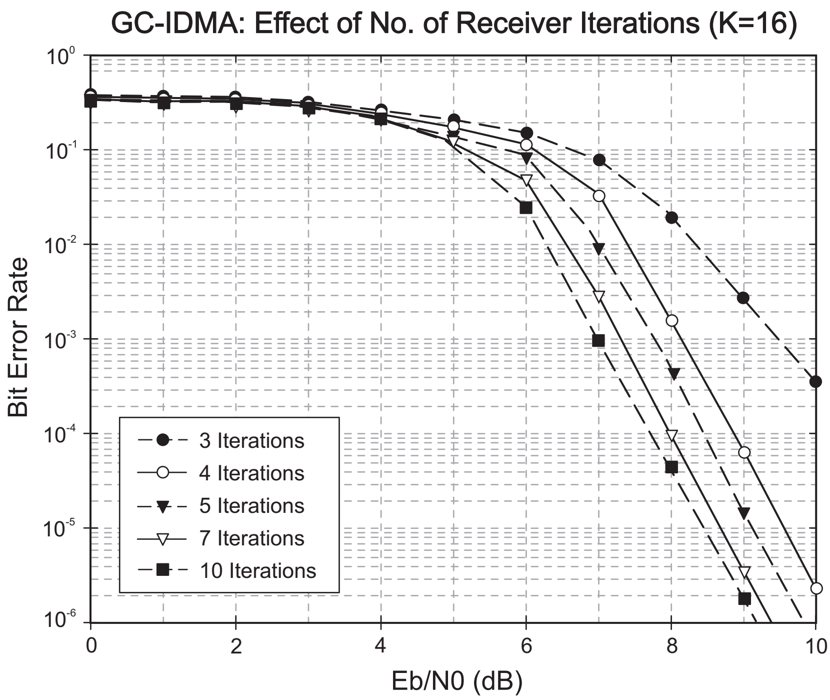

(a) Effect of Number of Receiver Iterations

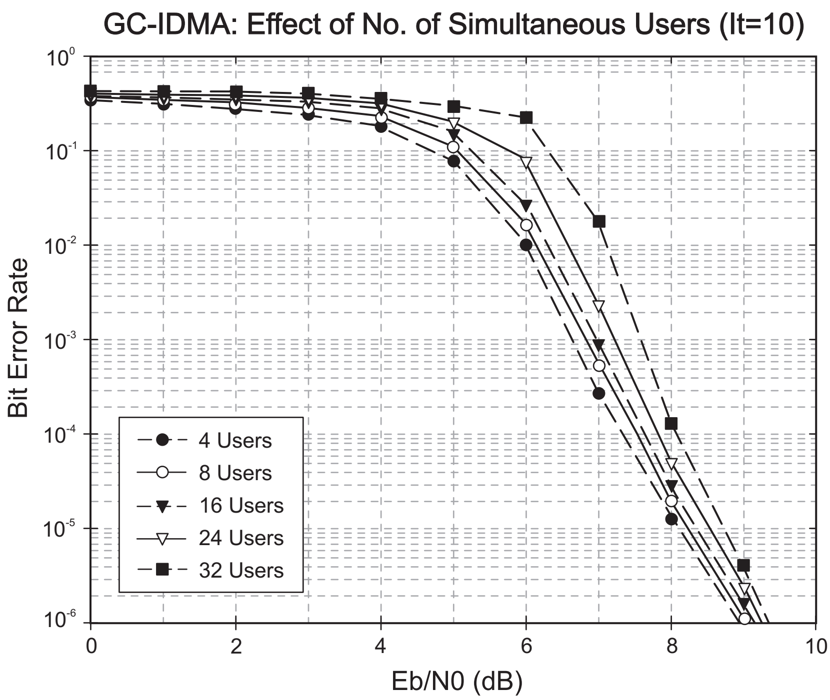

(b) Effect of Number of Simultaneous Users

Figure 4.8: GC-IDMA Performance for a) Various Number of Receiver Iterations; and b) Various Numbers of Users

Figure 4.8b compares the effect of the number of simultaneous users on the BER for Golden Code IDMA. The performance is shown for 10 receiver iterations. We observe almost identical performance for 1, 8 and 16 user systems over the simulated Eb/N0 range of 0dB to 10dB. For 24 and 32 user systems, we observe a slight degradation in performance (compared to 16-users) of up to 1dB and 0.5dB for 24 and 32 user systems respectively for $Eb/N0$ values of 5 to 7dB. For $Eb/N0$ values of 7dB and greater, the performance of 24 and 32 user systems is almost identical to the 1, 8 and 16 user systems.

4.9 Conclusion

In this chapter, the Golden Code—an optimal linear-dispersion (LD) code providing both diversity gain and full-rate—was presented.

First, the single-user case was considered and the performance of the Golden Code was been presented and compared with common multiple-antenna systems, namely the Alamouti code and V-BLAST (spatial multiplexing). The Golden Code was shown to provide superior performance at high-SNR levels while using the same low-complexity linear dispersion code decoding schemes typically used to decode Alamouti and V-BLAST schemes.

Simulation results of a single-user MIMO system using the Golden Code at various Doppler frequencies were presented. These results showed that the Golden Code maintains its superior performance when compared to the Alamouti scheme over the range of Doppler frequencies that would typically be encountered in a mobile communications system. For a symbol error rate of 10^{-4} the Eb/N0 requirement for the Golden code is 5dB less than the Alamouti code and V-BLAST.

Next, the multiuser case was considered and a MIMO framework for incorporating LD codes into an IDMA multiple-access scheme was developed. The performance of the 2×2 MIMO-IDMA multiuser scheme using the Golden Code (GC-IDMA) was then presented and compared with other 2×2 MIMO-IDMA schemes using the Alamouti code and V-BLAST space-time codes. GC-IDMA was shown to provide superior performance at moderate and high SNR levels while using the same low-complexity iterative decoding receiver structure as the other MIMO-IDMA schemes.

In a Rayleigh flat-fading environment, simulation results show that GC-IDMA outperforms Alamouti and V-BLAST IDMA at moderate and high SNR levels. For bit error rate of 10^{-5} or less, the $Eb/N0$ requirement for the GC-IDMA is 1dB less than the Alamouti-IDMA and V-BLAST-IDMA. Simulation results showing the effect of the number of simultaneous users and the effect of the number of receiver iterations on GC-IDMA performance were also presented.

Chapter 5

Multiuser Detection for Delay-Spread Underwater Acoustic Channels

Underwater sensor networks enable a broad range of applications including environmental monitoring, undersea exploration, assisted navigation, and distributed surveillance [2]. A robust and efficient communications scheme between the underwater network nodes is an essential foundation for reliable high-performance sensor networks.

The shallow water acoustic channel is an exceptionally difficult medium for data transmission, and developing reliable communications systems for this environment has proved to be very challenging. One of the main channel impairments is multipath interference caused by multiple reflections of the acoustic signal from the water surface and bottom. These reflections occur at small grazing angles and with small reflection losses. This effect causes both long time-delay spread and large multipath amplitudes to be present in the received signal [51].

Over the past decade, CDMA has been successfully employed as the modulation scheme for shallow water networks [15] [119] [111]. Spread-spectrum schemes, such as CDMA, employ a transmission bandwidth that is considerably greater than the information rate. Utilization of the bandwidth in this manner introduces a number of benefits, including multiple-access interference suppression capability and improved immunity against multipath effects.

Unfortunately, the long time-delay spreads that are typical for shallow water acoustic channels cause severe inter-symbol interference (ISI). This ISI degrades the performance of many CDMA receiver detection schemes. Multi-carrier modulation (MCM) is an attractive alternative because it is particularly resilient to long time-delay spreads.

The basic principle of MCM is to split a high-rate data stream into a number of lower-rate streams that are transmitted simultaneously over a number of sub-carriers. This significantly reduces the ISI span because the lower-rate parallel sub-carriers have increased symbol duration [126].

In [75], Orthogonal Frequency Division Multiplexing (OFDM), a low-complexity spectrally-efficient MCM technique, was combined with an IDMA overlay to develop a multiple-access scheme for multi-path fading channels. In this chapter we develop an OFDM-IDMA scheme that provides robust performance in the presence of large time-delay spread and the other impairments presented by the shallow water acoustic channel. The proposed scheme utilises a low-complexity iterative decoding algorithm based on the turbo-decoding concept [12].

The performance of the proposed OFMD-IDMA scheme is compared against other shallow water communication schemes, including single-carrier CDMA, single-carrier IDMA. Using ray-trace underwater channel models combined with noise models of commonly occurring oceanic noise phenomena, simulations of multiple-access sensor network systems are performed to assess the overall performance of the different schemes.

A Multiple-Input Multiple-Output (MIMO) extension to the OFDM-IDMA scheme is also investigated, where each transmitter and receiver use multiple transmitting and receiving elements respectively. This MIMO concept is used to exploit the multi-path nature of the underwater channel to provide improved performance in the form of either increased data robustness or increased data throughput.

Simulations of various underwater acoustic sensor network scenarios show that the OFDM-IDMA scheme consistently outperforms other common multiple-access schemes in the shallow water environment. The work in this chapter was published in [61] and [64].

5.1 Channel Model

Acoustic signals transmitted in shallow water are corrupted by interference from reflection and scattering at the water surface and bottom. For this reason, the shallow water channel is a difficult medium in which to achieve the high data rates needed for many applications. An especially difficult problem is that the acoustic signal transmitted over a shallow water channel has associated with it inherently small grazing angles and small reflection losses. This results in significant corruption due to large amplitude multi-path signals.

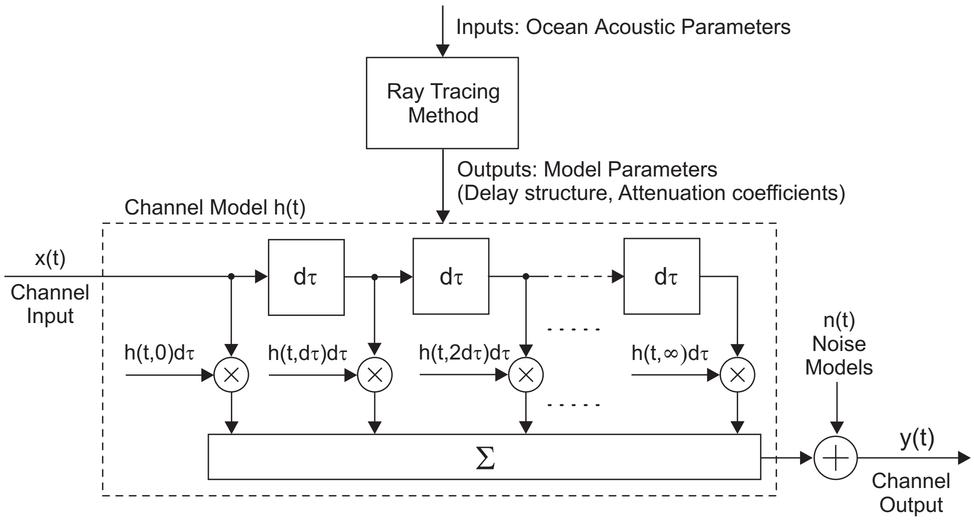

Figure 5.1: Channel Model Simulator Description

Ray tracing methods have been shown to provide realistic modeling of these effects for high frequency acoustic signals propagating in shallow water environments [27]. For our system simulations, we develop a ray-trace underwater channel model combined with noise models of commonly occurring oceanic ambient and intermittent noise sources. The channel model is shown in Figure 5.1.

5.1.1 Multipath Modeling

The shallow water propagation is modeled using the multipath channel model proposed by Zielinski, et al. [145]. This model is characterised by Ray theory and simplified with assumptions of constant sound velocity profile and constant bottom depth. Boundaries at the channel surface and bottom reflect an acoustic signal, resulting in multiple travel paths between transmitter and receiver. Therefore, the receiver can acquire signals arriving on different paths, each signal delayed according to the channel geometry.

We assume a channel geometry as shown in Figure 5.2 where the channel has uniform depth, h, and constant sound speed, c. The transmitter and receiver height are denoted by a, and b respectively. We only consider the case where the channel has a large range to channel depth ratio (L/h), such that it supports coherent, specular reflection.

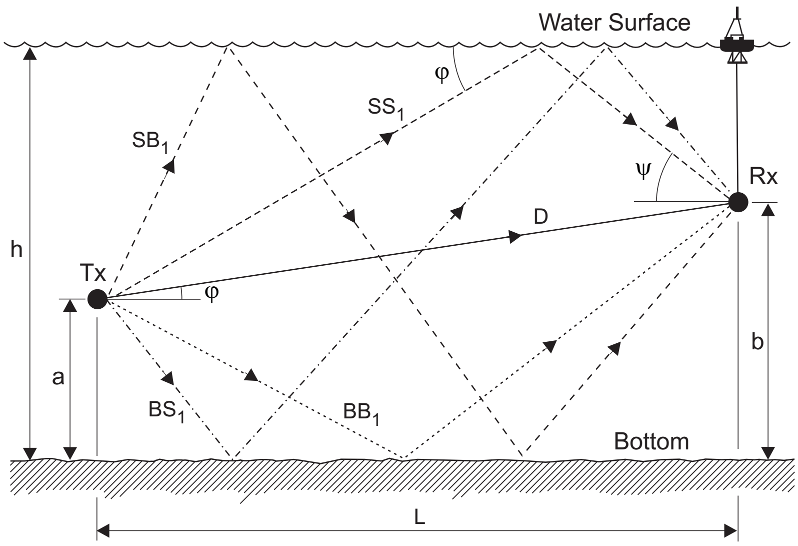

Figure 5.2: Multipath structure of a shallow water channel

The transmitted signal path can be classified as either the direct path D or multipath. Multipath signals are grouped into four types according to their first and last boundary reflection before arriving at the receiver. We use the following notation:

- SS_n denotes a multipath signal which has a first and last boundary reflection from the sea-surface;
- SB_n denotes a multipath signal which has first and last boundary reflections from the sea surface and bottom respectively;
- BS_n denotes a multipath signal which has first and last boundary reflections from the sea bottom and surface respectively; and
- BB_n to denote multipath signals which make a first and last boundary reflection from the sea bottom.

The subscript n denotes the multipath "order". Multipath signals with an order, n, of 2 or more have an additional $(n-1)$ intermediatory boundary reflections. Figure 5.2 shows these four types of multipath signals for the primary $(n = 1)$ path.

Multipath Signal Amplitude Calculation

The normalised amplitudes of each of the four types of multipath signals can be calculated from the following:

$$\begin{aligned}\alpha_{SS_n} &= \left[\frac{L_D}{L_{SS_n}}\right] R_{SS_n}, & \alpha_{SB_n} &= \left[\frac{L_D}{L_{SB_n}}\right] R_{SB_n},\\ \alpha_{BS_n} &= \left[\frac{L_D}{L_{BS_n}}\right] R_{BS_n}, & \alpha_{BB_n} &= \left[\frac{L_D}{L_{BB_n}}\right] R_{BB_n}\end{aligned} \tag{5.1}$$

where L_D is length of the direct signal path; L_{SS_n}, L_{SB_n}, L_{BS_n}, L_{BB_n} are the lengths of the multipath signal paths; and R_{SS_n}, R_{SB_n}, R_{BS_n}, R_{BB_n} are the combined reflection attenuation coefficients for each of the multipath types.

The path lengths can be calculated using the channel geometry. Using the binomial expansion to simplify the equations, the path lengths for the direct signal and each of the multipath types is given by:

$$L_D \simeq \left[L + \frac{1}{2L}(b-a)^2\right]$$

$$\begin{aligned}L_{SS_n} &\simeq \left[L + \frac{1}{2L}(2nh-a-b)^2\right] & L_{SB_n} &\simeq \left[L + \frac{1}{2L}(2nh-a+b)^2\right]\\ L_{BS_n} &\simeq \left[L + \frac{1}{2L}(2nh+a-b)^2\right] & L_{BB_n} &\simeq \left[L + \frac{1}{2L}(2(n-1)h+a+b)^2\right]\end{aligned} \tag{5.2}$$

The combined reflection attenuation coefficients represent the total attenuation due to repeated surface and/or bottom reflections for each multipath type. The coefficient values are calculated as follows:

$$\begin{aligned}R_{SS_n} &= \tilde{r}_s^n \tilde{r}_b^{(n-1)} \simeq -|r_s|^n, & R_{SB_n} &= \tilde{r}_s^n \tilde{r}_b^n \simeq |r_s|^n,\\ R_{BS_n} &= \tilde{r}_s^n \tilde{r}_b^n \simeq |r_s|^n, & R_{BB_n} &= \tilde{r}_s^{(n-1)} \tilde{r}_b^n \simeq -|r_s|^{n-1}\end{aligned} \tag{5.3}$$

where $\tilde{r}_s$ is the surface reflection coefficient, and $\tilde{r}_b$ is the bottom reflection coefficient.

The surface reflection coefficient, r_s can be evaluated using the Bechmann-Spezzichino model, and the bottom reflection coefficient, r_b can be evaluated using either the Rayleigh model (Brekhovskikh) or the NUSC model (Yarger) [145]. In general, reflection coefficients depend on grazing angle and therefore on the order of the multipath.

Multipath Signal Arrival Time Calculation

The signal arrival times can be calculated from the signal path lengths and the sound speed. The difference in arrival times between the direct path and each of the four types of multipath signals can be calculated from the following:

$$
\begin{aligned}
\tau_{SS_n} &= t_{SS_n} - t_D \simeq \frac{2}{cL}\left[n^2h^2 - nh(a+b) + ab\right] \\
\tau_{SB_n} &= t_{SB_n} - t_D \simeq \frac{2}{cL}\left[n^2h^2 - nh(b-a)\right] \\
\tau_{BS_n} &= t_{BS_n} - t_D \simeq \frac{2}{cL}\left[n^2h^2 - nh(a-b)\right] \\
\tau_{BB_n} &= t_{BB_n} - t_D \simeq \frac{2}{cL}\left[(n-1)^2h^2 + (n-1)h(a+b) + ab\right]
\end{aligned} \tag{5.4}
$$

Combined Multipath Channel Response

The impulse response of a multi-path channel can be modeled by the weighted sum of delayed delta functions [93], therefore the received signal $y(t)$ can be represented by a weighted sum of the delayed transmitted signal $x(t)$, i.e.:

$$y(t) = \sum_{\ell=1}^{\infty} \alpha_\ell x(t - \tau_\ell) \tag{5.5}$$

where α_ℓ is the amplitude of the signal received from the ℓ-th path normalised by the amplitude of the direct path signal ($\ell = 1$), and τ_ℓ designates the difference in time of arrivals between the direct path signal ($\ell = 1$) and reflected signals ($\ell > 1$).

Elaborating (5.5) for the channel geometry shown in Figure 5.2, the received signal $y(t)$ constructed from the summation of image signals is given by:

$$
\begin{aligned}
y(t) = \frac{\exp\{j\omega(t-t_D)\}}{L_D} \Bigg\{ 1 + \sum_{n=1}^{\infty} \big(& \alpha_{SS_n}\exp\{-\tau_{SS_n}\} + \alpha_{SB_n}\exp\{-\tau_{SB_n}\} \\
& + \alpha_{BS_n}\exp\{-\tau_{BS_n}\} + \alpha_{BB_n}\exp\{-\tau_{BB_n}\} \big) \Bigg\}
\end{aligned} \tag{5.6}
$$

where $j = \sqrt{-1}$. In the computation of (5.6), the number of terms is usually limited to include only those with significant amplitudes. In our simulations, we neglect terms smaller than 2% of the amplitude of the direct path signal. An example multipath channel response for frequencies between 10kHz and 100kHz, and channel lengths (L)

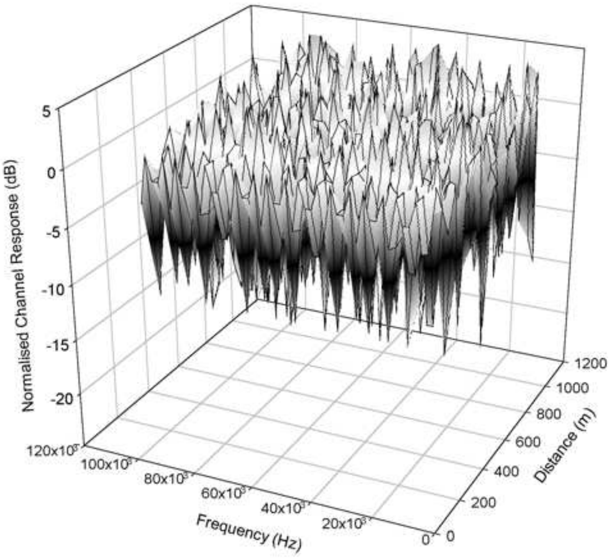

Figure 5.3: Shallow water multipath channel response example

from 100m to 1100m, is shown in Figure 5.3. In this example, the channel depth (h) is 20m, the transmitter height (a) and receiver height (b) is 10m. The surface reflection coefficient ($\tilde{r}_s$) is 0.33, bottom reflection coefficient ($\tilde{r}_b$) is 1.00, and sound speed (c) of 1500m/s.

5.1.2 Noise Modeling

The channel model includes models for ambient and significant intermittent noise sources. Ambient noise sources include surface agitation noise, and thermal nose. Intermittent noise sources include noise due to snapping shrimp and rain noise. Figure 5.4 shows the typical noise levels of the following common ambient and intermittent sources.

Shipping Noise. The noise level (in dB re 1μPa) due to shipping is given by [71][124]

$$NL_{\text{shipping}} = \begin{cases} NL_{100} & f \leq 100Hz \\ NL_{100} - 20\log(10f) & f > 100Hz \end{cases} \tag{5.7}$$

where NL_{100} is typically between 60 and 80 dB re 1μPa (depending on shipping density), and f is the frequency in kHz.

Surface Agitation Noise. The noise caused by the bursting of bubbles of dissolved air at the air-water interface, gives rise to noise which is mainly dependant on wind

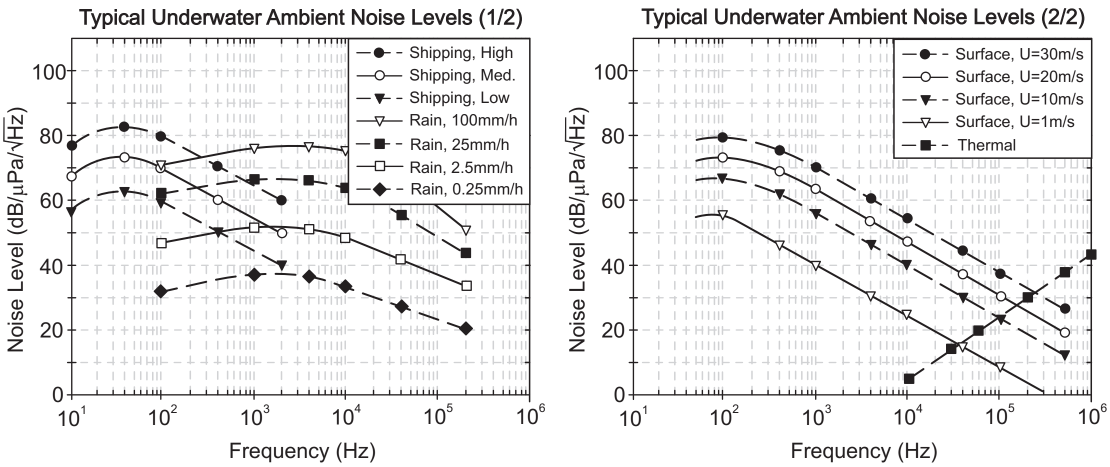

Figure 5.4: Typical noise levels of ambient and intermittent sources

speed [35].

$$N_{\text{wind}} = 20.5 + 22.4 \log U \tag{5.8}$$

where U is the wind speed in m/s at a reference height of 10m above the surface of the water. The frequency dependent ambient noise level due to surface agitation can be given by [5]

$$N_{\text{surface agitation}} = N_{\text{wind}} + 20.7 - 15.9 \log f \tag{5.9}$$

where f is the frequency in kHz.

Thermal Noise. The noise due to the thermal excitation of the water can be modeled by [124]

$$N_{\text{thermal}} = -15 + 20 \log f \tag{5.10}$$

where f is the frequency in kHz.

Rain Noise. The noise level for rain is a function of the size and velocity of the water droplets when they hit the water surface. Both of these factors are dependent on the rainfall rate [124]. In addition, rain noise is also effected by wind speed [5]. The noise level (in dB re 1μPa) due to rain is given by

$$NL_{\text{rain}} = b + a \log RR \tag{5.11}$$

where

$$a = \begin{cases} 25.0 & U \leq 1.5 \\ 5.0 + 5.7(5.0 - U) & 1.5 < U < 5.0 \\ 5.0 & U \geq 5.0 \end{cases} \tag{5.12}$$

and

$$b = \begin{cases} 41.6 & U \leq 1.5 \\ 50.0 + 2.4(5.0 - U) & 1.5 < U < 5.0 \\ 50.0 & U \geq 5.0 \end{cases} \tag{5.13}$$

RR is the rainfall rate in mm/h, and U is the wind speed in m/s.

Noise due to Snapping Shrimp. There are currently no theoretical models for modeling the noise due to snapping shrimp [35]. The empirical formula developed by Urick [124] for modeling snapping shrimp noise (in dB re 1μPa) is

$$N_{\text{shrimp}} = -15 + 20 \log f \tag{5.14}$$

where f is the frequency in kHz.

5.2 Single-Carrier IDMA for Multipath-Fading

5.2.1 Transmitter Structure and Signal Model

The single-carrier IDMA transmitter structure and multipath-channel signal model is shown in Figure 5.5. The transmitter operates as described in Section 2.10.1.

We consider the case of underwater acoustic channels with memory due to multipath delay dispersion. Each received sample can be expressed using an L-tap model as

$$y[i] = \sum_{k=1}^{K} \sum_{l=0}^{L-1} h_{k,l}\, x_k[i-l] + n[i] \tag{5.15}$$

where $x_k(i)$ is the i-th chip transmitted by user k, $h_{k,l}$ is the channel coefficient for user k (corresponding to a delay of l chip durations), and $n[i]$ is a noise sample. For a particular user k, we can rewrite (5.15) as

$$y[i] = h_{k,l}\, x_k[i - l] + \zeta_{k,l}[i] \tag{5.16}$$

where $\zeta_{k,l}[i]$ is the distortion (including additive noise, interference from other users as well as ISI from the same user) contained in $y[i]$ with respect to $x_k[i - l]$.

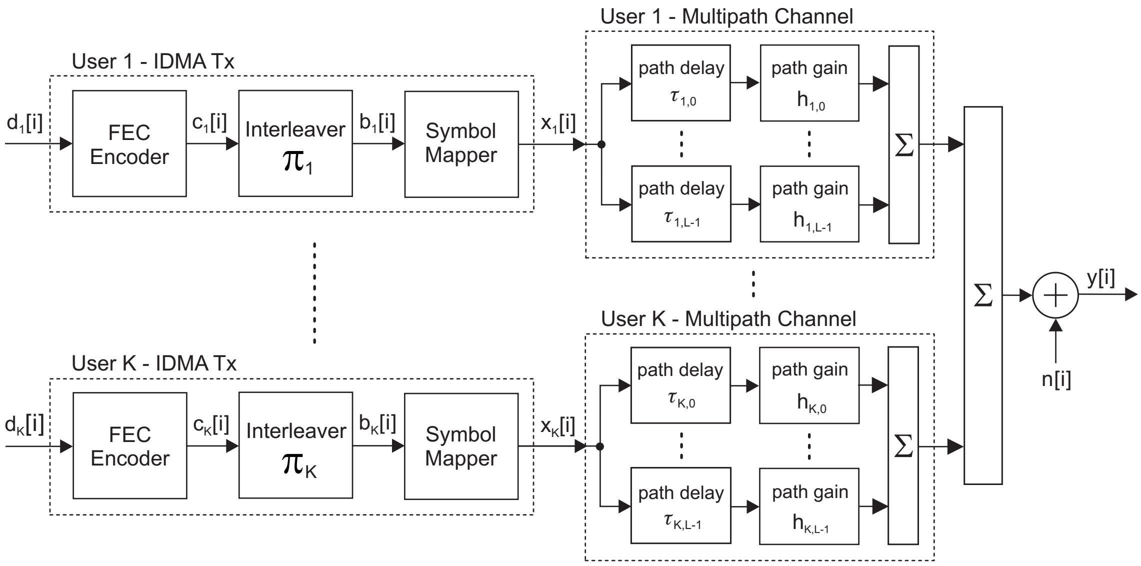

Figure 5.5: Single-Carrier IDMA transmitter structure and multipath-channel signal model

5.2.2 Iterative Receiver Structure

The joint multiple-access system with FEC coding in Figure 5.5 can be considered as a serially concatenated coding system, in which the FEC code takes the role of the outer code, and the multiple-access channel takes the role of the inner code [102]. Using this interpretation, an iterative receiver algorithm based on the turbo decoding concept [12] can be developed.

The iterative receiver structure for the multiuser IDMA system is shown in Figure 5.6. It consists of a soft-output elementary signal estimator (ESE) and K single users *a posteriori* probability decoders (DECs). The two stages are separated by by interleavers and deinterleavers.

Using the received signal, $y[i]$, and the interleaved extrinsic information (in LLR form) of the code bits of the K-users (from the K single-user DECs), $\{\lambda_2(b_k[i]\}_{i,k}$, as inputs, the soft-output ESE calculates the *a posteriori* probabilities (in LLR form) of

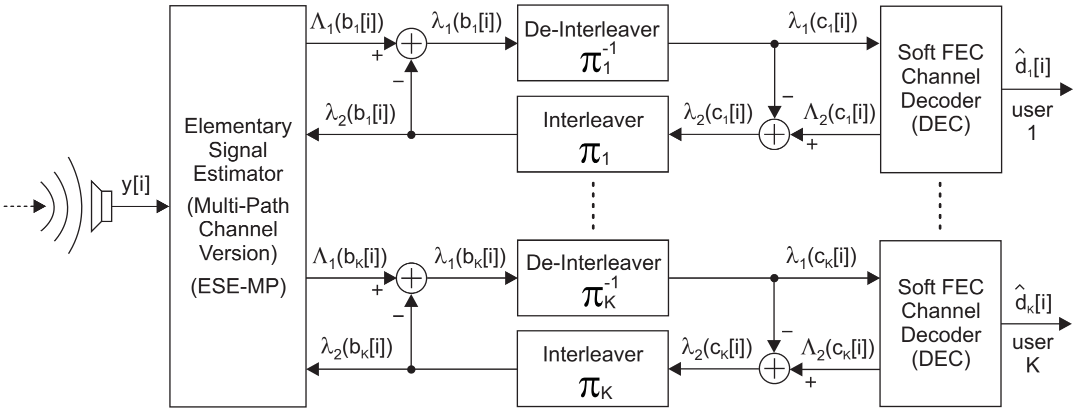

Figure 5.6: Receiver structure for the multiuser IDMA system

the code bits of all K-users. These *a posteriori* LLRs are then deinterleaved (producing $\{\lambda_1(c_k[i]\}_{i,k})$ and fed to the DECs.

Using the deinterleaved extrinsic information of the code bits from the soft-output ESE as input, the DEC of the k-user calculates the *a posteriori* probabilities (in LLR form) of the code bits, $\{\Lambda_2(c_k[i]\}_{i,k}$. These *a posteriori* LLRs are then interleaved and fed back to the ESE.

The components of the receiver are described next.

Elementary Signal Estimator (ESE) for Multipath-Fading Channels

The ESE described in Section 2.10.2 is now extended to account for the multipath-fading channel. This is developed from [85]. At a given iteration, the ESE estimates the *a posteriori* LLRs of the code bits $b_k[i]$, i.e.,

$$\Lambda_1(b_k[i]) \triangleq \log \frac{P(b_k[i] = 1 \mid \mathbf{y})}{P(b_k[i] = 0 \mid \mathbf{y})} \tag{5.17}$$

for $i = 0, \ldots, J-1$, and $k = 1, \ldots, K$. Here, $\mathbf{y}$ denotes the received vector. Note that the real and imaginary components of symbol $x_k[i]$ are decoded independently. Using Bayes' rule, (5.17) can be rewritten as

$$\Lambda_1(b_k[i]) = \underbrace{\log \frac{P(\mathbf{y} \mid b_k[i] = 1)}{P(\mathbf{y} \mid b_k[i] = 0)}}_{\lambda_1(b_k[i])} + \underbrace{\log \frac{P(b_k[i] = 1)}{P(b_k[i] = 0)}}_{\lambda_2(b_k[i])} \tag{5.18}$$

The first term in (5.18), denoted as $\lambda_1(b_k[i])$, is the extrinsic information calculated by the ESE. The second term, denoted as $\lambda_2(b_k[i])$ is the *a priori* probability (in LLR form) of $b_k[i]$. An estimate of the *a priori* probability is calculated by the DEC of the k-th user at the previous iteration. At the first iteration, no prior information about the code bits is available, therefore all bit values are assumed equiprobable and the *a priori* LLR values are set to zero.

The calculation of the extrinsic information for each user is now described in detail. By rewriting (5.16), the received signal from user-k via path-l can be described as

$$y[i+l] = h_{k,l}\, x_k[i] + \zeta_{k,l}[i]. \tag{5.19}$$

Let $h^*_{k,l}$ denote the conjugate of $h_{k,l}$, and define

$$\begin{aligned} \tilde{y}[i+l] &\triangleq h^*_{k,l}\, y[i+l] \\ &= |h_{k,l}|^2 x_k[i] + \tilde{\zeta}_{k,l}[i] \end{aligned} \tag{5.20}$$

where

$$\tilde{\zeta}_{k,l}[i] = h^*_{k,l}\, \zeta_{k,l}[i]. \tag{5.21}$$

By the central limit theorem, $\tilde{\zeta}_{k,l}[i]$ can be approximated as a Gaussian variable. The phase shift due $h_{k,l}$ is canceled out in (5.20), which means that the real and imaginary parts of $x_k[i]$ can be decoded independently. This reduces the complexity of decoding the QPSK mapping.

The extrinsic information for user-k and path-l can be written as

$$\begin{aligned} \lambda_1(b_k[i])_l &\triangleq \log \frac{P(\tilde{y}[i+l] \mid b_k[i]=1)}{P(\tilde{y}[i+l] \mid b_k[i]=0)} \\ &= 2|h_{k,l}|^2 \left(\frac{\tilde{y}[i+l] - \mathrm{E}\left\{\tilde{\zeta}_{k,l}[i]\right\}}{\mathrm{Var}\left\{\tilde{\zeta}_{k,l}[i]\right\}} \right) \end{aligned} \tag{5.22}$$

where $\mathrm{E}\{\cdot\}$ and $\mathrm{Var}\{\cdot\}$ denote expectation and variance, respectively. Finally, the extrinsic information for user-k, considering all l-paths of the channel can be written as

$$\lambda_1(b_k[i]) = \sum_{l=0}^{L-1} \lambda_1(b_k[i])_l. \tag{5.23}$$

Soft Channel Decoding (DEC)

The channel decoder for the k-th user estimates the *a posteriori* probabilities (in LLR form) of the code bits, $\Lambda_2(c_k(i))$, which are given by

$$\begin{aligned}\Lambda_2(c_k[i]) &\triangleq \log \frac{P(c_k[i]=1 \mid \{\lambda_1(c_k[i])\}_i \,;\, \text{code structure})}{P(c_k[i]=0 \mid \{\lambda_1(c_k[i])\}_i \,;\, \text{code structure})}, \\ &= \lambda_2(c_k[i]) + \lambda_1(c_k[i]).\end{aligned} \tag{5.24}$$

These *a posteriori* probabilities are computed using the BCJR algorithm [6] based on the *a priori* information from the ESE, $\{\lambda_1(c_k[i])\}$, and knowledge of the code structure. Additionally, the DEC estimates the *a posteriori* LLRs of the information bits, $\{\Lambda_2(d_k[i])\}$, and at the final iteration, performs a hard decision on the information bits, producing $\{\hat{d}_k[i])\}$.

5.3 Multi-Carrier IDMA (OFDM-IDMA)

The concept of multicarrier modulation is to split a high-rate data stream into a number of lower-rate streams that are transmitted simultaneously over a number of subcarriers. These lower-rate parallel streams have increased symbol duration, and therefore the relative amount of time dispersion caused by multipath delay spread is decreased. The bandwidth of each subcarrier is made sufficiently narrow so that the frequency response characteristics of the individual sub-channels are nearly flat [126].

OFDM is an efficient realization of multicarrier modulation communication in which the subcarriers are made mutually orthogonal. The orthogonality attribute allows the subcarrier spectra to overlap, while still allowing the subcarrier signals to be received and decoded without interference from the adjacent carriers.

Consider an OFDM system with N_c subcarriers. The frequency spacing of the N_c subcarriers is $\triangle f$. The total system bandwdith B is divided into N_c equidistant sub-channels. All subcarriers will be mutually orthogonal within a time interval of length $T_s = 1/\triangle f$. The n-th subcarrier signal, denoted by $\tilde{s}^{(n)}(t)$, can be given by

$$\tilde{s}^{(n)}(t) = \exp\{j2\pi n \triangle f t\}, \qquad n = 0, 1, \ldots N_c - 1; \quad 0 \leq t \leq T_S, \tag{5.25}$$

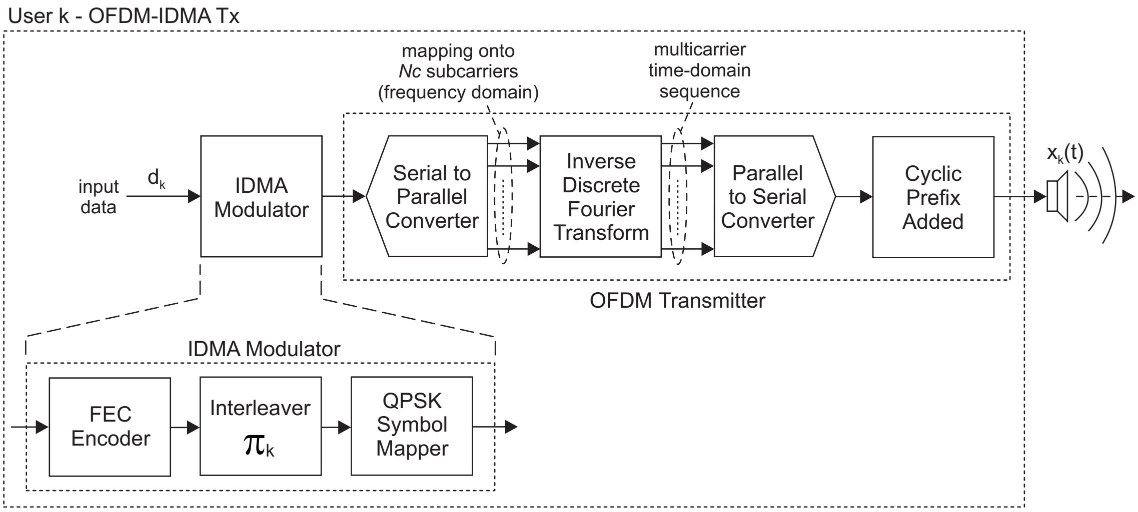

Figure 5.7: Transmitter structure for the multiple-access OFDM-IDMA system

where $j = \sqrt{-1}$. Since the system bandwidth B is subdivided into N narrowband channels, the OFDM block duration T_S is N times as large as in the case of a single-carrier transmission system covering the same bandwidth. Typically, for a given system bandwidth, the number of subcarriers is chosen such that the symbol duration is large compared to the maximum delay of the channel. The composite OFDM baseband signal, $\tilde{x}(t)$, for symbol time i is then given by

$$\tilde{x}(t) = \sum_{n=0}^{N_c-1} x^{(n)}[i]\, \tilde{s}^{(n)}(t - iT_S), \qquad iT_S \leq t \leq (i+1)T_S, \tag{5.26}$$

where $x^{(n)}[i]$ are the input IDMA symbols. The complex baseband OFDM signal (5.26) exactly described the inverse discrete Fourier transform of N_c input symbols (where N_c is the number of sub-carriers) [76]. Therefore the OFDM modulator can be readily implemented using the inverse discrete Fourier transform. To improve computational efficiency, the fast Fourier transform (FFT) algorithm is generally used to compute the inverse DFT.

Usually the subcarrier signal $\tilde{s}^{(n)}(t)$, (5.25), is extended by a cyclic prefix with the length T_{CP} yielding the following signal

$$s^{(n)}(t) = \exp\{j2\pi n \triangle f t\}, \qquad -T_{CP} \leq t \leq T_S. \tag{5.27}$$

The cyclic prefix is added to the subcarrier signal in order to reduce or eliminate ISI from a multipath channel. At the receiver, the cyclic prefix is removed and only the time interval $0 \leq t \leq T_S$ is evaluated. The total OFDM block duration is $T = T_S + T_{CP}$.

Figure 5.7 shows the transmitter structure of the OFDM-IDMA scheme. After IDMA processing (FEC encoding, interleaving and symbol mapping), a serial to parallel (S/P) buffer sub-divides the chip sequence into N_c substreams. Then each substream is modulated onto a sub-carrier by IFFT operation. Finally, the cyclic prefix is added.

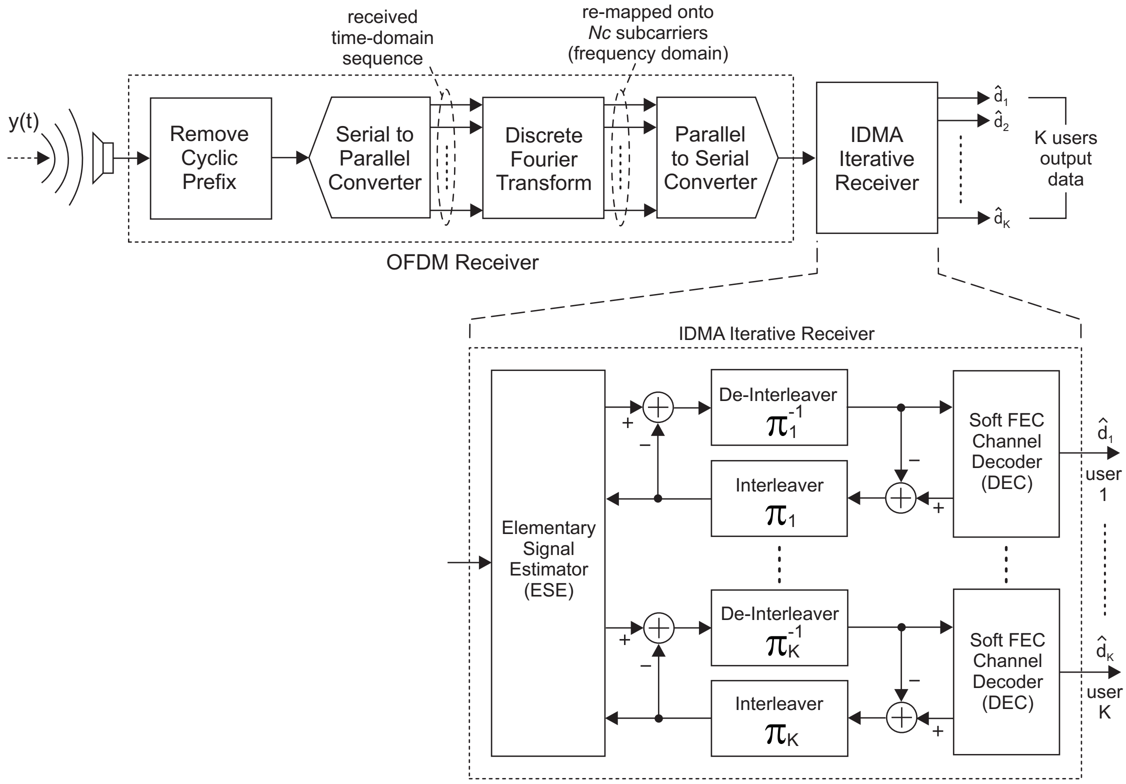

Figure 5.8: Receiver structure for the multiple-access OFDM-IDMA system

Figure 5.8 shows the receiver structure of the OFDM-IDMA scheme. OFDM demodulation is performed before iterative multiuser detection. OFDM demodulation can be readily performed by a discrete Fourier transform, which for computational efficiency, is usually implemented using the FFT algorithm. In this scheme, ISI and MAI are independently processed by the OFDM demodulator and the ESE, respectively. Note that the multipath-fading version of the ESE (from Section 5.2.2) is not required here, and the lower-complexity version of the ESE (for flat-fading) from Section 2.10.2 is used.

5.4 MIMO-OFDM-IDMA

MIMO (Multiple-Input and Multiple-Output) is a general term that refers to communication systems where each transmitter and receiver use multiple transmitting and receiving elements respectively. These systems exploit the spatial diversity of the multipath transmission channel underwater channel to provide improved performance in the form of either increased data robustness or increased data throughput.

At the transmitter side of a MIMO system, Space-Time Block Codes (STBCs) are used to map the input data stream into multiple sub-streams that are dispersed in linear combinations over space (i.e., transmit elements) and time. A STBC is defined by a $(P \times N)$ code matrix $\mathbf{X}$, where N denotes the number of transmit antennas or the *spatial* transmitter diversity order, and P denotes the number of channel usages for transmitting a STBC codeword or the *temporal* transmitter diversity order.

The STBC encoder takes as input a code vector, $\mathbf{x}$, and transmits each row of symbols as specified in $\mathbf{X}$ at P consecutive channel usages. At each channel usage, the symbols contained in the N-dimensional row vector of $\mathbf{X}$ are transmitted through N transmitter antennas simultaneously [114].

As an example, consider the 2×2 Alamouti STBC (ie., $P = 2, N = 2$) [3]. The Alamouti STBC matrix $\mathbf{X}$ is defined by

$$\mathbf{X} = \begin{bmatrix} x(1) & x(2) \\ -x^*(2) & x^*(1) \end{bmatrix} \tag{5.28}$$

where $(\,\cdot\,)^*$ denotes the complex conjugate operation. The input to this STBC is the code vector $\mathbf{x} = [\,x(1),\, x(2)\,]^T$. During the first channel use, the two symbols of the top row of $\mathbf{X}$, $[\,x(1),\, x(2)\,]$, are transmitted simultaneously from the two transmit elements; and during the second channel use, the symbols in the second row of $\mathbf{X}$, $[\,-x^*(2),\, x^*(1)\,]$, are transmitted. The Alamouti STBC provides diversity gain (compared to a single-input single-output systems), but not multiplexing gain.

In this chapter, we restrict our investigation to 2×2 MIMO systems (transmitters and receivers with 2 transmitting and 2 receiving elements respectively), using the Alamouti STBC (5.28).

Figure 5.9 shows the transmitter structure of the MIMO-OFDM-IDMA scheme. The input data sequence is encoded and interleaved by the FEC encoder and interleaver

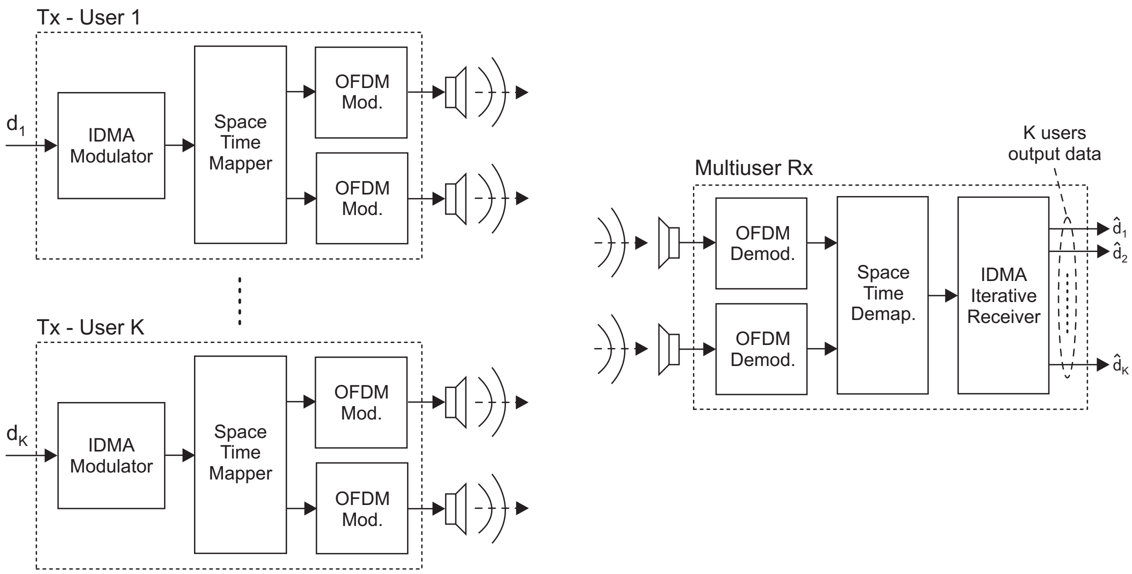

Figure 5.9: Multiuser MIMO-OFDM-IDMA system

respectively. The interleaved chip sequence is then QPSK-modulated followed by space-time mapping as specified by the Alamouti code matrix, $\mathbf{X}$. Finally, each STBC output sub-stream is independently OFDM modulated.

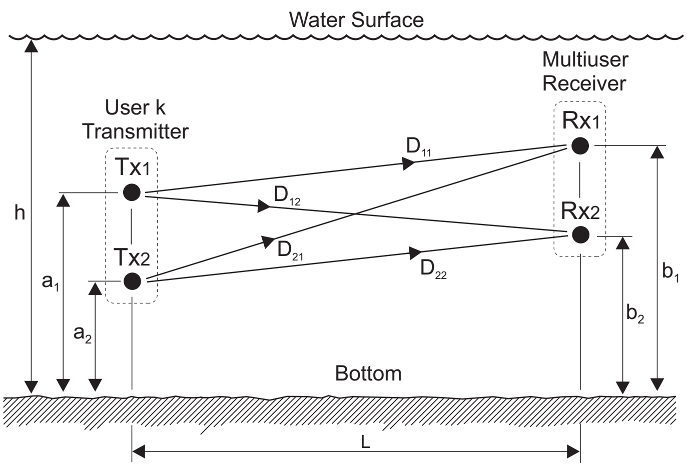

Figure 5.10: Shallow water channel model for a 2 x 2 MIMO system

The channel model for the MIMO system is shown in Figure 5.10. For simplicity the multipath signals are not shown.

5.5 System Performance

The application of an underwater sensor network is used to assess the performance of the various multiuser communication schemes. A star topology network is considered where multiple sensor nodes transmit directly (single-hop) to the central gateway node. Each sensor node is located within the receiving range of the gateway node. Data transmission may be ad hoc, and multiple nodes can transmit data simultaneously to the central gateway node.

Channel Model	Range, L (m) min.	nom.	max.	Depth, h (m)
1	117	130	143	16
2	306	340	374	16
3	495	550	605	16

Table 5.1: Underwater Acoustic Channel Model Parameters

The system performance of the three communications schemes presented (single-carrier IDMA, OFDM-IDMA, and MIMO-OFDM-IDMA), and single-carrier CDMA, are evaluated using the ray-trace multipath channel model. For the CDMA scheme, the coded-CDMA transmitter of Section 2.8 is used (Figure 2.17), and at the receiver side, the CDMA turbo multiuser detector described in Section 2.9 is used, which is suitable for asynchronous CDMA over multipath fading channels. The simulations assume the receiver has perfect channel knowledge.

Each schemes is simulated with 8 simultaneous users (transmitting sensor nodes) over three different channel ranges. The parameters for the channel models are shown in Table 5.1. The range (L) between the receiver and each transmitter is randomly selected between the minimum and maximum values listed to ensure each user has different multipath channel characteristics. The surface reflection coefficient ($\tilde{r}_s$) is 0.33, and bottom reflection coefficient ($\tilde{r}_b$) is 1.00. The transmitter and receiver heights are 6m and 11m respectively (i.e., $a = 6$, $b = 11$), except for the MIMO systems where $a_1 = 5$, $a_2 = 7$, $b_1 = 10$, and $b_2 = 12$.

In the IDMA schemes, the transmitter FEC code is a 1/4-rate convolutional code serially concatenated with a 1/8-rate repetition code (producing an overall code rate of $R = 1/32$). Each transmitter generates QPSK symbols and has a symbol rate of

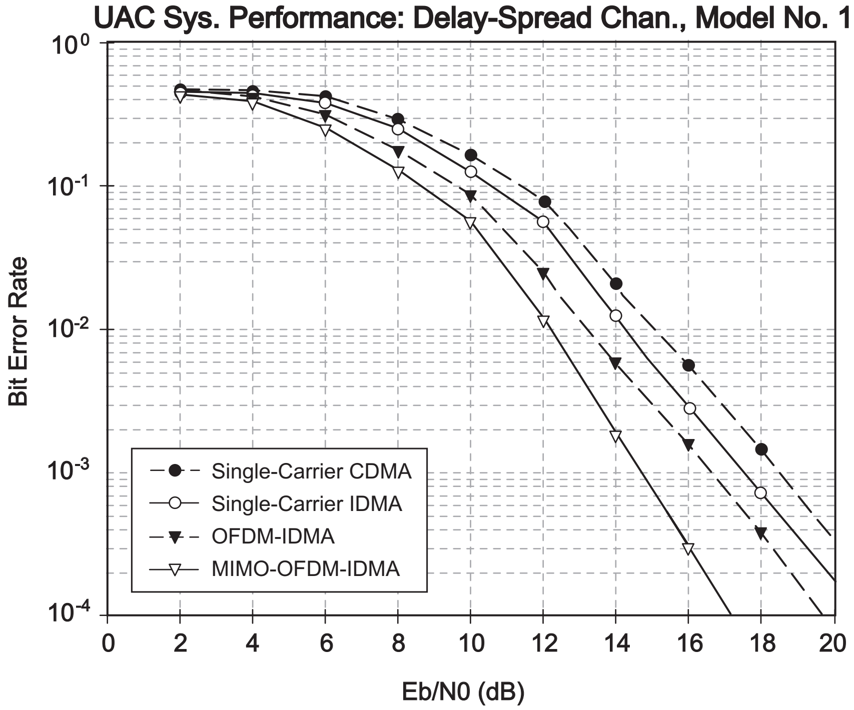

(a) Channel Model No. 1

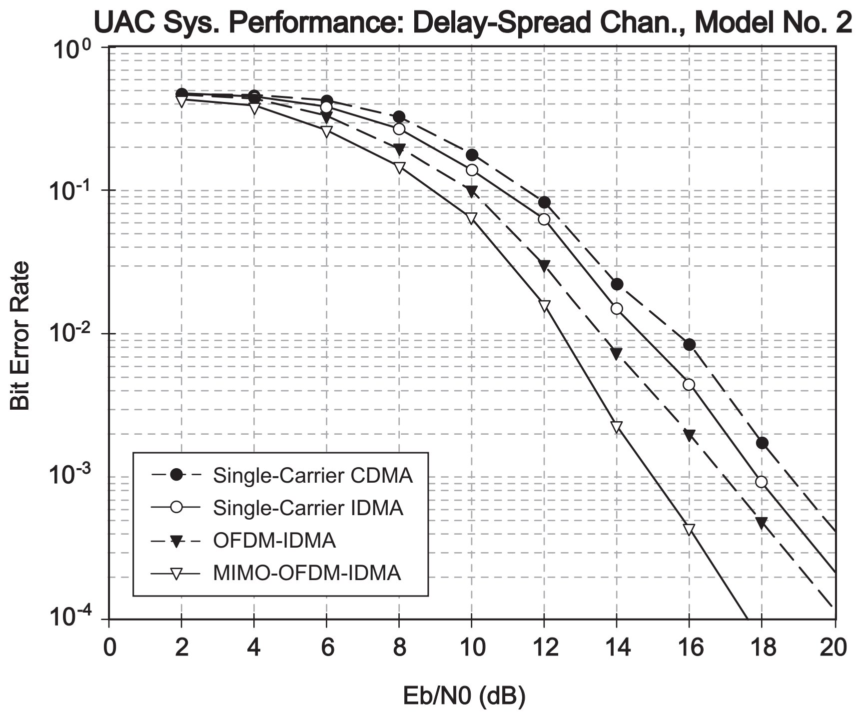

(b) Channel Model No. 2

Figure 5.11: UAC System Performance in Delay-Spread Channels (Model Nos. 1 & 2)

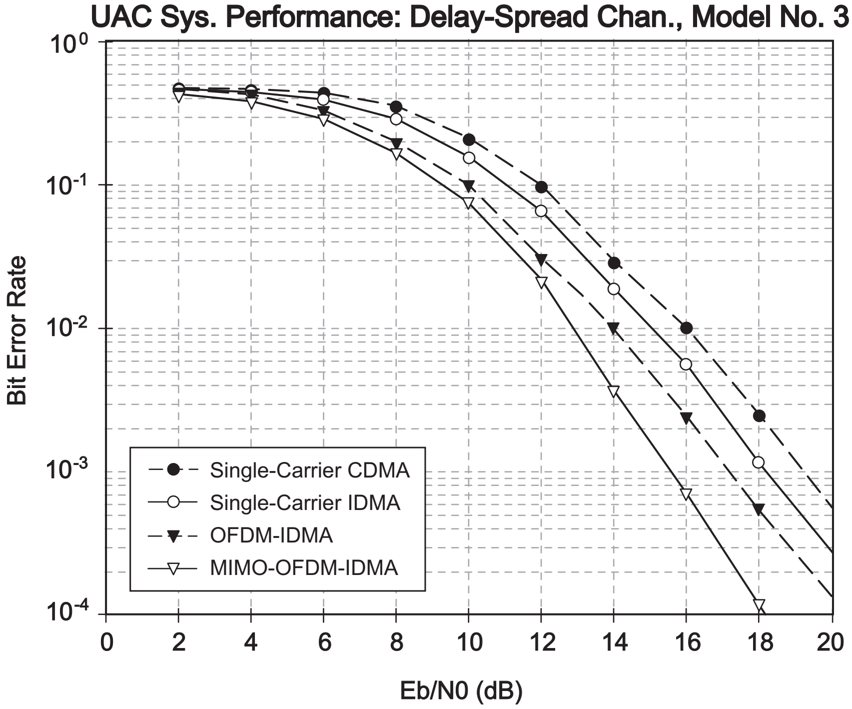

Figure 5.12: UAC System Performance in Delay-Spread Channels (Model No. 3)

1200 symbols per second (producing an aggregate rate of 9600 symbols per second). The OFDM systems uses 128 sub-carriers. In the single-carrier CDMA scheme, the transmitter FEC code is a 1/2-rate convolutional code, and the spreader uses a 16-chip sequence (producing the same bandwidth expansion as the IDMA schemes).

Figures 5.11a, 5.11b, and 5.12 compare the bit error rate (BER) performances of the comunications schemes over channel models 1, 2, and 3 respectively. A slight performance degradation is observed over all four communication schemes for increasing channel range. The BER performance at the longest range (550m) is degraded by approximately 1dB when compared to the shortest range (130m).

In general, the single-carrier IDMA scheme provides a 1dB performance improvement compared to the single-carrier CDMA scheme. This can be attributed to the coding-gain of the IDMA scheme. In CDMA, the spreading operation produces redundancy, and therefore bandwidth expansion, since a single chip alone can carry one bit of information. This redundancy is used to distinguish different users, but this is not ideal from a coding perspective because redundancy is introduced without coding gain. Whereas in IDMA, the bandwidth expansion is entirely achieved by a low-rate FEC code. This code can be a combination of a repetition code (for bandwidth expansion) and a stronger code (for coding gain), which provides a trade-off between performance and complexity.

The OFDM-IDMA scheme provides a performance improvement of approximately 1dB compared to single-carrier IDMA. This improvement in BER comes with the cost of reduced bandwidth efficiency because of the addition of cyclic-prefix to each transmitted OFDM block. Finally, the MIMO-OFDM-IDMA provides an improvement in BER performance of approximately 2dB, which can be attributed to the diversity-gain of the Alamouti STBC. The rich multipath nature of the underwater acoustic channel makes it an ideal candidate for MIMO systems.

5.6 Conclusion

In this chapter, multiuser communications schemes for shallow water acoustic channels were presented. The underwater acoustic channel is characterised by strong multipath signals and long delay spreads, and is considered to be an exceptionally difficult medium for data transmission.

Three IDMA schemes were developed for the underwater channel:

- single-carrier IDMA with a modified multiuser detector for multipath channels;
- OFMD-IDMA, combining multicarrier-modulation with an IDMA overlay; and
- MIMO-OFDM-IDMA, a multiple-input multiple-output extension added to the OFDM-IDMA scheme employing space-time coding to provide diversity gain.

The performance of the three schemes was presented and also compared to single-carrier CDMA.

The single-carrier IDMA scheme was shown to consistently outperform CDMA over the range of conditions tested. The use of low-rate FEC codes to generate bandwidth expansion in IDMA provides additional coding gain compared to CDMA, which uses spreading sequences for bandwidth expansion (producing redundancy without coding gain). The OFDM-IDMA and MIMO-OFDM-IDMA provided further performance improvement, outperforming CDMA by approximately 2dB and 4dB respectively.

The efficient use of bandwidth makes IDMA an attractive spread-spectrum modulation scheme for underwater channels that are severely limited in bandwidth. MIMO systems with space-time coding are able to exploit the rich multipath nature of the underwater channel and are also attractive for underwater communications schemes. The results demonstrate that both OFDM-IDMA and MIMO-OFDM-IDMA schemes are strong candidates for shallow water sensor communication schemes, and are worthy of further research.

Chapter 6

Multiuser Detection for Doubly-Spread Underwater Acoustic Channels

Designing reliable multiple-access communication systems to underpin underwater acoustic sensor networks has proved challenging. For single-carrier modulation schemes with time-domain equalization, the long delay-spread inherent in shallow water channels dictates that a large number of equalizer taps must be used. The resulting computational complexity means that these schemes are often considered unattractive. Multicarrier modulation schemes, such as orthogonal frequency division multiplexing (OFDM), are commonly used for delay-spread channels. However, shallow water channels are often both delay- and Doppler-spread. In Doppler-spread channels, the orthogonality of OFDM is lost, leading to subcarrier interference which complicates data detection and degrades performance. In this chapter, we develop an adaptive multiuser single-carrier system where time-domain equalization is performed using a Kalman filter (KF). KF-based equalization has been shown to outperform traditional linear transversal equalizers, and have much lower complexity. Low-level pilot sequences are superimposed on each users' transmitted data to enable semi-blind channel estimation at the receiver. An adaptive receiver is created by embedding an extended Kalman filter (EKF) into a turbo multiuser detector. The EKF-based equalizer jointly optimizes the estimates of the channel coefficients and data symbols in each iteration of the detection process. EKF state-space modelling is performed using low-rank basis expansion models which provide accurate tracking of time-varying channels at minimal computational complexity. Experimental results demonstrate that the proposed multiple-access scheme with adaptive turbo receiver provides robust performance in doubly-spread underwater acoustic channels.

6.1 Introduction

Underwater sensor networks facilitate a wide range of applications including environmental monitoring, undersea exploration, distributed surveillance, and assisted navigation [2]. A robust and efficient multiple-access communications scheme between the underwater network nodes is an essential foundation for reliable high-performance sensor network operation. However, the shallow water acoustic channel has proved to be a difficult medium for data transmission, and developing reliable communications systems for this environment has been challenging [51].

Code-division multiple-access (CDMA) has been successfully employed as the modulation scheme for shallow water networks [15] [119] [111]. CDMA is a spread-spectrum technique that can provide simultaneous access for multiple users. By employing a transmission bandwidth that is considerably greater than the information rate, spread-spectrum schemes provide a number of benefits, including multiple-access interference (MAI) suppression capability and improved immunity against multipath effects.

The underwater channel is generally impaired by significant multipath interference which produces both long time-delay spread and large multipath amplitudes in the received signal [51]. These long time-delay spreads cause severe inter-symbol interference (ISI) which degrades the performance of many CDMA receiver detection schemes. To alleviate the effects of long time-delay spreads, Multi-carrier modulation (MCM) schemes, such as the spectrally-efficient orthogonal frequency division multiplexing (OFDM), are often used. The basic principle of MCM is to split a high-rate data stream into a number of lower-rate streams that are transmitted simultaneously over a number of sub-carriers. This significantly reduces the ISI span because the lower-rate parallel sub-carriers have increased symbol duration [126].

In [64], a multiple-access communications system that provides robust performance over delay-spread shallow water acoustic channels was developed by combining OFDM with an interleave-division multiple-access (IDMA) overlay. IDMA [85] is a new multiple-access spread-spectrum scheme that uses a low-complexity iterative receiver structure to perform multiuser detection, and has been shown to outperform coded CDMA. However, many practical shallow water acoustic channels are not only delay-spread but are also significantly Doppler-spread. Channels that are both delay- and Doppler-spread are said to be *doubly-spread*. In the case of doubly-spread channels, the orthogonality of OFDM is lost, leading to subcarrier interference which greatly complicates data-detection and degrades performance. For Doppler-spread (time-varying) channels, guard bands can be used in OFDM systems to maintain sub-carrier orthogonality, but this is at the expense of spectral efficiency. For channels with large Doppler-spread, this loss of spectral efficiency would be severe.

In this chapter, we develop a multiple-access IDMA system that would be suitable for underwater acoustic sensor networks. The receiver using a turbo multiuser detection (MUD) algorithm with time-domain equalization. The application of the turbo processing principle to data detection of coded transmission systems with ISI is commonly referred to as *turbo equalization* [23]. For underwater acoustic channels, time-domain equalization using traditional linear traversal equalizers would require a large number of equalizer taps, and may be considered impractical due to the computational complexity. However, we consider equalization based on the Kalman filter (KF). KF-based equalizers have been shown to perform significantly better than linear transversal equalizers, and at much lower complexity (fewer equalizer taps) [101], [55]. Additionally, the state-space formulation of the Kalman equalizer is well suited for iterative receivers and can easily incorporate the soft *a-priori* information from forward error correction (FEC) channel decoders.

For practical systems, it is necessary to perform channel estimation at the receiver because the channel coefficients will be unknown. Channel estimation schemes are generally categorized into one of two methodologies: pilot-aided methods that use information induced from known pilot symbols or training sequences that are interspersed with the data symbols; and blind methods that only use information contained in the receive data symbols. However, with turbo processing, the receiver's the channel estimator can begin with a coarse channel estimate deduced from the pilot symbols, and then utilize the *a posteriori* decision on data symbols obtained from previous iterations to further improve the channel estimate. This type of scheme that combines both pilot symbols and blind information is called a *semi-blind* method and is more powerful than the two methods separately [22].

In [109], an iterative linear channel estimator employing Kalman filtering was developed for turbo processing, where channel estimation and equalization are performed separately in each iteration. However this type of scheme generally only works well for slow fading channels. Also, there can be significant correlation between the estimates of the channel and data symbols because the estimator and equalizer use the estimates obtained from each other.

In [58], an adaptive turbo equalizer was developed using nonlinear Kalman filtering to incorporate channel estimation into the equalization process. The resulting adaptive soft nonlinear Kalman filter (NKF) takes the soft decisions of data symbols from the soft decoder as its *a priori* information, and performs equalization iteratively. With such an approach, the proposed scheme jointly optimizes the estimates of the channel and data symbols in each iteration. This avoids the convergence to a local minima problem that can occur when channel estimation and equalization are performed separately.

Linear channel estimation schemes using pilot-symbols has been shown to provide good performance in delay-spread (multipath) channels and in Doppler-spread (fast-fading) channels. However, in doubly-spread channels, the number of unknown channel parameters often exceeds the number of known data variables (pilot symbols) and the underlying linear system used by the estimation algorithm becomes underdetermined. To alleviate this problem, the number of unknown channels parameters must be reduced so that the linear system becomes tractable. This can be achieved by using low-dimensional models to approximate the time-varying nature of the channel. The accuracy of the channel model employed by the estimation scheme will largely determine the system performance.

Low-order autoregressive (AR) processes are popular low-complexity models of discrete-time random processes. The first-order AR model, AR(1), has been shown to be effective for modelling Rayleigh channels with slow- and moderate-fading on a symbol-by-symbol basis [132] [131], and was employed as state-space model in the NKF-based turbo equalizer of [58].

The basis expansion model (BEM) is low-dimensional low-rank model that can accurately capture the fast time-variations of a doubly-spread channel over a period of time. A BEM consists of superpositions of time-varying basis functions weighted by time-invariant coefficients. Modelling of linear systems by basis functions can turn a time-varying identification problem into a time-invariant one, thereby reducing the number of channel parameters to estimate. The usefulness of using BEMs to model underwater acoustic channels was first recognised in [95] and [96].

In [52], an adaptive NKF-based turbo equalizer was developed using a Fourier BEM channel model. The NKF is used to track the changes in the BEM coefficients instead of tracking the actual channel changes, since the time-variations of BEM coefficients generally evolve much slower that the time-variations of the channel itself. For fast-fading channels, the NKF with Fourier BEM model [52] achieves better performance than the

NKF scheme in [58] where the channel is modelled as an AR process. The Fourier BEM is the time-domain equivalent of the (frequency-domain) Doppler-line filters used in [24] to equalize underwater Doppler-spread channels.

For the multiple-access IDMA system developed in this chapter, the receiver embeds a NKF-based channel estimator/equalizer into the turbo multiuser detection framework. This approach will be shown to be considerably more effective at tracking and equalizing doubly-spread channels than the traditional linear systems-based schemes for IDMAS multiuser channel estimation [86]. The channel estimation and equalization scheme are based on the nonlinear Kalman filtering approach of [58] and [52], but are extended to the multiuser case, adapted to IDMA with superimposed training sequences, and generalised to accommodate different BEM and AR models. The performance of the proposed scheme is evaluated using shallow-water acoustic channel simulation models that been verified by sea trial data. A number of BEM and AR channel estimation models are evaluated to assess the channel estimation/tracking ability and also the system bit error rate performance.

6.2 Underwater Acoustic Channels and Channel Modelling

In a shallow water environment, transmitted acoustic signals undergo multiple reflections at the water surface and sea floor. These reflections occur at small grazing angles and with small reflection losses creating large multipath amplitudes and long time-delay spread in the received signal [51].

Relative movements between the transmitters and the receiver, and the movements of the propagation medium induce Doppler effects, which can be significant even for slow changes. Additional amplitude and phase fluctuations may also result from scattering which is caused by the roughness of the channel surface and bottom. When the sea surface is rough, the vertical motion of the surface modulates the amplitude of the incident wave and superposes its own spectrum as upper and lower sidebands on the spectrum of the incident sound. Moreover, when there is a surface current, the horizontal motion will appear in the scattered sound and cause a Doppler-shifted and Doppler-smeared spectrum [123], [27]. The frequency of the signal received might differ significantly from the frequency of the signal transmitted (by up to 1% typically) [71].

6.2.1 Models for Channel Simulation

Practical methods for modelling refraction effects can be derived from geometrical acoustic theory. The acoustic energy is followed along its various propagation paths, accounting for refractions of the wave direction with sound velocity and gradient. This commonly-used method is based on ray tracing, and is considered to be accurate and computationally efficient for short ranges at high frequencies (where high frequencies are considered to be acoustic frequencies above 500Hz) [47], [27]. An example geometry-based model using ray tracing is shown in Figure 6.1.

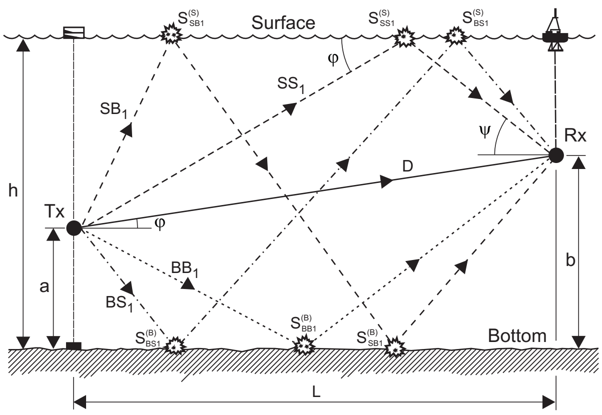

Figure 6.1: Geometry-based ray tracing model of a shallow water acoustic channel

The shallow water propagation is modeled using the multipath channel model proposed by Zielinski, et al. [145]. This model is based on the ray tracing method and simplified with assumptions of constant sound velocity profile and constant bottom depth. Boundaries at the channel surface and bottom reflect the acoustic signal, resulting in multiple travel paths between transmitter and receiver. Consequently, the receiver acquires signals arriving on different paths, each signal delayed according to the channel geometry and attenuated by path and reflection losses.

Figure 6.2 compares the channel impulse responses of the ray tracing model from [145] against published channel measurements from sea trials for four different channel configurations. For the modelling parameters, we assume a surface reflection coefficient ($\tilde{r}_s$) of 0.33, a bottom reflection coefficient ($\tilde{r}_b$) of 1.00, and the underwater speed of sound (c) of 1500m/s. The sea trial measurements are from Aliesawi et al. [4] for Figure 6.2a and Figure 6.2b, and from Coatelan and Glavieux [21] for Figure 6.2c and Figure 6.2d. The comparison results show that the ray theory model provides a reasonable representation of the physical underwater acoustic channel.

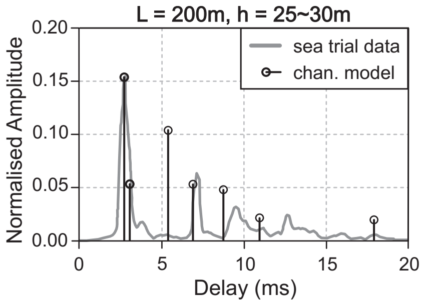

(a) Channel A: L=200m, h=25-30m

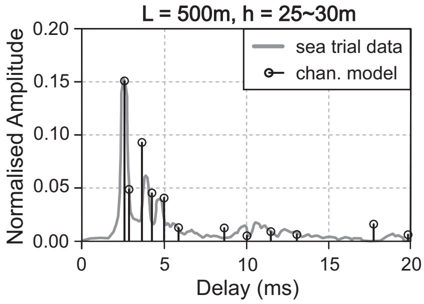

(b) Channel B: L=500m, h=25-30m

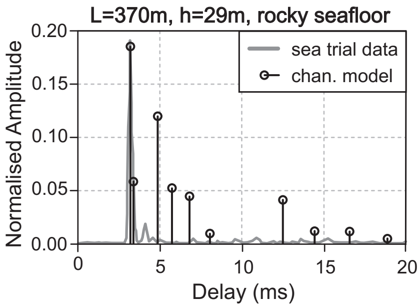

(c) Channel C: L=370m, h=29m

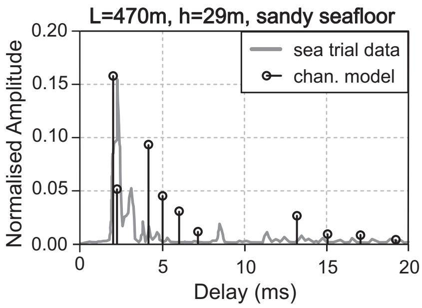

(d) Channel D: L=470m, h=35m

Figure 6.2: Normalised channel impulse responses from sea trial data and channel models

Additionally, the Doppler effects and micropath scattering can be modelled using Rayleigh random processes. Independent and uncorrelated Rayleigh random processes are applied to each path within the ray-theory multipath model. Each Rayleigh process is generated by the method in [143] and satisfies Jakes' model [46].

6.2.2 Models for Channel Estimation

The shallow water acoustic channel can be modelled as a stochastic linear time-variant (LTV) system, with Bello system functions [8] employed to characterize the system in terms of time (t); frequency (f); delay (τ); and Doppler shift (ν).

The input-output relation of the channel is defined by

$$y(t) = \int_{-\infty}^{\infty} h(t,\tau)x(t-\tau)\, d\tau \tag{6.1}$$

where $y(t)$ is the channel output at time t, $x(t)$ is the channel input at time t, and $h(t,\tau)$ is the *input delay-spread function* and is interpreted as the response of the channel at time t to a unit impulse input that stimulated the channel at the time $t-\tau$.

The *delay-Doppler-spread function* $S(\tau, \nu)$ of the channel is defined by the Fourier transform of $h(t, \tau)$ with respect to time t, i.e.,

$$S(\tau, \nu) = \int_{-\infty}^{\infty} h(t, \tau) \exp\{-j2\pi f \tau\} \, dt \tag{6.2}$$

Expressing the time-variant impulse response $h(t, \tau)$ by the inverse Fourier transform of $S(\tau, \nu)$, allows the representation of (6.1) in the form

$$y(t) = \int_{-\infty}^{0} \int_{-\infty}^{\infty} S(\tau, \nu) x(t - \tau) \exp\{-j2\pi\nu t\} \, d\nu \, d\tau \tag{6.3}$$

This relation shows that the output signal $y(t)$ can be represented by an infinite sum of delayed, weighted, and Doppler shifted replicas of the input signal $x(t)$. Signals delayed during transmission in the range of $[\tau, \tau + d\tau)$ and affected by a Doppler shift within $[\nu, \nu + d\nu)$ are weighted by the differential part $S(\tau, \nu) \, d\nu \, d\tau$. Therefore, $S(\tau, \nu)$ explicitly describes the dispersive behaviour of the channel as a function of both the propagation delays τ and the Doppler frequencies ν.

In the discrete-time setting, the channel's input-output relation becomes

$$y(i) = \sum_{l=0}^{L-1} h(i, l) x(i - l) \tag{6.4}$$

and the delay-Doppler-spread function in discrete-time form becomes

$$S(l, d) = \sum_{i=0}^{N-1} h(i, l) \exp\left\{\frac{-j2di}{N}\right\} \tag{6.5}$$

Here, $x(i)$, $y(i)$, $h(i, l)$ and $S(l, d)$ are sampled versions of $x(t)$, $y(t)$, $h(t, \tau)$ and $S(\tau, \nu)$, respectively, from (6.1) and (6.2). The sampling frequency $f_s = 1/T_s$ is assumed to be larger than $B + \nu_{max}$, where B is the transmit bandwidth, and ν_{max} is the maximum Doppler frequency. Furthermore, $L = \lceil \tau_{max}/T_s \rceil$ is the number of discrete channel taps, i.e., the maximum discrete-time delay.

Estimating the complete mathematical description of a doubly-spread LTV channel is a complex task. For every N received samples, we need NL channel coefficients to accurately characterize the channel. Even with superimposed training, where a pilot-symbol is superimposed onto each of the N data symbols, we cannot solve for NL coefficients as the number of unknown variables exceeds the known data variables (i.e.

N pilot symbols). Fortunately, most practical channels exhibit some additional structure which simplifies the description so that a smaller number of parameters are sufficient to model the channels behavior. Such low-dimensional low-rank representations of LTV channels are often referred to as *parsimonious* models.

A popular class of low-rank channel model is the basis expansion model (BEM) [118], [32] which employs a basis expansion $\{g_q(l)\psi_q(i)\}_{q=0}^{Q-1}$, with respect to time i, for each tap of the channel impulse response $h(i,l)$, i.e.,

$$h(i,l) = \sum_{q=0}^{Q-1} g_q(l)\psi_q(i). \tag{6.6}$$

The BEM is motivated by the observation that the temporal (i) variation of $h(i,l)$ is generally smooth due to the channels limited Doppler spread, and hence $\{\psi_q(i)\}_{q=0}^{Q-1}$ can be chosen as a small set of smooth functions. In most cases, the BEM (6.6) is considered only within a finite interval, which we assume to be $i \in [0, N-1]$. The q-th coefficient for the l-th tap in (6.6) is given by

$$g_q(l) = \langle h(\,\cdot\,,l), \tilde{\psi}_q\rangle = \sum_{n=0}^{N-1} h(i,l)\tilde{\psi}_q(i), \tag{6.7}$$

where $\{\tilde{\psi}_q(i)\}_{q=0}^{Q-1}$ is the bi-orthogonal basis for the span of $\{\psi_q(i)\}_{q=0}^{Q-1}$ (i.e., $\langle\psi_q, \tilde{\psi}_{q'}\rangle = \delta_{qq'}$ for all q, q') [42].

The BEM of (6.6) is useful because the complexity of characterizing $h(i,l)$ for the interval $i \in [0, N-1]$ is reduced from NL to QL parameters, where $Q \ll N$. Although, in general, an extension of the time interval will require a proportional increase in the BEM model order (i.e., $Q \propto N$). Using the basis expansion of (6.6) in the channel input-output relation of (6.4) results in

$$\begin{aligned} y(i) &= \sum_{l=0}^{L-1}\sum_{q=0}^{Q-1} g_q(l)\psi_q(i)x(i-l) \\ &= \sum_{q=0}^{Q-1} \psi_q(i) \sum_{l=0}^{L-1} g_q(l)x(i-l) \\ &= \sum_{q=0}^{Q-1} \psi_q(i)\tilde{y}_q(i) \quad \text{where} \quad \tilde{y}_q(i) = \sum_{l=0}^{L-1} g_q(l)x(i-l) \end{aligned} \tag{6.8}$$

Hence, the channel can be viewed as a bank of Q time-invariant filters (convolutions) with impulse responses $g_q(l)$ whose outputs $\tilde{y}_q(i)$ are multiplied by the (time-varying) basis functions $\psi_q(i)$ and added. This BEM structure is shown in Figure 6.3.

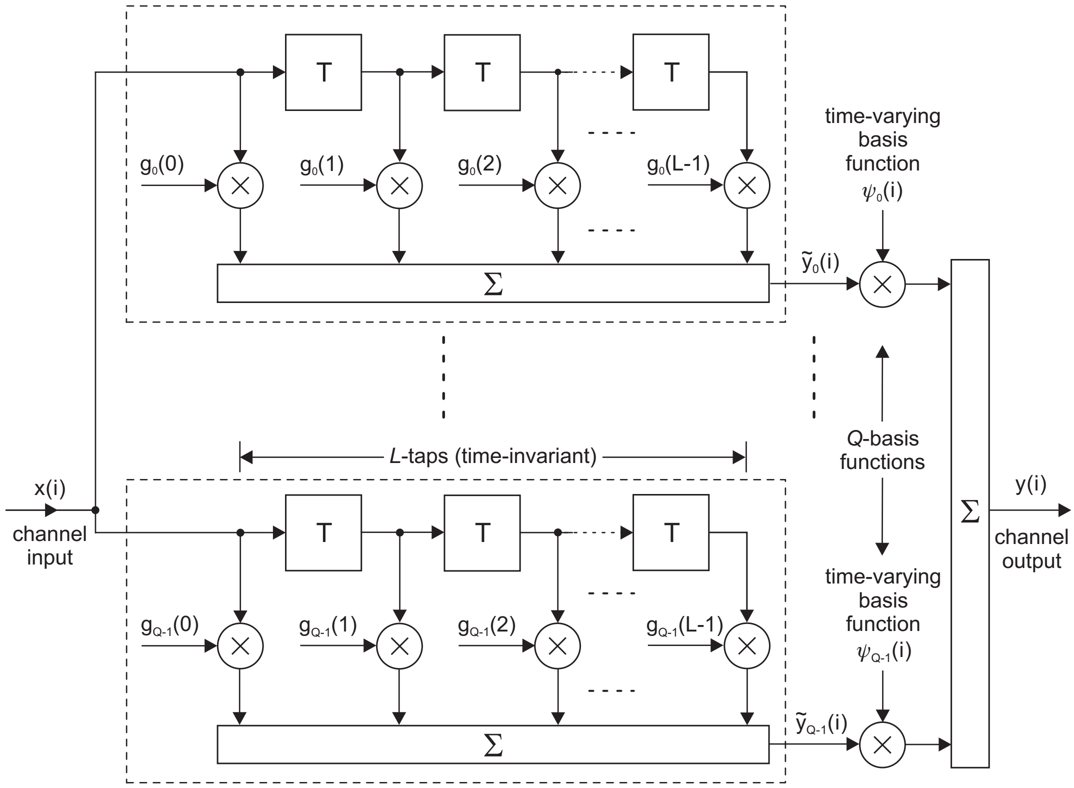

Figure 6.3: Basis expansion model (BEM) of a linear time-variant (LTV) channel

Discrete Fourier (Complex-Exponential) BEM

A basis expansion using complex-exponential basis functions is the most common form of BEM used in practice [118] [32]. This is motivated by taking the inverse discrete Fourier transform of the discrete delay-Doppler-spread function, $S(l, d)$, of (6.5), i.e.,

$$h(i, l) = \frac{1}{N} \sum_{d=0}^{N-1} S(l, d) \exp\left\{\frac{-j2ni}{N}\right\}. \tag{6.9}$$

Denoting the discrete Doppler shift and the maximum discrete Doppler shift as d and d_{max} respectively, and assuming that $S(l, d) = 0$ for $|d| > d_{max}$ results in the so-called *critically sampled* complex-exponential (CE) BEM. Here, the model order equals $Q = 2d_{max} + 1$

with the basis functions given by

$$\psi_q(i) = \exp\left\{\frac{-j2\pi(q-d_{max})i}{N}\right\}, \qquad 0 \le i \le N-1; \quad 0 \le q \le Q-1 \tag{6.10}$$

and the corresponding BEM coefficients given by

$$g_q(l) = \frac{1}{N} S(l, q-d_{max}), \qquad 0 \le q \le Q-1. \tag{6.11}$$

The BEM coefficients, $\{g_q(l)\}_q$, remain invariant during the block of N symbols, but may change from block to block. The Fourier basis functions $\{\psi_q(i)\}_q$ are common for every block. the basis functions of the CE-BEM can be inferred if the delay spread and the Doppler spread (or at least their upper bounds) are known [72]. Treating the basis functions as known, estimation of a time-varying process is reduced to estimating the invariant coefficients over a block of N symbols.

Oversampled Complex-Exponential (CE) BEM

The critically-sampled CE BEM often suffers from spectral leakage introduced by the the (time-limited) rectangular window of the truncated discrete Fourier transform. This Doppler leakage often requires a rather large value of d_{max} to achieve satisfactory modeling accuracy. An alternative interpretation of this problem is that the uniformly-spaced discrete Doppler frequencies d/N (i.e., Doppler resolution $1/N$) usually do not coincide with the actual Doppler frequencies of the continuous channel. In the time domain, this manifests as a Gibbs (or ringing) phenomenon, which degrades the quality of the CE-BEM particulary near the interval boundaries.

These issues of Doppler leakage and Gibbs phenomenon can be alleviated by oversampling [117]. The basis functions for the *oversampled* CE-BEM are given by

$$\psi_q(i) = \exp\left\{\frac{-j2\pi(q-\xi d_{max})i}{\xi N}\right\}, \qquad 0 \le i \le N-1; \quad 0 \le q \le Q-1 \tag{6.12}$$

where ξ is the oversampling factor ($\xi \in \mathbb{N}^*$), and $Q = 2\xi d_{max} + 1$. The oversampling reduces the frequency spacing of complex exponentials and gives a better representation of the channel impulse response [56]. Although in the oversampled model, the basis functions are no longer orthogonal. Example critically-sampled and oversampled CE BEMs are shown in Figure 6.4.

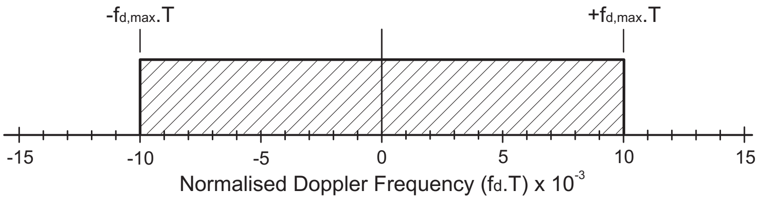

(a) Example Doppler spectrum

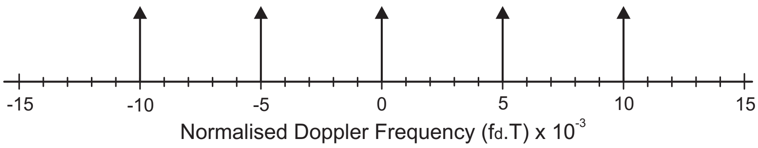

(b) Critically-sampled model (ξ=1, d_{max}=2, Q=5)

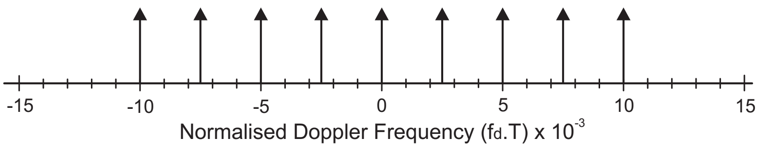

(c) Oversampled model (ξ=2, d_{max}=2, Q=9)

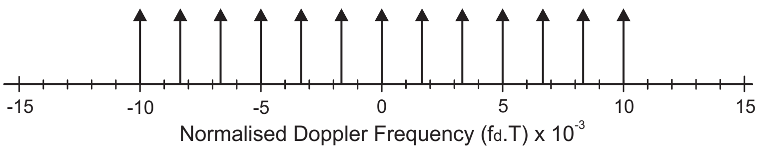

(d) Oversampled model (ξ=3, d_{max}=2, Q=13)

Figure 6.4: Example Doppler spectrum and CE-BEM frequencies

Discrete Prolate Spheroidal Sequences (DPSS) BEM

The Doppler leakage that afflicts the CE-BEM can be significantly reduced by replacing the complex-exponential basis functions with truncated versions of discrete prolate spheroidal sequences (DPSSs) [141]. DPSSs are functions that are band-limited as well as maximally time-concentrated in the sense of having minimum energy outside a prescribed time interval $[0, N-1]$. For a given time sequence of length N and a given maximum normalized Doppler frequency ν_{max}, the DPSSs are the solutions $\psi_q(i)$ to the eigenvalue problem [108]:

$$\sum_{i'=0}^{N-1} \frac{\sin(2\pi\nu_{max}(i-i'))}{\pi(i-i')}\psi_q(i') = \lambda_q\psi_q(i), \qquad i \in \mathbb{Z}. \tag{6.13}$$

Equivalently, the eigenvalues $\{\lambda_q\}_q$ are the eigenvalues of the $N \times N$ matrix $\mathbf{C}$ where

$$\mathbf{C}\boldsymbol{\psi}_q = \lambda_q \boldsymbol{\psi}_q \qquad \text{and} \qquad \{\mathbf{C}\}_{i,i'} = \frac{\sin[2\pi(i-i')\nu_{max}]}{\pi(i-i')} \qquad 0 \leq i, i' \leq N-1$$

where $\{\mathbf{C}\}_{i,i'}$ denotes the (i, i')-th element of $\mathbf{C}$. The N-elements of the corresponding eigenvectors for this matrix, $\boldsymbol{\psi}_q \triangleq [\psi_q(0), \psi_q(1), \ldots, \psi_q(N-1)]^T$, are the length-$N$ subsequences of the DPSSs [84]. The DPS sequences, $\psi_q(i)$, form an orthogonal basis on $[0, N-1]$ and also an orthonormal basis on $\mathbb{Z}$. Assuming that the maximum Doppler frequency can be established with reasonable accuracy, DPS sequences usually provide better modelling accuracy than complex-exponential (Fourier) sequences with the same number of basis functions.

Karhunen-Loève Expansion (K-L) BEM

The normalised mean square (MS) error $E\{|h(t) - \tilde{h}(t)|^2\}$ between $h(t)$ and its series representation $\tilde{h}(t)$ depends on the number of terms in the series and the basis functions used in the series expansion. A series expansion is considered optimum in a MS sense if it yields the smallest MS error for a given number of terms. The Karhunen-Loève (K-L) expansion is optimum in a MS sense for expanding a stationary random process over a finite time interval $[-T/2, T/2]$. The orthonormal set of basis functions, $\{\psi_q(t)\}_q$, used in the K-L expansion of $h(t)$ are obtained from the solutions of the integral equation [106]:

$$\int_{-T/2}^{T/2} R_{hh}(t-\tau)\psi(\tau)d\tau = \lambda\psi(t) \quad -T/2 < t < T/2, \tag{6.14}$$

where $R_{hh}(t-\tau)$ denotes the autocorrelation of $h(t)$ and is defined as $\mathrm{E}\{h(t)h^*(t+\tau)\}$. The solution yields a set of eigenvalues $\lambda_1 > \lambda_2 > \ldots > \lambda_Q$, and eigenfunctions $\{\psi_q(t)\}_{q=1}^{Q}$, and the K-L expansion is written in terms of the eigenfunctions as

$$\tilde{h}(t) = \sum_{q=1}^{Q} g_q \psi_q(t) \qquad -T/2 < t < T/2 \tag{6.15}$$

where

$$g_q = \int_{-T/2}^{T/2} h(t)\psi_n^*(t)\,dt \qquad q = 1, 2, \ldots, Q \tag{6.16}$$

The K-L expansion is often of limited use because of the difficulty in finding eigenfunctions of the appropriate random process. However, for the fast Rayleigh fading process the eigenfunctions can be found using the method in [128].

6.3 Single-User Channel Equalization using the Kalman Filter

The Kalman filter (KF) was first applied to the problem of intersymbol interference (ISI) channel equalization in [55]. The received signal model is stated in terms of a dynamic system driven by white noise, and the system state variables are tracked by the KF using only the outputs of noisy linear combinations of certain states. The following overview of KF-based equalization summarizes the work from [55], [9], [50], and [40].

6.3.1 State-Space System Model

The single-user ISI channel can be modelled in discrete-time as a finite tapped delay line as shown in Figure 6.5.

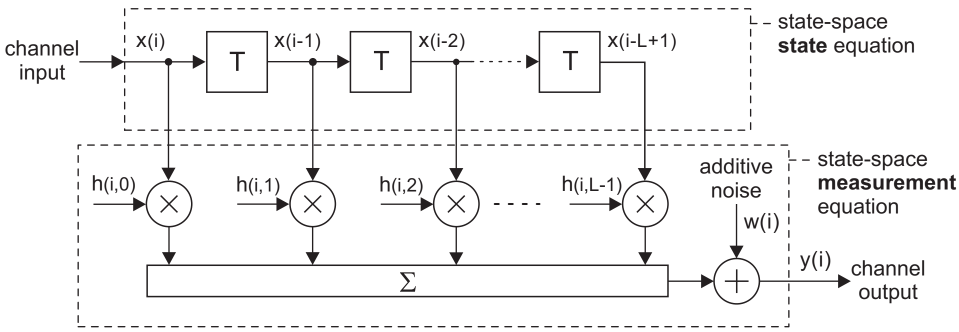

Figure 6.5: Channel model

The sequence of transmitted symbols, $x(i)$, that form the input data into the delay line are assumed to be uncorrelated complex random variables, and are treated as random binary white noise with mean $\mathrm{E}\{x(i)\} = 0$ and covariance $\mathrm{Cov}\{x(i), x(j)\} = \sigma_x^2 \delta_{ij}$. The overall channel is characterized by the causal impulse response, $\{h(i,l)\}_{l=0}^{L-1}$, with the channel output being a finite weighted sum of input pulses. The received signal, $y(i)$, is given by

$$y(i) = \sum_{l=0}^{L-1} h(i,l)x(i-l) + w(i) \tag{6.17}$$

where $w(i)$ is the so-called additive *measurement noise*. This is a discrete-time complex white noise process with mean $\mathrm{E}\{w(i)\} = 0$ and covariance $\mathrm{Cov}\{(w(i), w(j)\} = \sigma_w^2 \delta_{ij}$. The measurement noise, $w(i)$, is statistically independent of the channel input, $x(i)$.

In state-space form, the L-tap delay line and transmit data sequence are modelled using two equations: the *state* equation; and the *measurement* equation. The *state* equation is defined as:

$$\mathbf{s}(i+1) = \mathbf{\Phi}\mathbf{s}(i) + \mathbf{\Gamma}u(i+1) \tag{6.18}$$

where $\mathbf{\Phi}$ is a $L \times L$ matrix (termed the *state transition matrix*), $\mathbf{\Gamma}$ is a $L \times 1$ vector, and $u(i)$ is the so-called *process* noise, with definitions:

$$\mathbf{\Phi} = \begin{bmatrix} \mathbf{0}_{1\times(L-1)} & 0 \\ \mathbf{I}_{L-1} & \mathbf{0}_{(L-1)\times 1} \end{bmatrix}, \quad \mathbf{\Gamma} = \begin{bmatrix} 1 \\ \mathbf{0}_{(L-1)\times 1} \end{bmatrix}, \quad u(i+1) = x(i+1). \tag{6.19}$$

The $L \times 1$ state vector, $\mathbf{s}(i)$, represents the state of the system at time i. The components of the state vector, $s_1(i), s_2(i), \ldots, s_L(i)$, are thus, respectively, the channel input $x(i)$ at time i, and the $L-1$ successive outputs of the delay elements in the channel model (Figure 6.5), i.e.,

$$\mathbf{s}(i) = \begin{bmatrix} s_1(i) \\ s_2(i) \\ \vdots \\ s_L(i) \end{bmatrix} \triangleq \begin{bmatrix} x(i) \\ x(i-1) \\ \vdots \\ x(i-L+1) \end{bmatrix} \tag{6.20}$$

The *measurement* equation describes the channel output at time i, i.e.,

$$y(i) = \mathbf{H}(i)\mathbf{s}(i) + w(i) \tag{6.21}$$

where y is the (scalar) measured output; $\mathbf{H}(i)$ is the $1 \times L$ row vector of channel coefficients defined as $\mathbf{H}(i) \triangleq [h(i,0), h(i,1), \ldots, h(i,L-1)]$, and $w(i)$ is the so-called *observation* noise. The observation noise is assumed to be scalar Gaussian white noise with mean $\mathrm{E}\{w(i)\} = 0$ and covariance $\mathrm{Cov}\{w(i), w(j)\} = \sigma_w^2 \delta_{ij}$. From inspection, it can be seen that the state space model of (6.18) and (6.21) has the same expression as the signal model of (6.17).

6.3.2 Equalization of Channels with Known Coefficients

The Kalman filtering algorithm calculates the minimum error-variance estimate of the state vector $\mathbf{s}(i)$ of the state space model ((6.18) and (6.21)), in the sense that it minimizes the mean square of the norm of the estimation error

$$\mathrm{E}\{||\tilde{\mathbf{s}}(i \mid i)||^2\} \triangleq \mathrm{E}\{||\mathbf{s}(i) - \hat{\mathbf{s}}(i \mid i)||^2\} \tag{6.22}$$

where $\hat{\mathbf{s}}(i \mid i)$ is the estimate of state vector $\mathbf{s}(i)$ based on the set of sequential observations $y(1), y(2), \ldots, y(i)$. The $L \times L$ error covariance matrix $\mathbf{P}(i \mid i)$ is defined as

$$\mathbf{P}(i \mid i) \triangleq \mathrm{E}\left\{[\hat{\mathbf{s}}(i \mid i) - \mathbf{s}(i)][\hat{\mathbf{s}}(i \mid i) - \mathbf{s}(i)]^H\right\} \tag{6.23}$$

and (6.22) becomes $\mathrm{E}\{||\tilde{\mathbf{s}}(i \mid i)||^2\} = \mathrm{tr}\,(\,\mathbf{P}(i \mid i)\,)$. The KF minimizes the trace of the error covariance matrix, or any linear combination of the main diagonal elements of the matrix. For the state vector defined in (6.20), the KF minimizes $\mathrm{E}\{|\hat{x}(i) - x(i)|^2\}$ [9].

The KF for the discrete state-space system of (6.18) and (6.21) is described by the following recursive equations for the state estimate vector and error covariance matrix [55], [9]:

1. Time update:

$$\hat{\mathbf{s}}(i \mid i-1) = \mathbf{\Phi}\hat{\mathbf{s}}(i-1 \mid i-1) \tag{6.24}$$

$$\mathbf{P}(i \mid i-1) = \mathbf{\Phi}\mathbf{P}(i-1 \mid i-1)\mathbf{\Phi}^T + \mathbf{\Gamma}\mathbf{Q}\mathbf{\Gamma}^T \tag{6.25}$$

2. Kalman gain:

$$\mathbf{K}(i) = \mathbf{P}(i \mid i-1)\mathbf{H}^T(i)\left[\sigma_w^2 + \mathbf{H}(i)\mathbf{P}(i \mid i-1)\mathbf{H}^T(i)\right]^{-1} \tag{6.26}$$

3. Measurement update:

$$\hat{\mathbf{s}}(i \mid i) = \hat{\mathbf{s}}(i \mid i-1) + \mathbf{K}(i)\,[\,y(i) - \mathbf{H}(i)\hat{\mathbf{s}}(i \mid i-1)\,] \tag{6.27}$$

$$\mathbf{P}(i \mid i) = [\mathbf{I} - \mathbf{K}(i)\mathbf{H}(i)]\,\mathbf{P}(i \mid i-1) \tag{6.28}$$

The resulting general form for the KF is shown in Figure 6.6. A new estimate, $\hat{\mathbf{s}}(i \mid i)$, is formed by predicting forward the old estimate, $\hat{\mathbf{s}}(i \mid i-1)$, and then correcting it with a combination of the observation error $\hat{y}(i \mid i-1) = y(i) - \hat{y}(i \mid i-1)$, which is usually known as *innovation*, weighted by the Kalman gain matrix $\mathbf{K}(i)$. Note that the output vector, $\hat{\mathbf{s}}(i \mid i)$, is an estimate of the last L inputs to the channel.

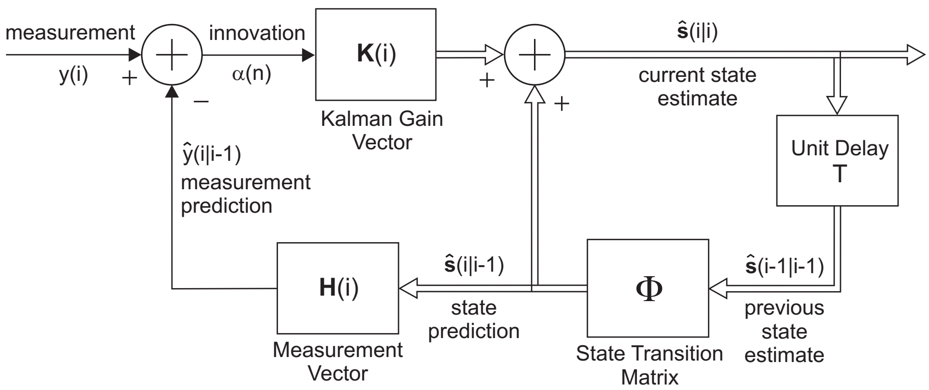

Figure 6.6: General form of the Kalman filter (KF)

The recursive algorithm of (6.24)-(6.28) requires the initial selection of $\hat{\mathbf{s}}(0 \mid 0)$ and $\mathbf{P}(0 \mid 0)$. This is usually achieved by assigning the mean value of $\mathbf{s}(0)$ as $\hat{\mathbf{s}}(0 \mid 0)$ and its corresponding covariance as $\mathbf{P}(0 \mid 0)$, i.e.,

$$\hat{\mathbf{s}}(0 \mid 0) = \mathrm{E}\{\,\mathbf{s}(0)\,\} = \mathbf{0} \tag{6.29}$$

$$\mathbf{P}(0 \mid 0) = \mathrm{E}\{\,\mathbf{s}(0)\,\mathbf{s}^H(0)\,\} = \sigma_x^2\mathbf{I}. \tag{6.30}$$

The variables and parameters used in the KF algorithm are summarized in Table 6.1. The KF-based ISI channel equalizer is shown in Figure 6.7. It is a form of recursive digital filter and is attractive for digital implementation. Note that the tap coefficients $k_1(i), \ldots, k_L(i)$ are the elements from the Kalman gain matrix, $\mathbf{K}(i) \triangleq [k_1(i), \ldots, k_L(i)]$. The Kalman filter contains the same number of delay elements as employed in the channel model, and that that the predicted measurement, $y(i \mid i-1)$, is the sum of the predicted states weighted by the appropriate tap coefficients from the measurement matrix, $\mathbf{H}(i)$.

Variable	Definition	Dimension
$\mathbf{s}(i)$	State vector at time i	$L \times 1$
$y(i)$	Observation at time i	1×1
$\mathbf{H}(i)$	Measurement matrix at time i	$1 \times L$
$\mathbf{Q}$	Covariance matrix of the process noise $u(i)$, $\mathbf{Q} = \sigma_x^2 \mathbf{I}$	$L \times L$
$\mathbf{K}(i)$	Kalman gain at time i	$L \times 1$
$\hat{\mathbf{s}}(i \mid i-1)$	Predicted estimate of the state at time i, given the observations $y(0), y(1), \ldots, y(i-1)$	$L \times 1$
$\hat{\mathbf{s}}(i \mid i)$	Filtered estimate of the state at time i, given the observations $y(0), y(1), \ldots, y(i)$	$L \times 1$
$\mathbf{P}(i \mid i-1)$	Error covariance matrix of $\hat{\mathbf{s}}(i \mid i-1)$, the *a priori* covariance	$L \times L$
$\mathbf{P}(i \mid i)$	Error covariance matrix of $\hat{\mathbf{s}}(i \mid i)$, the *a posteriori* covariance	$L \times L$

Table 6.1: Summary of Kalman filter (KF) variables and parameters

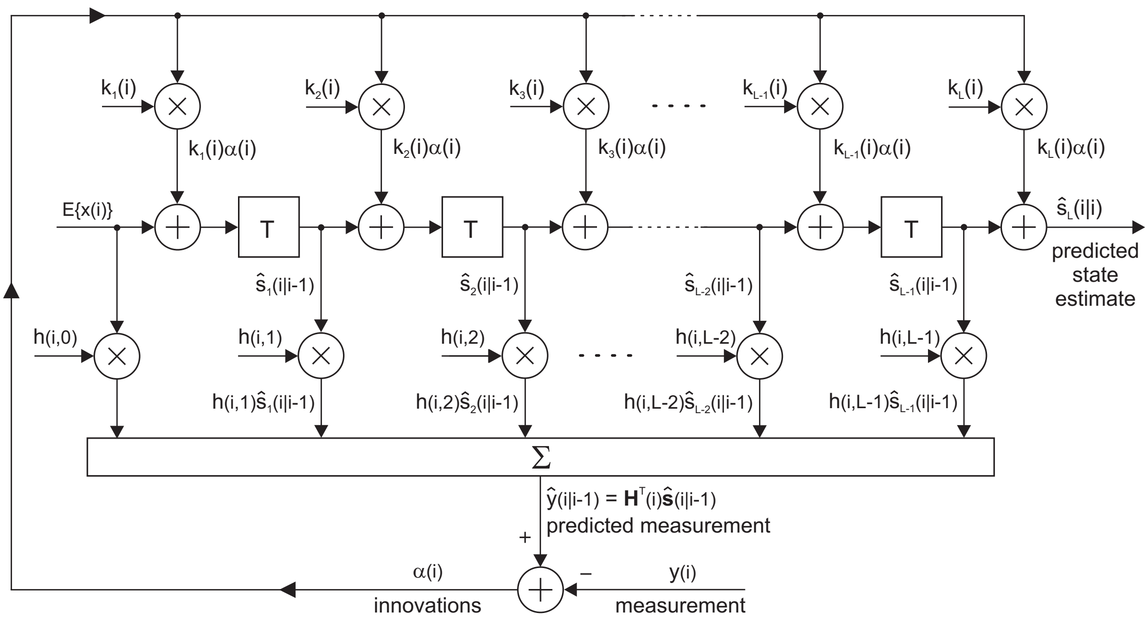

Figure 6.7: KF-based equalizer for ISI channels (single-user channel)

At time i, the estimates of L consecutive transmitted symbols, $\hat{x}(i-L+1), \ldots, \hat{x}(i)$, are available at the receiver. However, in an attempt to minimize the error variance, only the delayed estimates are generally used. The greater the estimation delay, the more information (observations) there is available to form the estimate, and hence the smaller the error variance. In this case, the best symbol estimate at time i is

$\hat{x}(i-L+1) = \{\hat{\mathbf{s}}(i \mid i)\}_L$. This is a so-called *fixed-lag* estimate with delay-δ, where $\delta = L - 1$

6.3.3 Adaptive Equalization of Channels with Unknown Coefficients

To account for unknown coefficients, the equalizer must estimate the channel coefficients and use these values to estimate the signal. This is accomplished by extending the state vector to include the channel parameters as states, i.e.

$$\mathbf{s}(i) = \begin{bmatrix} \mathbf{s}_1^T(i) & \mathbf{s}_2^T(i) \end{bmatrix}^T \qquad (2L \times 1 \text{ vector}) \tag{6.31}$$

where

$$\mathbf{s}_1(i) = [\, x(i),\, x(i-1), \ldots\, x(i-L+1)\,]^T \qquad (L \times 1 \text{ vector}) \tag{6.32}$$

$$\mathbf{s}_2(i) = [\, h(i,0),\, h(i,1), \ldots\, h(i,L-1)\,]^T \qquad (L \times 1 \text{ vector}) \tag{6.33}$$

and hence the state equation is appended with L additional difference equations:

$$h(i+1,l) = h(i,l), \qquad 0 \leq l \leq L-1 \tag{6.34}$$

assuming a time-invariant channel. (The case of a time-varying channel is considered in Section 6.5.) The state equation then assumes the form

$$\mathbf{s}(i+1) = \mathbf{F}\mathbf{s}(i) + \mathbf{G}u(i+1) \tag{6.35}$$

where $\mathbf{F}$ is a $2L \times 2L$ matrix, and $\mathbf{G}$ is a $2L \times 1$ vector, with definitions:

$$\mathbf{F} = \begin{bmatrix} \mathbf{\Phi} & \mathbf{0}_{L\times L} \\ \mathbf{0}_{L\times L} & \mathbf{I}_L \end{bmatrix}, \quad \mathbf{G} = \begin{bmatrix} \mathbf{\Gamma} \\ \mathbf{0}_{L\times 1} \end{bmatrix}, \quad u(i+1) = x(i+1) \tag{6.36}$$

The $2L \times 1$ state vector $\mathbf{s}(i)$ represents the state of the system at time i, the first L components of the vector are the last L transmitted signals, and the last L components are the channel coefficients. Matrices $\mathbf{\Phi}$ and $\mathbf{\Gamma}$ are as defined in (6.19).

The adaptive equalizer formulaton of the KF includes a non-linearity in the measurement equation:

$$y(i) = \mathbf{h}\left(\mathbf{s}(i)\right) + w(i), \tag{6.37}$$

where the function $\mathbf{h}\left(\mathbf{s}(i)\right)$ represents the transformation from the state variables to the ideal observations (without noise), and is defined as

$$\mathbf{h}\left(\mathbf{s}(i)\right) = s_1(i)s_{L+1}(i) + \cdots + s_L(i)s_{2L}(i) = \sum_{n=1}^{L} s_n(i)s_{L+n}(i) \tag{6.38}$$

and $s_{L+n}(i)$ is the channel coefficient corresponding to the n-th input $s_n(i)$

The KF is a linear filter and is unable to process non-linear equations intrinsically. However, an approximate solution can be achieved by linearizing $\mathbf{h}$. The result of this linearization and the subsequent application of the linear KF of (6.24)-(6.28) results in the *extended Kalman filter* (EKF). We linearize $\mathbf{h}\left(\mathbf{s}(i)\right)$ about the estimate of $\mathbf{s}(i)$ based on the previous data or predicted estimate $\hat{\mathbf{s}}(i \mid i-1)$, since a linearized observation equation is needed to determine $\hat{\mathbf{s}}(i \mid i)$ in (6.27). Using a first-order Taylor expansion to linearize $\mathbf{h}\left(\mathbf{s}(i)\right)$ yields

$$\mathbf{h}\left(\mathbf{s}(i)\right) \approx \mathbf{h}\left(\mathbf{s}(i \mid i-1)\right) + \left.\frac{\partial \mathbf{h}}{\partial \mathbf{s}(i)}\right|_{\mathbf{s}(i)=\hat{\mathbf{s}}(i|i-1)} \left(\mathbf{s}(i) - \hat{\mathbf{s}}(i \mid i-1)\right) \tag{6.39}$$

Denoting the Jacobian matrix by

$$\mathbf{H}(i) = \left.\frac{\partial \mathbf{h}}{\partial \mathbf{s}(i)}\right|_{\mathbf{s}(i)=\hat{\mathbf{s}}(i|i-1)} \tag{6.40}$$

the linearized version of the observation equation from (6.37) becomes

$$y(i) = \mathbf{H}(i)\mathbf{s}(i) + \left(\mathbf{h}(\hat{\mathbf{s}}(i \mid i-1)) - \mathbf{H}(i)\hat{\mathbf{s}}(i \mid i-1)\right) + w(i) \tag{6.41}$$

For the function $\mathbf{h}\left(\mathbf{s}(i)\right)$ defined in (6.38), the Jacobian matrix, $\mathbf{H}(i)$, is a $1 \times 2L$ vector defined as

$$\mathbf{H}(i) = \left[s_{L+1}(i \mid i-1), \ldots, s_{2L}(i \mid i-1), s_1(i \mid i-1), \ldots, s_L(i \mid i-1)\right] \tag{6.42}$$

The linear KF for this model is the EKF which is defined by the following equations [50]:

1. Time update:

$$\hat{\mathbf{s}}(i \mid i-1) = \mathbf{F}\hat{\mathbf{s}}(i-1 \mid i-1) \tag{6.43}$$
$$\mathbf{P}(i \mid i-1) = \mathbf{F}\mathbf{P}(i-1 \mid i-1)\mathbf{F}^T + \mathbf{G}\mathbf{Q}\mathbf{G}^T \tag{6.44}$$

2. Kalman gain:

$$\mathbf{K}(i) = \mathbf{P}(i \mid i-1)\mathbf{H}^T(i)\left[\sigma_w^2 + \mathbf{H}(i)\mathbf{P}(i \mid i-1)\mathbf{H}^T(i)\right]^{-1} \tag{6.45}$$

3. Measurement update:

$$\hat{\mathbf{s}}(i \mid i) = \hat{\mathbf{s}}(i \mid i-1) + \mathbf{K}(i)\left[y(i) - \mathbf{h}\left(\hat{\mathbf{s}}(i \mid i-1)\right)\right] \tag{6.46}$$
$$\mathbf{P}(i \mid i) = \left[\mathbf{I} - \mathbf{K}(i)\mathbf{H}(i)\right]\mathbf{P}(i \mid i-1) \tag{6.47}$$

6.4 Multiple Access IDMA

Interleave division multiple-access (IDMA) [85] is a new spread-spectrum multiple-access scheme, that when used with low-complexity iterative receivers has been shown to outperform coded CDMA. In contrast to CDMA, which separates users by specific spreading codes, IDMA separates users by unique interleaver sequences. IDMA can be regarded as a special case of chip interleaved CDMA, and therefore inherits many advantages of CDMA including dynamic channel sharing, asynchronous transmission, and robustness against fading [74].

In an IDMA system, bandwidth expansion is entirely achieved by low-rate forward error correction (FEC) code. A compromise between complexity and performance can be achieved by constructing the FEC code as a combination of simple repetition code (for bandwidth expansion) and strong code (for coding gain).

6.4.1 Transmitter Structure

Fig 6.8 shows the transmitter structure of the multiple-access IDMA scheme with K simultaneous users [85]. The input data sequence $\mathbf{d}_k$ of user-k is encoded by the FEC encoder generating a coded sequence $\mathbf{c}_k \triangleq [c_k(1), \ldots, c_k(i), \ldots c_k(N)]^T$, where N is the frame length. The elements in $\mathbf{c}_k$ are referred to as coded bits. Then $\mathbf{c}_k$ is passed through

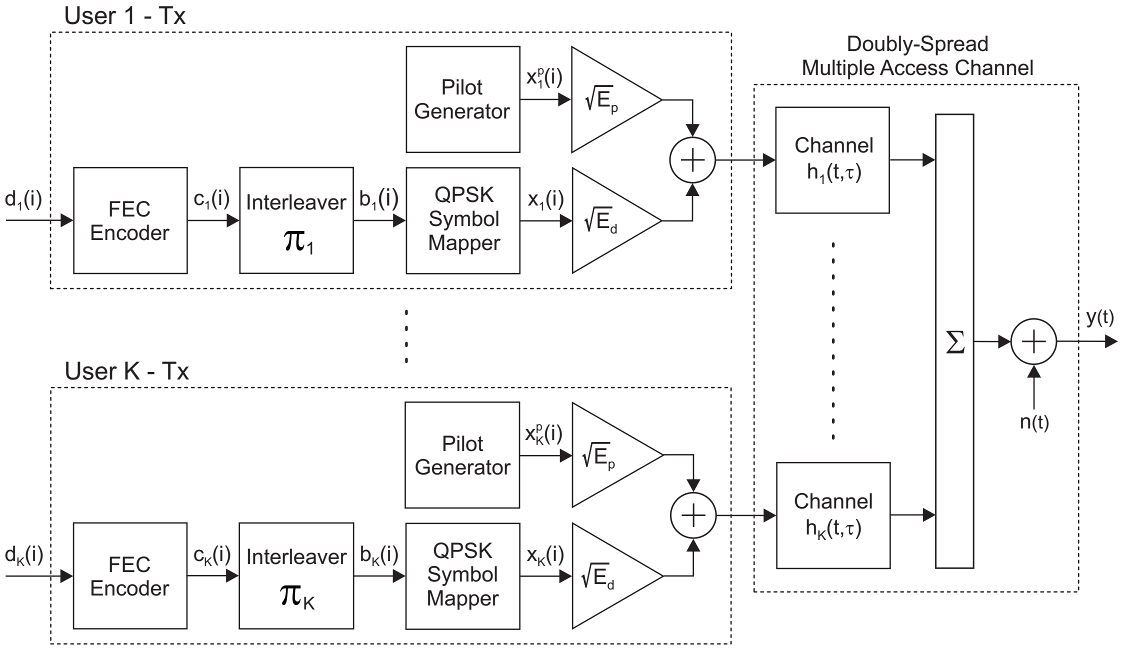

Figure 6.8: Transmitter structure for a multiple-access IDMA system

a random interleaver π_k, generating the interleaved coded bit sequence $\mathbf{b}_k(i) = \pi_k[\mathbf{c}_k(i)]$. Finally, the interleaved chip sequence is QPSK modulated, producing $\mathbf{x}_k$. The QPSK symbols are assumed to have unity average energy, with mean $\mathrm{E}\{x_k(i)\} = 0$ and variance $\mathrm{E}\{|x_k(i)|^2\} = 1$. The elements of $\mathbf{x}_k$ are referred to as chips in accordance with CDMA convention.

The interleaver sequence for each user, π_k, must be unique since IDMA system users are distinguished solely by their interleaver sequence. These interleavers disperse the coded sequences so that the adjacent chips are approximately uncorrelated.

Our proposed scheme employs a pilot-embedding method, where low-level pilots are transmitted concurrently with the data, is used to obtain an initial coarse estimate of the channel such that the iterative detection process at the receiver can be started. The soft information obtained from the turbo decoder is subsequently used to improve channel estimates.

For each user, the pilot sequences are superimposed over the entire transmission block. For each chip, $x_k(i)$, there is one pilot chip, $x_k^p(i)$. Therefore, the channel memory length does not need to be smaller than the spreading length. Additionally, as the training is performed in parallel to the data transmission, it is possible to track rapidly time-varying channels. Compared with the more conventional approach of time-multiplexing pilot symbols with data, superimposing the pilot-sequences has the advantage of not increasing the transmission bandwidth [45].

In this chapter, the pilot symbols are transmitted at 10dB below the signal level of the data symbols, and the pilot sequence design is from [80].

6.4.2 Receiver Structure

The joint multiple-access system with FEC coding in Figure 6.8 can be considered as a serially concatenated coding system, where the FEC code and the multiple-access channel assume the roles of outer code and inner code, respectively [102]. Using this interpretation, an iterative receiver algorithm based on the turbo decoding concept [13] can be developed.

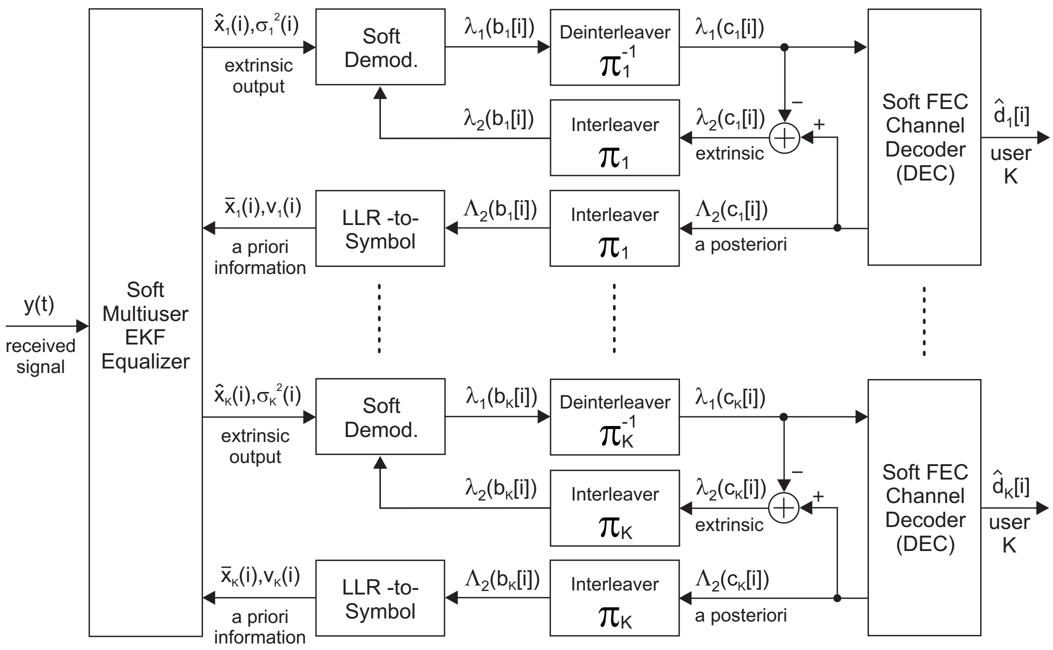

Figure 6.9: Receiver structure for a multiple-access IDMA system

The iterative receiver structure for the multiuser IDMA system is shown in Fig. 6.9. This structure is based on the IDMA iterative receiver structure for joint channel estimation and multiuser detection from [86] and [144], except here an adaptive soft extended Kalman filter (EKF) is embedded into the iterative decoding process (in place of the elementary signal estimator (ESE) of [86]). The adaptive EKF combined with appropriate state-space channel models enables the receiver to effectively track and equalize time-varying frequency-selective fading channels. The EKF is developed from [58], [101], and [52].

The receiver structure consists of a soft-input soft-output (SISO) Kalman filter-based multiuser equalizer and K single-user *a posteriori* probability FEC decoders (DECs). The two stages are separated by interleavers and deinterleavers.

In each decoding iteration, the equalizer uses its *a priori* information to perform joint adaptive channel estimation and equalization. The *a priori* information consists of the the received signal $y(t)$, soft information about the data symbols (supplied by the K single-user FEC decoders from the previous iteration), and knowledge of the pilot symbols. The equalizer produces soft-valued extrinsic information consisting of updated sequences of soft symbol estimates $\hat{x}_k(i)$, and the associated error variance $\sigma_k^2(i)$, for the K users. The estimates $\hat{x}_k(i)$ are assumed to be complex Gaussian distributed with mean $x_k(i)$ and variance $\sigma_k^2(i)$.

The K single-user demodulators then perform symbol-by-symbol MAP demodulation using the extrinsic information from the equalizer, and the *a priori* information, $\lambda_2(b_k(i))$, for the coded bits, $b_k(i)$, from the soft FEC decoders (produced in the previous iteration). The demodulators produce extrinsic information, $\lambda_1(b_k(i))$, (in log-likelihood ratio (LLR) form) for the coded bits $b_k(i)$. The demodulator output LLRs, $\lambda_1(b_k(i))$, are then deinterleaved according to $\lambda_1(c_k(i)) = \pi_k^{-1}\{\lambda_1(b_k(i))\}$, where each user (k) has a unique interleaver sequence (π_k). The deinterleavers reorder the extrinsic information sequences into the correct order for the FEC decoding. The deinterleaver outputs, $\lambda_1(c_k(i))$, (which are now the extrinsic LLRs for the coded sequence $c_k(i)$) are then passed to the K single-user soft FEC decoders which then use the BCJR algorithm [6] to perform MAP decoding.

The K FEC decoders generate both the extrinsic information $\lambda_2(c_k(i))$ and the *a posteriori* probabilities $\Lambda_2(c_k(i))$ for each user's coded sequence $\{c_k(i)\}_i$. The interleaved extrinsic LLRs $\lambda_2(b_k(i)) = \pi\{\lambda_2(c_k(i))\}$ are then used as *a priori* information for the demodulator, while the *a posteriori* LLRs $\Lambda_2(b_k(i)) = \lambda_1(b_k(i)) + \lambda_2(b_k(i))$ are used to compute the mean $\bar{x}_k(i)$ and variance $v_k(i)$ for data symbols $x_k(i)$ as

$$\bar{x}_k(i) = \mathrm{E}\{x_k(i)\} = \sum_{x\in\mathcal{X}} x\, P(x_k(i) = x), \tag{6.48}$$

and

$$\begin{aligned} v_k(i) = \mathrm{Var}\{x_k(i)\} &= \sum_{x \in \mathcal{X}} |x - \bar{x}_k(i)|^2 \, P(x_k(i) = x), \\ &= 1 - |\bar{x}_k(i)|^2 \end{aligned} \tag{6.49}$$

where $\mathcal{X}$ denotes the set of possible symbol constellations, and the probability $P(x_k(i) = x)$ is calculated based on the assumption of independent bit sequence $\{b_k(i)\}_i$. Finally, $\bar{x}_k(i)$ and $v_k(i)$ are fed back into the equalizer as *a priori* information for the next iteration.

6.5 Multiuser Adaptive Soft EKF-Based Equalizer for Doubly-Spread Channels

In this section, we describe the multiuser adaptive EKF-based equalizer that is embedded in the turbo multiuser detector (MUD). The doubly-spread channels are modelled using basis expansion models, and the EKF performs joint channel estimation and equalization where their correlation is implicity considered. The multiuser EKF design is based on the single-user channel EKF designs of [58] and [52], except here it is extended to the multiuser case, adapted for IDMA systems with superimposed training, and incorporates different channel models.

6.5.1 Multiuser System Model

The single-user channel of (6.17) is now extended to the doubly-spread multiuser case with K users. The sequence of transmitted symbols from the k-th user is denoted $\{x_k(i)\}$, and the channel response for the k-th user at time i to a unit impulse at time $i - l$ is denoted $\{h_k(i,l)\}_{l=0}^{L}$. The received signal, $y(i)$, is given by

$$y(i) = \sum_{k=1}^{K} \sum_{l=0}^{L} h_k(i,l) x_k(i-l) + w(i) \tag{6.50}$$

where $w(i)$ is the additive *measurement noise*, described previously. The channels $\{h_k(i,l)\}$ are modelled using the wide-sense stationary uncorrelated scattering (WSSUS) assumption [8], and are independent for different users, k. The transmitted symbols,

$x_k(i)$, are assumed mutually independent and identically distributed (i.i.d.) with mean $\mathrm{E}\{x_k(i)\} = 0$ and variance $\mathrm{E}\{x_k(i)x_k^*(i)\} = \sigma_{x_k}^2 = \sigma_x^2 \ \forall\, k$.

For a block of N_B consecutive received symbols, the BEM representation of the channel for user-k is

$$h_k(i,l) = \sum_{q=1}^{Q} g_{k,q}(l)\psi_q(i), \qquad 0 \le i \le N_B - 1; \quad 0 \le l \le L-1 \tag{6.51}$$

where $\{g_{k,q}(l)\}_{q=1}^{Q}$ are the BEM coefficients for k-th user, and $\{\psi_q(i)\}_{q=1}^{Q}$ are the basis functions. The BEM coefficients are time-invariant during the block $i \in [0, N-1]$, but may change from block to block. The basis functions vary with time i, but are common for every block (and all users). For a given set of basis functions, estimation of the time-varying channel $\{h_k(i,l)\}_{i,l}$ is reduced to estimating the invariant coefficients $\{g_{k,q}(l)\}_{q,l}$ over a block of N_B symbols.

The basis functions in (6.51) are stacked into the following vector:

$$\mathbf{\Psi}(i) \triangleq [\,\psi_1(i),\, \psi_2(i), \ldots,\, \psi_Q(i)\,]^T \qquad (Q \times 1 \text{ vector}) \tag{6.52}$$

and the BEM coefficients (for all K users) are stacked into the following vectors:

$$\mathbf{g}_q^{(l)} \triangleq [\,g_{1,q}(l),\, g_{2,q}(l),\, \ldots,\, g_{K,q}(l)\,]^T \qquad (K \times 1 \text{ vector}) \tag{6.53}$$

$$\mathbf{g}^{(l)} \triangleq [\,\mathbf{g}_1^{(l)T},\, \mathbf{g}_2^{(l)T}, \ldots,\, \mathbf{g}_Q^{(l)T}\,]^T \qquad (KQ \times 1 \text{ vector}) \tag{6.54}$$

$$\mathbf{g} \triangleq [\,\mathbf{g}^{(0)T},\, \mathbf{g}^{(1)T}, \ldots,\, \mathbf{g}^{(L)T}\,]^T \qquad (J_1 \times 1 \text{ vector}) \tag{6.55}$$

where dimension $J_1 \triangleq KQ(L+1)$. Define the following transmit symbol vectors:

$$\mathbf{x}(i) \triangleq [\,x_1(i),\, x_2(i),\, \ldots,\, x_K(i)\,]^T \qquad (K \times 1 \text{ vector}) \tag{6.56}$$

$$\mathbf{X}(i) \triangleq [\,\mathbf{x}^T(i),\, \mathbf{x}^T(i-1), \ldots,\, \mathbf{x}^T(i-L)\,]^T \qquad (K(L+1) \times 1 \text{ vector}) \tag{6.57}$$

Then, with the time restriction of $i \in [0, N_B - 1]$, the multiuser system model of (6.56) using the BEM channel representation of (6.51), can be restated in vector form as

$$y(i) = \mathbf{X}^T(i)[\,\mathbf{I}_{(L+1)} \otimes (\mathbf{\Psi}(i) \otimes \mathbf{I}_K)\,]^H \mathbf{g} + w(i), \qquad 0 \le i \le N_B - 1 \tag{6.58}$$

where $\otimes$ denotes the Kronecker product.

6.5.2 State-Space Model Incorporating A Priori Information

Using the approach of [52], the time-varying channels are modelled using BEMs, with the BEM coefficients tracked by the EKF employing a low-order vector autoregressive (VAR) process as state-space model. A VAR process of dimension $KQ(L+1)$ is used to track the corresponding number of BEM coefficients.

Although the BEM coefficients in (6.58) are invariant over the block of N_B symbols, they can change from block to block, therefore, in the broader sense, the BEM coefficient vectors can be considered to be varying with time i. Consequently, the coefficient vector of (6.55) can be denoted as $\mathbf{g}(i)$. With the assumption that the channel BEM coefficients follow an AR(1) model [52], a first-order VAR model is used to track the time-variations of the BEM coefficient vector, $\mathbf{g}(i)$, as follows:

$$\mathbf{g}(i) = \mathbf{A}_1\mathbf{g}(i-1) + \mathbf{z}(i) \tag{6.59}$$

where $\mathbf{A}_1 = \alpha\mathbf{I}_{J_1}$ is the VAR coefficient matrix, and the driving noise vector $\mathbf{z}(i)$ is zero-mean complex Gaussian with variance $\sigma_z^2\mathbf{I}_{J_1}$ and statistically independent of $\mathbf{g}(i-1)$. The Yule-Walker method (autocorrelation method) [49] can be used to calculate α. Typically $\alpha \approx 1$ but $\alpha < 1$. Assuming the multiuser channel is wide-sense stationary (WSS) and the BEM coefficients $\{g_{k,q}(l)\}$ are independent, we have

$$\sigma_z^2 = \sigma_h^2(1-|\alpha|^2)/Q \tag{6.60}$$

where $\sigma_h^2 \triangleq \mathrm{E}\{|h_k(i;l)|^2\}$, based on the assumption that all users (k) and all taps (l) have the same Doppler spectrum.

The KF-equalization is performed with a fixed-lag of δ symbols ($\delta > 0$) in order to minimize the symbol estimate error variance. Generally, the equalization delay (δ) should be greater than the maximum discrete delay-spread (L) to capture all the available information. Define $D \triangleq \max\{\delta+1, L+1\}$.

The state vector must include estimates of both the transmitted symbols and the BEM channel coefficients to enable the EKF to adaptively equalize the multiuser channel with unknown coefficients. The state vector, $\mathbf{s}(i)$, is defined as follows:

$$\mathbf{s}(i) = \begin{bmatrix} \mathbf{s}_1^T(i) & \mathbf{s}_2^T(i) \end{bmatrix}^T \qquad (J \times 1 \text{ vector}) \tag{6.61}$$

where

$$\mathbf{s}_1(i) \triangleq [\mathbf{x}^T(i), \mathbf{x}^T(i-1), \ldots, \mathbf{x}^T(i-D+1)]^T, \qquad (KD \times 1 \text{ vector}) \tag{6.62}$$

$$\mathbf{s}_2(i) \triangleq \mathbf{g}(i). \qquad (J_1 \times 1 \text{ vector}) \tag{6.63}$$

and $J \triangleq KD + KQ(L+1) = KD + J_1$. Transmit symbol vector, $\mathbf{x}(i)$, is the $K \times 1$ vector defined in (6.56).

For the EKF to be used within a turbo processing framework, the standard EKF formulation (of Section 6.3.3) must be modified to incorporate soft *a priori* information from the FEC channel decoders. This is achieved by considering each user's transmit symbol sequence, $\{x_k(i)\}_i$, to be a WSS stochastic process [109]. Then, using Wold's theorem [49], the symbol sequence of the k-th user, $x_k(i)$, can be expressed as

$$x_k(i) = \bar{x}_k(i) + \tilde{x}_k(i), \tag{6.64}$$

where $\bar{x}_k(i) = \mathrm{E}\{x_k(i)\}$ is a deterministic sequence, and $\tilde{x}_k(i)$ is approximated as an uncorrelated stochastic process with mean $\mathrm{E}\{\tilde{x}_k(i)\} = 0$ and autocorrelation $\mathrm{E}\{\tilde{x}_k(i)\tilde{x}_k^*(i+j)\} = v_k(i)\delta(j)$ (assuming an ideal interleaver).

The statistical characteristics of $x_k(i)$, namely $\bar{x}_k(i)$ and $v_k(i)$, are calculated from the *a priori* information. For data symbols, $\bar{x}_k(i)$ and $v_k(i)$ are calculated from (6.48) and (6.49), respectively. While for pilot symbols, $\bar{x}_k(i) = x_k^p(i)$ and $v_k(i) = 0$, since the pilot symbols are known to the equalizer.

Collecting the K users together, the following vectors are defined:

$$\bar{\mathbf{x}}(i) = [\, \bar{x}_1(i), \bar{x}_2(i), \ldots, \bar{x}_K(i) \,]^T \qquad (K \times 1 \text{ vector}) \tag{6.65}$$

$$\tilde{\mathbf{x}}(i) = [\, \tilde{x}_1(i), \tilde{x}_2(i), \ldots, \tilde{x}_K(i) \,]^T \qquad (K \times 1 \text{ vector}) \tag{6.66}$$

Using the state vector, $\mathbf{s}(i)$ in (6.61), the state equation (incorporating *a priori* information) can be written as

$$\mathbf{s}(i) = \mathbf{F}\mathbf{s}(i-1) + \mathbf{G}\bar{\mathbf{x}}(i) + \mathbf{u}(i), \tag{6.67}$$

with the following definitions:

$$\mathbf{F} = \begin{bmatrix} \mathbf{\Phi} & \mathbf{0}_{KD \times J_1} \\ \mathbf{0}_{J_1 \times KD} & \mathbf{A} \end{bmatrix} \qquad (J \times J \text{ matrix}) \tag{6.68}$$

$$\mathbf{A} = \alpha \mathbf{I}_{J_1} \qquad (J_1 \times J_1 \text{ matrix}) \tag{6.69}$$

$$\mathbf{\Phi} = \begin{bmatrix} \mathbf{0}_{1 \times (D-1)} & 0_{1 \times 1} \\ \mathbf{I}_{(D-1)} & \mathbf{0}_{(D-1) \times 1} \end{bmatrix} \otimes \mathbf{I}_K \qquad (KD \times KD \text{ matrix}) \tag{6.70}$$

$$\mathbf{G} = \begin{bmatrix} \mathbf{I}_K & \mathbf{0}_{K \times (J-K)} \end{bmatrix}^T \qquad (J \times K \text{ matrix}) \tag{6.71}$$

$$\tag{6.72}$$

The vector $\mathbf{u}(i)$ is zero-mean uncorrelated process noise, defined as

$$\mathbf{u}(i) = \begin{bmatrix} \mathbf{\Gamma}^T \tilde{\mathbf{x}}(i) & \mathbf{z}^T(i) \end{bmatrix}^T, \qquad (J \times 1 \text{ vector}) \tag{6.73}$$

where

$$\mathbf{\Gamma} = [\,1 \quad \mathbf{0}_{1 \times (D-1)}\,]^T \otimes \mathbf{I}_K \qquad (KD \times K \text{ matrix}) \tag{6.74}$$

and $\mathbf{z}(i)$ is the $J_1 \times 1$ vector defined in (6.59). The covariance matrix of $\mathbf{u}(i)$ is given by

$$\mathbf{Q}(i) = E\{\mathbf{u}(i)\,\mathbf{u}^H(i)\} = \tilde{\mathbf{Q}} + \mathbf{G}\mathbf{V}\mathbf{G}^T, \qquad (J \times J \text{ matrix}) \tag{6.75}$$

where

$$\mathbf{V} = \operatorname{diag}\{\, v_1(i),\, v_2(i), \ldots,\, v_K(i) \,\} \qquad (K \times K \text{ matrix}) \tag{6.76}$$

$$\tilde{\mathbf{Q}} = \begin{bmatrix} \mathbf{0}_{KD \times KD} & \mathbf{0}_{KD \times J_1} \\ \mathbf{0}_{J_1 \times KD} & \sigma_z^2 \mathbf{I}_{J_1} \end{bmatrix} \qquad (J \times J \text{ matrix}) \tag{6.77}$$

The measurement equation is given by

$$y(i) = \mathbf{h}[\mathbf{s}(i)] + w(i), \tag{6.78}$$

and the nonlinear function for $\mathbf{h}[\mathbf{s}(i)]$ is defined as

$$\mathbf{h}[\mathbf{s}(i)] \triangleq \mathbf{X}^T(i) \left[\, \mathbf{I}_{(L+1)} \otimes (\mathbf{\Psi}(i) \otimes \mathbf{I}_K)\,\right]^H \mathbf{g}(i), \tag{6.79}$$

where both $\mathbf{X}(i)$ and $\mathbf{g}(i)$ can be obtained from the the state vector, $\mathbf{s}(i)$.

6.5.3 Fixed-Lag Soft Input Extended Kalman Filtering

The EKF is applied to the state and measurement equations of (6.67) and (6.78), respectively, to jointly decode the data symbols and track the channel BEM coefficients. The EKF is initialized with

$$\hat{\mathbf{s}}(-1 \mid -1) = \mathbf{0}_{J\times 1} \quad \text{and} \quad \mathbf{P}(-1 \mid -1) = \tilde{\mathbf{Q}},$$

The EKF is described by the following recursive equations:

1. Time update:

$$\hat{\mathbf{s}}(i \mid i-1) = \mathbf{F}\hat{\mathbf{s}}(i-1 \mid i-1) + \mathbf{G}\bar{\mathbf{x}}(i), \tag{6.80}$$

$$\mathbf{P}(i \mid i-1) = \mathbf{F}\mathbf{P}(i-1 \mid i-1)\mathbf{F}^T + \tilde{\mathbf{Q}} + \mathbf{G}\mathbf{V}\mathbf{G}^T. \tag{6.81}$$

2. Kalman gain:

$$\mathbf{H}(i) = \left.\frac{\partial \mathbf{f}[\mathbf{s}]}{\partial \mathbf{s}}\right|_{\mathbf{s}=\hat{\mathbf{s}}(i|i-1)} \qquad \text{(Jacobian matrix)}, \tag{6.82}$$

$$\mathbf{K}(i) = \mathbf{P}(i \mid i-1)\mathbf{H}^H(i)\left[\sigma_w^2 + \mathbf{H}(i)\mathbf{P}(i \mid i-1)\mathbf{H}^H(i)\right]^{-1}. \tag{6.83}$$

3. Measurement update:

$$\hat{\mathbf{s}}(i \mid i) = \hat{\mathbf{s}}(i \mid i-1) + \mathbf{K}(i)\{y(i) - \mathbf{h}[\hat{\mathbf{s}}(i \mid i-1)]\}, \tag{6.84}$$

$$\mathbf{P}(i \mid i) = [\mathbf{I}_J - \mathbf{K}(i)\mathbf{H}(i)]\mathbf{P}(i \mid i-1). \tag{6.85}$$

The EKF recursions are shown diagrammatically in Figure 6.10. The *a priori* information $\{\bar{x}_k(i), v_k(i)\}_{k=1}^K$ is the soft information (at time i) obtained from the K single-user FEC channel decoders, via the LLR-to-symbol blocks (as shown in Figure 6.9). The output $\hat{x}_k(i) = \{\hat{\mathbf{s}}(i+\delta \mid i+\delta)\}_{(K\delta+k)}$ is the delayed *a posteriori* estimate of the data symbol $x_k(i)$ for the k-th user, $k \in [1, K]$.

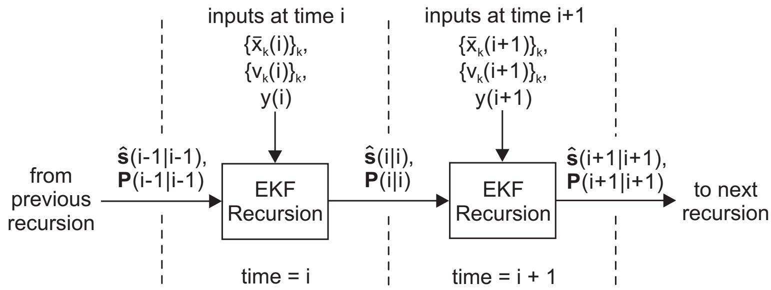

Figure 6.10: Extended Kalman filter (EKF) recursions

6.5.4 Generating Extrinsic Information

The fixed-lag EKF generates delayed *a posteriori* estimates for $\{x_k(i)\}_{k=1}^K$. However, if the EKF equalizer is to be used within a turbo framework, it must produce delayed *extrinsic* estimates. To generate extrinsic estimates, $\{\hat{x}_k(i)\}_{k=1}^K$, that are independent of the *a priori* information $\{\bar{x}_k(i), v_k(i)\}_{k=1}^K$, the *comb* structure shown in Figure 6.11 (adapted from [58]) is used in conjunction with the EKF.

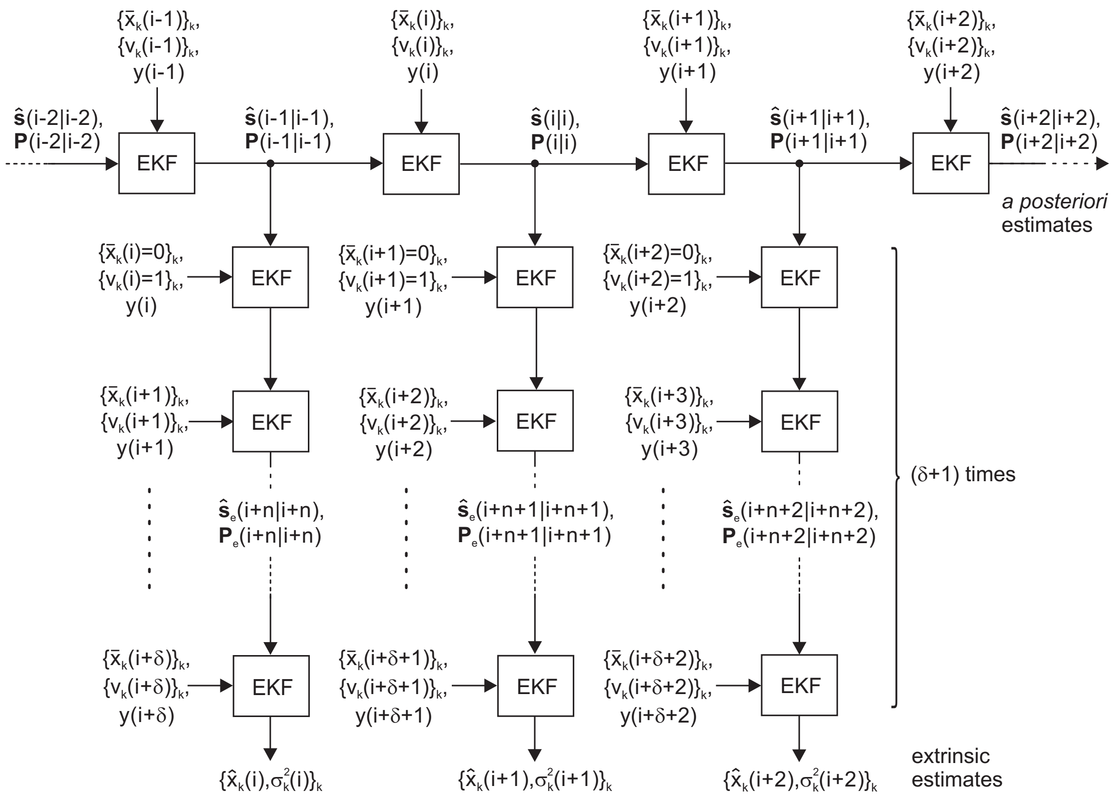

Figure 6.11: Adaptive SISO equalizer using fixed-lag extended Kalman filters (EKFs).

At each time i, the vertical branch composed of $(\delta + 1)$ EKFs produce the extrinsic estimates for each user, $\{\hat{x}_k(i)\}_{k=1}^K$, while the horizontal branch keeps updating the *a posteriori* estimate $\hat{\mathbf{s}}(i \mid i)$ and its error covariance $\mathbf{P}(i \mid i)$. In order to exclude the effect of the *a priori* information, the first EKF in the vertical branch assigns $\{\hat{x}_k(i) = 0, v_k(i) = 1\}_{k=1}^{K}$ to the *a priori* inputs, in place of the information generated by the FEC decoders, Let $\hat{\mathbf{s}}_e(i+n \mid i+n)$ and $\mathbf{P}_e(i+n \mid i+n)$ denote the state estimate and its error covariance matrix, respectively, generated by the $(n+1)$-th vertical filtering branch. Then the δ-delayed estimate $\hat{x}_k(i)$ and its error covariance $\sigma_k^2(i)$, which form the extrinsic information for $x_k(i)$, are given by

$$\hat{x}_k(i) = \{\, \hat{\mathbf{s}}_e(i+\delta \mid i+\delta)\,\}_{(K\delta+k)}\,, \quad \text{and} \tag{6.86}$$

$$\sigma_k^2(i) = \{\, \mathbf{P}_e(i+\delta \mid i+\delta)\,\}_{(K\delta+k),(K\delta+k)}\,, \tag{6.87}$$

respectively (for user k).

6.6 Performance Evaluation

We consider an underwater sensor network multiuser system where multiple sensor nodes can directly transmit (single-hop) to the central gateway node. Sensor node data transmission may be ad hoc, and multiple nodes may transmit data simultaneously to the central gateway node. Each sensor node must be located within the receiving range of the gateway node. The adaptive equalization schemes are evaluated with 8 simultaneous users (transmitting sensor nodes). The transmitter FEC code (which is common to all users) is a 1/4-rate convolutional code serially concatenated with a 1/8-rate repetition code (producing an overall code rate of $R = 1/32$). Each transmitter generates QPSK symbols and has a symbol rate of 1200 symbols per second (producing an aggregate rate of 9600 symbols/second).

A multiple-access random doubly-spread underwater acoustic channel is simulated by a tapped delay line (multipath) structure derived from the ray-tracing methods of [145], with independent and uncorrelated Rayleigh processes applied to each tap. Within the multiuser channel, the channel coefficients $\{h_k(i,l)\}_{k,l}$ are mutually independent for each user k and for each tap l. Each tap is generated via the method in [143] and satisfies Jakes' model [46]. Channel ranges of 200 to 500m, and water depth of 25 to 30m are considered, using the models described in Section 6.2.1. From the channel fading rate definitions in Table 6.2, we consider fast- and very-fast-fading rates with normalised Doppler frequency range of 2.5×10^{-3} to 15×10^{-3}.

Fading Term	Norm. Doppler frequency $(f_d \cdot T_c)$	Velocity (m/s) (for $f_c = 12$kHz)
Slow fading	$0.15 \times 10^{-3} - 0.50 \times 10^{-3}$	$0.07 - 0.22$
Moderate fading	$0.50 \times 10^{-3} - 2.50 \times 10^{-3}$	$0.22 - 1.10$
Fast fading	$2.50 \times 10^{-3} - 5.00 \times 10^{-3}$	$1.10 - 2.20$
Very fast fading	$5.00 \times 10^{-3} - 15.0 \times 10^{-3}$	$2.20 - 6.60$

Table 6.2: Normalised Doppler frequencies and corresponding velocities (for speed of sound in water $c = 1500$m/s, chip duration $T_c \approx 280us$ and carrier frequency $f_c = 12$kHz).

The channel model includes models for significant ambient and intermittent noise sources. Significant ambient noise sources include surface agitation, and thermal excitation, while significant intermittent noise sources include shipping, and rain. The typical levels of these common noise sources are shown in Fig 6.12. These values are calculated from the empirical formulae and observations in [5], [71], and [124].

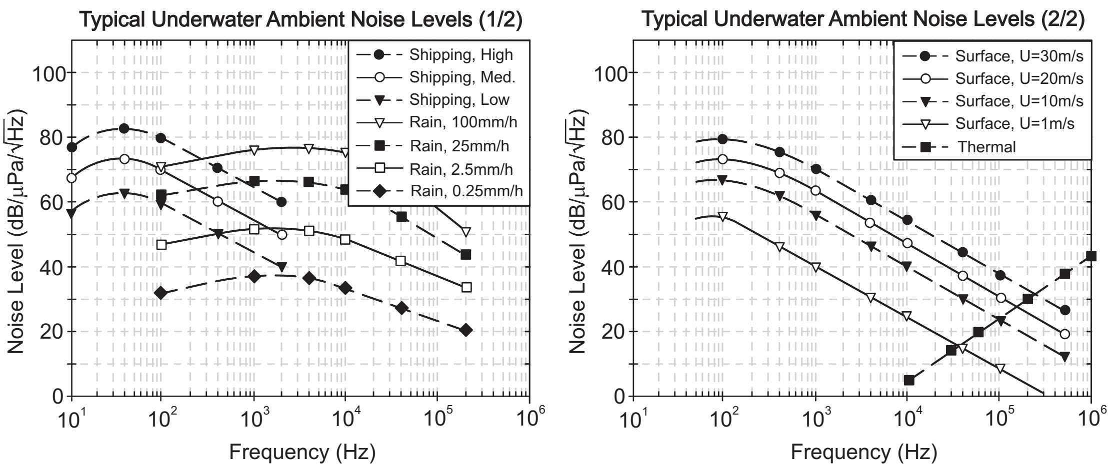

Figure 6.12: Typical noise levels of ambient and intermittent sources

The bit error rate performance of any adaptive receiver scheme will be dependent on the accuracy of the channel estimation methods employed. Therefore, the estimation accuracy of various BEM models is investigated first. The channel estimation normalised mean square error (NMSE) achieved with CE, DPSS, and K-L basis functions for a channel with normalized Doppler spread, f_dT, of 15×10^{-3} is shown in Figure 6.13. The results for different model orders, Q, is also shown.

For the CE-BEM, the critically-sampled ($\xi = 1$), and oversampled ($\xi = 2, 3, 4$) forms are considered. At $Eb/N0 = 25$dB, the critically-sampled CE-BEM (with model order,

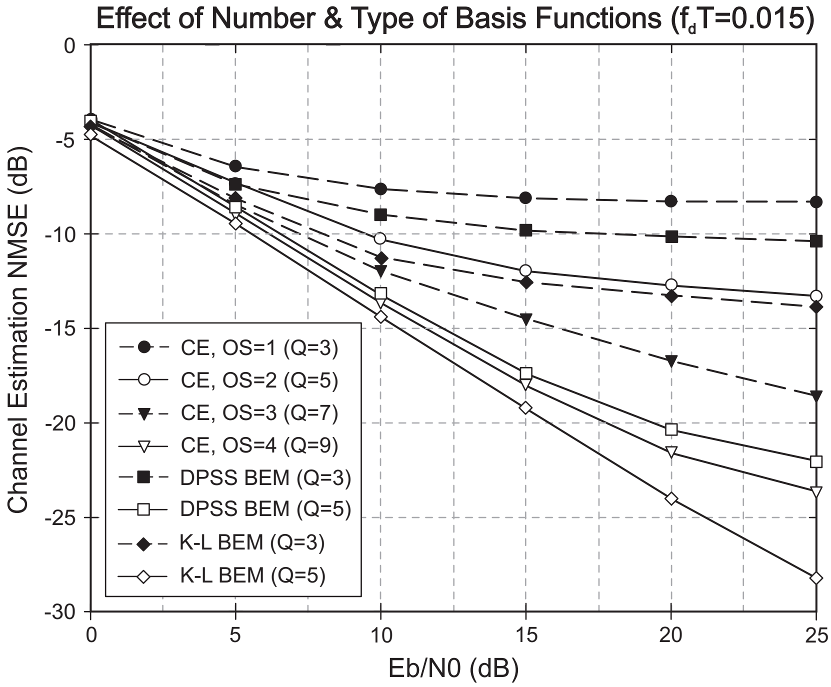

Figure 6.13: Channel estimation NMSE for CE, DPSS, and K-L basis expansion models of a Rayleigh channel with normalized Doppler spread, $f_dT = 15 \times 10^{-3}$.

$Q = 3$) has a channel estimation NMSE of -8dB. This result improves with oversampling. For oversampling factors of 2,3, and 4, the NMSE reduces to -13dB, -18dB and -23dB, respectively (at $Eb/N0 = 25$dB). Note that oversampling also increases the model order, with oversampling factors 2, 3, and 4 producing model orders of 5, 7 and 9 respectively. Computational complexity increases linearly with model order, and so we observe a trade-off between model accuracy and computational complexity.

For the DPSS and K-L BEMs, model orders of Q=3, and Q=5 are considered. For a model order of 3 ($Q = 3$), the channel estimation NMSE for the DPSS BEM and K-L BEM is -10.5dB and -12.8dB, respectively, at $Eb/N0 = 25$dB. Increasing the model order to 5 (Q=5), the channel estimation NMSE reduces to -22dB and -28dB for the DPSS BEM and K-L BEM, respectively. The K-L BEM provides the best NMSE performance for a given model order, but requires exact knowledge of the Doppler frequencies and expects the channel to be Rayleigh distributed. In these simulations, the channel model has correct statistics and the Jakes' model simulators pass the Doppler spread parameters to the K-L BEM. In practical implementation, the Doppler frequencies will not be known (with any accuracy) and the channel may not be Rayleigh distributed, but we have included the K-L BEM here to demonstrate the performance bound of the channel estimation/equalization scheme.

Both the CE BEM and DPSS BEM only require an upper bound on the Doppler spread (not knowledge of the exact Doppler frequencies), so the performance of these two models should be more representative of what is achievable in practice.

As a general rule, for a coded system to achieve an acceptable receiver bit error rate performance (e.g., a BER in the order of 10^{-4} or better), the channel estimation scheme should have a NMSE performance of approximately -12dB or better. From the results of Figure 6.13, this suggests that a minimum BEM order of 5 (Q=5) is required for channels with normalised Doppler spread up to 15×10^{-3}. Therefore the following results all use BEM models of order 5 or greater.

Figure 6.14 compares the performance of channel estimation models employed by the iterative multiuser detector over a range of normalised Doppler spread. The linear equalizer is the standard IDMA channel estimation scheme of [86] and [144]. The auto-regressive (AR) model and basis expansion models (CE, DPSS, K-L) are the state-space models employed by the extended Kalman filter (EKF) embedded in the IDMA turbo multiuser detector. Figure 6.14a shows the channel estimation normalised mean square error (NMSE), while Figure 6.14b shows the bit error rate performance.

The linear equalizer scheme performs well at lower Doppler spreads (with NMSE of 18.8dB and BER of 1.7×10^{-5} at $f_dT = 1 \times 10{-}3$ and $E_b/N_0 = 10\text{dB}$) but at higher Doppler spreads the performance rapidly deteriorates, with a BER greater than 1×10^{-1} for $f_dT \geq 5 \times 10{-}3$.

The EKF using the 10th-order AR model, AR(10), also performs well for slow and moderate fading channels, with a BER of 4×10^{-5} at $f_dT = 1 \times 10^{-3}$ and $E_b/N_0 = 10\text{dB}$, but performance also deteriorates significantly with increasing Doppler spread, with a BER of greater than 1×10^{-2} for $f_dT \geq 6.25 \times 10{-}3$.

The EKF using the BEM state-space models provides better performance. The critically-sampled CE-BEM (OS=1) has a channel NMSE of -14.6dB or better for $f_dT \leq 8.75 \times 10^{-3}$, deteriorating to -9.6dB for $f_dT = 15 \times 10^{-3}$. Similarly the BER performance is 2.6×10^{-5} at $f_dT = 1 \times 10^{-3}$ and slowly rises to 7×10^{-4} for $f_dT = 15 \times 10^{-3}$.

The oversampled CE (OS=2), DPSS, and K-L BEMs provide the best performances, all providing BER of 2×10^{-5} or better and channel NMSE values of -18dB or better for $f_dT \leq 10 \times 10^{-3}$. At $f_dT = 15 \times 10^{-3}$, the channel NMSE is -12.5dB or better and the BER is 2×10^{-4} or better.

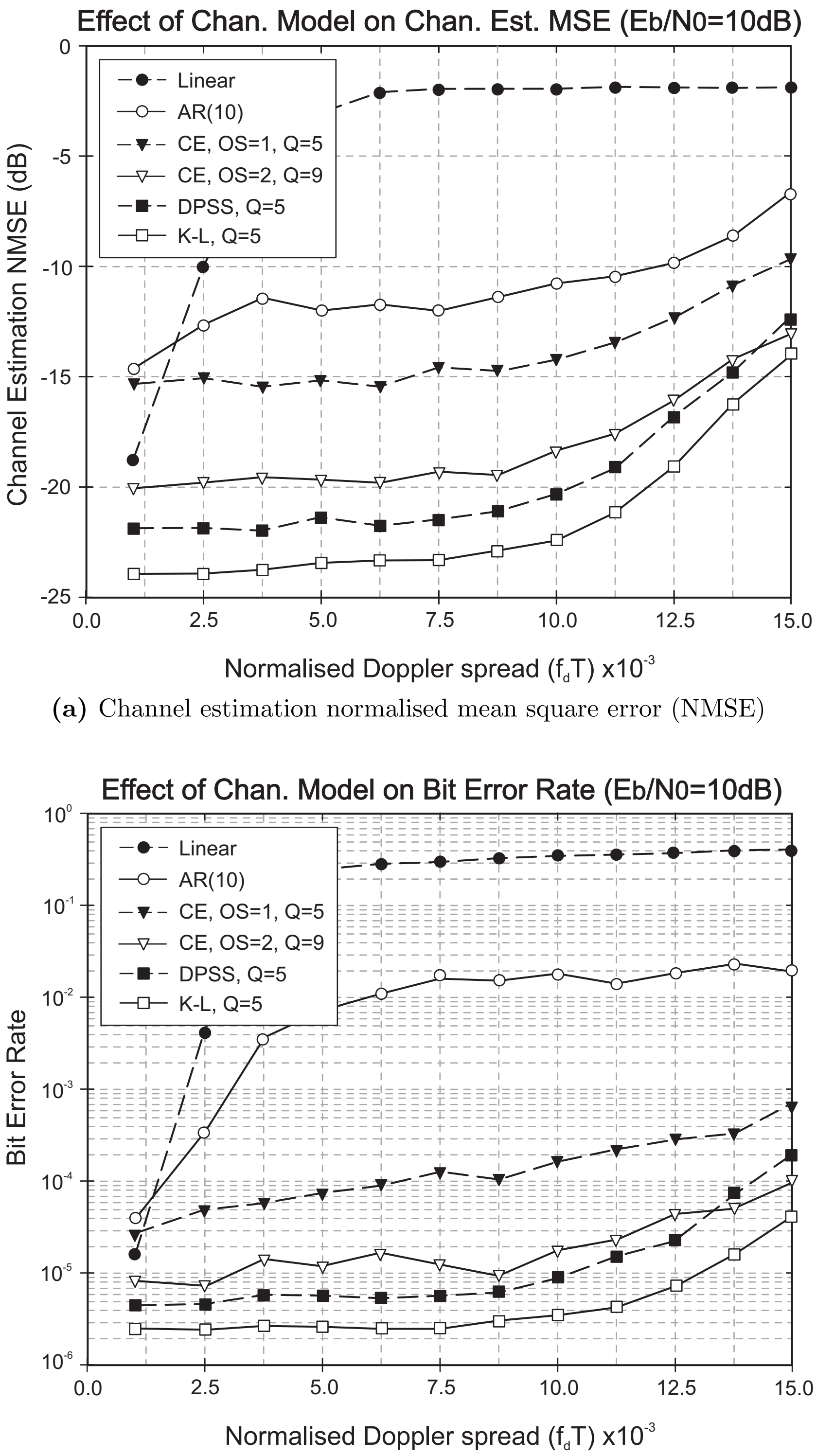

(a) Channel estimation normalised mean square error (NMSE)

(b) Bit error rate performance

Figure 6.14: Effect of channel estimation scheme and Doppler spread on system performance: a) channel estimation NMSE; and b) bit error rate. ($E_b/N_0 = 10\text{dB}$)

As the maximum normalised Doppler frequency increases, the number of significant eigenvalues in the BEM representation increases and thus a larger number of basis functions, Q, need to be used for an accurate approximation. As a general case, the BEM accuracy deteriorates with increasing f_dT. The accuracy can be improved by increasing the number of basis functions used (Q), but this comes with the cost of increasing computational complexity.

Figure 6.15 compares the performance of the channel estimation schemes over a range of signal-to-noise ratios at maximum Doppler spread ($f_dT = 15 \times 10^{-3}$). Figure 6.15a shows the channel estimation normalised mean square error (NMSE), while Figure 6.14b shows the bit error rate performance.

As discovered previously, the linear equalization scheme performs poorly at theis high Doppler spread, with channel NMSE and BER values of approximately -3dB and 3×10^{-1} respectively, over the range of E_b/N_0 values. The EKF with autoregressive model achieves better performance than the linear scheme, but still only attains a BER of 1.2×10^{-3} and channel NMSE of -8dB at $E_b/N_0 = 20$dB.

The four basis expansion models all achieve good performance at high Doppler spread. The K-L BEM achieves a channel NMSE and BER of -16.5dB and 4.8×10^{-6} respectively at $E_b/N_0 = 12.5$dB. The K-L BEM is exactly matched to the Jakes' model Rayleigh spectrum, so this represents the best case performance of the multiuser EKF scheme (for 5 basis functions, $Q = 5$). The DPSS BEM achieves a channel NMSE and BER of -15dB and 1.3×10^{-5}, respectively, at $E_b/N_0 = 12.5$dB. This is within 2dB of the K-L BEM performance and the DPSS BEM doesn't require detailed knowledge of he channel spectrum, only the maximum Doppler frequency.

The critically-sampled CE-BEM achieves a channel NMSE and BER of -10.5dB and 9×10^{-5}, respectively, at $E_b/N_0 = 12.5$dB. While the over-sampled CE-BEM achieves a channel NMSE of -15.5dB and 6.5×10^{-6}, respectively, for the same E_b/N_0 ratio. The over-sampled CE-BEM performance is within 1.5dB of the K-L BEM, but this comes at the expense of computational complexity with the oversampled CE-BEM requiring 9 basis functions compared to 5 for the K-L BEM (and other BEM types evaluated).

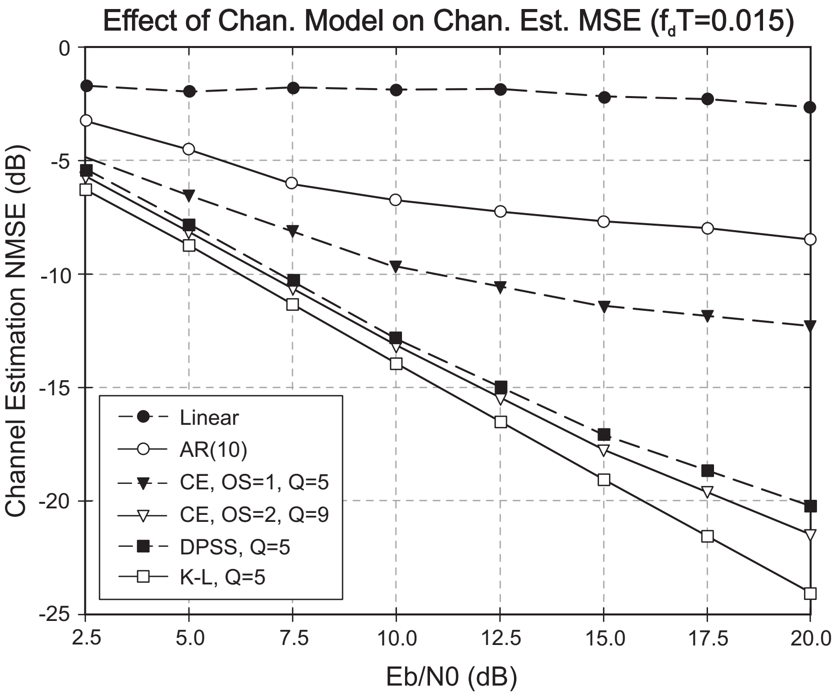

(a) Channel estimation normalised mean square error (NMSE)

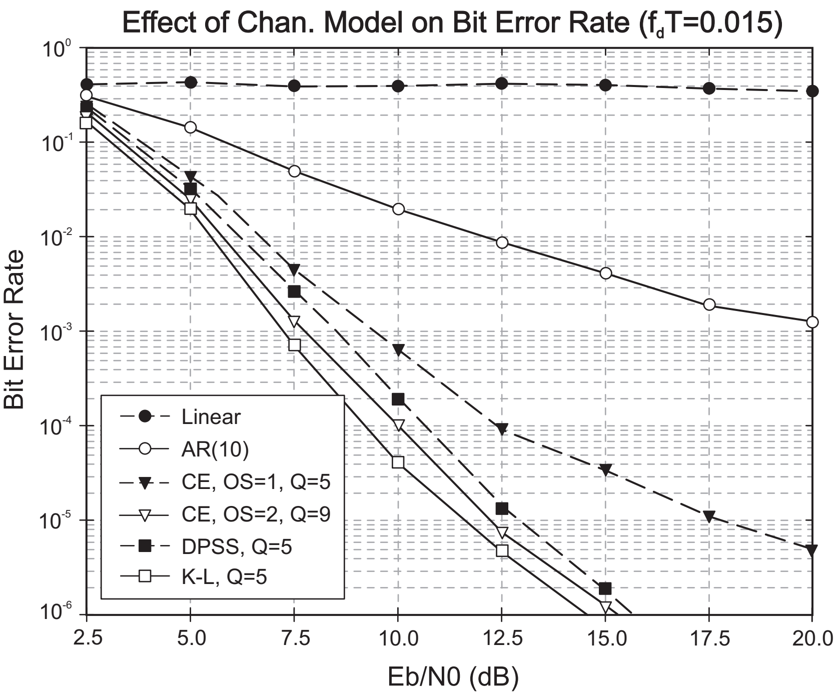

(b) Bit error rate performance

Figure 6.15: Effect of channel estimation scheme and E_b/N_0 ratio on system performance: a) channel estimation NMSE; and b) bit error rate. ($f_dT = 15 \times 10^{-3}$)

6.7 Conclusion

In this chapter, a multiple-access communications scheme for doubly-selective underwater acoustic channels was developed. It is envisaged that the schmee could be used to support an underwater sensor network.

The communications scheme uses interleave-division multiple access (IDMA), a scheme where users are separated by unique interleaver sequences. When used with low-complexity iterative receivers, IDMA has been shown to outperform coded CDMA.

To enable joint channel estimation and data detection, low-level pilot symbols are superimposed onto the transmitted data. These pilots, which are at a level much lower that the signal level, are used by the receiver to obtain the initial coarse estimates of the channel. Improved estimates of the channel are then obtained by integrating the estimation of the channel into the decoding loop. Soft information from the iterative decoder is used to improve channel estimation after every iteration of the decoder.

Such schemes have been shown to provide good performance in multipath (delay-spread) channels, and in fast-fading (Doppler-spread) channels. However in doubly-spread channels, the number of unknown channel variables exceeds the number of known data variables (pilot symbols). The underlying system of equations used by the channel estimation algorithm becomes underdetermined, and accurate channel estimation becomes intractable.

To alleviate this problem, we model the doubly-selective channel using basis expansion models (BEMs). A BEM is an economical or parsimonious model that can provide a good approximation of a time-varying channel using a a reduced number of parameters. Modelling of linear systems by basis expansion models can turn a time-varying system identification problem into a time-invariant one. Using BEM representations of the channel, estimation of doubly-spread channels from using pilot symbols becomes tractable.

An adaptive turbo multiuser receiver was developed where time-domain equalization is performed using a Kalman filter (KF). KF-based equalization has been shown to outperform traditional linear transversal equalizers, and have much lower complexity. An extended Kalman filter (EKF) is embedded into the turbo multiuser detector to create a multiuser equalizer that jointly optimizes the estimates of the channel coefficients and data symbols in each iteration of the detection process. EKF state-space modelling is performed using basis expansion models to provide a tractable means of estimating doubly-spread channels at minimal computational complexity.

Experimental results demonstrate that the proposed multiple-access scheme with adaptive turbo receiver provides robust performance in doubly-spread underwater acoustic channels.

Chapter 7

Conclusion

This thesis explores and applies iterative and adaptive processing techniques to multiple-access IDMA systems. The research consists of two parts. The first is concerned with the optimisation of the iterative detection process, this is achieved through power allocation, FEC code allocation and perfect space-time coding. The second part is concerned with the application of IDMA systems with iterative receivers to underwater acoustic communications. The underwater acoustic channel is a challenging environment characterised by long delay-spreads and limited bandwidth. An OFDM-IDMA system was presented as a solution for underwater channels with delay spread, and an iterative receiver for IDMA using a non-linear Kalman filter to perform joint decoding and channel equalization was presented for doubly-spread underwater acoustic channels. The non-linear Kalman filter utilised low-rank basis expansion models (BEMs) to track the temporal variation of the channels.

In this final chapter, the main conclusions from the novel findings and future research directions on this work are presented. The following section summarises the work that has been conducted in this thesis which highlights the contributions of this research work. Thereafter, directions for further research are discussed.

7.1 Summary and Thesis Contributions

7.1.1 IDMA Performance Optimisation using Variance Transfer Analysis

Variance Transfer (VT) charts were used as a tool for analysing the iterative receiver performance. VT charts track the variance in the log-likelihood ratio (LLR) values that are exchanged between the multiuser detector (MUD) and the channel decoders, providing a graphical representation of the receiver's convergence process. The variance transfer (input/output) characteristic curves of the constituent receiver components, the multiuser detector (MUD) and the forward error correction (FEC) channel decoders, were calculated and then the iterative receiver performance was optimised by matching the VT characteristic curves. Two optimisation schemes were developed:

Power Allocation. Chayat et. al. [18] have shown that the performance of an iterative receiver is optimised if different users transmit at different powers, allowing the iterative decoder to operate in an "onion peeling" mode, where the higher-power layers converge first, decreasing their contribution to the residual noise, and then the lower-power layers converge.

The IDMA concept was extended to a multi-rate system where different users transmit data at different rates, but the same low-complexity iterative receiver structure could still be used. High-rate users were supported by breaking up the input data stream into multiple sub-streams. An IDMA layer was created from each sub-stream, and the multiple IDMA layers are then combined and transmitted from a single antenna. The iterative receiver treats each IDMA layer as a virtual user.

VT charts where then used to analyse the iterative receiver performance, and to develop an optimal power allocation strategy for assigning transmit power levels to IDMA layers. In a Rayleigh flat-fading environment, simulation results demonstrated that the performance of the proposed scheme is close to the theoretical limit.

FEC Code Allocation. Ten Brink [116] demonstrated that different FEC codes generate different FEC channel decoder VT characteristics. The allocation of FEC codes can also be used to manipulate the reciever VT characteristics and thereby optimise system performance.

Using numerical methods and VT Charts, a simple FEC code allocation strategy is devised so that new users are allocated FEC codes according to the existing system load, this allows the FEC decoder VT curve to dynamically match the MUD VT curve as it changes with system load, providing optimal system performance over a range of operating conditions. For small multiuser systems, results demonstrated that the performance of the proposed system approaches the theoretical single user bound.

7.1.2 Optimal Space-Time Coding using the Golden Code

Multiple antenna systems (commonly referred to as multi-input multi-output or MIMO systems) have proven to be an effective method for realising high-rate reliable wireless communications. While coding strategies for MIMO systems have generally focused on providing either higher-rate or increased diversity over traditional single antenna (SISO) systems, linear dispersion (LD) codes are a generalised class of space-time codes that can theoretically provide both diversity gain and high-rate.

LD codes are defined as codes that break up the input data stream into sub-streams that are dispersed in linear combinations over space and time. Recently, cyclic division algebra techniques have provided the means for constructing LD codes that provide both full-diversity and full-rate. Codes that achieve both full-diversity and -rate (and meet a few energy efficiency criteria) are known as *perfect* STBCs or *perfect* codes. The golden code is a perfect STBC for 2×2 multiple-antenna systems.

The *Golden Code* system was extended to the multiuser case, and a MIMO-IDMA multiuser detector to decode LD codes was developed. The complexity of the receiver was linear in the number of users. The performance of this GC-IDMA scheme was compared with MIMO-IDMA schemes employing the Alamouti STBC and V-BLAST, and also against the single-user bound. In a Rayleigh flat-fading environment, simulation results demonstrated that GC-IDMA outperforms both Alamouti- and V-BLAST-IDMA at moderate and high SNR levels. For signal to noise ratios of 8dB and greater, the GC-IDMA scheme employing 16 users approaches within 0.25dB of the single-user bound.

7.1.3 Multiuser Communications for Underwater Acoustic Channels

Underwater sensor networks enable a broad range of applications including environmental monitoring, undersea exploration, assisted navigation, and distributed surveillance [2]. Reliable high-performance sensor networks would need to be underpinned by a robust and efficient multiple-access underwater communications scheme.

Transmission of acoustic waves is considered the most practical means of underwater communications. Radio systems are not feasible because the only radio waves in the extra-low frequency range (< 300Hz) are capable of propagating any distance through conductive sea water. Optical systems are also not suitable because optic waves, while not suffering as significantly from attenuation, are severely affected by scattering and absorption [110].

However, designing reliable underwater acoustic communications (UAC) systems has proven to be very challenging. One of the main channel impairments is multipath interference caused by multiple reflections of the acoustic signal from the water surface and bottom. These reflections occur at small grazing angles and with small reflection losses. This effect causes both long time-delay spread and large multipath amplitudes to be present in the received signal [51].

Delay-spread underwater acoustic channels

Large delay-spread implies that single-carrier communication will be plagued by inter-symbol interference (ISI) that, for practical signal bandwidths, spans many symbols. As an alternative, multi-carrier modulation (MCM) has been proposed to increase the symbol interval and thereby decrease the ISI span. Multicarrier modulation (MCM) is a popular transmission scheme in which the data stream is split into several substreams and transmitted, in parallel, on different subcarriers. MCM transforms the inter-symbol interference (ISI)-inducing frequency selective channel into a set of independent parallel subchannels.

Orthogonal frequency division multiplexing (OFDM) [135], [20] has emerged as one of the most practical MCM techniques for data communication over frequency-selective fading channels. In OFDM, the computationally-efficient fast Fourier transform (FFT) is used to transmit data in parallel over a large number of orthogonal subcarriers. The principle advantage of multi-carrier schemes like OFDM, relative to single-carrier schemes, is that they facilitate simple equalization of delay-spread (i.e., frequency-selective) channels. When an adequate number of subcarriers are used in conjunction with a cyclic prefix of adequate length, subcarrier orthogonality is maintained, even in the presence of frequency-selective fading. Orthogonality implies a lack of subcarrier interference and permits simple, high-performance data detection.

Orthogonal Frequency Division Multiplexing (OFDM) was combined with an IDMA overlay to develop a multiple-access communications system that provides robust performance in the presence of large time-delay spread and the other impairments presented by the shallow water acoustic channel. A low-complexity iterative decoding algorithm based on the turbo-decoding concept was developed for the OFDM-IDMA system receiver, and experimental results demonstrate good performance.

Doubly-spread underwater acoustic channels

The underwater acoustic channel was extended to the doubly-spread case. The relative motion between the transmitter, receiver, and scattering objects imparts each path with a unique Doppler shift, so that multipath propagation also induces a frequency-domain spreading effect on the information signal. Such channels are both delay- and Doppler-spread (or equivalently, frequency- and time-selective), and are referred to as "doubly-spread" or "doubly-selective".

OFDM schemes can been used successfully for time-invariant and slowly time-varying (TV) channels, but they become problematic for doubly-spread (or rapidly TV) channels. For time-invariant channels, the data stream can be split up and transmitted in parallel on non-interfering subcarriers, with equalization being just a simple matter of adjusting the gain and phase on each received subcarrier. This approach can be easily extended to slowly TV channels, where a time-invariant channel is simulated by choosing an OFDM symbol duration that is shorter than the coherence time of the channel. For time-invariant or slowly TV channels, the loss in spectral efficiency due to the inclusion of the guard intervals can be made small, since the channel delay spread (and hence the guard interval) is much smaller than the channel coherence time (and hence the OFDM symbol length). But for rapidly TV channels, the OFDM symbol length would need to be made extremely short, at which point the loss of spectral efficiency due to guard insertion would be severe [104]. Hence, OFDM schemes become impractical for rapidly TV channels.

As a result, a single-carrier system with adaptive channel-estimation is considered for the doubly-spread underwater channel. A single-carrier system with linear traversal equalizer would face complexity issues due to the large number of equalizer taps required to compensate for the long delay-spread. Instead, a Kalman filter (KF) is used as equalizer. KF-based equalizers have been shown to perform significantly better than linear traversal equalizers at a much lower complexity. Additionally, the state-space formulation of the Kalman equalizer is well suited for iterative receivers and allows easy incorporation of soft (a-priori) information for channel-coded systems.

The Kalman filter utilises basis expansion models (BEMs) to model the doubly-selective underwater channels. A basis expansion model is a parsimonious low-rank channel model that exploits the inherent structure in the channel response [32]. Modelling of linear systems by basis functions turns a time-varying system identification problem into a time-invariant one, thereby reducing the number of channel parameters to estimate and simplifying the equalization task.

The receiver uses a semi-blind iterative channel estimation algorithm to initially estimate the channels using only the pilot sequences and then iteratively includes the decoded data into the channel estimates to improve the estimation accuracy. Experimental results showed that the proposed system provides robust performance in doubly-spread underwater acoustic environments.

7.2 Future Work

For future work, we would like to examine multiple directions, including:

- Further investigation into iterative receiver optimisation. For example, as an alternative to the power and code allocation methods presented, allocation of Low-Density Parity-Check (LDPC) codes [31] with different degree sequences could be considered.
- The MIMO-IDMA scheme for the 2×2 Golden code could be extended to accommodate optimal space-time codes of higher dimensions, for example, the 3×3, 4×4, and 6×6 perfect space-time codes proposed by Oggier, et al. [82].
- Further investigation of the nonlinear Kalman filter equalizer. Potentially improved accuracy may be achieved by using other forms of non-linear Kalman filter instead

of the extended Kalman filter, for example, the particle filter. Complexity reduction could also be addressed be considering lower-complexity variants of the Kalman filter, for example, the reduced-complexity Kalman filter proposed by Roy and Duman [101].

- Sea trials of the underwater acoustic communications schemes would provide insight into the performance of the both the OFDM-IDMA scheme and the non-linear Kalman Filter based single-carrier IDMA scheme. Sea trial data would also help improve the accuracy of the simulation channel models.

- Channel tracking using Basis Expansion Models. Additional types of basis expansion model could be considered for the channel tracking function. The Wavelet BEM is a potential candidate. Also, sea trial data could allow the KL BEM to be better customised to the underwater environment, instead of just matching the KL BEM to the Jakes-model spectrum.

- To maximise the performance of the underwater communications schemes, the optimisation methods proposed in the first part of the thesis could be applied to the underwater schemes. Namely power allocation, FEC code allocation and perfect space-time codes.

Bibliography

[1] O. Aitsab and R. Pyndiah, "Performance of reed-solomon block turbo code," in *IEEE GLOBECOM*, London, UK, 1996, pp. 121–125.

[2] I. F. Akyildiz, D. Pompili, and T. Melodia, "Underwater Acoustic Sensor Networks: Research Challenges," *Ad Hoc Networks (Elsevier)*, no. 3, pp. 257–279, 2005.

[3] S. M. Alamouti, "A simple transmit diversity technique for wireless communications," *IEEE Journal on Selected Areas in Communications*, vol. 16, no. 8, pp. 1451–1458, Oct. 1998.

[4] S. A. Aliesawi, C. C. Tsimenidis, B. S. Sharif, and M. Johnston, "Iterative Multiuser Detection for Underwater Acoustic Channels," *IEEE Journal of Oceanic Engineering*, vol. 36, no. 4, pp. 728–744, Oct. 2011.

[5] *APL-UW High-Frequency Ocean Environmental Acoustic Models Handbook, Technical Report APL-UW TR9407*, Applied Physic Laboratory, Univeristy of Washington, Seattle WA, USA, 1994.

[6] L. R. Bahl, J. Cocke, F. Jelinek, and J. Raviv, "Optimal decoding of linear codes for minimizing symbol error rate," *IEEE Transactions on Information Theory*, vol. 20, pp. 284–287, Mar. 1974.

[7] J.-C. Belfiore, G. Rekaya, and E. Viterbo, "The golden code: a 2 x 2 full-rate space-time code with nonvanishing determinants," *IEEE Transactions on Information Theory*, vol. 51, no. 4, pp. 1342–1436, Apr. 2005.

[8] P. A. Bello, "Characterization of randomly time-variant linear channels," *IEEE Trans. Comm. Syst.*, vol. 11, no. 4, pp. 360–393, 1963.

[9] S. Benedetto and E. Biglieri, "On linear receivers for digital transmission systems," *IEEE Transactions on Communications*, vol. 22, no. 9, pp. 1205–1215, Sep. 1974.

[10] ——, *Principles of Digital Transmission with Wireless Applications.* New York:

Kluwer Academic / Pelnum Publishers, 1999.

[11] S. Benedetto and G. Montorsi, "Unveiling turbo codes: Some results on parallel concatenated coding schemes," *IEEE Transactions on Information Theory*, vol. 42, pp. 409–428, Mar. 1996.

[12] C. Berrou and A. Glavieux, "Near optimum error correcting coding and decoding: Turbo codes," *IEEE Transactions on Communications*, vol. 44, no. 10, pp. 1261–1271, Oct. 1996.

[13] C. Berrou, A. Glavieux, and P. Thitimasjshima, "Near Shannon limit error-correcting coding and decoding: Turbo-codes(1)," in *IEEE International Conference on Communications, 1993 (ICC '93)*, Geneva, Switzerland, May 1993, pp. 1064–1070.

[14] R. C. Bose and D. K. Ray-Chaudhuri, "On a class of error correcting binary group codes," *Information and Control*, vol. 3, pp. 68–79, Mar. 1960.

[15] C. Boulanger, G. Loubet, and J. R. Lequepeys, "Spreading sequences for underwater multiple-access communications," in *MTS/IEEE OCEANS '98*, Sep.-Oct. 1998, pp. 1038–1042.

[16] D. Brady and J. C. Preisig, "Underwater acoustic commmunications," in *Wireless Communications: A Signal Processing Perspective*, H. V. Poor and G. W. Wornell, Eds. Prentice Hall, Mar. 1998, ch. 8, pp. 330–379.

[17] G. Caire, R. R. Muller, and T. Tanaka, "Iterative multiuser joint decoding: optimal power allocation and low-complexity implementation," *IEEE Transactions on Information Theory*, vol. 50, no. 9, pp. 1950 – 1973, Sep. 2004.

[18] N. Chayat and S. Shamai, "Iterative soft onion peeling for multi-access and broadcast channels," in *The Ninth IEEE International Symposium on Personal, Indoor and Mobile Radio Communications, 1998,*, vol. 3, Sep. 1998, pp. 1385–1390.

[19] J. F. Cheng and R. J. McEliece, "Unit-memory hamming turbo codes," in *IEEE International Symposium on Information Theory*, 1995, p. 33.

[20] L. J. Cimini Jr., "Analysis and simulation of a digital mobile radio channel using orthogonal frequency division multiplexing," *IEEE Transactions on Communications*, vol. COM-33, pp. 665–765, Jul. 1985.

[21] S. Coatelan and A. Glavieux, "Design and test of a coding OFDM system on the

shallow water acoustic channel," in *MTS/IEEE OCEANS '95*, vol. 3, Oct 1995, pp. 2065–2070.

[22] E. de Carvalho and D. Slock, "Blind and semi-blind FIR multichannel estimation: (global) identifiability conditions," *IEEE Transactions on Signal Processing*, vol. 52, no. 4, pp. 1053–1064, Apr. 2004.

[23] C. Douillard, M. Jezequel, C. Berrou, A. Picart, P. Didier, and A. Glavieux, "Iterative correction of intersymbol interference: Turbo equalization," *European Transactions on Telecommunications*, vol. 6, pp. 507–511, Sep.-Oct. 1995.

[24] T. H. Eggen, A. B. Baggeroer, and J. C. Preisig, "Communication over Doppler spread channels. Part I: Channel and receiver presentation," *IEEE Journal of Oceanic Engineering*, vol. 25, no. 1, pp. 62–71, Jan. 2000.

[25] P. Elia, K. R. Kumar, S. A. Pawar, P. V. Kumar, and H. F. Lu, "Explicit, Minimum-Delay Space-Time Codes Achieving the Diversity Multiplexing Gain Tradeoff," *IEEE Transactions on Information Theory*, vol. 52, no. 9, pp. 3869–3884, Sep. 2006.

[26] P. Elias, "Coding for noisy channels," in *IRE Convention Record*, vol. 4, 1955, pp. 37–47.

[27] P. C. Etter, *Underwater Acoustic Modeling and Simulation*, 3rd ed. London, UK: Spon Press, 2003.

[28] K. Fazel and S. Kaiser, *Multi-carrier and Spread Spectrum Systems: From OFDM and MC-CDMA to LTE and WiMAX*, 2nd ed. Chichester, U.K.: John Wiley & Sons, 2008.

[29] G. D. Forney, *Concatenated Codes.* Cambridge, MA: MIT Press, 1966.

[30] G. J. Foschini, "Layered Space-Time Architecture for Wireless Communication in a Fading Environment When Using Multiple Antennas," *Bell Labs Technical Journal*, vol. 1, no. 2, pp. 41–56, Autumn 1996.

[31] R. Gallager, "Low density parity check codes," *IRE Trans. Inform. Theory*, vol. 8, pp. 21–28, Jan. 1962.

[32] G. B. Giannakis and C. Tepedelenlioğlu, "Basis expansion models and diversity techniques for blind identification and equalization of time-varying channels," *Proceedings of the IEEE*, vol. 86, no. 10, pp. 1969–1986, Oct. 1998.

[33] A. Glavieux, C. Laot, and J. Labat, "Turbo equalization over a frequency selective channel," in *Proc. Intern. Symp. Turbo Codes*, Brest, France, Sep. 1997, pp. 96–102.

[34] M. J. E. Golay, "Notes on digital coding," *Proceedings of the IEEE*, vol. 37, p. 657, 1949.

[35] S. R. Govilkar, "A simulator for the microcontroller-based underwater ultrasonic communications," Master's thesis, North Carolina State University, Raleigh, North Carolina, USA, 2006.

[36] J. Hagenauer, "Source-controlled channel decoding," *IEEE Transactions on Communications*, vol. 43, pp. 2449–2457, Sep. 1995.

[37] ——, "Forward error correcting for CDMA systems," in *1996 International Symposium on Spread Spectrum Techniques and Applications (ISSSTA '96)*, Mainz, Germany, Sep. 1996, pp. 566–569.

[38] R. W. Hamming, "Error detecting and correcting codes," *Bell System Technical Journal*, vol. 29, pp. 147–160, 1950.

[39] B. Hassibi and B. M. Hochwald, "High-rate codes that are linear in space and time," *IEEE Transactions on Information Theory*, vol. 48, no. 7, pp. 1804–1824, Jul. 2002.

[40] S. Haykin, *Adaptive Filter Theory*, 4th ed. New Jersey, USA: Prentice Hall, 2002.

[41] W. Hirt and J. Massey, "Capacity of the discrete-time gaussian channel with intersymbol interference," *IEEE Transactions on Information Theory*, vol. 34, pp. 380–388, May 1988.

[42] F. Hlawatsch and G. Matz, *Wireless Communications over Rapidly Time-Varying Channels*. Amsterdam, The Netherlands: Academic Press, 2011.

[43] A. Hocquenghem, "Codes correcteurs d'erreurs," *Chiffres*, vol. 2, pp. 147–156, 1959.

[44] P. Hoeher, "On channel coding and multi-user detection for DS-CDMA," in *IEEE International Conference on Universal Personal Communications*, Ottawa, Canada, Oct. 1993, pp. 641–646.

[45] P. Hoeher and F. Tufvesson, "Channel estimation with superimposed pilot sequence," in *IEEE Global Telecommunications Conference, 1999 (GLOBECOM '99)*, Rio de Janeiro, Brazil, Dec. 1999, pp. 2162–2166.

[46] W. C. Jakes, *Microwave Mobile Communications*, 1st ed. New York: Wiley, 1974.

[47] F. B. Jensen, "Numerical models of sound propagation in real oceans," in *MTS/IEEE OCEANS '82*, 1982, pp. 147–154.

[48] S. J. Johnson, *Iterative Error Correction: Turbo, Low-Denisty Parity-Check and Repeat-Accumulate Codes*. Cambridge, UK: Cambridge University Press, 2010.

[49] S. M. Kay, *Modern Spectral Estimation: Theory and Application*. New Jersey, USA: Prentice Hall, 1988.

[50] ——, *Fundamentals of Statistical Signal Processing, Volume 1: Estimation Theory*. New Jersey, USA: Prentice Hall, 1993.

[51] D. B. Kilfoyle and A. B. Baggeroer, "The state of the art in underwater acoustic telemetry," *IEEE Journal of Oceanic Engineering*, vol. 25, no. 1, pp. 4–27, Jan. 2000.

[52] H. Kim and J. K. Tugnait, "Turbo equalization for doubly-selective fading channels using nonlinear Kalman filtering and basis expansion models," *IEEE Transactions on Wireless Communications*, vol. 9, no. 6, pp. 2076–2087, Jun. 2010.

[53] R. Koetter, A. C. Singer, and M. Tüchler, "Turbo equalization," *IEEE Signal Processing Magazine*, vol. 21, no. 1, pp. 67–80, Jan. 2004.

[54] K. Larsen, "Short convolutional codes with maximmal free distance for rates 1/2, 1/3, and 1/4," *IEEE Transactions on Information Theory*, vol. 19, no. 5, pp. 371 – 372, May 1973.

[55] R. Lawrence and H. Kaufman, "The Kalman filter for equalization of a digital communications channel," *IEEE Transactions on Communication Technology*, vol. COM-19, no. 6, pp. 1137–1141, Dec. 1971.

[56] G. Leus, "On the estimation of rapidly time-varying channels," in *12th European Signal Processing Conference, EURASIP 2004*, Vienna, Austria, Sep. 2004, pp. 2227–2230.

[57] Q. Li, X. Wang, and C. Georghiades, "Turbo mulituser detection for turbo coded CDMA in multipath fading channels," *IEEE Transactions on Vehicular Technology*, vol. 51, no. 5, pp. 1096–1108, Sep. 2002.

[58] X. Li and T. F. Wong, "Turbo equalization with nonlinear Kalman filtering for

time-varying frequency-selective fading channels," *IEEE Transactions on Wireless Communications*, vol. 6, pp. 691–700, Feb. 2007.

[59] S. Lin and J. J. Costello, *Error Control Coding*, 2nd ed. Englewood Cliffs, NJ: Prentice-Hall, 2004.

[60] L. Linton, P. Conder, and M. Faulkner, "On the Performance of Golden Codes in Rayleigh Fading Channels with Doppler Spread," in *1st International Conference on Signal Processing and Communication Systems, ICSPCS 2007*, Gold Coast, Australia, Dec. 2007.

[61] ——, "Multiuser Communications for Underwater Acoustic Networks using MIMO-OFDM-IDMA," in *2nd International Conference on Signal Processing and Communication Systems, ICSPCS-2008*, Gold Coast, Australia, Dec. 2008.

[62] ——, "Multiuser MIMO Communications using Interleave-Division Multiple-Access and Golden Codes," in *2008 IEEE 67th Vehicular Technology Conference, VTC2008-Spring*, Marina Bay, Singapore, May 2008.

[63] ——, "Multi-Rate Communications Using Layered Interleave-Division Multiple Access with Power Allocation," in *IEEE Wireless Communications and Networking Conference, WCNC 2009*, Budapest, Hungary, Apr. 2009.

[64] ——, "Multiple-Access Communications for Underwater Acoustic Sensor Networks using OFDM-IDMA," in *MTS/IEEE Oceanic Engineering Conference, OCEANS 2009*. Biloxi, Mississippi, USA: MTS/IEEE, Oct. 2009, pp. 1–8.

[65] ——, "Improved Interleave-Division Multiple Access (IDMA) Performance Using Dynamic FEC Code Allocation," in *IEEE Wireless Communications and Networking Conference, WCNC 2010*, Sydney, Australia, Apr. 2010.

[66] J. Lodge and M. Gertsman, "Joint detection and decoding by turbo processing for fading channel communications," in *International Symposium on Turbo Codes and Related Topics*, Brest, France, Sep. 1997, pp. 88–95.

[67] B. Lu and X. Wang, "Iterative receivers for multiuser space-time coding systems," *IEEE Journal on Selected Areas in Communications*, vol. 18, no. 11, pp. 2322 – 2335, Nov. 2000.

[68] R. W. Lucky, *Silicon Dreams: Information, Man, and Machine.* New York, NY: St. Martin's Press, 1989.

[69] R. Lupas and S. Verdu, "Linear multiuser detectors for synchronous code-division multiple-access channels," *IEEE Transactions on Information Theory*, vol. 35, no. 1, pp. 123–136, Jan. 1989.

[70] ——, "Near-far resistance of multiuser detectors in asynchronous channels," *IEEE Transactions on Communications*, vol. 38, no. 4, pp. 496–508, Apr. 1990.

[71] X. Lurton, *An Introduction to Underwater Acoustics: Principles and Applications*. Chichester, UK: Praxis Publishing Ltd, 2002.

[72] X. Ma, G. B. Giannakis, and S. Ohno, "Optimal training for block transmissions over doubly selective channels," *IEEE Transactions on Signal Processing*, vol. 51, no. 5, pp. 1351–1366, May 2003.

[73] U. Madhow and M. L. Honig, "MMSE interference suppression for direct-sequence spread-spectrum CDMA," *IEEE Transactions on Communications*, vol. 42, no. 12, pp. 3178–3188, Dec. 1994.

[74] R. H. Mahadevappa and J. G. Proakis, "Mitigating multiple access interfence and intersymbol interference in uncoded CDMA systems with chip-level interleaving," *IEEE Transactions on Wireless Communications*, vol. 1, no. 10, pp. 781–792, Oct. 2002.

[75] I. M. Mahafeno, C. Langlais, and C. Jego, "OFDM-IDMA versus IDMA with ISI cancellation for quasistatic rayleigh fading multipath channels," in *4th International Symposium on Turbo Codes and Related Topics*, Apr. 2006, pp. 1–6.

[76] T. May and H. Rohling, "Orthogonal frequency division multiplexing," in *Wideband Wireless Digital Communications*, A. F. Molisch, Ed. New Jersey, USA: Prentice Hall PTR, 2001.

[77] T. K. Moon, *Error Correction Coding: Mathematical Methods and Algorithms*. Hoboken, NJ, USA: John Wiley and Sons, 2005.

[78] D. E. Muller, "Application of boolean algebra to switching circuit design," *IEEE Transactions on Computers*, vol. 3, pp. 6–12, Sep. 1954.

[79] A. F. Naguib, N. Seshadri, and A. R. Calderbank, "Applications of space-time block codes and interference for high capcaity and high data rate wireless systems," in *32nd Asilomar Conference on Signals, Systems, and Computers*, Nov. 1998, pp. 1803 – 1810.

[80] J. C. L. Ng, K. B. Letaief, and R. D. Murch, "Complex optimal sequences with constant magnitude for fast channel estimation initialization," *IEEE Transactions on Communications*, vol. 46, no. 3, pp. 305–308, Mar. 1998.

[81] C. Novak, F. Hlawatsch, and G. Matz, "MIMO-IDMA: Uplink multiuser communications using interleave-divison multiple access and low-complexity iterative receivers," in *IEEE International Conference on Acoustics, Speech and Signal Processing, 2007 (ICASSP '07)*, vol. 3, Apr. 2007, pp. 225 – 228.

[82] F. Oggier, G. Rekaya, J.-C. Belfiore, and E. Viterbo, "Perfect Space-Time Block Codes," *IEEE Transactions on Information Theory*, vol. 52, no. 9, pp. 3885–3902, Sep. 2006.

[83] R. Ouertani, A. Saadani, G. R.-B. Othman, and J.-C. Belfiore, "On the Golden Code Performance for MIMO-HSDPA System," *64th IEEE Vehicular Technology Conference, 2006 (VTC-2006 Fall)*, pp. 1–5, 2006.

[84] D. P. Percival and A. T. Walden, *Spectral Analysis for Physical Applications: Multitaper and Conventional Univariate Techniques.* Cambridge, UK: Cambridge University Press, 1993.

[85] L. Ping, L. Liu, K. Wu, and W. K. Leung, "Interleave-divison multiple-access," *IEEE Transactions on Wireless Communications*, vol. 5, no. 4, pp. 938–947, Apr. 2006.

[86] L. Ping, L. Liu, K. Y. Wu, and W. K. Leung, "Interleave-Division Multiple-Access (IDMA) Communications," in *International Symposium on Turbo Codes and Related Topics, 2003. (ISTC 2003)*, Brest, France, Sep. 2003, pp. 173–180.

[87] H. V. Poor, *An Introduction to Signal Detection and Estimation*, 2nd ed. New York: Springer-Verlag, 1994.

[88] ——, "Iterative multiuser detection," *IEEE Signal Processing Magazine*, vol. 21, no. 1, pp. 81–88, Jan. 2004.

[89] H. V. Poor and S. Verdú, "Probability of error in MMSE multiuser detection," *IEEE Transactions on Information Theory*, vol. 43, pp. 858–871, 1997.

[90] E. Prange, "Cyclic error-correcting codes in two symbols," Air Force Cambridge Research Center, Cambridge, MA, Tech. Rep. Tech. Rep. TN-57-103, Sep. 1957.

[91] R. Price and P. E. Green, "A communication technique for multipath channels,"

Proceedings of the IRE, vol. 46, no. 3, pp. 555–570, Mar. 1958.

[92] J. G. Proakis and M. Salehi, *Communication Systems Engineering*, 2nd ed. Upper Saddle River, NJ: Prentice-Hall, 2002.

[93] J. Proakis, *Digital Communications*, 4th ed. New York, USA: McGraw-Hill, 2001.

[94] R. Pyndiah, A. Glavieux, A. Picart, and S. Jacq, "Near optimum decoding of product codes," in *IEEE GLOBECOM*, 1994, pp. 393–343.

[95] F. Qu and L. Yang, "Orthogonal space-time block-differential modulation over underwater acoustic channels," in *MTS/IEEE OCEANS 2007 Conference*, Vancouver, BC, Canada, Sep. 2007, pp. 1–5.

[96] ——, "Basis expansion model for underwater acoustic channels?" in *MTS/IEEE OCEANS 2008 Conference*, Quebec City, QC, Canada, Sep 2008, pp. 1–7.

[97] L. Rabiner, "A tutorial on hidden Markov models and selected applications in speech recognition," *Proceedings of the IEEE*, vol. 77, pp. 257–286, Feb. 1989.

[98] D. Raphaeli and A. Saguy, "Linear equalizers for turbo equalization: A new optimization criterion for determining the equalizer taps," in *2nd Intern. Symp. Turbo Codes*, Brest, France, Sep. 2000, pp. 371–374.

[99] I. S. Reed, "A class of multiple-error-correcting codes and a decoding structure," *IEEE Transactions on Information Theory*, vol. 4, pp. 38–49, Sep. 1954.

[100] I. S. Reed and G. Solomon, "Polynomial codes over cerain finite fields," *SIAM Journal on Applied Mathematics*, vol. 8, pp. 300–304, 1960.

[101] S. Roy and T. M. Duman, "Soft input soft output Kalman equalizer for MIMO frequency selective fading channels," *IEEE Transactions on Wireless Communications*, vol. 6, no. 2, pp. 506–514, Feb. 2007.

[102] C. Schlegel and A. Grant, *Coordinated Multiuser Communications.* Dordrecht, The Netherlands: Springer, 2006.

[103] C. Schlegel, Z. Shi, and M. Burnashev, "Optimal power-rate allocation and code selection for iterative joint detection of coded random cdma," *IEEE Transactions on Information Theory*, vol. 52, no. 9, pp. 4286–4294, Sep. 2006.

[104] P. Schniter, S.-J. Hwang, S. Das, and A. P. Kannu, "Equalization of time-varying channels," in *Wireless Communications over Rapidly Time-Varying Channels*,

F. Hlawatsch and G. Matz, Eds. Oxford, U.K.: Academic Press, 2011, ch. 6, pp. 237–284.

[105] B. A. Sethuraman, B. S. Rajan, and V. Shashidhar, "Full-diversity, high-rate space-time block codes from division algebras," *IEEE Transactions on Information Theory*, vol. 49, no. 10, pp. 2596–2616, Oct. 2003.

[106] K. S. Shanmugan and A. M. Breipohl, *Random Signals: Detection, Estimation and Data Analysis.* New York, USA: John Wiley and Sons., 1988.

[107] C. E. Shannon, "A mathematical theory of communication," *Bell System Technical Journal*, vol. 27, pp. 379–423, 623–656, 1948.

[108] D. Slepian, "Prolate spheroidal wave functions, Fourier analysis, and uncertainty-V: The discrete case," *Bell Labs Technical Journal*, vol. 57, no. 5, pp. 1371–1430, May-Jun. 1978.

[109] S. Song, A. C. Singer, and K. Sung, "Soft input channel estimation for turbo equalization," *IEEE Transactions on Signal Processing*, vol. 52, no. 10, pp. 2885–2894, Oct. 2004.

[110] M. Stojanovic., "Underwater acoustic communication," in *Wiley Encyclopedia of Electrical and Electronics Engineering.* New York, USA: John Wiley & Sons, 1999.

[111] M. Stojanovic and L. Freitag, "Multiple Detection for Wideband Underwater Acoustic CDMA Communications," *IEEE Journal of Oceanic Engineering*, vol. 31, no. 3, pp. 685–695, Jul. 2006.

[112] G. L. Stüber, *Principles of Mobile Communication.* New York: Springer, 2012.

[113] V. Tarokh, H. Jafarkhani, and A. Calderbank, "Space-time block codes from orthogonal designs," *IEEE Transactions on Information Theory*, vol. 45, no. 5, pp. 1456–1467, Jul. 1999.

[114] V. Tarokh, N. Seshadri, and A. Calderbank, "Space-time codes for high data rate wireless communication: performance criterion and code construction," *IEEE Transactions on Information Theory*, vol. 44, no. 2, pp. 744–765, Mar. 1998.

[115] S. ten Brink, "Convergence of iterative decoding," *Electronics Letters*, vol. 35, no. 10, pp. 806–808, May 1999.

[116] ——, "Design of conatenated coding schemes based on iterative decoding conver-

gence," Ph.D. dissertation, Institite of Telecommunications, University of Stuttgart, Germany, Apr. 2001.

[117] T. A. Thomas and F. W. Vook, "Multi-user frequency-domain channel identification, interference suppression, and equalization for time-varying broadband wireless communications," in *IEEE Workshop Sensor Array & Multichannel Signal Process.*, Boston, MA, USA, Mar. 2000, pp. 444–448.

[118] M. K. Tsatsanis and G. B. Giannakis, "Modeling and equalization of rapidly fading channels," *Int. J. Adapt. Control Signal Process.*, vol. 10, pp. 159–176, Mar. 1996.

[119] C. C. Tsimenidis, O. R. Hinton, A. E. Adams, and B. S. Sharif, "Underwater acoustic receiver employing direct-sequence spread spectrum and spatial diversity combining for shallow-water multiaccess networking," *IEEE Journal of Oceanic Engineering*, vol. 26, no. 4, pp. 594–603, Oct. 2001.

[120] M. Tüchler and J. Hagenauer, "Turbo equalization using frequency domain equalizers," in *Proc. Allerton Conf.*, Monticello, IL, Oct. 2000.

[121] M. Tüchler, R. Koetter, and A. C. Singer, "Turbo equalization: Principles and new results," *IEEE Transactions on Communications*, vol. 50, no. 5, pp. 754–767, May 2002.

[122] M. Tüchler, A. Singer, and R. Kötter, "Minimum mean squared error (MMSE) equalization using a priori information," *IEEE Transactions on Signal Processing*, vol. 50, no. 3, pp. 673–683, Mar. 2002.

[123] R. J. Urick, *Principles of underwater sound, 3rd ed.* Los Altos Hills, CA, USA: Peninsula Publishing, 1983.

[124] ——, "Ambient noise in the sea," Naval Sea Systems Command, Department of the Navy, Washington DC, USA, Tech. Rep., 1984.

[125] M. Valenti, "Iterative detection and decoding for wireless communications," Ph.D. dissertation, Virginia Polytechnic Institute and State University, Blacksburg, Virginia, USA, Jul. 1999.

[126] R. van Nee and R. Prasad, *OFDM for wireless multimedia communications.* Boston, USA,: Artech House, 2000.

[127] S. Verdú, *Multiuser Detection.* Cambridge, UK: Cambridge Univ. Press, 1998.

[128] M. Vistintin, "Karhunen-Loève expansion of a fast Rayleigh fading process," *IEE Electronic Letters*, vol. 32, no. 18, pp. 1712–1713, Aug. 1996.

[129] A. J. Viterbi, "Error bounds for convolutional codes and an asymptotically optimum decoding algorithm," *IEEE Transactions on Information Theory*, vol. 13, pp. 260–269, Apr. 1967.

[130] B. Vucetic and J. Yuan, *Turbo Codes: Principles and Applications.* Boston, USA: Kluwer Academic Publishers, 2000.

[131] H. S. Wang and P.-C. Chang, "On verifying the first-order Markovian assumption for a Rayleigh fading channel model," *IEEE Transactions on Vehicular Technology*, vol. 45, no. 2, pp. 353–357, May 1996.

[132] H. S. Wang and N. Moayeri, "Finite-state Markov channel-a useful model for radio communication channels," *IEEE Transactions on Vehicular Technology*, vol. 44, no. 1, pp. 163–171, Feb. 1995.

[133] X. Wang and H. V. Poor, "Iterative (turbo) soft interference cancellation and decoding for coded CDMA," *IEEE Transactions on Communications*, vol. 47, no. 7, pp. 1046–1061, 1999.

[134] ——, *Wireless Communication Systems: Advanced Techniques for Signal Reception.* Upper Saddle River, NJ: Prentice-Hall, 2004.

[135] S. B. Weinstein and P. M. Ebert, "Data transmission by frequency division multiplexing using the discrete Fourier transform," *IEEE Transactions on Communications*, vol. COM-19, pp. 628–634, Oct. 1971.

[136] C. Weiss, C. Bettstetter, and S. Riedel, "Code construction and decoding of parallel concatenated tail-biting codes," *IEEE Transactions on Information Theory*, vol. 47, no. 1, pp. 366–386, Jan. 2001.

[137] S. Wicker, *Error Control Systems for Digital Communications and Storage.* Englewood Cliffs, NJ: Prentice Hall,, 1995.

[138] J. M. Wozencraft and B. Reiffen, *Sequential Decoding.* Cambridge, MA: MIT Press, 1961.

[139] Z. Wu and J. Cioffi, "Turbo decision aided equalization for magnetic recording channels," in *IEEE Global Telecommunications Conference, 1999 (GLOBECOM '99)*, Dec. 1999, pp. 733–738.

[140] Z. Xie, R. T. Short, and C. K. Rushforth, "A family of suboptimum detectors for coherent multiuser communications," *IEEE Journal on Selected Areas in Communications*, vol. 8, no. 4, pp. 683–690, May 1990.

[141] T. Zemen and C. F. Mecklenbrauker, "Time-variant channel estimation using discrete prolate spheroidal sequences," *IEEE Transactions on Signal Processing*, vol. 53, no. 9, pp. 3597–3607, Sep. 2005.

[142] L. Zheng and D. N. C. Tse, "Diversity and Multiplexing: A Fundamental Tradeoff in Multiple Antenna Channels," *IEEE Transactions on Information Theory*, vol. 49, no. 5, pp. 1073–1096, May 2003.

[143] Y. R. Zheng and C. Xiao, "Simulation models with correct statistical properties for Rayleigh fading channels," *IEEE Transactions on Communications*, vol. 51, no. 6, pp. 920–928, Jun. 2003.

[144] H. Zhu, B. Farhang-Boroujeny, and C. Schlegel, "Pilot embedding for joint channel estimation and data detection in MIMO communication systems," *IEEE Communications Letters*, vol. 7, no. 1, pp. 30–32, Jan. 2003.

[145] A. Zielinski, Y.-H. Yoon, and L. Wu, "Performance analysis of digital acoustic communication in a shallow water channel," *IEEE Journal of Oceanic Engineering*, vol. 20, no. 4, pp. 293–299, Oct. 1995.

List of Figures

List of Tables